Hydrogen doped Thin Film Diamond: Properties and Application for Electronic Devices

Hui Jin Looi

This thesis is submitted for the degree of Doctor of Philosophy.

Department of Electronic and Electrical Engineering
University College
University of London
DECEMBER 1999

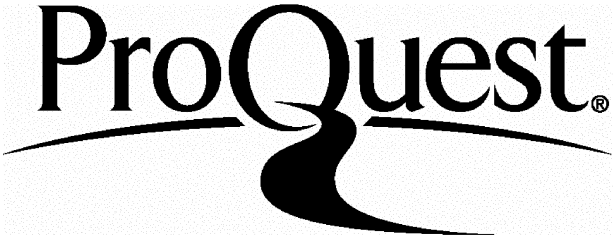

University of London

Abstract of Thesis

The face centered cubic allotrope of carbon, diamond, is a semiconducting material which possesses a valuable combination of extreme properties such as super-hardness, highest thermal conductivity, chemical hardness, radiation hardness, wide bandgap and others. Advances in chemical vapour deposition (CVD) technology have lead to diamond becoming available in previously unattainable forms for example over large areas and with controllable purity. This has generated much research interest towards developing the knowledge and processing technology that would be necessary to fully exploit these extreme properties.

Electronic devices fabricated on oxidised boron doped polycrystalline CVD diamond (PCD) displayed very poor and inconsistent characteristic. As a result, many electronic applications of polycrystalline diamond films were confined to ultra-violet (UV) and other forms of device which relied on the high intrinsic resistivity on undoped diamond films. If commercially accessible PCD films are to advance in areas which involve sophisticated electronic applications or to compete with existing semiconductors, the need for a more reliable and fully ionised dopant is paramount.

This thesis describes a unique dopant discovered within the growth surface of PCD films. This dopant is related to hydrogen which arises during the growth of diamond films. The aim of this study is to characterise and identify possible applications for this form of dopant. The mechanism for carrier generation remains unknown and based on the experimental results in this work, a model is proposed. The Hall measurements conducted on this conductive layer revealed a p-type nature with promising properties for electronic device application. A more detailed study based on electrical and surface science methods was carried out to identify the stability and operating conditions for this dopant. The properties of metal-semiconductor contacts on these surfaces were investigated. The fundamental knowledge is essential for exploring more advanced electronic devices such as the field effect transistors (FETs). Diamond is the only material suitable for detecting UV in the 220nm wavelength without any appreciable visible response. The prospect of introducing a doped layer based on Schottky mode for UV detection is important as it allows monolithic integration with other electronic devices.

Acknowledgements

I would like to acknowledge the UCL Graduate School for the award of a Graduate School Scholarship and the CVCP committee for the award of an ORS Scholarship. Without both awards, it would not be possible for me to pursue this degree. I am also indebted to the Public Service Department (JPA) of Malaysia for a government grant between 1991-1996 where it all started.

I would like to thank Dr Jeff Harris and his group in UCL and the IRC in Imperial College for access to their brilliant Hall effect kit. This facility has enabled me to conduct most of the material characterisation in this study. The enlightening discussion with Dr Harris and his courteous help in the laboratory is also gratefully acknowledged. I am also very grateful to Dr. John Foord and his group from Oxford University for the collaboration and helped especially in the UPS and XPS measurements. Kevin Lee, David Prescott, Chris Nice and Vic Law are also thanked for their advice in device fabrications and numerous clean room processing.

The UCL Diamond group, according to seniority, Dr. Duncan Marshall, a cheerful, creatively dressed man having a strong affinity for bikes for his help in the RIE system, lab and proof reading this thesis. Dr. Simon Chan, the original device and clean room processing guy for useful advice, his'lucky' desk and a good chat before I started. Dr. Robert McKeag for revealing me the secret of handling rough surfaces. Dr. Bhaswar Baral for cheering me, motivation and removing my guilt after spending hours on computer games. Dr. Mike Whitfield, conveniently having almost everything on his desk, exhausting the hard disk space, useful discussion on FET's, diodes, MSM and how to crash computers,. Dr Lisa Pang, a charming 'big sister', easy to beat up person, good cook, however < 1 pint, great company, for half believing in my extrapolated results and not believing my Au coated probes! Olivier Gaudin, a good discussion about politics, defects, gain, a warm place to stay and for making me run a lot in badminton. Stuart Lansley, for believing in the OPFET and keeping things organised in the lab and office. Oliver Williams, the only serious strategy game player in the group apart from me, maintaining, downloading and restoring the Mac's and for disliking PC!.

My flatmates namely, Moo Man, Sharon, Wei Siong, Loon Chian, Chye Seong, Johnnie and Dodo for their support, help and warm company throughout the 3 years in London. Also enjoyed those 'interesting' subject that we talk or quarrel about. Chien Ping (little one) for her long and cheerful emails :)

I would like to thank my supervisor Dr Richard B. Jackman for the motivation, advice, encouragement, enthusiasm and support throughout this PhD. Those famous phrases.... lets make a transistor ! ...how ? Place two diodes back to back! ...amazingly almost everything works after that.....

And in Malaysia, Dad, Mum, Ee Li, Chui Li and others for their endless support and encouragement. ..... 'When are you going to finish ?' .....errrr.....I am not sure.....

Research is exciting and fun. Most of the time tough, confusing and risky. Too many riddles '.....what is going to happen when.....?' '..will it work....?' .....well just do it.....

And finaly to all the intelligent and highly creative activities I indulged in namely Warcraft II, FF7, Red Alert, Heroes II and III, Age of Empires, Ceaser III, freecell, bubbles, while waiting for the evaporator to pump down .....sometimes it can take up to weeks believe me.....

Hui Jin
November 1999

Contents

Chapter 1

Introduction

The semiconducting properties of natural diamond had been discovered as early as the 1950's [Brophy, 1955]. Long ago, before this discovery, diamond was more renowned as a precious gem stone for its brilliance when cut and polished, its elegance, status and fame inherited from the past. Even today, there is still a strong demand for optically flawless diamonds for the same reasons.

The outstanding properties of diamond have been widely acknowledged in the last few decades. However, the high cost of diamond and restricted availability prevents its extreme physical properties from being exploited industrially. Furthermore, natural diamond being the hardest of all material comes in different shapes, quality and sizes (mostly small). Even if not for the cost, it will be extremely difficult to obtain and process natural diamonds into a uniform standard shape and size which would be advantageous for applications in the drills and tool sector compared with other materials. Diamonds are thermodynamically unstable with respect to graphite hence attempts to purify diamond generally lead to material degradation.

As diamond became more thoroughly researched, the extreme physical properties became better understood and its potential as a semiconductor became clear to the scientific community. Diamond is often regarded as the 'ideal' semiconductor. It consists of carbon covalently bonded to neighbouring carbon atoms in a tetrahedral orientation, similar to the most well known and used semiconductor, silicon. Many physicists have shown that the combination of physical, chemical and electronic properties of diamond will make it far more superior to existing semiconductor materials. Diamond began to receive attention when a possible dopant boron was identified [Collins, 1970]. Only later, when methods of depositing diamond uniformly and reproducibly over large areas became established, did it really become viable to consider this material for industrial and electronic applications. These methods of depositing diamond films in

a controllable manner were based on a concept known as chemical vapour deposition (CVD). It involved deposition of diamond from the gas phase at a relatively low substrate temperature ~900°C and pressure (~30mbar) in contrast to the natural process occurring only deep in the earth crust which normally require pressures of ~30kbar and temperatures exceeding 2000°C. To reproduce these natural conditions in the laboratory is extremely costly and technically very demanding. The CVD method stemmed from Deryagin's [1970] idea of using an atomic hydrogen rich atmosphere to suppress the growth of non diamond carbon phase. An account of the CVD methods of growing diamond will be presented in Chapter 2. The ability to deposit high quality diamond on non diamond substrate in a controllable manner has significantly increased the availability of and reduced the cost of diamonds for research and industry.

In this study, it is the semiconducting properties of CVD diamond and the electronic devices that it will support that are of interest. Much effort has been expended in order to introduce an impurity dopant into diamonds in a controllable manner, essential for the realisation of most devices. The most well known dopant boron has been studied in great depth. Different techniques have been employed to incorporate boron and other possible atomic species into the lattice to change this material from semi-insulating to semiconducting. Chapter 3 discusses some of the techniques used and the experimental results achieved by many workers. The immediate success in doping diamond films with boron and other elements has lead to the fabrication of unipolar electronic devices. Devices such metal insulator semiconductor field effect transistor (MISFET), metal oxide semiconductor field effect transistor (MOSFET), metal semiconductor field effect transistor (MESFET) and Schottky diodes have been demonstrated on natural, polycrystalline CVD diamond and homoepitaxial CVD diamond. Theoretical predictions of the performance of diamond devices compared with experimental results are explored in chapter 4.

Recently, a fully ionised dopant related to a hydrogen terminated layer of CVD grown diamond has emerged. This form of p-type dopant have been used successfully to fabricate high performance devices such as MESFET, MISFET and Schottky diodes on homoepitaxial CVD diamond [Kawarada, 1994]. The experimental sections in this study aimed to characterise the properties of this conductive layer and explore its potential application for electronics on the more economical and commercial polycrystalline CVD diamond. In order to achieve this goal, various characterisation methods and fabrication process are required. Chapter 5 will provide a brief description of the main techniques used in this course of study.

The experimental results commence in chapter 6 with an investigation into the electrical properties of surface conductive layer on polycrystalline CVD diamond films. This was conducted in different environments to determine the effect of different treatments on the stability of this layer. The experimental results were very positive indicating that the next step would be to fabricate simple devices on these surfaces. The electronic properties of 6 different metallisation contacts were investigated on these surfaces in Chapter 7. Apart from Au all the other metallisation contact displayed rectification characteristics. Schottky diodes using a combination of Au and the other metallisation contact have been realised. Chapter 8 concentrates on

engineering low resistive electrical contact on these films. Au and carbide forming metals such as Ti have been introduced. The electrical properties of these contacts were characterised using the specific contact resistance measurement. The mechanical integrity and electrical stability of these electrical contacts are of great importance for the applications addressed here.

The fabrication of active electronic devices is demonstrated in chapter 9. MESFETs were fabricated using Al as the gate with point ohmic contacts as the source and drain. These devices were the first to be fabricated from polycrystalline diamond; they performed satisfactorily at room temperature and displayed good characteristics. The operation of a depletion or enhancement mode MESFET on polycrystalline CVD diamond film had previously not been achieved. Previous transistors using a boron doped channel on PCD film suffered from poor current-voltage characteristics. Chapter 10 reveals the possibility of using the hydrogen terminated layer to detect electromagnetic radiation in the deep UV region (~220nm) which correspond to the bandgap of diamond. The detectors are primarily based on the metal semiconductor contact; different modes of operation will also be demonstrated. The detection of UV in the 220nm region based on the Schottky contact mode is rarely reported in the literature. The difficulty associated with this mode of operation on boron doped polycrystalline material was the uncertainty related to the leakage current of the Schottky metallisation contact. The simple action of a phototransistor based on a MESFET mode of detection will also be discussed. This is the first reported operation of such a device on diamond. Chapter 11 summaries the project and present conclusion based on the new data recorded.

References :-

Brophy, J.J., Phys. Rev., [1955] **99**, 1336.

Collins, A.T., Lightowlers, E.C. and Williams, A.W.S. [1970] Diamond Res. (Suppl. Industrial Diamond Review), 19-22.

Deryagin, B.V. and Fedoseev, D.V. [1970] Russ. Chem. Rev., **39**, 783.

Kawarada, H., Aoki, M. and Ito, M., [1994] Appl. Phys.Lett., **65**, 1563.

Chapter 2

The Properties and CVD Deposition of Diamond

Contents

Section 2.1 Introduction to the Properties of Diamond

Diamond possess a valuable combination of extreme physical and chemical properties. Many demanding applications can be satisfied by exploiting these properties making diamond a particularly useful material rather than merely a decorative item in the gem stone industry. The sparsity, controlled market and the great demand for high quality diamond in the lucrative jewellery sector has increased its value to a stage where it is not economical to utilise it for any other commercial application. Nevertheless, the extreme properties of diamond will continue to suggest new applications. There is currently much effort directed to seek ways of producing cheaper and higher quality synthetic diamond films. This is to encourage the use of synthetic diamonds in industry and more importantly to lower the cost of diamond to the level where it will be an economical viable material. In 1993, the market consumption of natural and synthetic diamond (grown by the High Pressure High Temperature method) comprised of 65% for abrasives, 20% for micron size powder, 10% for drilling diamonds and 5% for tools [Bakon, 1993]. The physical, chemical and quality of most natural diamonds are far from ideal. Only a small percentage of these stones are of high quality enough to be considered as useful for the gem industry. The rest go into other applications like drill and tool bits. The major problem with natural diamond is that each stone has slightly different characteristics. It is impossible to manufacture electronic devices or production equipment from randomly shaped, varying

impurity content and quality stones which cannot be purified. These problems and the uncertainty about the effect of impurities contribute to the considerable spread in the reported properties. Furthermore, the quality and properties of diamond will degrade with the amount of contamination in these stones. Table 2.1 presents a few selected extreme properties of diamond.

Property	Diamond	Notes/comparison
Knoops Hardness ($kgmm^{-2}$)	7000	hardest material known, SiC(2480), Si (850) Stainless steel (660)
Coefficient of friction	0.1 (in air)	very low in air
Youngs's Modulus ($10^{11}Nm^{-2}$)	10.35	highest mechanical strength SiC (7), Si (1.9) stainless steel (2)
Sound propagation velocity (kms^{-1})	18.2	1.6 times the value of alumina
Chemical inertness		inert to all acids, bases and solvent at room temperature
Range of high transmittance (μm)	0.22-2.5 and > 6	orders of magnitude lower than other infra red material
refractive index	2.41	1.6 times the value of silica]
Thermal conductivity at 300K ($Wcm^{-1}K^{-1}$)	20	highest value at 300K Si (2.3), SiC(3.2) Cu(5)
Thermal expansion($10^{6}K^{-1}$)	1	Si (2.33), SiC (3.3) stainless steel (17.3)

Table 2.1 Selected properties of diamond [Bachmann, 1991]

In this study, the potential of synthetic diamond grown on non diamond substrates by chemical vapour deposition (CVD) methods as a semiconducting material will be investigated. The synthesis of diamond is revealed in section 2.2. Realising the uncertainty and the high cost associated with natural diamonds, numerous scientific studies have been conducted to improve the deposition of diamond through CVD. Most of the work was centred on improving the quality of the deposited film, increasing the growth area, the deposition rate and maintaining a low

production cost. Besides the advantage offered by its extreme physical properties, diamond is predicted to possess superior semiconducting properties compared to other materials. This has been confirmed by the discovery of high quality naturally occurring semiconducting diamonds [Brophy, 1955]. Such findings have also contributed towards the drive of improving the CVD method of synthesis, which offers the advantage of a good impurity control in the deposited film with the use of high purity carbon and hydrogen gaseous sources. As a result, synthetically deposited diamond films are more reliable, consistent and uniform relative to the natural source. Moreover, the ability to coat a large surface area with a diamond film allows the realisation of many applications which normally require a large active surface area, in contrast to the limited area of randomly shape natural diamond. The electronic properties of diamond compared with other semiconducting materials are displayed in table 2.2 for comparison.

Property	Diamond	Si	GaAs	3C-SiC	GaN
Bandgap (eV)	5.45	1.1	1.43	2.2	3.39
Electron mobility ($cm^2v^{-1}s^{-1}$)	2000	1500	8500	1000	900
Hole mobility ($cm^2v^{-1}s^{-1}$)	1800	600	400	40	150
Breakdown field (10^6Vcm^{-1})	10	0.3	0.4	4	5
Intrinsic resistivity (Ωcm)	10^{16}	10^3	10^9	$>10^9$	$>10^9$
Saturation electron velocity (10^7cms^{-1})	2.7	1	2	2	2.7
Dielectric constant	5.7	11.9	12.8	9.7	9
Work function (eV)	NEA {111} surface	4.8	4.7	-	-

Table 2.2 Electronic properties of diamond compared with other semiconductor [Yoder, 1993; Morkoc, 1994]

Diamond has the highest thermal conductivity of any material. More importantly, diamond based electronic devices do not require additional heat sinking as the material itself is the most efficient heat spreader. Another useful property of diamond is the electron has one of the highest saturation velocities. A high speed device can be realised from this property. In addition, the breakdown field is also the highest on diamond. These two properties combined allowed a high electric field to be applied in the material at the saturation velocity promising RF devices capable of delivering larger output power. Furthermore, the large bandgap of diamond will maintain a high intrinsic bulk resistivity even at high temperatures. Thus, electronic devices with a low leakage current and capable of operating at high temperature are possible. The

potential and merits of electronic and power devices fabricated from diamond will be discussed in Chapter 4. The chemical inertness of diamond, its radiation hardness, visible blind characteristic and its electronic potential made this material suitable for detection of alpha particles, X-rays, UV light and allow for operation in harsh environments where other semiconductors would fail. These extreme properties make diamond attractive for specific applications where there is no alternate choice. The combination of electronics and the superior mechanical properties of highly oriented diamond (HOD) films currently find much interest for various applications in micro-electro-mechanical systems (MEMS).

Section 2.2 Chemical Vapour Deposition (CVD) of Diamond

Angus *et al.* [1968] demonstrated that the mass of diamond grit can be increased by passing methane gas over it under chemical vapour deposition conditions and confirmed that the net increase of mass is due to the formation of diamond. Later, Deryagin *et al.* [1970] increased the efficiency of this method by incorporating a super-equilibrium concentration of atomic hydrogen to suppress the deposition of graphite and simultaneously enhance the growth of diamond. The method was further refined by Matsumoto *et al.* [1982]. The concept of using a super-equilibrium concentration of hydrogen now forms the basis of all CVD diamond deposition techniques at low pressure. The CVD of diamond can be separated into three stages. They are:

a) The formation of atomic hydrogen and development of gas phase chemistry.
b) The nucleation of diamond on the surface of a non diamond substrate.
c) The growth of diamond via surface chemical reactions.

In the first stage, energy is required to produce a high concentration of atomic hydrogen from its molecular form. The energy needed to break the hydrogen bonds is most often supplied by microwave injection or hot filament activation although other sources have been used effectively [Hirose, 1989]. Once achieved, atomic hydrogen being highly reactive and unstable reacts with either a hydrogen molecule or other gas phase hydrocarbon molecule (e.g. CH_4, C_2H_6) resulting in hydrogen abstraction. This gives rise to either a molecular hydrogen or a highly reactive intermediate (free radical) which may then undergo chemical reactions.

Many reaction intermediates have been identified [Sunkara, 1990] and diamond nucleation is believed to begin with the adsorption of such species on the non diamond substrate. Following adsorption, these species desorb, etched by atomic hydrogen or form a stable nucleation site. The rate of spontaneous nucleation on non diamond substrates varies considerably from non-existent on mirror polished silicon to highly dense (~10^6 nucleation sites cm^{-2}) on Si scratched by diamond powder. Intentional damaging of the substrate surface creating microscopic sharp edges also gives positive results [Dennig, 1992; Polini, 1992]. In general, carbide forming species are found to be much more effective compared to non carbide forming substrates as they increase the adsorption probability and stability of nucleation species. An amorphous carbide layer is normally found at the interface between the diamond film and the

carbide forming substrate, implying that this layer provides defects and dangling bonds that may energetically favour the growth of diamond [Ravi, 1990 b]. To achieve a continuous growth of diamond film, it is necessary to have a high density of nucleation sites at least 10^9 cm^{-2} [Bauer, 1993].

The key principle in the growth of diamond is the incorporation of a hydrocarbon species into the lattice at an active site followed by the loss of residual hydrogen through hydrogen abstraction, in conjunction with the suppression of sp^2 species. Each carbon on the growth surface cannot be totally terminated by more than a single hydrogen due to steric constraints. However, if this hydrogen is not present then the surface will reconstruct to form the energetically favoured graphitic bonds. The individual hydrogen bonds have to be removed through hydrogen abstraction to allow active sites for the addition of carbon. Non diamond forming radicals can be reduced by lowering the methane concentration relative to hydrogen, enhancing the production of useful small free radical hydrocarbons group like the methyl [Harris, 1989], acetylene [Martin, 1993] and acetyl [Rau, 1993] groups instead. These small groups have been proposed as the growth species supported with extensive kinetic analysis and computer modeling. Methyl radicals have been widely accepted as the main growth precursor especially on {100} planes [D'Evelyn, 1992]. However, the range of growth conditions used indicate the possibility that other species of hydrocarbon can contribute and dominate this event [Frenklach, 1992; Sun, 1993; Kondoh, 1993]. Incorporation of carbon takes place gradually through hydrogen abstraction allowing the carbon atom of the molecule to become bonded to neighboring carbon atoms. When the last hydrogen atom attached is removed, it opens an active site and the whole process recommences. An estimated 10,000 hydrogen atoms are required for every carbon added to the diamond lattice [Banholzer, 1992]. This explains the kinetic oriented mechanism of growth rather than thermodynamics and the relatively low growth rates associated with the CVD of diamond.

The use of only hydrogen and carbon chemistry for growth constrains the development of CVD processes as carbon can be only added in a very narrow concentration range. The low growth rate is essential to produce low defect density diamond; higher carbon to hydrogen (C/H) ratio will lead to faster growth which results in an increased density of sp^2 bonds and other defects [Liou, 1990]. Oxygen was first introduced into the growth chemistry by Hirose *et al.* [1986] in the form of acetone to explore the possibility of increasing the efficiency of the CVD process. Positive experimental results with an increase in the growth rates of low defect density diamond were achieved. The incorporation of oxygen augments the role of hydrogen in the gas phase reaction [Takeuchi, 1992] by preferential etching non diamond carbon [Ohtake, 1993]. OH groups are more aggressive etchants of non diamond carbon than hydrogen [Harris, 1989 b]. Once the potential of oxygen became understood, it was introduced in diamond growth in many forms including molecular [Kawato, 1987], carbon monoxide [Cerio, 1992] carbon dioxide [Chen, 1993] and acetone [Okoli, 1989]. Oxygen allows a more diverse chemistry than otherwise available. However, too much oxygen can cause excessive etching thus destroying nucleation sites.

Section 2.3 General growth techniques

Diamond film can be grown by using different type of reactors; they differ in the principle used to achieve gas phase activation, generation of atomic hydrogen and formation of important radical species. Four of the most commonly used methods will be briefly reviewed in this section. The arc jet offers a high deposition rate, microwave offers slower growth but higher quality film, combustion techniques offer low capital cost and hot filament systems offers low operating cost.

In the hot filament method, thermal dissociation of molecular hydrogen is used as a means of producing atomic hydrogen. The thermal energy is supplied by a refractory metal filament (tungsten or tantalum) usually heated to about 1900 - 2000°C. At these temperatures a dissociation efficiency of approximately 10% can be achieved [Setaka, 1989]. The substrate has to be placed close to the filament and sometimes water cooling is necessary. Adding a bias between the filament and substrate increases the nucleation density [Lee, 1990] while modifying the surface morphology of the grown film. This method offers the advantage of producing highly oriented diamond films over large area at a relatively low capital cost. Uniform deposition over a large area is possible because the activation of gas species is dependent upon the positioning of filament, unlike plasma deposition and most combustion processes. However, the physical and chemical changes to the filament over time affect the uniformity of the growth layer. Physical degradation of the filament usually contaminates the diamond film with metallic impurities. As a result, diamond films grown by hot filament methods are unsuitable for electronic application. Furthermore, carburisation of the filament leads to premature filament failure. The diamond film deposited tends to be thickest in regions closest to the filament [Jansen, 1990] therefore shape changes and filament sagging are critical areas to control [Wolden, 1992]. The hot filament system is frequently used for mathematical modeling as the thermally driven chemistry is much simpler and more straight-forward compared to a plasma based system.

A more efficient way of producing atomic hydrogen is by electromagnetic radiation induced dissociation. The frequency used most commonly is 2.45 GHz [Setaka, 1988]. The reactor is designed such that the microwave is launched into the growth chamber either in a direction normal [Liou, 1990] or parallel [Setaka, 1989] to the substrate surface. Gas activation is achieved by inelastic collision between electrons and neutrals. This gives an average hydrogen dissociation of about 0.1 - 10%. At high power densities, a substrate in direct contact with the plasma will become heated. The ions produced by the plasma do not appear to have an important role in growth and may cause detrimental effects by reducing the long range order of the film [Amaratunga, 1989]. Incorporation of impurities in the film is avoided by preventing the plasma from making any contact except with the substrate [Kamo, 1988]. This method suffers from radial nonuniformity as the density of radicals is the highest in the center of the plasma and reduces rapidly with radial distance away. Uniformity is confined to only a few centimeters, primarily dependent on the radiation wavelength. Microwave enhanced systems at 2.45 GHz are now commercially available making it one of the most popular deposition techniques. In general

the substrate temperature and growth rate is the highest where the density of plasma is the highest. In-situ diagnostics are difficult to implement in a plasma system as any probe inserted will distort the original plasma. In addition, the complexity of the chemical reactions and electrical component in a plasma prevents simple modeling. Due to the commercial availability and the relatively high quality of the film produced, diamond films grown by this technique have been used for many applications [McKeag, 1998; Kawarada, 1998].

Plasma torch activation systems provide the fastest growth rate reported. This type of system can use a high power, high density plasma sustained by a DC arc [Kurihara, 1989], inductively coupled RF [Matsumoto, 1992] or microwave excitation [Gasworth, 1992]. The high power density generates electrons at temperatures of around 10,000K. The gas temperature at 2100K [Raiche, 1993] is similar to the hot filament method. Gas activation is mainly achieved through thermal dissociation unlike the microwave enhanced method. A 99.5% dissociation from methane to carbon and hydrogen has been reported [Suzuki, 1988] while the atomic hydrogen dissociation can reach about 10%. Direct contact between the substrate and plasma is avoided as the plasma temperature can exceed the graphitisation temperature of diamond. Hence, water cooling of the substrate is necessary. The substrate has to be positioned as close as possible to the plasma in order to conserve the reactive chemistry. This results from the high collision frequency due to operating conditions at atmospheric pressure. A high gas flow rate is required to minimise the transport time of active radicals and to maintain the desired substrate temperature. Diamond films grown by this method are predominantly sp^3 and highly faceted. Typical growth rates between 60 μm/h [Matsumoto, 1987] up to 1mm/hour have been reported [Ohtake, 1990]. Films grown by this technique have shown some potential for particle detectors which require high carrier mobility and long lifetime [Pan, 1993]. Drawbacks include the high gas flow rate (1 - 100 litres/min) for maintaining the gas chemistry, electrode erosion, huge power consumption, high operating cost and limited area deposition (1 - 2cm) with poor uniformity [Matsumoto, 1992]. Plasma stability can be difficult to achieve due to high power, pressure and flow rates.

The combustion system relies on the exothermic reaction between acetylene and oxygen to provide the gas phase activation suitable for diamond growth [Hirose, 1989]. The combustion products of these gaseous species are CO, atomic and molecular hydrogen, CO_2 and H_2O. The design of the flame nozzle is critical to produce a uniform flame which is useful for the growth of a uniform film. In this method, the substrate is kept in contact with the flame and temperature is controlled by placing the substrate on a water cooled metal block. The flame temperature can be as high as 3700K at atmospheric pressure. This method offers the advantage of high growth rate (100μm/hour). The capital cost of this system is low but it is offset by the high consumption of reactant gas as the conversion efficiency of hydrocarbon to diamond is the worst among the methods discussed in this section. The diamond films grown usually contain some graphitic phase [Philips, 1992]. The temperature and chemical gradients coupled with high growth rates can lead to highly defective crystals. Growth using this method is not very suitable for electronic application as the deposition area is small and uniformity within this area is poor. The deposition area (typically 2 cm diameter) can be increased by using multiple burners with a rotational substrate holder [Tzeng, 1991].

Section 2.4 Electronic Grade CVD Diamond

The quality of the material deposited by the CVD technique depends on many factors, particularly on the growth substrate. The best quality CVD diamond to date is deposited through homoepitaxy. In this case, the growth of diamond is merely the addition of subsequent layer of diamond on a single crystal diamond substrate. However, the high cost, limited availability and small area of single crystal diamond prevents its use for production level device fabrication. Proof of concept devices devices such as FET's and logic circuits operating at 500°C have been reproducibly fabricated on homoepitaxial material exhibiting carrier mobilites close to theoretical prediction [Fox,1995].

Growth of CVD diamond proceeds most rapidly at defects and ledges, hence defects in a film normally propagate from substrate surface to film surface [Sutcu, 1992]. Homoepitaxy of CVD diamond growth proceeds the fastest on {110} surfaces while the smooth {100} surfaces are the slowest. Defect density is the highest on the {111} surfaces and about 1% of the {111} homoepitaxy material consists of twinned structures [Wild, 1991]. The surface roughness and high defect density on the {110} and {111} make {100} surface the best choice for growing electronic quality diamond. The growth on {100} surfaces is strongly influenced by the substrate temperature and carbon concentration in the gas phase. Growth proceeds laterally at steps and kinks rather than re-nucleation. Low growth temperatures can lead to pyramidal structures while high growth temperatures will produce a more defective film. Secondary nucleation is sometimes observed on these films [Wild, 1993].

Diamond films having electronic properties superior to most natural diamond have been demonstrated through homoepitaxy. However, the more realistic economically and large area deposition of CVD diamond through heteroepitaxy on non diamond substrate produces a material which is polycrystalline in nature [Kamo, 1988]. The high surface energy of diamond relative to most materials makes nucleation difficult without intentional introduction of nucleation sites [Kim, 1992]. The majority of these polycrystalline surfaces comprise of a mixture of the {111} and {100} planes. Heteroepitaxial growth normally requires a lower concentration of carbon in the gas phase compared to homoepitaxy. Growth conditions which allow deposition of homoepitaxial film may result in diamond like carbon or graphite during heteroepitaxy. The choice of substrate for nucleation and growth must be compatible with the growth environment (1000°C) at low pressures, the presence of atomic hydrogen and other reactive charged species. Substrates which form carbides and have little structural mismatch are favourable as they assist in providing nucleation sites and improve film adhesion. Generally, on such surfaces nucleation enhancement is necessary for growing a coalesced diamond film.

As in homoepitaxy, under certain growth conditions, heteroepitaxy growth proceeds more rapidly in a particular crystal direction. Favorable growth orientation allows these grains to dominate the morphology of polycrystalline film resulting in textured material. Textured polycrystalline film for (100) [Wild, 1993; Stoner, 1992] and other planes [Kobashi, 1990] has

been demonstrated. The mechanism responsible for the development of a textured film is described in terms of evolutionary selection [van der Drift, 1967]. This occurs when the majority of grains are oriented in a manner where the crystal direction of the most rapid growth is normal to the substrate. The dependence of morphology on the different growth rates of {100} and {111} faces is illustrated by a parameter known as α. Growth of <111> is expected for $\alpha = 1$, <110> for $\alpha = 1.5$ and <100> for $\alpha = 3$. The growth condition in a specific reactor can be optimised for the desired α. In general, α can be increased by decreasing the growth temperature and increasing the hydrocarbon concentration. A <100> textured film has a significantly smoother surface compared to the predominantly <110> and <111> textured film. However, this film still contains large angle grain boundaries and significant tilt. This will interfere with electronic and optical properties of the film. To further improve the quality of the film, the negative effect of grain boundary needs to be reduced.

Three factors which hinder heteroepitaxial diamond growth are :- its high surface energy, small lattice constant (3.7Å) and small coefficient of thermal expansion. Potential substrates for epitaxial growth of diamond can be divided into those that do not form an interlayer such as SiC, c-BN and BeO, those that form a carbide interlayer such as Si, Mo and W and finally those that form a graphitic layer such as Ni and Cu. Registry between the substrate and diamond film is more likely on material which does not form an interlayer. Heteroepitaxy of diamond has been demonstrated on c-BN with nucleation densities exceeding $10^{11}cm^{-2}$. However, single crystal c-BN is only available over small areas (several hundred microns in diameter) [Wang, 1993]. Improvement in heteroepitaxy on β-SiC has been demonstrated [Kawarada, 1998]. The author has successfully fabricated surface p-type channel MESFETs on this material.

Textured films where the grains are aligned with respect to one another are known as highly oriented diamond (HOD). Highly oriented diamond (HOD) has been successfully grown on β-SiC or Si [Jiang, 1993; Fox,1994; Kohl, 1993]. The quality of heteroepitaxial growth has been improved by using a bias enhanced nucleation (BEN) process [Stoner, 1993]. Significant increase in nucleation density was obtained by applying a negative bias prior to normal diamond deposition [Yugo, 1991]. The negative bias causes ions to bombard the surface of the substrate. These ions are critical for causing the enhanced nucleation. Robertson *et al.* [1995] proposed that the sub implantation of ions from biasing causes deposition of nanocrystalline graphitic sp^2 bonded C which acts as nucleation sites. In addition, the authors suggested that orientation of sp^2 planes perpendicular to the substrate surface may be caused by compressive stress due to ion bombardment. The biasing step is useful to deposit oriented diamond particles on Si (100) substrates. The (100) textured material was generated by controlling the relative growth rates of the crystal as proposed by van der Drift [1967] evolution theory. The orientation between the grains produces small angle grain boundaries between the individual grains and this is believed to reduce the density of interfacial traps by about 50% compared to randomly aligned polycrystalline material [Fox,1994].

References :-

Amaratunga, G., Putnis, A., Clay, K. and Milne, W. [1989] Appl. Phys. Lett., **55**, 634.

Angus, J.C., Will, H.A., and Stanko, W.S. [1968] J. Appl. Phys., **39**, 2915.

Anthony, T.R. [1990]" Metastable synthesis of diamond", The Physics & Chemistry of Carbides, Nitrides and Borides, R, Freer ed., p133.

Bachmann, P. [1991] Physics World, **April**, 32.

Bakon, A. and Szymanski A. [1993] "Practical Uses of Diamond", New York, USA.

Banholzer, W. [1992] Surf. Coat. Tech., **53**, 1.

Bauer, R.A., Sbrokey, N.M. and Brower, W.E. [1993] J. Mater. Res., **8**, 2858.

Brophy, J.J., Phys. Rev., [1955] **99**, 1336.

Butler, J.E. and Woodin, R.L. [1993] Phil. Trans. R. Soc. Lond., **A 342**, 209.

Cerio, F.M., Weimer, W.A. and Johnson, C.E. [1992] J. Mater. Res., **7**, 1195.

Chen, C.F., Hong, T.M. and Chen S.H. [1993] J. Appl. Phys., **74**, 4483.

Dennig, P.A., Shiomi, H., Stevenson, D.A. and Johnson, N.M. [1992] Thin Solid Films **212**, 63.

D'Evelyn, M.P., Chu, C.J., Hauge, R.H. and Margrave, J.L. [1992] J. Appl. Phys., **71(3)**, 1528.

Deryagin, B.V. and Fedoseev, D.V. [1970] Russ. Chem. Rev., **39**, 783.

Fox, B.A., Stoner, B.R., Malta, D.M., Ellis, P.J., Glass, R.C. and Sivazlian, F.R. [1994] Diamond & Relat. Mater., **3**, 382.

Frenklach, M. [1992] J. Chem. Phys., **97**, 5794.

Gasworth, S.M. [1992] Thin Solid Films, **212**, 186.

Harris, S.J. [1989 a] J. Appl. Phys., **65**, 3044.

Harris, S.J. and Weiner, A.M. [1989 b] Appl. Phys. Lett. **55**, 2179.

Hirose, Y. and Terasawa, Y. [1986] Jpn. J. Appl. Phys., **25**, 519.

Hirose, Y., Amanuma, S., Okada, N. and komaki, K. [1989] "1st International Symp. on Diamond and Diamond Like Films", The electrochemical Soc, Inc; Pennington, NJ, p 80.

Jansen, F. [1990] J. Vac. Sci. Technol., **A8**, 3785.

Jiang, X., Klages, C-P., Zachai, R., Hartweg, H. and Fusser, H. J. [1993] Appl. Phys. Lett. **62**, 3438.

Kamo, M., Yurimoto, H. and Sato, Y. [1988] Appl. Surf. Sci., **33/34**, 553.

Kawarada, H., Wild, C., Nerres, N., Koidl, P., Mizouchi, Y., Hokazono, A. and Nagasawa, H. [1998] Appl. Phys. Lett., **72**, 1878.

Kawato, T. and Kondo, K.I. [1987] Jpn. J. Appl. Phys., **26**, 1429.

Kim, J.W., Baik, Y.-J., Eun, K.Y. and Yoon D.N. [1992] Thin Solid Films, **212**, 104.

Kobashi, K., Nishimura, K., Miyata, K. Kumagai, K. and Nakaue [1990] J. Mater. Res., **5**, 2469.

Kohl, R., Wild, C. Herres, N. Koidl, Stoner, B.R. and Glass, J.T. [1993] Appl. Phys. Lett., **63**, 1792.

Kondoh, E, Tanaka, K. and Ohta, T. [1993] J. Appl. Phys., **72**, 5926.

Kurihara, K., Sasaki, K.I. and Kawarada, H. [1989] Fujitsu Sci. Tech. J., **25**, 44.

Lee, Y.H., Richard, P.D., Bachmann, P.K. and Glass, J.T. [1990] Appl. Phys. Lett., **56**, 620.

Liou, Y., Inspektor, A., Weimer, R., Knight, D. and Messier, R. [1990] J. Mater., Res., **5**, 2305.

Martin, L.R. [1993] J. Mat. Sci. Lett., **12**, 246.

Matsumoto, S., Sato, Y., Tsutsumi, M. and Setaka, N. [1982] J. Mater. Sci., **17**, 3106.

Matsumoto, S., Hino, M. and Kobayashi T. [1987] Appl. Phys. Lett., **51**, 737.

Matsumoto, S., Hosoya, I., Manabe, Y. and Hibino, Y. [1992] Pure & Appl. Chem., **64**, 751.

Morkoc, H., Strite, W.S., gao, G.B., Lin, M.E., Sverdlov, B. and Burns, M. [1994] J. Appl. Phys. **76**, 1363.

Ohtake, N. and Yoshikawa, M. [1990] J. Electrochem. Soc., **137**, 717.

Ohtake, N. and Yoshikawa, M. [1993] Jpn. J. Appl. Phys., **32(1)** , 2067.

Okoli, S., Haubner, R. and Lux, B [1989] J. Phys. **C5** (5), 159.

Pan. L.S., Karnia, D.R., Pianetta, P., Ager, J.W., Landstrass, M.I. and Han, S. [1993] J. Appl. Phys., **73**, 2888.

Phillips, R., Wei, J. and Tzeng, Y. [1992] Thin Solid Films, **212**, 30.

Polini, R. [1992] J. Appl. Phys., **72**, 2517.

Raiche, G.A. and Jeffries, J.B. [1992] Appl. Optics, **32**, 4629.

Rau, H. and Picht F. [1993] J. Mater., Res., **8 (9)**, 2250.

Ravi, K.V., Koch, C.A., Hu, H.S. and Joshi, A. [1990 a] J. Mater. Res., **5(11)**, 2356.

Ravi, K.V. and Koch, C.A. [1990 b] Appl. Phys. Lett., **57**, 348.

Robertson, J., Gerber, J., Sattel, S., Jung, K. and Ehrhardt, H. [1995] Appl. Phys. Lett., **66**, 3287.

Sun, B., Zhang, X., Zhang, Q. and Lin, Z. [1993] Appl. Phys. Lett., **62**, 31.

Setaka, N. [1989] J. Mater. Res., **4**, 664.

Stoner, B.R. and Glass. J.T. [1992] Appl. Phys. Lett., **60**, 698.

Stoner, B.R., Sahaida, S.R., Bade, J.P., Southworth, P. and Ellis, P.J. [1993] J. Mater., Res., **8**, 1334.

Sunkara, M., Angus, J.C., Hayman, C.C. and Buck, F.A. [1990] Carbon, **28**, 745.

Sutcu, L.F., Chu, C.J., Thompson, M.S. Hauge, R.H. Margrave, J.L. and D'Evelyn, M.P. [1992] J. Appl. Phys., **71**, 5930.

Suzuki, K., Sawabe, A. and Inuzuka, T. [1988] Appl. Phys. Lett., **53**, 1818.

Takeuchi, K. and Yoshida, T. [1992] J. Appl. Phys., **71**, 2636.

Tzeng, Y., Phillips, R., Cutshaw, C., Srivinyunon, T., Loo, B.H. and Wang P. [1991] Appl. Phys. Lett., **58**, 239.

van der Drift, A. [1967] Phillips Res. Repts., **22**, 267.

Wang, L., Piruoz, P., Argoitia, A., Ma, J.S. and Angus, J.C. [1993] Appl. Phys. Lett., **63**, 1336.

Watanabe, I., Matsukura, N. and Machi, Y. [1992] Jpn. J. Appl. Phys., **31**, 1958.

Wild, C., Koidl, P. Herres, N. Muller-Serbert, W. and Eckermann, T. [1991] " Anisotropic growth and twinning in polycrystalline CVD diamond films", 2nd International Conference on Diamond Materials, The Electrochemical Soc. Inc.; Pennington, N.J., p 152.

Wild, C., Koidl, P., Muller-Serbert, W., Walcher, H., Kohl, R., Herres, N., Locher. R., Samlenski, R. and Brenn. R. [1993] Diamond & Relat .Mater., **2**,158.

Wolden, C. Mitra, S. and Gleason, K.K. [1992] J. Appl. Phys., **72**, 3750.

Yoder, M.N. [1993] "In diamond Films and Coatings", ed. R.F. Davis, (Noyes Publications) New Jersey, USA.

Yugo, S., Kania, T., Kimura, T. and Muto, T. [1991] Appl. Phys. Lett., **58**, 1036.

Chapter 3

The Progress of Doping Diamond

Contents

Section 3.1 Introduction

In Chapter 2, the potential of semiconducting diamond for high temperature, high power and high speed devices have been discussed in terms of inherit material physical and electronic properties. Although these extreme properties coupled with theoretical predictions suggest its superiority over other semiconductors, these properties will only be available for further exploitation provided it becomes possible to dope and control the p-type and n-type electrical conduction in diamond. And hence, this will be the main discussion of this chapter.

In a solid, when atoms are closely packed together, energy levels converge and form a continuous band of energy. The diamond zinc blend structure is such that the valence band is completely filled with electrons at 0K and the conduction band is empty. Hence there is no charge transport conduction within the valence band as there are no empty states for carriers to move. On the other hand, the conduction band is empty, although states exist, there are no

electrons available for conduction. With a bandgap of 5.45eV separating the valence and conduction band, intrinsic diamond is a good insulator [Field, 1979].

Recently, the cost of diamond has been significantly reduced with the advent of gas phase synthesis of diamond on non diamond and diamond substrate through the CVD technique [Spitsyn, 1981]. It is also through this gas phase synthesis where potential impurity dopant can be added during the growth stage. Further improvement and developement in these areas which allow the deposition of higher quality homoepitaxial and CVD films is one of the major steps forward in diamond electronics [Fox, 1994 and 1995].

Section 3.2 Choices of Dopant

Doping can be accomplished by incorporating certain impurity ions which are electrically active at the substitutional site in the diamond lattice. Ideally these impurities should be compatible in terms of chemical bonds and physical size without disturbing the original lattice itself. Unwanted impurities may generate additional defects which can be deep in the bandgap resulting in the compensation of the original useful carriers. The impurities must also be uniformly distributed throughout the lattice and not segregated and accumulated at certain sites.

Of all the impurities to date only boron and nitrogen have been shown to be substitutional. This is due to the closely packed diamond structure with a lattice parameter 3.567Å coupled with a small tetrahedral radius of carbon 0.77Å [Gildenblat, 1991]. With the exception of boron, other larger impurities will deform the diamond lattice to a certain extend. Boron has been successfully incorporated as an acceptor in HPHT synthesis, CVD diamond and is also found in natural diamond. There were reports indicating that boron actually improves the structural quality of diamond by reducing the concentration of planar defects and vacancies in polycrystalline films[Wang, 1992]. It was found that boron reduces the graphitic component in the CVD diamond. This effect can be explained if one assumes that boron doping allows better annealing of the defects. The Raman Spectrum of the film is affected by the amount of boron incorporated in the diamond film. The shift and widening of the sp^3 Raman peak in boron doped diamond film in figure 3.1 has been reported and interpreted in terms of the lattice strain [Gildenblat, 1991].

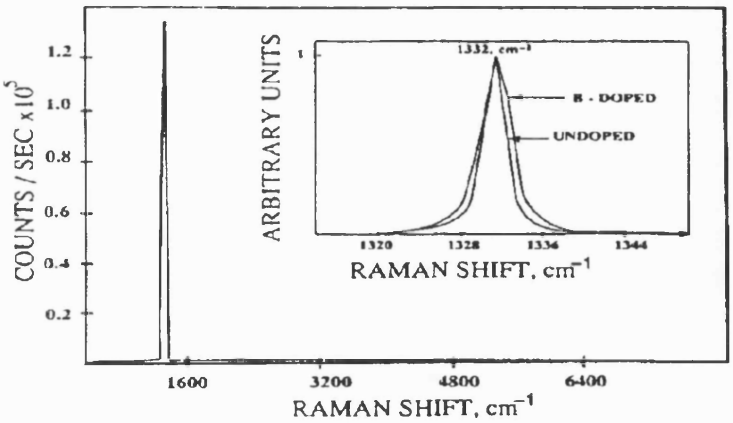

Figure 3.1 shows the widening and shift of Raman Spectra due to boron incorporation in natural diamond

Nitrogen exists in most diamond but it forms a deep level in the bandgap and is therefore electrically inactive. Nitrogen however, plays an important role in compensating acceptors and generating re-combination centers. In contrast to boron, isolated nitrogen at substitutional sites has donor like properties with an ionization energy of 1.7eV [Davies, 1977]. It has been reported to increase the growth rate of diamond films and encourages growth of {100} textured film if added in small quantities (<100ppm) [Badzian, 1993] but deteriorates the structural quality of diamond if added in large quantity [Bergman, 1994].

Carbon atoms are much smaller in size compared to phosphorus. This explains the low solubility of phosphorus into the diamond lattice. Contrary to nitrogen, theoretical computation for phosphorus suggests a low donor activation energy of only 0.2eV and predicts phosphorus to be a substitutional impurity [Kajihara, 1989]. Okano *et al.* [1992] introduced phosphorus into diamond by vaporizing a solution of P_2O_5 in methanol diluted with acetone. Carrier concentrations of $10^{15}cm^{-3}$ and an electron Hall mobility of $50cm^2/Vs$ have been measured. However, the film resistivity was too high for any practical use. Incorporation of phosphorus in large concentrations has adverse affects on the diamond lattice structure. It alters the surface morphology and deteriorates the Raman spectra [Haubner, 1998]. The low solubility of phosphorus in diamond films can be explained by its negative formation energy (E_f = -10.7eV) [Kajihara, 1989].

Section 3.3 P-type Diamond from Boron Doping

Brophy *et al.* [1955] conducted the first Hall measurement for type IIb diamond using indium and silver paint as ohmic contacts. Type IIb diamond is classified according to its blue phosphorescence and high conductivity [Custers, 1952], to distinguish them from type IIa, the more transparent and insulating natural diamond. They reported a p-type conduction with a sheet carrier concentration of 7×10^{13} cm^{-2}, a resistivity of 760Ωcm and a Hall mobility of $100cm^2/Vs$

at room temperature. Point contact rectification confirmed the existence of p-type conduction over the entire surface. Austin *et al.* [1956] performed Hall characterisation over a wider temperature range to determine the activation energy of the carriers in natural diamond. Based on the model containing both acceptor and donor levels, an activation of 0.38eV was measured. In addition, a hole concentration of 1.8 x $10^{13}cm^{-3}$, a Hall mobility of 1550 cm^2/Vs and resistivity of 270Ωcm at room temperature was reported. They suspected that the impurity element responsible for this p-type behaviour was either boron or aluminium.

Collins *et al.* [1970] used a similar model to Austin to determine the activation energy of the p-type behaviour in their type IIb diamond. They measured a mean value of 0.368eV. Later Lightowlers *et al.* [1976] utilised the I-V and C-V characteristic of a Au Schottky barrier to correlate quantitatively the active carriers in the diamond film to the boron concentration in the film. They concluded that the acceptors responsible were most probably substitutional boron.

The most effective method of modifying electronic properties of a material is through intentional doping. To date, only boron has clearly demonstrated and established itself conclusively to be an electrically active dopant. The lack of other types of dopant especially the n-type cast serious doubt on possible application and development of diamond electronics. In addition boron itself lies quite deep at 0.37eV above the valence band and efficient generation of active carriers at low temperature is very low.

Section 3.4 Doping during HPHT Synthesis

Wentorf *et al.* [1962] reported the preparation of semiconducting diamond using the High Pressure and High Temperature (HPHT) technique. Doping was conducted by addition of boron to the mixture of carbon and diamond forming catalysts (Fe, Ni, etc.) followed by exposure to conditions suitable to produce diamond. The resistivity obtained averaged about 10^5Ωcm with an activation energy of only 0.17 to 0.18eV. The unexpectedly high resistivity measured is most probably caused by compensation effects from nitrogen impurities in the diamond. A hole will be annihilated when an electron from the nitrogen donor level drops to the boron level creating no net change in conductivity. Calculation by Davies [1977] revealed that nitrogen acts as a deep donor and lies at 1.7eV below the conduction band. Doping by this process does not grant easy control over the amount of impurity of dopant required. It also suffers from inevitable contamination by nitrogen and other catalysts during the application of high pressure. Furthermore, it is not cost effective and the growth equipment cannot be easily developed. Other important parameters such as uniformity, the thickness of the doped layer, the large surface area and selective area doping were difficult to control.

Section 3.5 Ion Implantation

In this well known method, a beam of the desired, impurity ions is accelerated to the energy required normally ranging from several keV to several MeV and is directed onto the surface of the semiconductor. The impinging ions enter the crystal, giving up their energy by collision to the lattice and finally settle down at an average penetration depth. The penetration depth is dependent on the kinetic energy of the incidence ions, the target material and the angle of the incidence ions to the target. The distribution of the implanted ions can be approximated to a Gaussian.

Vavilov *et al.* [1966] successfully produced semiconducting diamond films by implanting lithium and boron ions with an energy of 40keV in a plane perpendicular to the (111) and (110) surface of diamond. The activation energy of lithium doped films decreased from 0.30eV to 0.23eV with increasing carrier concentration from 10^{17} to $10^{20}cm^{-3}$. Thermo-emf measurement confirmed the boron implanted diamond to be p-type. Later, Vavilov *et al.* [1972] reported the formation of a p-n junction through implantation of boron and phosphorous ions. Boron ions were implanted with 25 keV energy at a dose of 2 x $10^{14}cm^{2}$ at room temperature followed by a 5keV at a dose of 1.5 x $10^{15}cm^{2}$ to form ohmic contact. The large implanted doses resulted in graphitisation of diamond, hence an immediate anneal at 1400°C for 2 hours was performed to remove the implantation damage. P was then implanted at a temperature of 600°C at a dose of 1.6 x $10^{14}cm^{-2}$ with an energy of 80keV to define the n-type region.

Implantation on diamond is complicated due to the tendency of the damaged site to relax into non diamond carbon upon annealing as under these conditions diamond was not the favourable thermodynamic phase. Prins [1988] demonstrated the control of boron doping using a 2 step method. Boron was implanted cold into diamond at 77K followed by a rapid anneal at 1400K. At 77K the defects together with the vacancies created freeze and the following anneal promotes the boron atoms into the substitutional site created by the implantation damage.

A MISFET which displayed current saturation and pinch off was demonstrated by Zeisse *et al.* [1991] on type IIa diamond using ion implantated boron channel. Multiple implantation to achieve a uniformly doped channel 210nm thick was carried out at 80K. A quick anneal at 1203K in nitrogen ambient was performed to remove the implantation damage and activate the implanted boron. This was followed by a standard etching in a boiling solution of CrO_3 in H_2SO_4 to eradicate the remaining graphitic phase from the surface [Gildenblat, 1991].

Implantation offers the precise control of dopant concentration as ion beam current can be measured. It also offers uniformity over the wafer surface, uniformity in depth by multiple implantation at different energies and selective doping at preferred sites. However, the disadvantage of lattice damage caused by ion bombardment is inevitable. Normally a high temperature anneal is employed to remove some of this damage. This technique is especially useful for the formation of ohmic contacts [Uzan-Saguy, 1995]. However, the uniformity of ion

implanted species over a rough polycrystalline surface can be difficult to achieve especially when the average grain size is larger than the average penetration depth of the ions.

Later, Fontaine *et al.* [1996] further optimised the 2 steps suggested by Prins. A more refined technique called Cold Implantation and Rapid Anneal was introduced (CIRA). At 77K the low diffusity of defects created by implantation process increases the probability of implanted boron occupying the substitutional sites during the subsequent rapid anneal at 1450°C in vacuum for 10 minutes. Later, using a similar technique, Uzan-Saguy *et al.* [1998] reported the formation of a delta doped buried conductive layer in type IIa diamond with room temperature Hall mobility of 600cm^2/Vs at carrier concentration of 4 x 10^{18}cm^{-3} and an activation energy of 0.354eV, as shown in Figure 3.2(a) and Figure 3.2(b) respectively. This is the highest mobility ever achieved at that level of boron concentration through implantation. They used high energy B implanted at 2MeV with a penetration depth of 1.6μm at 77K which produced less graphitic defects [Prawer, 1997]. In addition, these defects can be easily annealed compared to the lower energy (keV) implant. The use of delta doped layers can also achieve higher film conductance than the equivalent uniform doped layers [Aleksov, 1999].

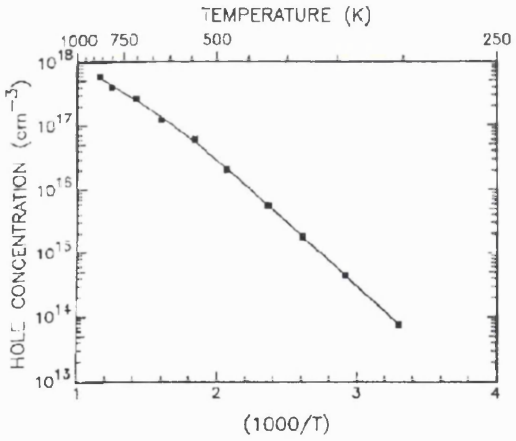

Figure 3.2 (a)

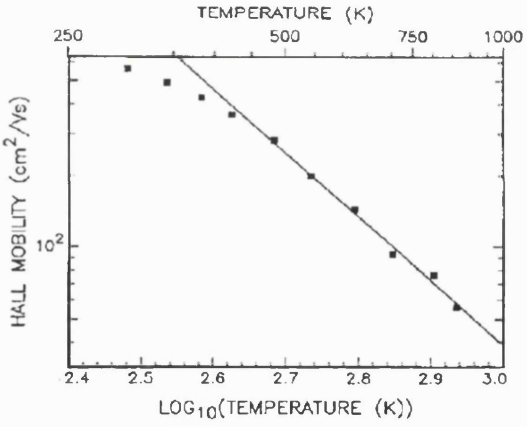

Figure 3.2(b)

Figure 3.2(a) shows the variation of hole concentration with temperature and Figure 3.2(b) shows the Hall mobility dependence on temperature on natural diamond implanted with boron

Section 3.6 In-situ Doping of Diamond during growth

In this case, the dopant is introduced during the growth of the diamond film itself. This technique became popular stemming from the development of the microwave CVD process for synthesising diamonds from the gas phase at high temperature and low pressure. Boron can be introduced to the CVD growth environment in solid, liquid and gaseous form. The common gaseous form of boron is diborane. It has been widely used as a dopant [Gildenblat, 1991] but it is highly toxic. Alternative choices such as solid sources include boron powder and boron trioxide (B_2O_3) while boric acid (H_3BO_3) and cyclic organic borinate esters have been used as liquid sources.

The first attempt to fabricate a p-n junction using dopant introduced by this method was reported by Alexenko *et al.* [1990] on the (111) face of natural diamond crystal. Diodes were fabricated on boron and phosphorus doped films, a p-n junction was formed at the interface. However, the diode was leaky. Fujimori *et al.* [1986] reported the synthesis of p-type semiconducting diamond using MPECVD technique with diborane (B_2H_6) as the dopant. Boron concentration in both the polycrystalline and homoepitaxial film was measured by SIMS. It was estimated to be about ~$10^{20}cm^{-3}$. The activation of the carriers was only about 0.013eV. In a later study Fujimori *et al.* [1990] demonstrated that the activation energy of the conducting film was affected by doping concentration. They also pointed to the dependency of mobility of holes and the carrier concentration on temperature.

Okano *et al.* [1990] explored the possibility of using boron trioxide (B_2O_3) [Okano, 1989] and diphosphorus pentaoxide (P_2O_5) [Okano, 1990], both being a non poisonous compound as a dopant source for synthesising a p and n-type semiconducting diamond films. The resistivities of the films were inversely proportional to the B/C ratio in the gas phase. Impurity profiles by SIMS confirmed that the impurity concentration in these films were related to the amount added during the growth stage. In addition, a Hall mobility of ~$40cm^2/Vs$ was recorded for the p-type characteristic.

The reduction of activation energy with increasing concentration of boron acceptors has been suggested to be caused by the formation of an impurity band [Mort, 1991; Nishimura, 1991]. Nishimura *et al.* [1991] proposed that the formation of impurity band will occur for acceptor level higher than 2 x $10^{18}cm^{-3}$. The advantage of having a pulse doped diamond film with lower activation energy and hence higher conductance has been fully utilised for the fabrication of homoepitaxial diamond MISFETs which displayed high performance at 200°C [Aleksov, 1999].

Lagrange *et al.* [1998] conducted a comprehensive study on the conduction behaviour of boron doped homoepitaxial films on {100} type IIb synthetic diamond doped by diborane for a temperature range of 300-1000K. Saturation of conductivity was observed between 680K and 1000K for samples doped below 2 x $10^{17}cm^{-3}$. For the range 10^{18} to 10^{19} cm^{-3}, an activation of 0.185eV was recorded from 500 - 1000K and 0.368eV between 300 and 500K as shown in Figure 3.3(a). Metallic properties of diamond films began to surface at concentration above 3 x $10^{20}cm^{-3}$ in agreement to the Mott transition. Others have also recorded similar values [Werner, 1997]. Hopping conduction at a temperature of 100K to 500K for carriers of 2.5 x $10^{19}cm^{-3}$ shown in figure 3.3(b) is in agreement with a value of 2.7 x $10^{19}cm^{-3}$ predicted by Werner *et al.* [1997]. Different conduction mechanisms for a range of carrier concentration are revealed in Figure 3.3(b).

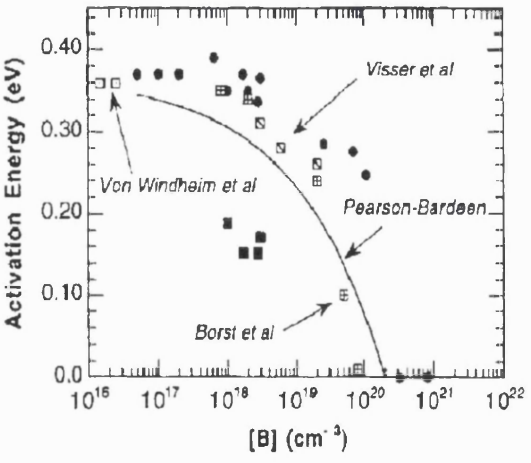

Figure 3.3(a)

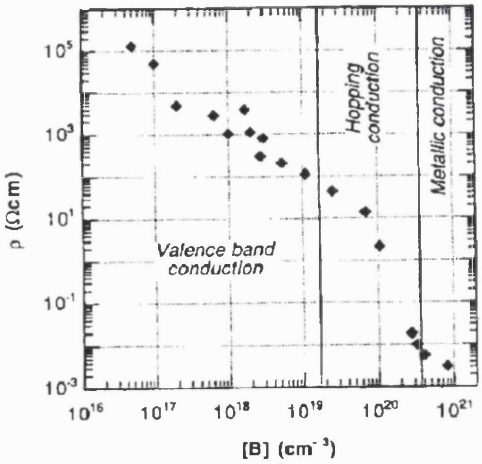

Figure 3.3(b)

Figure 3.3(a) shows the variation of activation energy with boron concentration and Figure 3.3(b) shows the resistivity of diamond film at different boron concentration [Lagrange, 1998]

Good control over the boron concentration in diamond films during growth was demonstrated by Gheeraert *et al.* [1998]. In figure 3.4 the boron concentration was determined by using the infra red absorption coefficient at 160meV from Davis [1977] calibration which agrees closely to the actual SIMS measurement.

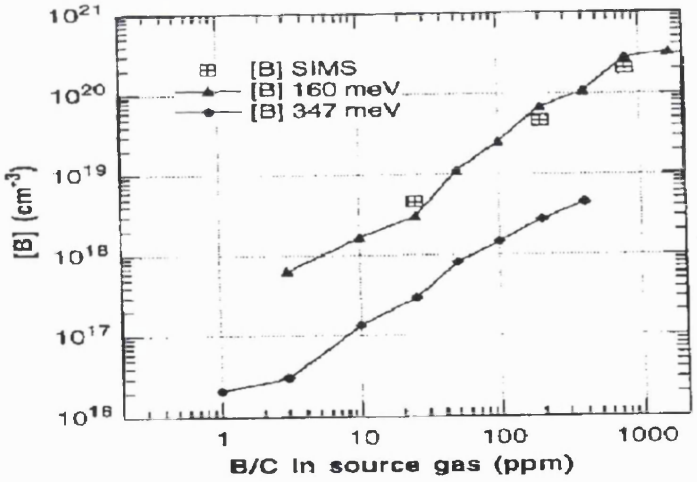

Figure 3.4 shows correlation between Boron concentration determined by SIMS and the infra red absorption at 160meV and 347meV [Gheeraert, 1998]

Fox *et al.* [1995] deposited homoepitaxial films in the {100} orientation with Hall mobilities up to 1400cm^2/Vs with reproducible values within the 1100-1300cm^2/Vs range as shown in Figure 3.5(a). These results compared well with the ~2000cm^2/Vs in Figure 3.5(b) for the best natural type IIb sample with a boron concentration of $10^{15}cm^{-3}$. FET's which exhibit current saturation and pinch off at 773K, transconductance of 1.3mS/mm have been fabricated on these films. These FETs were combined into analogue and digital circuits capable of operating at 523K and 673K.

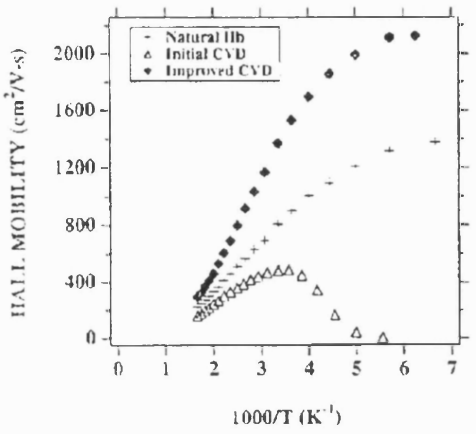

Figure 3.5(a)

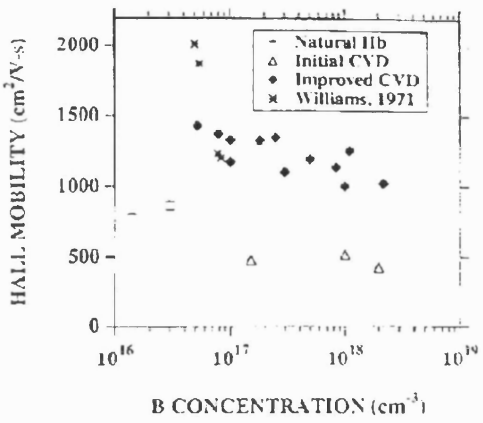

Figure 3.5(b)

Figure 3.5(a) shows the Hall mobility of different types of diamond film at a temperature range and Figure 3.5(b) shows the variation of Hall mobility with carrier concentration [Fox, 1995]

The improvement originated from the progress in the CVD technique for depositing diamond films. It is now possible to improve the electronic properties of boron doped homoepitaxial film to surpass that of natural diamond. Natural diamond which contain defects and impurities may underestimate the true potential of diamond. Moreover, natural diamond samples are not controllable form of diamond suitable for electronic application.

Section 3.7 Hydrogenated Surface Conductive Layer

Natural intrinsic diamond, a good insulator exhibits resistivity of the order of $10^{16}\Omega$cm due to the 5.45eV bandgap of diamond. However, it is well known that continuous intrinsic diamond films grown by MPECVD technique can exhibit resistivity of the order $10^{6}\Omega$cm, approximately 10 orders of magnitude lower than expected [Grot, 1990; Landstrass, 1989]. Subsequent annealing of these films in air at temperature above 400°C restored the resistivity to their original level. Subjecting natural diamond to atomic hydrogen in a plasma causes a reduction of resistivity again to about $10^{6}\Omega$cm. As undoped samples were used and conduction appeared after exposure to a hydrogen plasma, hydrogen was believed to be one of the reasons for this behaviour. Landstrass *et al.* [1989] proposed the passivation of deep traps by hydrogen as the reason for low conductivity.

Gildenblat *et al.* [1991] recorded a sheet resistance of 8kΩ/square on as-deposited homoepitaxial diamond, a value that was independent of the amount of boron incorporated into the bulk. However, this conductive layer can be removed by exposing the diamond to a strong oxidising wet chemical etch solution comprising a mixture of $CrO_3 + H_2SO_4$ at 170°C for 30 minutes followed by a rinse in a 1:1 boiling solution of H_2O_2 and NH_4OH [Grot, 1990]. They concluded that a thin non diamond surface layer is formed on the top of the CVD diamond film giving rise to the conductivity. After the cleaning procedure, the resistivity of the material is

dependent on the boron in the bulk.

Shiomi, *et al.* [1991] observed that the carrier concentration in homoepitaxial as-grown films is higher than those from activated boron acceptors. Hence they suggested the additional generation of carriers related to hydrogen. Maki *et al.* [1992] carried out re-hydrogenation using an ECR microwave system and concluded a deep acceptor level was forming as deduced from Seebeck effect measurements and temperature dependence resistivity.

Kawarada *et al.* [1994] fabricated an enhancement MESFET on as-deposited homoepitaxial hydrogen terminated undoped diamond and achieved a transconductance of 100μS/mm, drain to source current saturation and pinch off was observed. They also reported a Schottky barrier height which is dependent on metal electronegativity on similar surfaces. This evidence not only confirmed the semiconducting p-type nature of this layer but also demonstrated that this conductive layer is thin enough for realising a normally off MESFET. Al Schottky diodes using Au as ohmic contact display an ideality factor of 1.1, the nearest to unity ever reported on diamond and with barrier height of 0.8eV

Hall measurements on hydrogen terminated undoped, hydrogen terminated boron doped and oxidised boron doped homoepitaxial synthetic type Ib diamond were conducted by [Hayashi, 1997]. On the hydrogenated samples, they recorded carrier concentration of ~10^{18} cm^{-3} (assuming the conductive layer is 20nm thick an estimation from their SIMS profile of hydrogen) with a Hall mobility of around 30cm^2/Vs. The mobility of hydrogenated samples showed a positive power of $T^{1.1}$ indicating a different scattering mechanism (ionised impurity) exists in these films compared to a value of $T^{-0.5}$ recorded for the oxidised boron doped samples. The potential of this conductive layer for electronic applications has not been fully explored. Currently most of the studies on this layer are concentrated on {100} homoepitaxial layer.

Section 3.8 Doping on Polycrystalline CVD Diamond

Most of the early works on boron doping were carried out either on natural type IIa, natural type IIb or homoepitaxially grown epilayers on a diamond substrate. Renewed interest is generated emerging from the possibility to grow thin film diamond on non diamond substrate such as silicon, silicon dioxide, Al_2O_3 and on carbide forming metals using CVD technique. However, the deposition of thin film diamond on non diamond substrate produces a material which is polycrystalline in nature and true heteroepitaxy is not observed. Nevertheless, by careful control of the deposition technique and growth parameters, the quality of these more economical sources can be improved and purity can be enhanced to electronic grade near comparable to the single crystal diamond [Stoner, 1993].

The electrical and material characteristic of B_2H_6 doped polycrystalline diamond grown by MPECVD on highly resistive Al_2O_3 substrate was carried out by Nishimura *et al.* [1991(a)].

They obtained a low Hall mobility, ohmic behaviour and a low activation energy for heavily doped film (7 x 10^{20} cm^{-3}). The low activation energy and ohmic behaviour were caused by the formation of an impurity band. Uncontrollable dopant incorporation into these films will lead to heavily doped samples which are not very useful for fabricating active electronic devices.

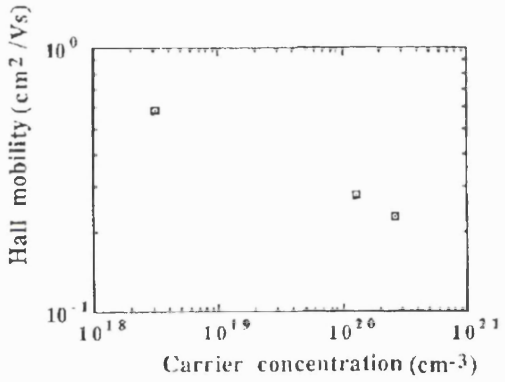

Figure 3.6(a)

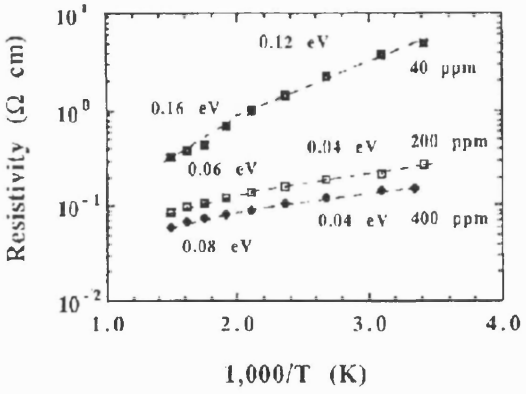

Figure 3.6(b)

Figure 3.6(a) shows the Hall mobility against carrier concentration and Figure 3.6(b) shows the variation of resistivity with temperature [Nishimura, 1991 (a)]

Dopant control during growth was demonstrated by Masood *et al.* [1993] using in-situ doping with pure boron powder. Hot filament CVD was used and diamond film was deposited on thermally grown SiO_2. The film resistivity and mobility decreases with carrier concentration as shown in Figure 3.7(a). They obtained a mobility of 30 cm^2/Vs, much higher than reported by Nishimura. Figure 3.7(b) shows the changes in the activation energy with Hall concentration.

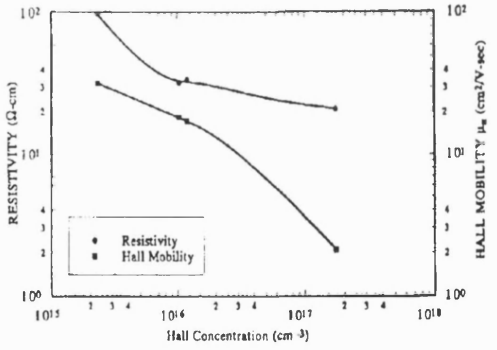

Figure 3.7(a)

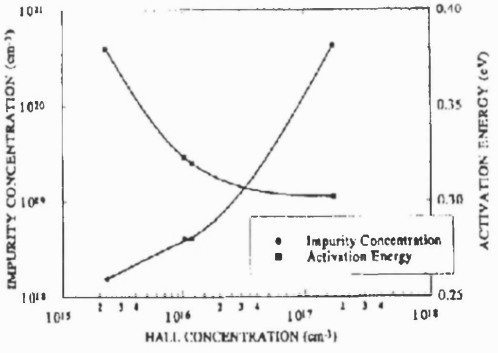

Figure 3.7(b)

Figure 3.7(a) shows the variation of resistivity, mobility with Hall concentration and Figure 3.7(b) shows the variation of activation energy and carrier concentration. [Masood, 1993]

A study of boron implanted polycrystalline diamond film was conducted by Fontaine *et al.* [1994]. Implantation was carried out at 77K followed by an annealing at 800°C in a furnace. The author reported a critical amorphisation threshold of 3 x $10^{15}$$cm^{-2}$ at 90keV, this was evident from their Raman spectra and resistance measurements shown in figure 3.8(a) and 3.8(b).

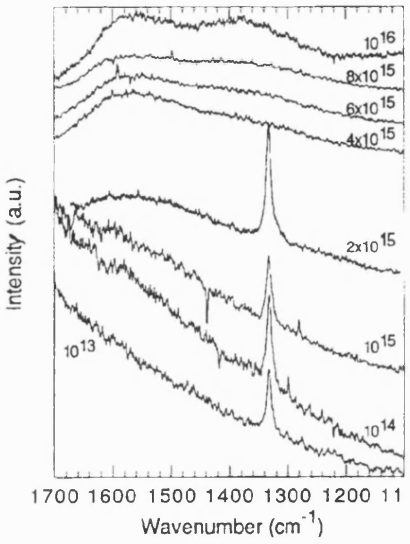

Figure 3.8(a)

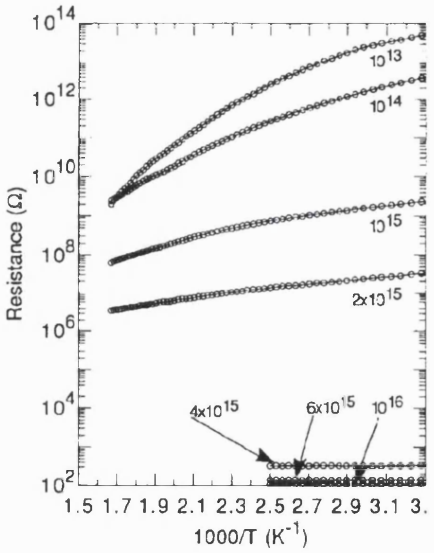

Figure 3.8(b)

Figure 3.8(a) shows the Raman spectra of diamond film after implantation with boron at different doses and figure 3.8(b) shows the corresponding resistance measured [Fontaine,1994].

Highly orientated textured diamond (HOD) can be deposited on Si substrates using a bias process [Wolter, 1993; Jiang, 1993]. Thin film diamond grown by this method allows relative improvement in electronics properties resulting from the orientated growth of diamond film compared with the randomly orientated grains on polycrystalline films. Hall measurement indicates an activation energy of 0.346eV at carrier concentration of 6.0 x 10^{13} cm^{-3} with an improved mobility of 165 cm^2/Vs compared with only about 1 to 30 cm^2/Vs for randomly orientated material [Malta, 1993].

The presence of grain boundaries has deleterious effect on the transport properties of a semiconductor. The way it affects the electronic properties of a semiconductor has been described by Seto and Baccarani. The Hall mobility of a polycrystalline film is less than one fifth that of the homoepitaxial film as shown in Figure 3.9(b) Improvements were confirmed by comparing the Hall mobility of HOD of (100) and polycrystalline material, a value of 165 cm^2/Vs against only about 30cm^2/Vs for the best polycrystalline material. In addition, the presence of grain boundaries leads to additional states, an increase in trap density and non diamond carbon phases which degrade the transport properties, even compensating useful active carriers [Fox, 1994].

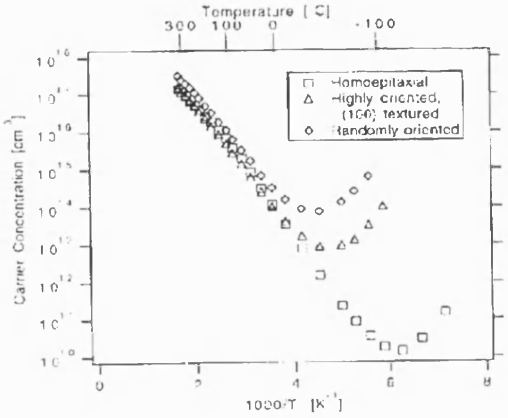

Figure 3.9(a)

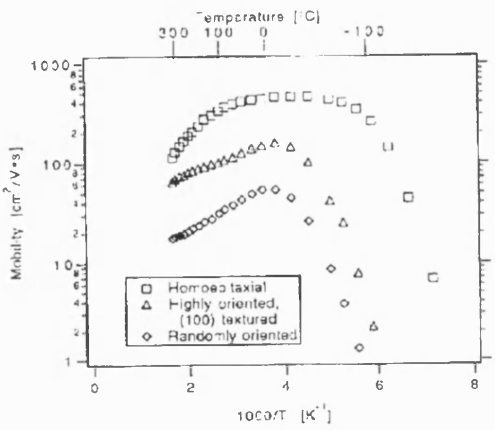

Figure 3.9(b)

Figure 3.9(a) shows variation of carrier concentration at different temperature and Figure 3.9(b) compares the Hall mobility of various diamond films [Fox, 1994]

Previous studies assumed boron was uniformly distributed in the *in-situ* doped PCD films. However, Huang *et al.* [1995] showed the presence of segregation of boron at the grain boundary of PCD films grown by HFCVD. Boron acid (H_3BO_3) was used as the doping source. They suggested that the segregation was caused by higher degree of oxidation of boron into B_2O_3 at the grain boundary. Ruan *et al.* [1992] and Erz *et al.* [1995] explained that the decrease in efficiency of boron doping in diamond films were attributed to the formation of B_2O_3 during the growth phase. Therefore, the presence oxygen in the gas phase will reduce the efficiency of boron incorporation.

Section 3.9 N-type doping of diamond

To date there are few reliable reports indicating the existence of n-type conduction on diamond [Okano, 1990; Koizumi, 1997]. The most convincing dopant for n-type conduction is phosphorus. Although nitrogen can be conveniently incorporated into the diamond lattice, it suffers from a very deep donor level (1.7eV) and remains inactive. Nitrogen has been used effectively to compensate the acceptor level of boron to produce a delta doped boron layer on homoepitaxial material [Aleksov, 1999]. N-type doping through lithium implantation has been reported by Prawer *et al.* [1993]. However, their experimental results were not supported by Hall measurement. In addition, the high dose of implantation needed can cause irrecoverable graphitisation. The high resistivity of the film despite high implantation doses suggests that lithium was not a suitable donor.

Incorporation of phosphorus has been investigated both by implantation [Hofsass, 1997] and *in situ* addition [Koizumi, 1997; Okano, 1990]. It appeared that the latter method produced a more positive result. Phosphorus in the form of diphosphorus pentaoxide (P_2O_5) was introduced into a microwave reactor by Okano *et al.* [1990] and the author reported an increase

in conductivity (10^{-2} Ωcm) of the diamond synthesized. Kozumi *et al.* [1997] used phosphine (PH_3) as a dopant source and successfully grew homoepitaxial layers on {111} surfaces using microwave CVD method. N-type conduction was confirmed by Hall measurement with a Hall mobility of 23 cm^2/Vs and an activation energy (E_A) of 0.43eV at 500K. They attributed their success to the reduction of hydrogen incorporation in the film during growth at 950°C. Nishimori *et al.* [1997] reported n-type properties from tri-n-butylphosphine ($P(C_4H_9)_3$) as a dopant source on homoepitaxial {100} surfaces grown using gas source molecular beam epitaxy. In addition, these authors successfully fabricated a p-n junction and carried out a Hall assessment. They reported an E_A of 0.12eV at a carrier concentration of 1.2×10^{18} cm^{-3} at 400°C. One of the main reasons for the difficulty in obtaining n-type properties is the deterioration of electrical conduction due to the incorporation of hydrogen together with the dopant especially when phosphine was used [Prawer, 1993]. Hydrogen atoms passivate the donor P atoms by inducing vacancies. In addition, hydrogenated P atoms incorporated at the interstitial sites cannot contribute to electrical conduction.

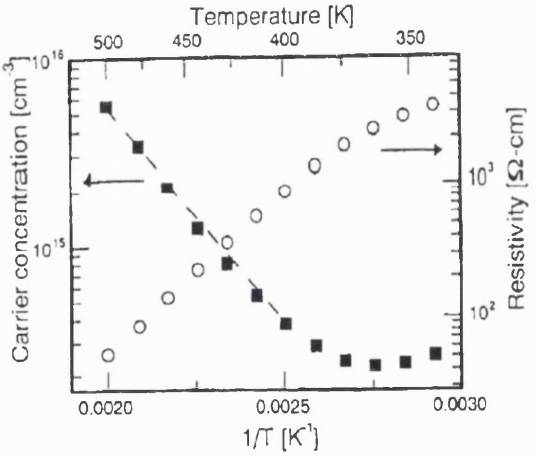

Figure 3.10 (a)

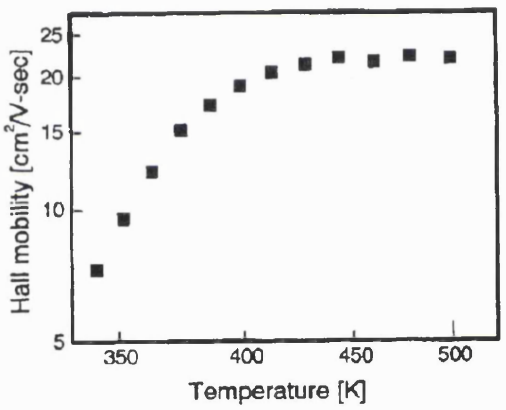

Figure 3.10(b)

Figure 3.10(a) shows the temperature dependence of phosphorus doped n-type films while Figure 3.10(b) shows the Hall mobility at different temperature [Kozumi, 1997]

Recently, sulfur has established itself as a useful n-type dopant on diamond [Gamo, 1999]. The n-type *in-situ* doping was performed by adding H_2S during the growth of homoepitaxial (100) CVD diamond surfaces. Hall measurement confirmed the n-type characteristic with Hall mobilities close to $1000cm^2/Vs$ for active carrier concentration at levels of $10^{16}cm^{-3}$. The activation energy is about 0.3eV measured over a large temperature range. A p-n junction which displays rectification ratio more than 3 orders of magnitude has been fabricated using boron as the p-type dopant.

References :-

Aleksov, A., Vescan, A., Kunze, M., Gluche,P., Ebert, W., Kohn, E., Bergmaier, A. and Dollinger, G. [1999] Diaond & Relat. Mater., **8**,941.

Alexenko, A.E. and Spitsyn, B.V., [1990] "Proc. NATO-advanced Study Institute on Diamond & Diamond like Films and Coatings", Castelveccio Pascoli, page 93.

Austin, I.G. and Wolfe, R. [1956] Proc. Phys. Soc., **69B**, 329.

Baccarani, G., Ricco, B. and Spadini, G., [1978] J. Appl. Phys., **49**, 5565.

Badzian, A. and Badzian, T. [1993] Appl. Ph6ys. Lett., **62**, 3432.

Bergman, L., McClure, M.T., Glass, J.T. and Nemanich, R.J. [1994] J. Appl. Phys., **76**, 3020.

Brophy, J.J., Phys. Rev., [1955] **99**, 1336.

Collins, A.T. and Williams, W.S., [1970] Solid State Phys., **4**, 1789.

Custers, J.F.H., [1952] Physica, **18**, 489.

Davies, G., [1977] "The Optical properties of diamond", Marcel Dekker Inc., New York.

Erz, R., Dotter, W., Jung, K. and Ehrhardt, H., [1995] Diamond & Relat. Mater., **4**, 469.

Field, J.E., [1979] "The Properties of Diamonds", New York : Academic.

Fujimori, N., Imai, T., and Doi, A. [1986] Vacuum, **36**, 99.

Fujimori, N., Nakahata, H. and Imai, T., [1990] Jpn. J. Appl. Phys., **29**, 824.

Fontaine, F., Deneuville, A., Gheeraert, E., Gonon, P., Abello, L. and Lucazeau, G. [1994] Diamond & Relat. Mater., **3**, 623.

Fontaine, F., Uzan-Saguy, C., Philosoph, B. and Kalish, R., [1996] Appl. Phys. Lett., **68**, 2264.

Fox, B.A., Stoner, B.R., Malta, D.M., Ellis, P.J., Glass, R.C. and Sivazlian, F.R., [1994] Diamond & Relat. Mater., **3**, 382.

Fox, B.A., Hartsell, M.L., Malta,D.M., Wynands, H.A., Kao, CT., Plano, L.S., Tessmer, G.J., Henard, R.B., Holmes, J.S., Tessmer, A.J. and Dreifus, D.L., [1995] Diamond & Relat. Mater., **4**, 622.

Gamo, M., Sakaguchi, I., Yasu, E., Ushizawa, K., Haneda, H., Suzuki, T. and Ando, T. [1999] 10th European Conference of Diamond, Diamond like Mater., Carbon Nanotubes, Nitries and Silicon Carbide, Prague, Czech Republic.

Gheeraert, E., Deneuville, A. and Mambou, J., [1990] Diamond & Relat. Mater., **7**, 1509.

Gildenblat, S.Sh., Grot, S.A. and Badzian, A., [1991] Proceedings of the IEEE, **79**,647.

Grot, S.A., Gildenblat, G.Sh., Hatfield, C.W., Wronski, C.R., Badzian, A.R., Badzian, T. and Messier, R., [1990] IEEE Electron Dev. Lett., **11**, 100.

Hayashi, K., Yamanaka, S., Watanabe, H., Sekiguchi, T., Okushi, H. and Kajimura, K. [1997] J. Appl. Phys., **81**, 744.

Haubner, R., Bohr, S. and Lux, B [1999] Diamond & Relat. Mater., **8**, 171.

Huang, J.T., Hu, C.S., Hwang, J., Chang, H. and Lee, L.J., [1995] Appl. Phys. Lett., **67**, 2382.

Jiang, X., Klages, C.P., Zachai, R., Hartweg, M. and Fusser, H.J., [1993] Appl. Phys. Lett. **62**, 3438.

Kajihara, S., Antonelli, A. and Bernholc, J., [1989] Proc. Fall MRS Meeting, **62**, 315.

Kawarada, H., Aoki, M. and Ito, M., [1994] Appl. Phys.Lett., **65**, 1563.

Koizumi, S., Kamo, M., Sato, Y., Ozaki, H. and Inuzuka, T. [1997] Appl. Phys. Lett., **71**, 1065.

Lagrange, J.-P., Deneuville, A. and Gheeraert, E., [1998] Diamond & Relat. Mater., **7**, 1390.

Landstrass, M.I. and Ravi, K.V., [1989] Appl. Phys. Lett., **55**, 1391.

Lightowlers, E.C. and Collins, A.T., [1976] J. Phys. D: Appl. Phys., **9**, 951.

Maki, T., Shikama, S., Komori, M., Sakagushi, Y., Sakuta, K. and Kobayashi, T., [1992] Jpn. J. Appl. Phys., **31**, 1446.

Malta, D.M., von Windheim, J.A. and Fox, B.A., [1993] Appl. Phys. Lett., **62**, 2926.

Malta, D.M., van Windheim, J.A., Wynands, H.A. and Fox, B.A., [1995] J. Appl. Phys., **77**, 1536.

Masood, A., Aslam, M., Tamor, M.A. and Potter, T.J., [1992] Appl. Phys. Lett., **61**, 1832.

Mort, J., Okumura, K. and Machonkin, M.A., [1991] Phil. Mag. B, **63**, 1031.

Nishimori, T., Nakano, K., Sakamoto, H., Takakuwa, Y. and Kono, S. [1997] Appl. Phys. Lett., **71**, 945.

Nishimura, K., Das, K. and Glass, J.T., [1991 (a)] Appl. Phys. Lett., **69**, 3142.

Nishimura, K., Das, K. and Glass, J.T., [1991 (b)] J. Appl. Phys., **69**, 3142

Okano, K., Naruku, H., Akiba, Y., Kurosu, T., Iida, M. and Hirose, Y., [1989] Jpn. J. Appl. Phys., **27**, 173.

Okano, K., Kiyota, H., Iwasaki, T., Nakamura, Y., Akiba, Y., Kurosu,T., Iida, M. and Nakamura, T., [1990] Appl. Phys. A, **51**, 344.

Prawer, S., Uzan-Saguy, C., Braunstein, G. and Kalish, R. [1993] Appl. Phys. Lett., **63**, 2502.

Prins, J.F., [1988] Phy. Rev. B, **38**, 5576.

Prawer, S., Nugent, K.W. and Jamieson, D.N., [1997] Diamond & Relat. Mater., **7**, 106.

Ruan, J., Kobashi, K. and Choyke, W.J., [1992] Appl. Phys. Lett., **60**, 1884.

Shiomi, H., Nishibayashi, Y. and Fujimori, N., [1991] Jpn. J. Appl. Phys., **30**, 1363.

Spitsyn, B.V., Bouilov, L.L. and Derjaguin, B.V., [1981] J. Crystal Growth, **52**, 219.

Stoner, B.R. and Glass, J.T., [1992] Appl. Phys. Lett., **60**, 698.

Stoner, B.R., Kao, C-T., Malta, D.M., Glass, R.G., [1993] Appl. Phys. Lett., **62**, 2347.

Uzan-Saguy, C., Kalish, R., Walker, R. Jamieson, D.N. and Prawer, S., [1998] Diamond & Relat. Mater., **7**, 1429.

Valivov, V.S., Guseva, M.I., Konorova, E.A. and Krasnopevtsev V.V., Sergienko, F. and Tutov, V.V., [1966] Soviet Phys.-Solid St., **8**, 1560.

Valivov, V.S., Gukasyan, M.A., Guseva, M.I., Konorova, E.A., Krasnopevtsev V.V. and Sergienko, F., [1972] Soviet Phys. Dokl., **16**, 856.

Wang, X.H., Ma, G.H.M., Zhu, W., Glass, J.T. and Nemanich, R.J. [1992] Diamond & Relat. Mater.,

Wentorf, R.H. and Bovenkerk, H.P., [1959] J. Chem. Phys., **36**, 1987.

Werner, M., Locher, R., Kolhy, W., Holmes, D.S., Kolse, S. and Fectht, H.J., [1997] Diamond & Relat. Mater., **7**, 308.

Williams, A.W.S. and Collins, A.T. [1971] J. Phys. C, **4**, 1789.

Wolter, S.D., Stoner, B.R., Glass, J.T., Ellis, P.J., Buhaenko, D.S., Jenkins, C.E. and Southwath, P., [1993] Appl. Phys. Lett., **62**, 1215.

Zeisse, C.R., Hewett, C.A., Nguyen, R., Zeidler, J.R. and Wilson, R.G., [1991] IEEE Electron Dev. Lett., **12**, 602.

Chapter 4

Electronic Devices on Diamond

Contents

Section 4.1 Introduction

The device applications for most moderate bandgap semiconductors (Si and Ge) are severely limited at high temperature. At a junction temperature of 300°C, silicon for example suffers from high intrinsic carrier concentration (n_i). As a result, the conductivity is no longer governed by the dopant. Degradation of device structure and material leading to device failure can also be caused by diffusion of dopants and metallisation contacts into the bulk during high temperature operation. The low diffusion coefficient of impurities in diamond, the wide bandgap 5.45eV (giving a low intrinsic carrier concentration at room temperature) and the low chemical

reactivity of diamond makes it one of the most promising wide bandgap material for these specific applications. This next section will explore the potential of electronic devices fabricated from diamond films based on the prediction by the figure of merits. More importantly, in the next few sections, the true performance of these devices will be revealed.

Section 4.2 Figure of Merits

In order to assess the potential of diamond compared with other semiconducting material for certain types of electronic application, the figures of merit is required. The Johnson figure of merit (JFM) allows comparison in terms of usefulness in power microwave applications [Johnson, 1963]. It is actually a product of maximum voltage and cut-off frequency and is given as

$$JFM = \frac{E_c v_s}{2\pi}$$

where v_s is the Saturated Electron Velocity (cm/s)
E_c is the Breakdown Field (V/cm)

The high saturated electron velocity of diamond (v_s= 2.8 x 10^7 cm/s) at room temperature [Ferry, 1975] combined with breakdown field (E_c = 10^7 V/cm) [Bogdanov, 1982] results in JFM of 90 times higher than silicon and in fact the highest among existing semiconductors [Davis, 1988; Yoder, 1987].

As for potential application in the field of digital integrated circuits, The Keyes figure of merits (KFM) is often used and is given as [Keyes, 1975]

$$KFM = \lambda \sqrt{\frac{c v_s}{2\pi\varepsilon_I}}$$

where λ is the Thermal Conductivity (W/Kcm)
ε_I dielectric permittivity (F/cm)

Again the high saturation velocity, the low dielectric permittivity of diamond (ε_I= 5.5) and high thermal conductivity (λ up to 20W/cmK) for natural type IIa crystal [Burgeneister, 1978] and up to 10W/cmK for CVD grown diamond film [Morelli, 1988] makes it superior to other existing materials [Davis, 1988; Yoder, 1987].

A figure of merit proposed by Shenai *et al.* [1987] and later corrected by Collins [1992] is based on the parameter σ_A which can be interpreted as the on state drift region conductance per unit area of an abrupt one sided p-n junction. σ_A is given as

$$\sigma_A = \frac{q \mu n_c}{W_m}$$

where	μ is the mobility of carriers	(cm^2/Vs)
	n_c is the active carrier concentration	(cm^{-3})
	W_m is the depletion layer depth at breakdown	(V/cm)

The breakdown field E_m is related to N_B (doping concentration) through

$$N_B = \frac{\varepsilon_I E_m^{\ 2}}{2 q V_B}$$

where	V_B is the breakdown voltage	(V)
	E_m is the breakdown field	(V/cm)
	N_B is doping concentration	(cm^{-3})

The breakdown voltage is fixed (V_B) so that equitable comparison can be made. For the calculation of σ_A, $n_c = N_B$ for Si and GaAs at or above room temperature, however as boron is a relatively deep acceptor in diamond, with E_A = 0.37eV above the valence band, diamond is actually operating at the freeze out regime at room temperature. If the hole mobility of high quality natural diamond is used in the calculations corrected by Collins [1992], the potential of diamond surpasses Si at about 1000 / 2.8 and GaAs 1000 / 2.2 K. Comparing with other wide bandgap semiconductor such as SiC, it is significant that diamond has higher carrier mobilities than SiC and other wide bandgap semiconductors at both room temperature and elevated temperature [Davis,1988; Reggiani, 1981; Fox, 1995]. One of the current objectives for the development of diamond based high temperature electronics is to increase the current driving capability.

It should be noted that JFM and KFM alone do not really reflect the true potential of a material for electronic purposes. The effectiveness of the dopants and the mobility of carriers are two of the very essential parameter not being taken into account. Other important issues related to the quality of the material in terms of defects, sub bandgap states and traps need to be considered. Reproducibility, flexibility, consistency, maturity of thin film diamond technology and cost effectiveness are other essential factors which interests the commercial industry.

Section 4.3 Metal Semiconductor Contacts on diamond

The technology and properties of metal semiconductor contacts are some of the most fundamental and important criteria for any semiconductor to be considered for device applications. This is the only means where current can be driven in and out of a device in a controllable manner or the simplest way of providing electrical connection to a material to extract

useful information. Obtaining a high quality metal semiconductor interface is the most frequently encountered problem in the development of a new material. The properties of these contacts directly contribute to the active device performance. Consequently, many early works in the diamond field have concentrated on improving the performance of this property [Gildenblat, 1991].

When a metal is deposited on a semiconductor, in general, a potential is developed at the interface due to the difference in the work function of the two materials. Sometimes, with the inevitable presence of an oxide layer between the two interfaces and imperfection of the surface terminating species, interface states in the bandgap will occur at or near the surface. These states were responsible for the well known Fermi level pinning, a model proposed by Bardeen and observed in most practical metal semiconductor interfaces. This model explained the reason behind the non dependency of Schottky barrier height on the work function of the metal. The barrier height at the interface is not dependent on the difference between the work function of the metal and semiconductor [Bardeen, 1947].

Section 4.4 Metal Semiconductor Ohmic Contacts

When a potential difference is applied across a material or a device, the potential drop across the ohmic contact must be negligible. This allows the domination of electrical characteristic either by the actual device itself or the material. It is difficult to fabricate a good ohmic contact on diamond due to its inertness and wide bandgap nature. An early popular method was carried out by intentionally damaging the surface of the diamond thus creating a graphitic layer followed by the deposition of metallisation contacts. Mechanical roughening of the surface creating minute cracks and corners leading to a high electronic field at these sharp cracks has also been reported[Collins, 1970] where colloidal graphite, silver paint and tungsten points have been used as electrical contacts.

Subjecting diamond surfaces to particle bombardment causes a transformation from diamond into a graphitic phase[Hoffman, 1990]. On sputtered damaged surfaces of lightly doped polycrystalline diamond, Tachibana *et al.* [1992(a) and 1992(b)] deposited Au, Al and Ti and reported the formation of ohmic contacts. They confirmed the presence of non diamond carbon phase by conducting Auger electron spectroscopy (AES) of the surface. Geis *et al.* [1989] used an ArF laser of 193nm radiation to modify the surface of diamond, on these damaged surfaces ohmic contacts were formed by various materials including W Probes, Ag paint and evaporated Al. These modified layers contained a mixture of diamond, graphite and unidentified non diamond carbon phases. However, contacts caused by damaged material can be electrically noisy, the damage may be extensive, normally uncontrollable and presence of graphitic phases may caused poor adhesion of metal to the semiconductor.

Later, a more reliable and less damaging method was introduced which involved the use of carbide transition metals namely titanium and molybdenum [Moazed, 1988 and 1989];

[Shiomi, 1989]. A typical example is 10 - 15nm of titanium followed by 150 nm of Au evaporated on diamond surfaces. A subsequent anneal at elevated temperature (>400°C) enhanced the carbide formation at the interfaces and changed the I-V characteristic as shown in figure 4.1(a) and 4.1(b). The Au layer acts as a capped layer, sometimes a Pt diffusion layer is added for high temperature durability, to avoid oxidation of the Ti. Specific contact resistivity as low as 10^{-5} Ωcm^2 was measured on single crystal diamond at a carrier concentration of $10^{16}cm^{-3}$. X-ray photoelectron spectroscopy (XPS) have been used to study the critical carbidisation temperature of Ti films on diamond, the authors reported the formation of $TiC_{0.56}$ at 430°C. Annealing at higher temperature resulted in increased carbidic concentration to Ti [Miller, 1997].

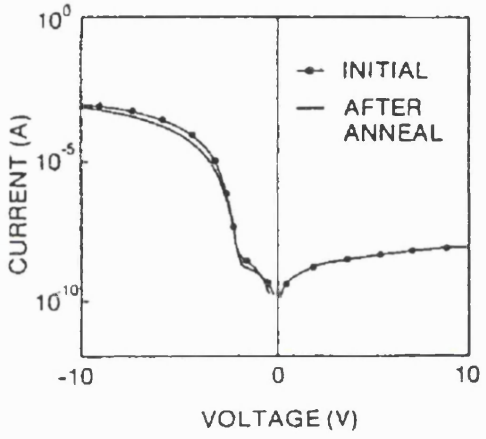

Figure 4.1(a)

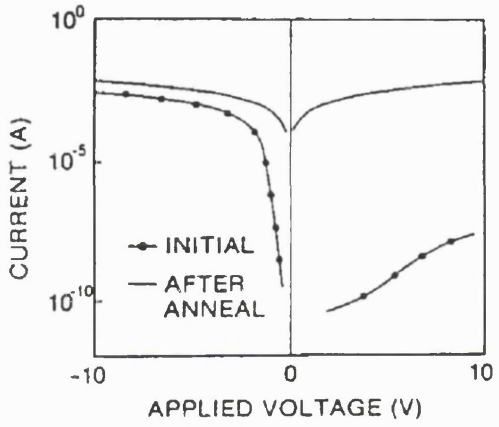

Figure 4.1(b)

Figure 4.1(a) shows no changes in the I-V characteristic of Au contacts after a 430°C and Figure 4.1(b) shows drastic changes in the Ti | Au contact after the same anneal. [Gildenblat, 1991 (b)]

Ion implantation offers the advantage of doping a selected area in a controllable manner and hence is a promising technique to modify the diamond surface especially for the fabrication of ohmic contacts. The impurity concentration and the penetration depth of the ions can be controlled. Prins [1989] demonstrated the first formation of ohmic contacts by heavy surface doping via an implantation step. A boron flux of 3 x $10^{16}cm^{-2}$ at 35keV energy was implanted with the substrate held at 200°C. A following anneal at 1200°C activated the implanted boron. This method was further refined by Venkatesan *et al.* [1992]. They employed a combination of a heavily boron doped region at the surface together with Ti | Au bilayer metallisation scheme. The specific contact resistance in the order of 10^{-6} and 10^{-5} Ωcm^2 was measured on single crystal and undoped polycrystalline diamond using the transfer length method (TLM). Formation of ohmic contacts via ion implantation damaged has also been studied, a vacancy of 1 x 10^{22} vac/cm^3 is required to reach the critical dose of graphitization for diamond [Uzan-Saguy, 1995]. Pang *et al.* [1997] have developed a polycrystalline MISFET by using implanted boron at 90keV and 120keV energy with the Ti | Au as metallisation to define ohmic contacts for the source and drain. MISFET operation at 300°C has been confirmed.

Heavily doped surfaces can also be achieved through *in-situ* doping. The dopant concentration in the deposited diamond films can be reasonably controlled by changing the

dopant gas phase concentration as demonstrated by Gheeraert *et al.* [1989] using gases like B_2H_6. Nishimura *et al.* [1991] reported a specific contact resistance of 10^{-4} Ωcm^2 on diamond films at a carrier concentration of 3 x 10^{20} cm^{-3}. The authors have employed this technique for the formation of source and drain contacts in their FETs. Other metallisation schemes such as Al | Si, Ti | Au and TiWN-Au on *in situ* heavily B-doped polycrystalline diamond films have been compared by Werner *et al.* [1996] using the transfer length method (TLM) method. The authors reported a value of 10^{-7} Ωcm^2 for the Al | Si contacts at a doping level exceeding $10^{20}cm^{-3}$. Current injection mechanism from the ohmic carbide metallisation contacts into the bulk semiconductor at doping level above 3 x 10^{20} cm^{-3} is dominated by the field emission theory (FE). At a concentration below 2.5 x 10^{18} cm^{-3}, it is dominated by thermionic field emission (TFE) [Yokoba, 1997].

Section 4.5 Metal Semiconductor Schottky Contacts

The difficulty of obtaining a reliable n-type dopant has hindered the development of p-n junction diodes on thin film diamond. As boron has established itself as the only reliable p-type dopant, the development of p-type Schottky contacts is critical to study the feasibility of diamond for electronic applications. Glover *et al.* [1973] obtained a Schottky barrier height (SBH) of 1.7eV ± 1.1eV for Au contacts thermally deposited on the surface of a natural boron doped diamond from the C-V measurement of these diodes conducted at room temperature. Barrier heights within the range of 1.7 to 2.2eV were reported by Mead *et al.* [1976] for Au, Al and Ba contacts on natural semiconducting diamond using current-voltage (I-V), capacitance-voltage (C-V) and internal photoemission spectroscopy (IPS) method. SBH of 1.3eV for Al and 1.5eV for Au were determined from the IPS measurements on the (111) surface of natural diamond [Himpsel, 1980]. In addition, a value of 1.13eV was measured for Al contacts on PCD.

In general, most of the reported SBH lie between 1.5 to 2.0eV for natural single crystal diamond. The SBH measured on natural diamond surfaces were not dependent on the properties of metallisation contacts. This observation is well known on other semiconductors resulting from the pinning of Fermi level. Contacts deposited on B-doped single crystal diamond are less leaky compared to PCD. In addition, metallisation contacts on (100) diamond surfaces performed better compared to (110) and (111) planes showing critical emphasis on the structural properties of the diamond surfaces. Gildenblat *et al.* [1990] suggested that the leakage current in these diodes were dependent on the area of the Schottky contact. Normally, the (100) surfaces are smoother and contain less structural defect density than on other planes such as (111), (110) and is far less than polycrystalline diamond.

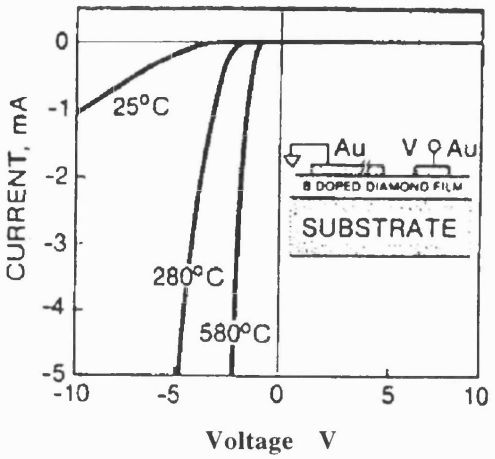

Figure 4.2(a)

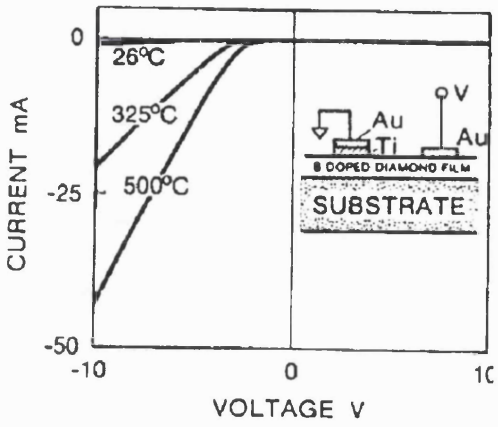

Figure 4.2(b)

Figure 4.2(a) shows I-V characteristics of Schottky diodes of Au at high temperature and Figure 4.2(b) shows the I-V characteristics of diodes using Ti | Au as ohmic contacts with Au as Schottky [Gildenblat, 1990]

Shiomi *et al.* [1989] demonstrated a Schottky diode with a rectification ratio more than 10^3 and a breakdown voltage exceeding 100V at room temperature. However, the device characteristic degraded above 300°C. A Au Schottky diode operating at 580°C from B doped homoepitaxial grown diamond was reported [Gildenblat, 1990]. Improvement in Schottky characteristic results from a cleaning treatment on the diamond surfaces prior to metallisation in a hot mixture of $CrO_3 + H_2SO_4$ at 170°C. Thermally deposited Ni contacts under ultra high vacuum (UHV) on (100) surface of natural diamond displayed rectification up to 400°C with an ideality factor of 2.4.

Miyata *et al.* [1991] reported point Schottky contacts which displayed the dependence of SBH on the work function of metals and hence suggesting the absence of Fermi level pinning. The diamond surfaces which they studied could be hydrogen terminated. Mori *et al.* [1991] obtained similar results using point Schottky contact. This author stressed the importance of surface terminating species on the electrical characteristics of metallisation contacts. The SBH on hydrogen terminated surfaces showed dependency on the electronegativity of metals. On contrary, no dependency was observed on oxidised surfaces. The importance of surface preparation of diamond for contacts deposition was demonstrated. However, thermally deposited contacts rarely exhibit dependence on the work function or electronegativity [Tachibana, 1993].

Homoepitaxial Au Schottky diode with ideality factor < 1.2, rectification ratio more than six orders of magnitude and breakdown (V_B) at 195V was reported by Ebert *et al.* [1998]. Leakage current less than 10^{-7} Acm^{-2} and barrier height in the range of 1.6 - 1.8eV were measured. The device characteristics were shown in figure 4.3(b). These Schottky diodes were capable of operating up to 573K, however with an increase in leakage current shown in figure 4.3(a). The dramatic improvement originated from a novel pulse boron doping technique carried out by immersing boron rod in a plasma in an ASTeX-PECVD system.

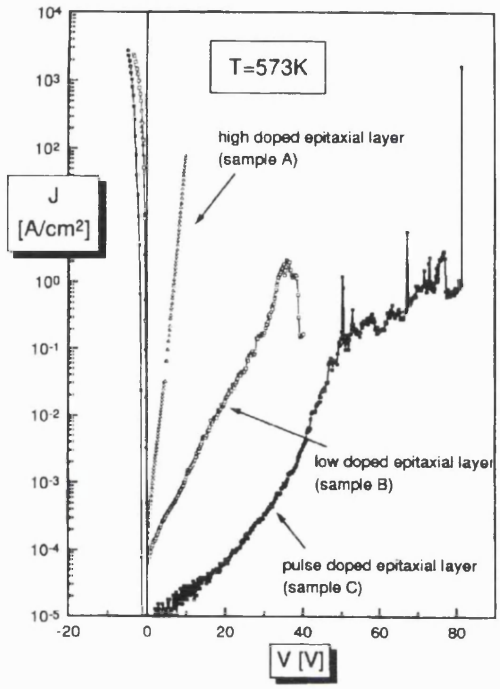

Figure 4.3(a)

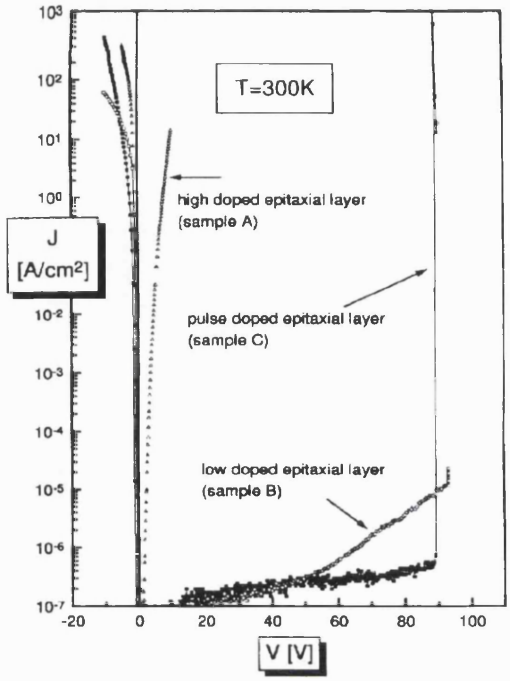

Figure 4.3(b)

Figure 4.3(a) and 4.3(b) shows rectification characteristics of Schottky diodes at 573K and 300K [Ebert, 1998]

Later, Vescan *et al.* [1998] fabricated a Schottky diode operating at 800°C. The outstanding performance at high temperature was achieved through utilisation of a Si-based contact with Au as a cap-layer for the Schottky contact. A diffusion barrier of Si : W doped with nitrogen was used. The Richardson plot of the diode revealed a barrier height of 1.9eV with a maximum breakdown field of 3 x 10^6V/cm at room temperature.

Section 4.6 Metal Intrinsic Semiconductor Structure

Most of the early Schottky devices suffered from large leakage currents. Many believed this was caused by inherit material defects, non diamond phases on the substrate surface, inefficiency of boron doping and high concentration of electric fields at the defective sites. Although high temperature, high rectification ratio and large breakdown capability have been demonstrated on natural and homoepitaxial diamond film, unfortunately, most Schottky contact on PCD remained poor and unreliable. Randomly oriented PCD films contain high defect densities and sharp peaks which led to high and uncontrollable leakage current. Inconsistency and unreproducible experimental results were a major problem on this form of material. Uniformity across the wafer cannot be demonstrated on randomly aligned grains.

In order to improve the device performance on PCD, a new approach was developed by Miyata *et al.* [1992 and 1993]. An incorporation of a thin insulating intrinsic diamond layer between the metal and doped diamond improved the rectification characteristic of the Schottky

diodes. In addition, the author correlated the reduction in leakage current with increased thickness of this intrinsic diamond layer as shown in figure 4.4(b). A thin SiO_2 layer about 2 nm thick replacing the intrinsic diamond layer also improved device performance by reducing the reverse leakage current of the Schottky contact [Venkatesan, 1992] as shown in figure 4.4(a). However, degradation of the I-V characteristics was observed at high temperature. The roughness of polycrystalline surfaces prevents uniform deposition of SiO_2. An introduction of a thin insulating layer inevitably increases the series resistance of the diode resulting in a smaller forward current. A Schottky diode with a very high breakdown voltage was realised in this manner on homoepitaxial CVD diamond [Shiomi, 1990].

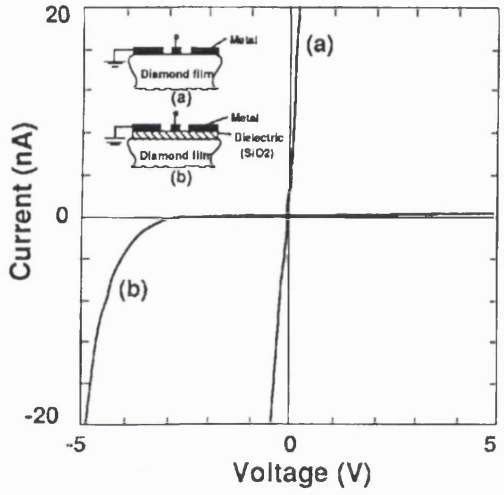

Figure 4.4(a)

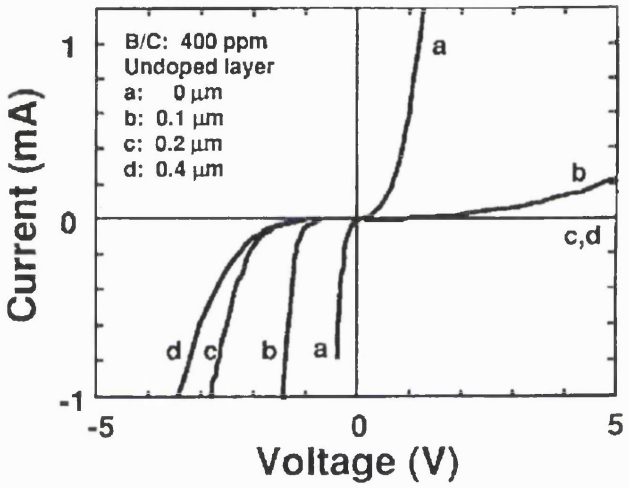

Figure 4.4(b)

Figure 4.4(a) shows rectification performance of MIS (SiO_2) structure [Venkatesan, 1992] and Figure 4.4(b) shows improvement of MIS rectificationwith increasing thickness of undoped layer [Miyata, 1993]

Section 4.7 Diamond Active Electronic Devices

The first diamond active electronic device successfully fabricated was a npn bipolar junction transistor [Prins, 1982]. The n-type region was created by bombarding C+ ions on to natural p-type diamond in 2 regions separated by a p-type boron doped region which acts as a base. Implantation damage resulted in an n-type conduction (caused by electron conduction through shallow donor states). Modulation and saturation of emitter collector current were observed, although the base current is in the same order of magnitude. Similar devices were also reported by Tzeng *et al.* [1987] where the n-type for the base was created by arsenic implantation in a natural p-type diamond. Geis *et al.* [1987] reported the first power gain point contact bipolar transistors operational at 510°C. B-doping was performed during HPHT growth, thermally deposited tungsten formed the base contact while point tungsten contacts were used as the collector and emitter. The n-type conductivity in these devices were most probably caused by shallow donor states near the conduction band. At present, the reproducibility and consistency of n-type doping is still under thorough investigation.

Shiomi *et al.* [1989] and Gildenblat *et al.* [1989] fabricated the first diamond Al gate MESFET on boron doped homoepitaxial film grown by CVD technique with B_2H_6 as the dopant during growth. These MESFETs displayed poor characteristic and suffered from large leakage current through the gate. To circumvent this problem, Shiomi *et al.* [1990] introduced an insulating layer (intrinsic diamond) between the doped diamond and the gate metallisation contact called the Metal I Intrinsic I Semiconductor structure or the MIS structure. A homoepitaxial CVD diamond MOSFET with a 100nm of sputtered SiO_2 as the gate dielectric was fabricated [Gildenblat, 1991]. The gate leakage current was reduced to only 10pA and the device is capable of operating at 300°C.

Tsai *et al.* [1991] developed a diamond MESFET with a transconductance of 0.7 μS/mm from bulk type IIa natural diamond. Solid state diffusion of boron into the diamond was performed by a rapid anneal at 1400°C for 30s with a boron nitride source sandwich on the surface on the diamond giving a 50nm thick channel. Annealed Ti I Au was used to define the drain and source contacts while the gate was formed by unannealed Ti I Au. A pulse doped channel MESFET with a self aligned recessed structure fabricated with assistance of reactive ion etching process was demonstrated by [Shiomi, 1994] .

The first diamond transistor which displayed saturation of drain current and full pinch off was a type IIa natural diamond MOSFET with a B-implanted channel shown in figure 4.5(a) [Zeisse, 1991]. SiO_2 was used as the dielectric layer for the gate and device exhibited a transconductance of 69 μS/mm at room temperature.

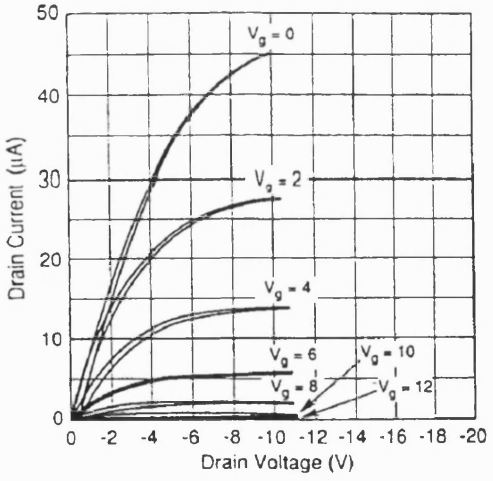

Figure 4.5(a)

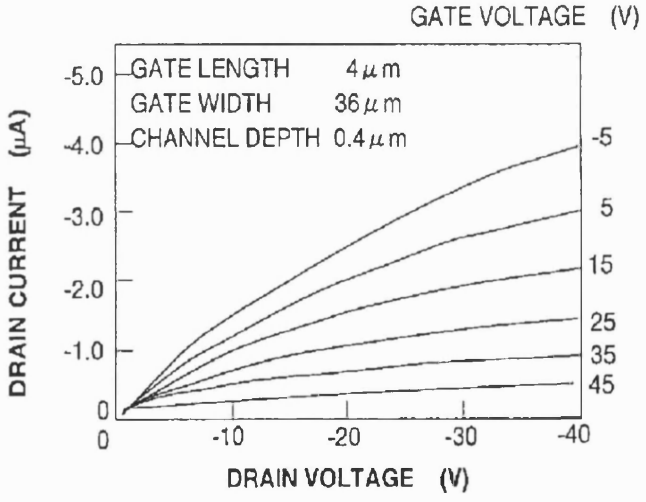

Figure 4.5(b)

Figure 4.5(a) shows current pinch off and saturation of B-implanted channel natural diamond MOSFET [Zeisse, 1991] and Figure 4.5(b) shows current pinch off and saturation of homoepitaxial recessed gate MESFET [Shiomi, 1994]

Nishimura *et al.* [1991] reported the first PCD MISFET using a 0.4μm thick intrinsic diamond as the dielectric material for the gate. The CVD diamond was grown on Si_3N_4 with 2μm

undoped buffer layer and 1μm B_2H_6 doped active channel. A transconductance of 5μS/mm was measured. Tessmner *et al.* [1992] fabricated a MOSFET on polished PCD surface with a channel defined by ion implantation of boron. A carrier concentration of 5 x $10^{18}cm^{-3}$ with a Hall mobility of 0.2 cm^2/Vs was measured on the active layer. A 75nm thick layer of SiO_2 was deposited and a transconductance of 121 μS/mm was recorded. Improved PCD MISFETs operating at 285°C were realised by the same group [Tessemer,1993] on unpolished surfaces with a 0.5 μm boron doped channel buffered by a 15μm thick intrinsic diamond. The peak transconductance at 285°C was 330 nS/mm shown in Figure 4.6(a). Pang *et al.* [1997] reported a MISFET operating at 300°C with a higher transconductance of 174 μs/mm. Doping was carried out by boron implantation.

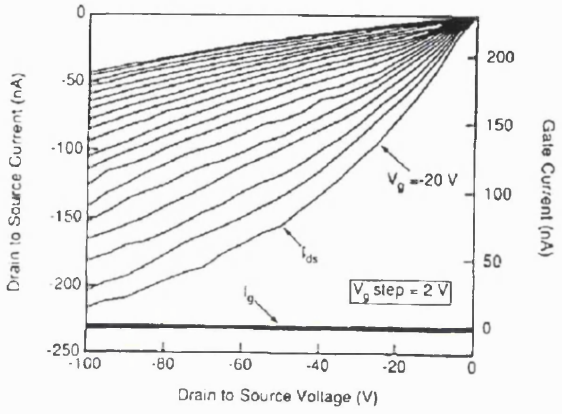

Figure 4.6(a)

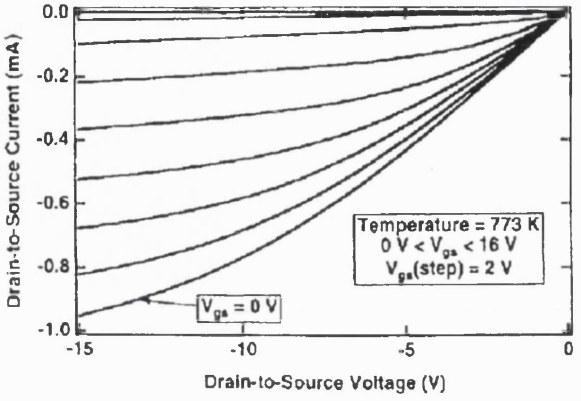

Figure 4.6(b)

Figure 4.6(a) shows improved performance of [Tessemer, 1992] MOSFET on polycrystalline diamond film at 285°C and Figure 4.6(b) shows homoepitaxial MOSFET fabricated by [Fox, 1995] operating at 773K with a transconductance of 1.3 mS/mm

An improved MPECVD deposition of homoepitaxial diamond films on a NIRIM type deposition system enabled the development of a homoepitaxial MOSFET operating at 773K with total drain current pinch off and fully saturation shown in Figure 4.6(b) [Fox, 1995]. The normalised transconductance was 1.3 mS/mm at 773K. Significant improvement was obtained through the use of higher quality film and more effective doping technique. Hence, a Hall mobility exceedinng 1000 cm^2/Vs was recorded for carrier concentration at 2 x 10^{18} cm^{-3}. Digital logic circuits were fabricated by combining two diamond FET's into NAND and NOR circuits. Synchronous TTL signals were used as inputs for the gates. Figure 4.7(a) shows the effective operation at 673K. The performance of the logic circuits are displayed in figure 4.7(b).

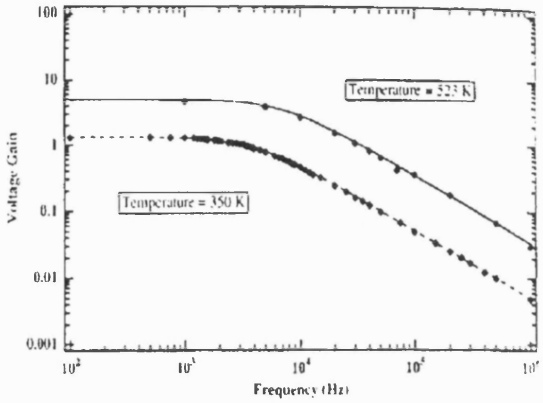

Figure 4.7(a)

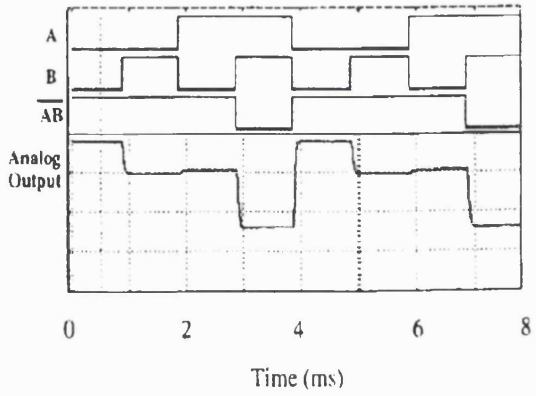

Figure 4.7(b)

Figure 4.7(a) shows relationship between voltage gain and frequency of homoepitaxial MOSFET [Fox, 1995] and Figure 4.7(b) shows output characteristic of a NOR gate fabricated using two of similar MOSFET.

Section 4.8 Surface Conducting Hydrogen Doped Devices

Most devices on diamond reviewed earlier were fabricated with p-type boron doped channels. The majority of these active devices were 'on-state' devices and high temperature performance displayed higher conductance than room temperature as more acceptors would be ionised. The activation energy can be reduced as discussed in Chapter 3 by the formation of an impurity band through heavily doping. However, excessive boron concentration during growth degrades the electronic properties of diamond film leading to lower carrier mobility resulting from ionised impurity scattering and higher leakage current in the Schottky characteristics. In this case the use of pulse doping will be useful. This makes diamond competitive only for high temperature applications.

Recently, a fully ionised p-type conductive layer was discovered on the surface of diamond grown by CVD process [Hayashi, 1996]. This conductive layer is related to the hydrogen layer which is present on the surface of as deposited CVD diamond films. A number of workers have fabricated high performance Schottky diodes using these layers which are present on as grown homoepitaxial films [Kawarada, 1994; Kiyota, 1996]. These diodes were high quality exhibiting an ideality factor close to 1.1, the nearest to unity ever reported on diamond. The Schottky barrier height of the point contact determined from the Richardson plot showed dependency on the electronegativity of its metallisation.

Utilising this conductive layer, Kawarada *et al.* [1994] fabricated enhancement mode MESFETs, the first normally off device on homoepitaxial CVD diamond, using Al as the gate and Au for both the source and drain. During that period, these devices displayed the highest room temperature transconductance reported on diamond at 25μS/mm. Later, with a better device design, reduced device dimension and smaller gate structure an improvement of device performance was reported [Hokazono, 1997; Gluche, 1997]. In addition, Hokazono *et al.*

[1997] reported the development of depletion mode and enhancement mode MESFET (transconductance of 7mS/mm) depending on the gate metallisation contact. Copper being a less electronegative element than Al displayed a depletion mode operation if used as the gate. Switching operations of logic circuits at 100kHz have also been confirmed. Gluche *et al.* [1997] showed that these devices can handle power levels of 6W/mm with a breakdown potential up to 200V.

Section 4.9 Variation of Electrical Properties in Diamond Films

McKeag *et al.* [1997] reported improvement of photoconductivity properties after employing a surface cleaning process followed by a series of gas treatments on PCD films. A latter work by the author demonstrated that repeated gas treatments improved the transient response at the expense of gain in photodetectors fabricated on free standing PCD [McKeag, 1998]. The surface terminating species have significant influence on the electrical properties of point and thermally deposited contacts on CVD diamond [Mori, 1991; Kawarada, 1994]. I-V characteristic revealed significant change in Schottky barrier height which correlates with the electronegativity of the metallisation contacts. Tachibana *et al.* [1993] did not observe the dependence of Schottky barrier height (measured by UPS) on electronegativity of different metal contacts deposited on hydrogen terminated surface in UHV. Van der Weide *et al.* [1994] reported the increase in Schottky barrier height of nickel contacts on diamond terminated by oxygen or hydrogen by using Ultraviolet photoelectron spectroscopy (UPS) and these findings were supported by Baumann *et al.* [1998] observation for other deposited metals (e.g. Zr, Cu and Co). They concluded that UHV cleaned surfaces exhibit the lowest metal Schotky barrier height.

The transient conductivity of CVD diamond film can be influenced by traps and interface states in the bandgap [Gonon, 1997]. These traps resulted from imperfection of the diamond lattice especially on polycrystalline samples. Traps can be filled by exposing samples to UV radiation. Once trapped, the carriers will take a long time to decay giving rise to persistent photoconductivity. The duration required to empty these traps depend on the relaxation time and the trapping energy levels. Annealing at higher temperature will increase the discharging rate from the traps.

Electrical properties of polycrystalline films were best on the large grain growth side and poorest at the diamond and growth substrate interface [Plano, 1993]. This is important as it relates to the defect density and traps which govern the electrical characteristics of a device as described in the previous paragraph. Devices fabricated on a thin film require a reasonably thick buffer layer for isolation from the substrate side and poor electrical characteristic of smaller grains [Pang, 1997]. This is due to the presence a non diamond layer at the substrate side as indicated by Ando *et al.* [1997] using a confocal Raman spectroscopy method. In addition, Yoneda *et al.* [1998] reported the dependency of carrier mobility and lifetime in PCD films on

the grain size. The authors concluded that a reduction in grain size is responsible for the increase in recombination at the grain boundaries and a reduction in carrier mobility values.

Section 4.10 Conclusion

Electronic devices fabricated on the best single crystal diamond using boron as the dopant did not achieve the performance predicted by the Figures of Merit. Although devices capable of operating at temperature as high as 500°C have been demonstrated, the performance of these devices at room temperature remained poor. The main difficulty encountered by these devices is the large activation energy of boron which lies at 0.37eV above the valence band. At room temperature only a very small number of these atoms are active. However when the operating temperature of these devices are raised, the conductivity of the diamond film increases exponentially, hence it is difficult to optimise the performance of these devices for operation over a range of temperature. The use of delta doping has been shown to reduce the activation energy significantly from 0.37eV to 0.15eV. Transistors and Schottky diodes displaying the best performance have been fabricated using this method. However, not many studies were available in the literature regarding the use of boron delta doped layers on diamond. Improvement and further work in this area is critical to enhance the performance of diamond devices.

Hydrogen related surface conductive channels provide a fully ionised dopant at room temperature. Schottky diodes fabricated on these devices demonstrated the dependency on the electronegativity of the metallisation contacts. MESFETs fabricated using this form of dopant displayed very high performance level with predicted transconductance exceeding SiC MOSFET. However, this form of conduction is unusual and little information is available regarding the properties and the origin of carriers. Research in this area is neccessary to harness its potential and uncover more attractive applications.

The type and quality of material are of the utmost importance for the fabrication of diamond electronic devices. Doping technique, surface preparation, surface termination species, contacts deposition and heat treatments in carefully chosen environments are critical in determining the electrical characteristic of the device fabricated. These explain the wide range of device characteristics obtained on various materials and differently treated samples. With a better understanding of how each of these properties affects the electrical properties of diamond film, significant progress has been achieved with the success in producing devices of higher quality than before, for example :- [McKeag, 1997; Hokazono, 1997; Gluche, 1997; Vescan, 1998; Fox, 1995; Ebert, 1997; Pang, 1997]. To date, devices fabricated on boron doped polycrystalline (heteroepitaxial) material are still way behind those fabricated on homoepitaxial material. This indicates the significance of grain boundary defects and other problems encountered on this material.

References :-

Albin, S and Watkins L. [1990] Appl. Phys. Lett., **56**, 1454.

Ando, T., Nishitani-Gamo, M., Yamamoto, K., Watanabe, K., Dennig, P.A., Sato, Y. and Sekita, M. [1997] Appl. Phys. Lett., **70**, 1530.

Bardeen, J. [1947] Phys. Rev. **71**, 717.

Baumann, P.K., and Nemanich, R.J. [1998] J. Appl. Phys., **83**, 2072.

Bogdanow, A.V., Vikulin, I.M. and Bogdanova, T.V., [1982] Sov. Phys. Semicond., **16**, 720

Burgemeister, E.A. [1978] Physica B, **93**, 165.

Collins, A.T., Lightowlers, E.C. and Williams, A.W.S. [1970] Diamond Res. (Suppl. Industrial Diamond Review), 19-22.

Collins, A.T. [1992] Materials Sceince and Engineering, **B11**, 257.

Davis, R.F., Sitar, Z., Williams, B.E., Kong, H.S., Kim, H.J., Palmour, J.W., Edmond, J.A., Ryu, J., Glassand, J.T. and Carter, Jr. [1988] Materials Science and Engineering, **B1**, 77.

Ebert, W., Vescan, A., Gluche, P., Borst, T. and Kohn, E. [1998] Diamond & Relat. Mater., **6**, 329.

Ferry, D.K., [1975] Phys. Rev. B, **12**, 2361.

Fox, B.A., Hartsell, M.L., Malta, D.M., Wynands, H.A., Kao, C.-T., Plano, l.S., Tessmer, G.J., Henard, R.B., Holmes, J.S., Tessmer, A.J. and Dreifus, D.L. [1995] Diamond & Relat. Mater., **4**, 622.

Geis, M.W., Rothschild, M., Kunz, R.R., Aggarwal, R.L., Wall, K.F., Parker, C.D., McIntosh, K.A., Efrenow, N.N., Zayhowski, J.J., Erlich, D.J. and Butler, J.E. [1989] Appl. Phys. Lett., **55**, 2295.

Geis, M.W., Efremow, N.N. and Rathman, D.D.[1988] J. Vac. Sci. Technol, A, **6**, 1953.

Gi, S.G., Mizumasa, T., Akina, Y., Hirose, Y., Kurosu, T. and Iida, M. [1995] Jpn. J. Appl. Phys., **34**, 5550.

Gildenblat, G.Sh., Grot, S.A., Badzian, A.R. Hatfield, C.W. and Badzian, T. [1990] IEEE Electron Dev. Lett., **11**, 371.

Gildenblat, G.Sh., Grot, S.A., Hatfield, C.W. and Badzian, A.R. [1991 (a)] IEEE Electron Dev. Lett., **12**, 37.

Gildenblat, S.Sh., Grot, S.A. and Badzian, A., [1991 (b)] Proceedings of the IEEE, **79**,647.

Glower, G.H. [1973] Solid State Electron. **16**, 937.

Gluche, P., Aleskov, A., Vescan, A., Ebert, W. and Kohn, E. [1997] IEEE Electron Dev. Lett., **18**, 547.

Gonon, P., Prawer, S., Boiko, Y. and Jamieson, D.N. [1997] Diamond & Relat. Mater., **6**, 860.

Hayashi, H., Yamanaka. S., Okushi, H. and Kajimura, K. [1996] Appl. Phys. Lett., **68**, 376.

Hoffman, A., Paterson, P.J.K. and Prawer, S. [1990] Nucl. Instrum. Methods Phys. Res. B, **52**, 63.

Hokazono, A, Ishikura, T., Nakamura, K., Yamashita, S. and Kawarada, H. [1997] Dia. & Relat. Mater., **6**, 339.

Johnson, E.O. [1963] "Physical limitation of frequency and power parameter of transistors', RCA Rev., **26**, 163.

Keyes, R.W. [1975] Proceeding of the IEEE, **63**, 740.

Kawarada, H., Aoki, M. and Ito, M., [1994] Appl. Phys.Lett., **65**, 1563.

Kiyota, H., Okushi, H., Ando. T., Kamo, M. and Sato, Y. [1996] Diamond & Relat. Mater., **5**, 718.

Kulkarni, A.K., Shrotriya, A., Cheng, P., Rodrigo, H., Bashyam, R. and Keeble, D.J. [1994] Thin Solid Film, **253**, 141.

Lightowlers, E.C. and Collins, A.T., [1976] J. Phys. D: Appl. Phys., **9**, 951.

McKeag, R., Marshall, R.D., Baral, B., Chan, S.S.M. and Jackman, R.B. [1997] Diamond & Relat Mater., **6**, 374.

McKeag, R. and Jackman, R.B. [1998] Diamond & Relat. Mater., **7**, 513.

Mead, C.A. and McGill, T.C. [1976] Phys. Lett., **58A(4)**, 249.

Miller, S., Fischer, R., Plank, H., Roth, J. and Dose, V. [1997] J. Appl. Phys., **82**, 3314.

Miyata, K., Matsui, Y., Kumagai, K., Miyauchi, S., Kobashi, K. and Nakaue, A. [1991] Proc. of 2nd Int. Conference New Diamond Science and Technol. Mterials Research Society, Pittsburg, 981.

Miyata, K., Dreifus, D.L. and Kobashi, K. [1992] Appl. Phys. Lett., **60**, 480.

Moazed, K.L., Nguyen, R. and Zeidler, J.R. [1988] IEEE Electron Dev. Lett., **9**, 350.

Moazed, K.L. and Zeidler, J.R. [1989] Proc. Fall 1989, MRS Meeting, **162**, 347.

Morelli, D.T., Bertz, C.P. and Perry, T.A. [1988] J. Appl. Phys., **64**, 3063.

Mori, Y., Show, Y., Deguchi, M. Yagi, H., Yagyu, H., Eimori, N., Okada, T., Hatta, H., Nishimura, K., Kitabatake, M., Ito, T., Hirao, T., Izumi, T., Sasaki, T. and Hiraki, A. [1993] Jpn. J. Appl. Phys., **32**, 987.

Mori, Y., Kawarada, H. and Hiraki, A. [1991] Appl. Phys. Lett., **58**, 940.

Muto, Y., Sugino, T., Shirafuji, J. and Kobashi, K. [1991] Appl. Phys. Lett., **59**, 843.

Nishimura, K., Kato, R., Miyaushi, S. and Kobashi, K. [1991] Japan New Diamond Forum, The 5th Diamond Symposium, Tsukuba, 34.

Pang, L.Y.S., Chan, S.S.M., Johnston, C., Chalker, P., and Jackman, R.B. [1997] Diamond & Relat., Mater., **6**, 333.

Plano, M.A., Zhao, S., Gardinier, C.F., Landstrass, M.I., Karnia. D.R., Kagan, H., Gan, K.K., Kass, R., Pan, L.S., Han, S., Schnetzer, S. and Stone, R. [1994] Appl. Phys. Lett., **62**, 193.

Prins, J.F., [1982] Appl. Phys. Lett., **41**, 950.

Prins, J.F. [1989] J. Appl. Phys. D., **22**, 1562.

Reggiani, L., Bosi, S., Canali, C. and Nava, F. [1981] Phys. Rev. B, **23(16)**, 3050.

Shenai, K., Scott, R.S. and Baliga, B.J. [1989] IEEE Transaction on Electron Devices, **36(9)**, 1811.

Shiomi, H., Nakahata, H., Imai, T. Nishibayashi, Y. and Fujimori, N. [1989] Jpn. J. Appl. Phys., **28**, 758.

Shiomi, H., Nishibayashi, Y. and Fujimori, N. [1990] Jpn. J. Appl. Phys., **29**, 2163.

Shiomi, H., Nishibayashi, Y., Toda, N., Shikata, S. and Fujimori, N. [1994] 4th International Conference on New Diamond Science and Technology, Kobe, 661.

Tachibana, T. and Glass, J.T. [1992 (a)] J. Appl. Phys., **72**, 5912.

Tachibana, T., Williams, B.E. and Glass, J.T., [1992 (b)] Phys. Rev. **B 45**, 11968.

Tessemer, A.J., Plano, L.S. and Dreifus, D.L [1992] Diamond & Relat. Mater., **1**, 89.

Tessemer, A.J., Plano, L.S. and Dreifus, D.L. [1993] IEEE Electron Dev. Lett., **14**, 66.

Tsai, W., Delfino, M., Hodul, D., Riaziat, M., Ching, L.Y., Reynolds, G. and Cooper C.B. [1991] IEEE Electron Device Lett., **12**, 157.

Tzeng, Y., Lin, T.H., Davidson, J.L. and Pan, L.S. [1987] Proc. 7th Biennial University | Government | Industry Microelectronics Symposium, IEEE, Rochewson, New York.

Uzan-Saguy, C., Cytermann, C., Brener, R., Richter, V., Shaanan, M. and Kalish, R. [1995] Appl. Phys. Lett., **67**, 1994.

van der Weide, J. and Nemanich, R.J. [1994] Physical Review B, **49**, 13629.

Venkatesan, V. and Das, K. [1992] IEEE Electron Dev. Lett., **13**, 126.

Vescan, A., Daumiller, I., Gluche, P., Ebert, W. and Kohn, E. [1997] Diamond & Relat. Mater., **7**, 581.

Werner, M., Job, R., Denisenko, A., Zaitsev, A., Fahrren, W.R., Johnston, C., Chalker, P.R. and Buckley-Golder, I.M. [1996] Diamond & Relat. Mater., **5**, 723.

Yoder, M.N. [1987] Naval Research Review, 27.

Yokoba, M., Koide, Y., Otsuki, A., Oku, T. and Murakami, M. [1997] J. Appl. Phys., **81**, 6815.

Yun, Y., Maki, T. and Kobayashi, T. [1997] J. Appl. Phys., **82**, 3422.

Zeidler, J.R., Hewett, C.A., Nguyen, R., Zeisse, C.R., and Wilson, R.G. [1993] Diamond & Relat., Mater., **2**, 1341.

Zeisse, C.R., Hewett, C.A., Nguyen, R., Zeidler, J.R. and Wilson, R.G. [1991] IEEE Electron Dev, Lett. **12**, 602.

Chapter 5

Experimental & Characterisation Techniques

Contents

Section 5.1 Introduction

This chapter presents a brief discussion on the various techniques that have been utilised throughout this thesis for the fabrication of electronic devices. The fabrication section will be mainly focused on photolithography and resistive deposition of metal contacts. It is essential that the electrical and chemical properties of a material are well understood before devices are actually defined. For this purpose, Hall effect measurements are employed for electrical characterisation, SIMS for detecting impurity elements, UPS and XPS for surface characterisation of the material coupled with SEM and Raman spectroscopy to asses the morphology and quality of the polycrystalline diamond film. Finally, the performance of devices which are successfully fabricated on material whose properties are known will be monitored using various electrical characterisation methods. These will be described at the beginning of each experimental chapter.

Section 5.2 Secondary Ion Mass Spectrometry (SIMS)

Secondary ion mass spectrometry (SIMS) is one of the most important and versatile analytical technique to determine the concentration of atomic species that are present on the surface and in a solid [Benninghoven, 1987; Janseen, 1991]. This technique is very sensitive and allows the detection limits of specific elements in the 10^{14} to 10^{15} cm^{-3} range. It has a typical lateral resolution of about 100μm to as high as 1μm while the depth resolution is about 50 to 100Å.

SIMS was developed by Castaing and Slodzian in the early 60's. Further development by Benninghoven *et al.* [1987] made this method popular for characterisation of impurity concentrations in semiconductors. The operating principle of SIMS is based primarily on the destructive removal of material from the target by sputtering and the analysis of the sputtered components by a mass spectrometer as shown in figure 1. Sputtering is normally carried out by means of an ion beam whose size marks the lateral resolution. Only a fraction of elements knocked out can be analysed by the mass spectrometer as about 99% of these are electrically neutral.

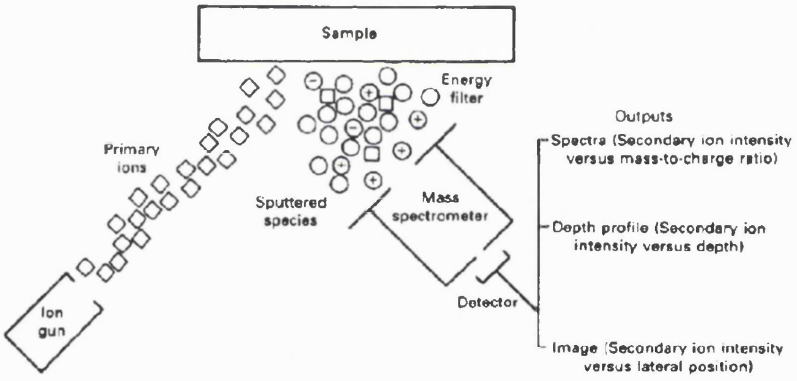

Figure 5.1 The basic principle operation of SIMS, the sputtering of sample by primary ions and the detection of secondary ions by mass spectrometer.

In an ultra high vacuum chamber, primary incident ions accelerated by an electric field to about 10 - 20 keV will be directed at the target. These energetic ions will penetrate the target and lose their energy to the surrounding atoms mainly by momentum transfer. Target atoms set in motion by impinging ions will transfer part of their energy to neighbouring atoms resulting in a collision cascade [Sigmund, 1969]. Sputtering occur when one atom receives enough energy from the collision cascade to overcome the surface binding energy. The sputtering yield (average number of sputtered atoms per incident ion) depends on the target material, energy of incoming projectiles, crystallographic orientation of the target and incidence angle of projectiles. Some of the sputtered atoms are charged (secondary ions). These secondary ions are the only kind of sputtered atoms that can be detected by the mass spectrometer. The secondary ion yield is influenced by the nature of primary ion. Given similar energy levels, more electronegative bombarding ions like oxygen (O_2^+) enhances the secondary ion yield for electropositive elements

(B and Al in Si) which produce positive ions. Similarly, electropositive primary ions (like Cesium Cs^+) enhances the yield for electronegative secondary ions (P, As and Sb in Si). In addition, the secondary ion yield can vary for the same element in different samples or matrix. This is know as the matrix effect. This effect is strongly based on the sample chemical environment [Morgan, 1980].

Ion bombardment will lead to implantation of the incident ions, lattice damage and displacement of target atoms from their original lattice sites [Werner, 1984]. The implantation and reallocation process will result in a broadening of the depth profile of an originally sharp interface [Turner, 1987]. This can be minimised by using low energy incidence ions, increasing incidence angle and using high pass projectiles. However, low energy ion beam will lead to poor primary beam focusing resulting in an error from the uncertainty in determining depth profiling as the crater created will not have steep walls and a flat bottom. The precision of the SIMS profile depends on the physical stability of the target during bombardment by primary ions. A electrically insulating target will charge up, disrupting accurate measurement by the mass spectrometer. It can be overcome by directing an electron beam on the target in a controlled manner (computerised) during sputtering to neutralise the positive charge accumulated from the primary ion beam [Stingeder, 1988].

A low sputtering rate (1 Å/h) will give a surface analysis known as static SIMS. At a higher sputtered rate alongside with a well focused beam (10 μm/h), with one particular mass measured in the mass spectrometer as a function of time, will give a depth profile known as dynamic SIMS. The secondary ion yield measured with time by the mass spectrometer can be converted to concentration versus depth. However, information about the primary ion beam current, the sputtered yield, the ionisation efficiency along with the fraction of neutral atoms to the secondary ion collected is necessary. Some of these parameters are difficult to determine as the secondary ion yield is target material dependent due to the matrix effect. An alternative assessment of elements by the use of ion implanted standards in a similar matrix are used for calibration. This provides an empirical determination of the depth profile rather than theoretical method. Ion implanted standards are capable of introducing an error less than 5%. Typical SIMS standards requirement for accurate empirical determination are

a) lateral target uniformity on a micrometer scale
b) stability of target composition over a period of time

For accurate and reliable determination of depth profile the target must satisfy the following conditions

a) Target must be smaller than 1 - 2 cm^2.
b) Sample composition must be homogeneous.
c) A flat bottom crater is required to ensure all detectable secondary ions arise from the same depth, target surface needs to be reasonably smooth.

Interface roughness and bombardment induced roughness will lead to depth profile distortion [Stevie, 1988].

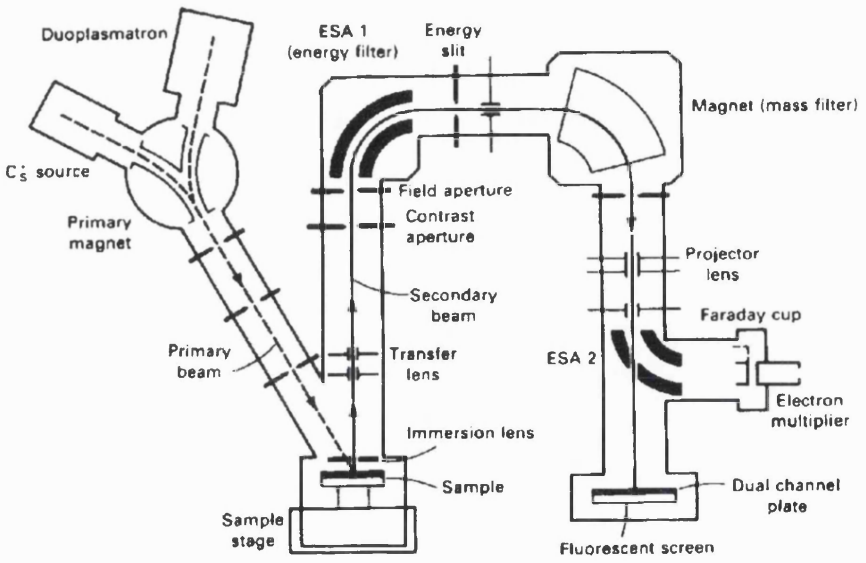

Figure 5.2 A more detail example of the SIMS setup including the isolation of the useful secondary ions by magnetic field and acceleration of primary ions to the sample.

Section 5.3 Raman Spectroscopy

Raman spectroscopy is a non destructive vibrational technique that can be employed to detect both organic and inorganic species [Exarhos, 1989; Gerrard, 1986]. Besides this, it is capable of performing molecular characterisation by directly probing the chemical bonds within the film and at the film substrate interface. To promote vibration in a solid which emits secondary emission measurable in the visible spectrum, this technique uses laser light scattering. Minimum sample preparation and a line of sight between the sample and analyser is the key advantage. Unlike SIMS and SEM, it avoids the problem associated with target charging and the use of high vacuum environment is not required.

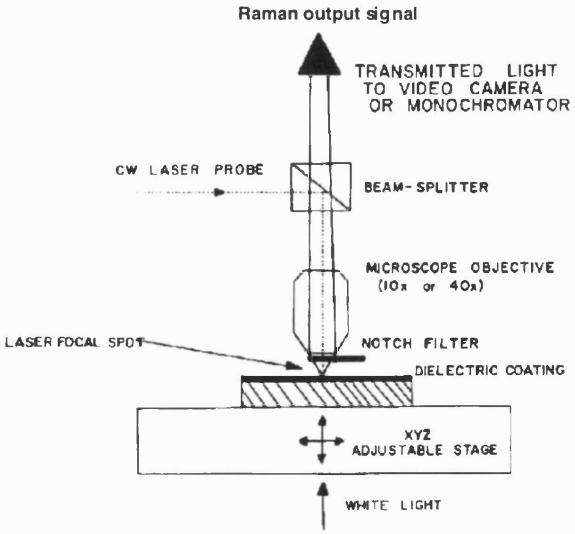

Figure 5.3 The basic Raman set up for measurement. The Notch filter is used to filter out the intense Rayleigh scattering. The measurement of Raman radiation is made perpendicular to the incident laser to increase the signal to noise ratio.

This method is named after the founder, Raman [1928]. When an intense monochromatic light source like a laser is incident on the target, interaction between incident electromagnetic laser radiation and the electrons in the target will induce a dipole moment. The frequency of the dipole moment will vary with the incident electromagnetic radiation frequency generating elastic Rayleigh scattering. More importantly, inelastic scattering will also be induced if the energy from the dipole moment can be coupled to a vibration excitation known as phonon in the solid. When the incident photon transfers part of its energy to the phonon the photon which emerges will have a lower energy. This results in a longer wavelength emission and is known as Stokes shifted scattering. However, if a photon interacts with a phonon in such a way that the part of the energy from the phonon is absorbed by the photon, then the emission of photons will be of a higher energy resulting in shorter wavelength emission. This condition is known as Anti Stokes shifted scattering. The difference between the incidence laser frequency and the scattered photon frequency is known as the Raman Shift. Normally the Stokes component has a higher intensity compared to the Anti-Stokes and therefore measurement is normally made based on Stokes scattering [Pankove, 1975]. In a complex molecule, the number of vibration modes and the mode frequency can be used as a finger print for identification of atoms or groups of atoms in different localised environment. The component that comes from the Rayleigh scattering is much more intense than the Raman scattering and this component needs to be removed by a sharp filter for the detection of the Stokes scattering component. The laser power is normally less than 5mW to reduce damage or heating of the sample [Raptis, 1983]. The basic set up for a Raman system is display in figure 5.3.

Laser Raman spectroscopy has been used extensively to qualitatively characterise diamond films grown by the CVD technique [Hayward, 1995]. The Raman spectrum of a perfect single crystal diamond contains a sharp peak at 1333cm^{-1} due to single phonon scattering. This peak is unambiguous evidence for the presence of diamond in a deposited film. The presence of other non diamond forms of carbon also give Raman excitations around this region. Non diamond carbon produces a broad band spectrum and this is normally superimposed on the sharp diamond peak. The sensitivity of the graphitic phase measured by the Raman cross section is about 50 times relative to diamond [Wada, 1981] while amorphous carbon is about 233 times [Sails, 1996]. In addition, the wavelength of the laser used for excitation affects the intensity and peak position of the non diamond carbon [Wagner, 1992; Yoshikawa, 1989]. These variations are believed to be caused by an increased laser absorption by the non diamond carbon at shorter wavelengths [Wagner, 1989] or a resonance effect [Fayette, 1994]. Leeds *et al.* [1998] conducted a systematic study of the quality of diamond CVD films grown by increasing methane concentration using 4 different laser wavelengths using 780nm (Infrared), 633nm (Red), 514nm (Green) and 244 nm (UV), the author reported the enhancement of the diamond peak at shorter wavelengths (514nm and 244nm). Little information about the non diamond carbon species can be gathered using this frequency. However, on a similar film for longer wavelength light (633nm and 780nm), the non diamond carbon band is significantly enhanced. These effects are illustrated in figure 5.4 for diamond films grown using different methane concentration with the lowest being label A and the highest label E.

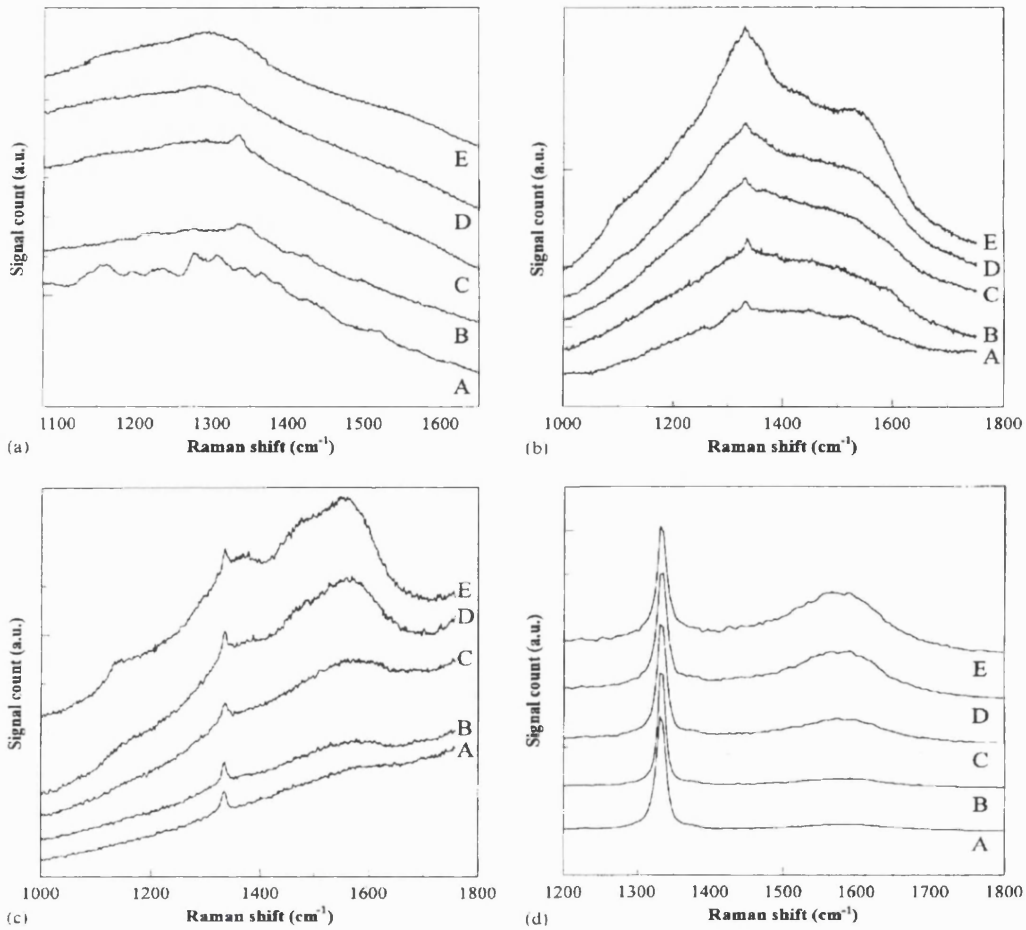

Figure 5.4 Raman Spectra of different diamond samples A - E (increasing non diamond carbon content). (a) Spectra taken at IR 780nm (b) Spectra taken at red light 633nm (c) Spectra taken at Green light 514nm (d) Spectra taken at UV 244nm [Leeds, 1998].

Section 5.4 Van der Pauw Hall Effect Measurement

Hall Effect is a powerful electrical-magnetic characterisation technique used to determine the electrical properties of semiconductors and metals. It is capable of determining the carrier transport properties of a piece of semiconductor. In addition, it also provides information about mobility, carrier type, carrier concentration and resistivity. If it is conducted with a variation of temperature it gives information about the scattering mechanism of carriers, activation energy of dopants and factors governing the resistivity of a material. This effect was named after its founder Hall in 1879 when he was investigating the nature of force acting on a conductor carrying a current in a magnetic field where he found a potential difference between both sides of the piece of conductor. The direction given in the following derivation is referenced according to Figure 5.5

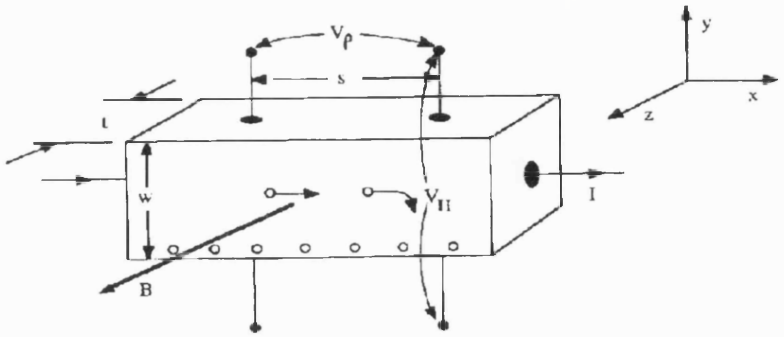

Figure 5.5

If a magnetic field is applied perpendicular to the direction of current flowing in a rectangular bar which is p-type, there will be a force acting on the carriers (holes) and it will be deflected to the bottom. The accumulation of carriers at the bottom of the bar will result in the existence of an electric field. The total force on the carriers will then be given by

$$F_y = q\,(E + v_x \times B_z)$$

where F_y is the force acting on the charge along the y direction
v_x is the drift velocity of the charge in the x direction
B_z is the magnetic field strength (T) in the z direction

An equilibrium will exist where the force caused by the magnetic field acting perpendicular on the carriers will balance with the force due to the electric field acting on the holes hence

$$E = v_x \times B_z \qquad \ldots\ldots(1)$$

The current flowing in the bar can be given as

$$I = q\,w\,t\,p\,v_x \qquad \ldots\ldots(2)$$

where I is the current flowing in the conductor (A)
q is the electronic charge (Q)
w is the thickness of the bar in the y direction (m)
p is the carrier density in the bar (m^{-3})
v_x is the average velocity of the charge (ms^{-1})
t is the width of the bar in the z direction (m)

Combining equation (1) and equation (2) will give

$$E_y = -\frac{B_z I}{q\,w\,t\,p} \qquad \ldots\ldots(3)$$

The electric field along the y direction will give a potential V_H if equation (3) is integrated with respect to y.

$$V_H = -\int_0^w \frac{B\,I}{q\,w\,t\,p}\,dy = \frac{B\,I}{q\,t\,p}$$

where V_H is the Hall voltage in the y direction (V).

However, most semiconductor material used for fabricating devices are in thin film form and the bar technique for determining the carrier concentration and mobility is not suitable. Van der Pauw developed a technique based on conformal mapping to determine the resistivity, carrier concentration and Hall mobility for thin films on arbitrary shaped samples without the need to know the current flow pattern in the sample. However, the following conditions must be met during the sample preparation before the theory is valid :-

a) The contacts must be placed at the circumference of the sample
b) The contact size is sufficiently small compared to the size of the sample
c) The sample must be uniformly thick
d) The sample must be singly connected with no isolated holes
e) The sample must have uniform doping.

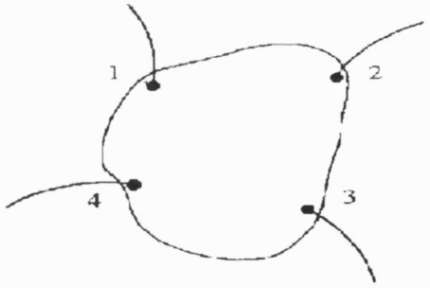

Figure 5.6 shows a typical contacts position for van der Pauw measurement on irregular shape sample

This technique relies on the use of a 4 point probe with 4 contacts placed at the circumference of the sample. The resistivity of the sample can be calculated from

$$\rho = \frac{\pi\,t}{\ln\,(2)}\,\frac{(R_{12,34} + R_{23,41})}{2}\,F$$

$$R_{12,34} = \frac{V_{34}}{I}$$

$$R_{23,41} = \frac{V_{41}}{I}$$

where ρ is the resistivity of the sample.

F is the correction factor for the van der Pauw measurement.

$R_{12,34}$ is the open circuit voltage measured between contact 3 and 4 with current flowing from contact 1 and 2.

$R_{23,41}$ is the open circuit voltage measured between contact 4 and 1 with current flowing from contact 2 and 3.

The measurement of open circuit voltage avoids potential drop across the contact resistance hence giving a more accurate measurement of the actual sample resistivity. The correction factor (F) is the ratio of $R_{12,34}$ and $R_{23,41}$ and can be obtained from a graph. If the thickness of the doped layer is not known then the sheet resistance is normally used instead.

Hall measurements are normally performed by passing a fixed current from a current source through two diagonal contacts with the open circuit Hall voltage measured between the other two contacts. Normally an offset voltage will be present before the magnetic field is applied and this has to be measured and subtracted to give the actual Hall voltage.

Section 5.5 Photolithography

Lithography is the process of defining a desired pattern on a planar surface or a plate. It is one of the most useful processing techniques to produce fine metallisation patterns and high resolution circuit structures on a semiconductor wafer [Diekmann, 1994]. Photolithography employs electromagnetic radiation from a suitable light source as the writing tool along with photosensitive material as an imaging medium and a chemical developer. Photolithography offers the advantage of high resolution capability and batch processing which is compatible for most commercial applications. It allows accurate placement of miniature structures with critical dimension in the micrometers scale and advancement to the nanometer region in the near future.

The electromagnetic radiation used as the writing tool is based on ultra-violet (UV) light. The most popular light source for UV is the xenon filled lamp. Spectral output from the xenon lamp can be modified with an addition of metal additives for example mercury. These lamps offer the advantage of reasonable spectral range with high intensity useful for most media in a cost effective manner. However, it requires a period of several minutes to stabilise the output spectrum while the mercury in the lamp vaporises.

In addition to light sources, an exposure system relies on optical lenses and mirrors to focus and reflect the radiation to the desired path. These must be made to allow sufficient transparency of the radiation from the source to the target. Diffraction of light will lead to loss of

sharp well defined pattern edges. As a rule of thumb these effects will become severe when the wavelength of light is comparable to the featured size.

Optical Materials Constructions

Region	Wavelength (nm)	Optics
Visible	400 - 750	soda lime glass
Near UV	350 - 400	white glass
Mid UV	300 - 350	Pyrex / Quartz
Deep UV	200 - 300	Quartz
Far UV	150 - 200	Calcium Flouride

For high resolution, it is critical to use parallel light rays incident in a perpendicular manner to the imaging medium to provide a steep side walls. Light sources are inherently non parallel rays (unless they are at infinite distance away) and hence a collimated optical system is required. The visible range of the spectrum also needs to be filtered out to avoid diffraction and unwanted exposure causing a poorly defined photoresist pattern.

The typical photosensitive medium used is the photoresist. In general to be considered satisfactory a medium needs to have the following properties:-
a) Absorption of light rays which matches with the spectral output of the light source (Xenon-Mecury lamp)
b) Chemical or physical changes in the exposed area.
c) A subsequent development step to clearly distinguished the exposed region from non exposed region.

The main important attributes of a given medium to provide a good quality image is sensitivity, contrast and resolution. Photoresist allows photo patterning of the substrate surfaces onto which they are applied in intimate contact. They are basically polymers in a liquid solution. There are two types of photoresist. The positive type where upon exposure to UV, the exposed region is weakened and can be dissolved away by the developer. The second kind the the negative type where region which is not exposed will be removed by the developer. Exposure to UV light causes chemical changes to the photoresist. The developing process relies on the differential of solubility of exposed versus no exposed resist. The aim is to remove the weakened resist section consistently and in a reproducible manner at a much faster rate than the other portion. The developing time, the strength of developer and the thickness of the photoresist spun is critical. Over and under development will lead to distortion of the resist pattern. Other important parameters such as the exposure time and bake out to harden the photoresist can also influence the end result.

Photoresist adhesion to the substrate, thickness and uniformity of the layer on the entire surface are the important parameters in selecting a photoresist type for a particular application. A clean surface is necessary for good adhesion. Commercial methods for applying liquid photoresist are spin coating, spray coating, roller coating and others. In the most common method, spin coating, the photoresist is deposited in bulk on the substrate and spun at speed up to 10,000 rev/min. This allows a uniform deposition of a thin coating and is the preferred method for IC fabrication. The spin speed, spin duration, viscosity of photoresist and the substrate surface roughness all have influenced on the uniformity and the thickness of the photoresist deposited.

Section 5.6 Resistive deposition of metal contacts

Metallisation contacts can be deposited via a few techniques namely resistive evaporation, flash evaporation, sputtering and electron evaporation. Resistive evaporation will be reviewed in this section as it is the main method for depositing thin metal film for most of the experimental work in the next few chapters. This process is the oldest means for depositing thin metal films. Evaporation is conducted by passing a current through a high resistance wire, filament or boat. The heat generated by the resistive element is used to melt and vaporise the metal required. The high resistive element is normally made from refractory metals such as tungsten and molydenum which have a very high melting points of 3380°C and 2610°C at atmospheric pressure. It is preferable that the metal sublimes, as this avoids interaction of the metal liquid phase with the filament or heating element. Some metals (such as Titanium) form alloys with tungsten at high temperature and this normally leads to the destruction of the filament during evaporation. A high vacuum ($< 10^{-6}$ mbar) is necessary to minimise contamination, prevents rapid oxidation of the metallic vapour and lower the vaporisation temperature. Aluminium, gold, silver, tin, nickel and chromium can be easily deposited in this manner. The key advantage of vacuum evaporation is the very high deposition rates achievable such that thick metal films (500nm) can be deposited. However, this method requires line of sight from the source to the target, as a result complex and irregular shape samples may not be uniformly coated.

The resistive evaporation system used for depositing thin metals film in this work is an Edwards 306. The base pressure during the evaporation is kept below 10^{-6}mbar. This pressure is achieved by a diffusion pump backed by a rotary pump. Liquid nitrogen cold trap is used in addition to removed unwanted contamination from the diffusion pump and to maintain low pressure during resistive heating itself. Evaporation for Al, Ti and Ni are carried out using a tungsten filament. Cu, Ag and Sn are performed using a molydenum boat while Cr is placed in a tungsten spiral.

Section 5.7 Photoelectron Spectroscopy

Electrons emitted or scattered from a surface can be used to determine the valence electronic properties (UPS), chemical composition (XPS and Auger) and elemental species (XPS) present. Most of these electrons after the various excitation methods escape the surface in the energy range between 5 to 2000eV. Figure 5.7 shows the experimentally determined inelastic scattering mean free path as a function of energy above the Fermi level [Seah & Dench, 1979].

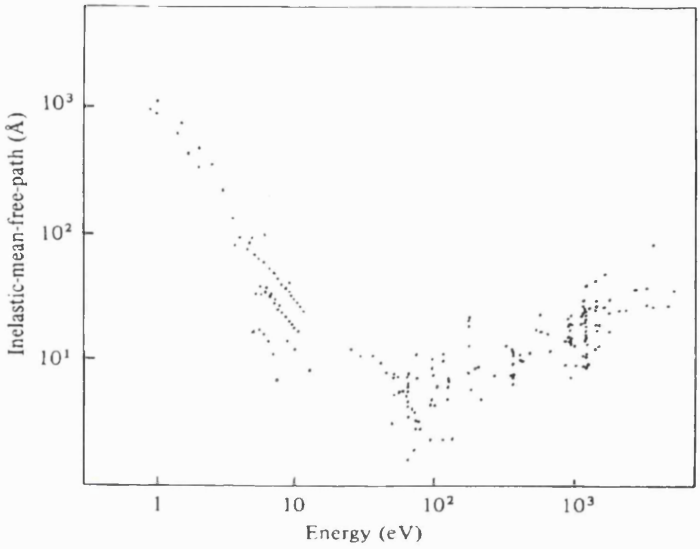

Figure 5.7 shows the spread of experimental determined inelastic mean free path of electrons and their kinetic energy on solids.

From figure 5.7, it can be seen that the mean free path for inelastic scattering of electron is tens of Å and at certain optimum energy (50 - 2000 eV) is typical less than 10 Å. Any technique involving the analysis of electron scattered from the solid in this energy range is highly surface sensitive and samples only a few atomic layers.

Photoelectron spectroscopy is a method based on using photons to generate electrons within the solid some of which then escape into a vacuum for energy analysis. There are 2 types of photoelectron spectroscopy X-ray photoelectron spectroscopy (XPS) and ultra-violet photoelectron spectroscopy (UPS). They are classified according to two different types of photon source.

a) UPS uses low energy photon source ($h\nu$ ~ 10.4 eV) from gas discharge lamps.
b) XPS uses high energy photon source ($h\nu$ ~ 1200 - 1400 eV)

Section 5.8 X-ray photoelectron spectroscopy (XPS)

X-ray photoelectron spectroscopy (XPS) is based on the photoelectric effect proposed by Einstein, however the radiation used for excitation in this case is much more energetic [Briggs, 1983]. It is also known as electron spectroscopy for chemical analysis (ESCA). It was first implemented in the 1950's by Seigbahn *et al.* [1964]. This technique is surface sensitive and allows surface probing from the upper 5 to 50 Å of the sample. Although the penetration depth of X-rays is further than that, this restriction is due to the shallow electron escape depth from the surface. Electrons emitted much deeper are unable to exit the surface due to their short mean free path.

When the X-ray is incident on the surface, electrons which have a binding energy less than that of the incidence photons will be emitted from any orbital. The measured energy of the ejected electrons at the spectrometer (E_{sp}) is related to the binding energy (E_b), and the energy of the primary X-ray (hv) through

$$E_b = hv - E_{sp} - \phi_{s_p}$$

where h is the plank constant.

v is the velocity of light in vacuum.

ϕ_{s_p} is the work function of the spectrometer (normally about 3 to 4 eV)

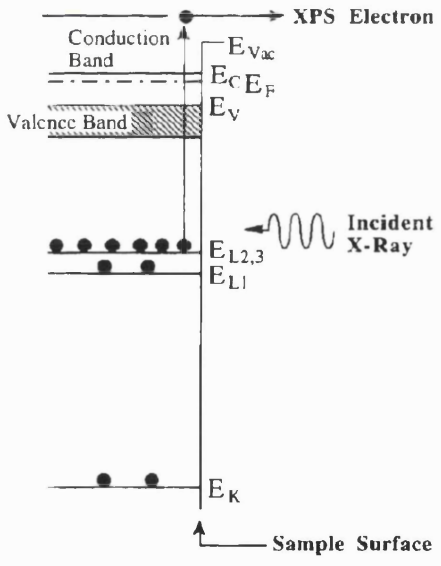

Figure 5.8 shows the ejection of core electrons by incidence X-Ray

The typical energy of the primary x-ray is about 1 to 2 keV and is much stronger compared to less than 50eV from the UPS. These energetic photons are sufficient to eject core levels electron from the sample surface. The binding energy of the core level electrons is influenced by the primary elements and their chemical surroundings. By knowing the primary elements, E_b can be used to determine the states of chemical bonds of the primary elements. This

is especially useful in determining the chemical nature of surfaces. Additionally, this technique is a non destructive method, however it does require an ultra high vacuum for the detection of emitted photoelectrons. The spectral shift recorded from the XPS peaks caused by changes in the chemical structure of the sample atoms at the surface provides vital information on oxidation states especially on semiconductors where the electrical properties of metal deposited on such surfaces is strongly influenced by the its chemical state. Binding energies for elements and compounds are well referenced [Wagner, 1979].

Sample charging may occur if continuous emission of electrons from the sample is not compensated. For a conductive sample, earthing the sample will overcome the problem, for insulating samples this can be overcome by an electron flood gun.

X-rays for an XPS experiment are created by bombarding a solid target with high energy electrons. The electron energy used for bombardment is normally higher than the K-shell binding energy and emission lines are associated with the filling of K-shell holes. Emission from Mg and Al is dominated by the $K_{\alpha 1,2}$ emission at 1486.6 and 1253.6 eV with a line width of about a few tenth of an eV. This limits the accurate detection of energy shifts and the position of photoelectron peaks.

Section 5.9 Ultraviolet Photoelectron Spectroscopy (UPS)

Ultraviolet photoelectron spectroscopy (UPS) applies similar concepts to the XPS except that photons of much lower energy are used instead (< 50eV). This lower energy regime is useful to probe the more weakly bound electrons and less localised valence electronic states.

To excite these weakly held electrons, a He gas discharge is used as a photon source. An HeI source gives a photon energy of 21.2eV while HeII provides radiation of 40.8eV. Other inert gas species emit photons of lower energy range. UPS is a surface sensitive technique but it is not as specific as XPS as the electron mean free path for this energy range is typically higher than for XPS. This technique is particularly useful to investigate the surface band structure. It can be also used to determine the Schottky barrier height for different metallisation contacts deposited on diamond and indicate the presence of an negative electron affinity (NEA) surface with the appearance of a sharp peak in the photoemission spectra [Baunmann, 1998]. Shifts in the spectrum normally indicate modification to the electronic levels.

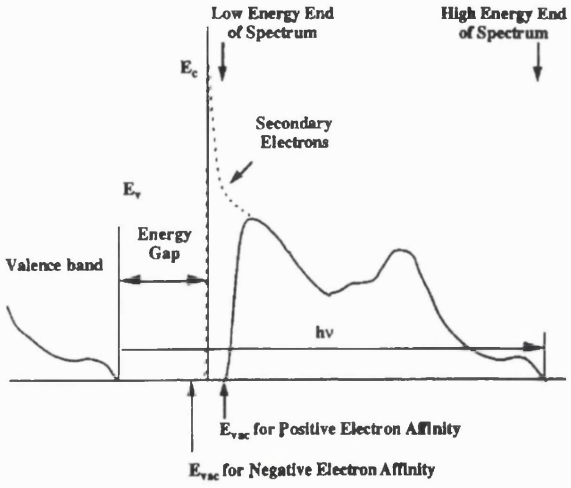

Figure 5.9(a)

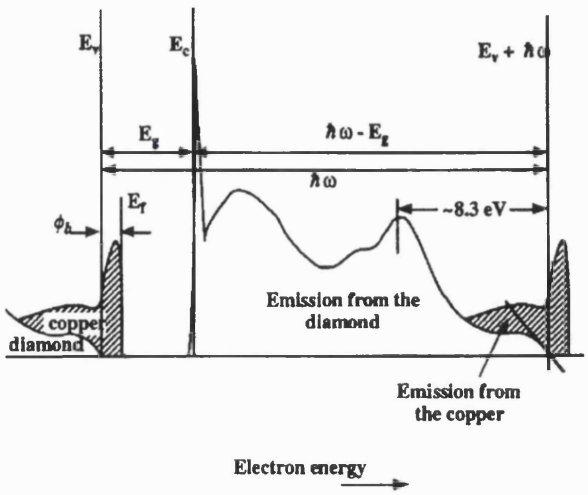

Figure 5.9(b)

Figure 5.9(a) shows the schematic diagram of photoemission spectra for a negative electron affinity surface(dotted line) and a positive electron affinity surface (solid line) while Figure 5.9(b) shows the schematic diagram of photoemission spectra for Cu deposited on diamond [Baunmann, 1998].

The Schottky barrier height is determined from the difference between the position of the valence band edge of diamond E_V and the metal Fermi-level E_F. as demonstrated in figure 5.9(b). Apart from determining the band structure of a semiconductor, UPS can also be used in the study of adsorbed molecules on surfaces. The UPS fingerprint of species in the gas phase allow the identification of the species which is chemisorbed on the surface.

Section 5.10 Scanning Electron Microscopy (SEM)

An electron microscope uses an electron beam to produce a magnified image of the sample. Electron microscopy has two distinctive advantages over optical microscopy. A higher magnification is possible on an electron microscope (within the nm region) as electrons have a much shorter wavelength than photons and the depth of field for an electron microscope is much larger. There are 3 principle types of electron microscope scanning, transmission and emission. Unlike an optical microscope, a scanning electron microscopy (SEM) basically consists of an electron gun, a electron beam focusing system, scanning coils, an electron detector and a cathode ray tube (CRT). The basic set up for this system is display in figure 5.10.

In the SEM [Schroder, 1998] a focused electron beam (1 to 10nm in diameter) is incident on the sample. The primary electron beam is scanned across the selected area of the sample. Secondary and back scattered electrons are generated at each beam location. X-ray photons will be induced as well due to bombardment of the primary electrons at the sample. Secondary electrons are collected by a detector and converted into electron beam induced current. This form of signal can be amplified to control the brightness of the CRT display. The brightness of the CRT display is scanned in synchronism with the primary beam scan on the sample. The magnification ratio is measured by taking the length of the CRT display to the dimension scan by

the primary beam. Magnification levels as high as 100,000 times are possible. The primary electron beam is typically provided with up to 20keV of energy with a beam current of 10μA. Different scan speeds are available with the lowest scan speed for best picture quality on the CRT. The sample stage normally allows precise 3 dimensional movement in addition to rotation. The contrast is influenced by the sample topography. This can be improved by tilting the sample stage with respect to the primary beam. Secondary electrons are emitted from approximately the top 10nm surface. The tilting increases the electron beam path lying within this 10nm. Contrast is dependent on the angle as :-

$$C = \tan(\theta)\ d\theta$$

where C is the contrast

θ is the angle from normal incidence ($\theta = 0^{\circ}$ for normal incidence)

The dependency of contrast with tilt is responsible for the 3 dimensional image of the area scanned. Furthermore, the secondary electrons emitted at different directions from the detector are attracted and collected as well. The image from an SEM is formed by the amplification of secondary electrons and image information is mapped onto a CRT screen unlike optical microscopy where light is reflected and passed through lenses.

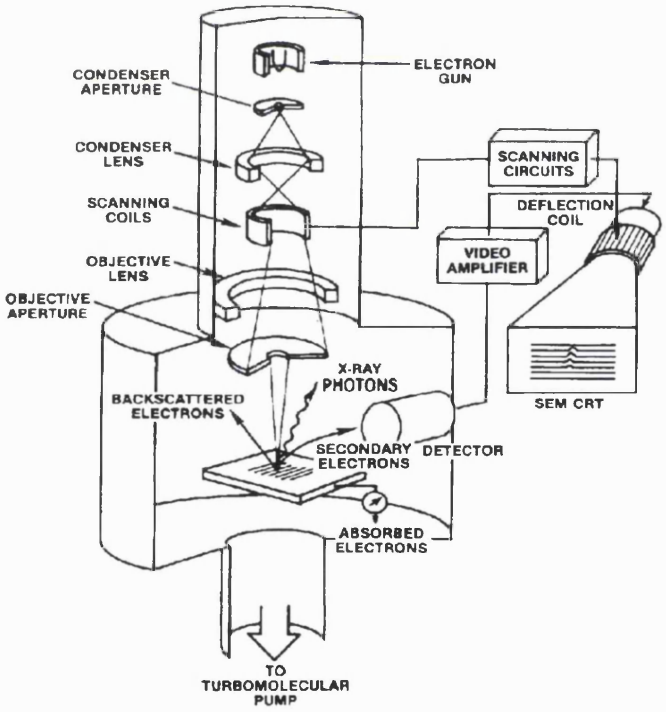

Figure 5.10 The basic set up for an SEM [Young, 1986]

SEM is used mainly to monitor the surface of semiconductor for various device designs and applications. It requires the use of high vacuum environment as it involves detection of electrons. For an insulating sample, a thin Au layer is sputtered on to the surface to ensure charging of sample by the primary electron beam can be grounded.

References :-

Baumann, P.K. and Nemanich, R.J. [1998] Diamond & Relat. Mater., **7**, 612.

Benninghoven, A., Rudenarer, F.G. and Werner, H.W., [1987] "Secondary Ion Mass Spectroscopy", Wiley, New York.

Briggs, D. and Seah, M.P. [1983] "Practical Surface Analysis by Auger and X-Ray Photoelectron Spectrsocopy", John Wiley, New York, 1983.

Diekmann, J. [1994] "Electronic Materials & Process Handbook", McGraw Hill, Singapore, Chapter 10.

Exarhos, G.J. [1989] "Characteristic of Semiconductor Materials" principle and method vol.1, Noyes Publication, New Jersey, 242.

Fayette, L., Marcus, B., Mermoux, M., Abello, L. and Lucazeau, G. [1994] Diamond & Relat. Mater., **3**, 438.

Gerrard, D.L. and Bowley, H.J. [1996] "Raman Spectroscopy", Anal. Chem., **58**, 6R.

Hall, E.H., [1879] Amer. J. Math., **2**, 287.

Hayward, I.P., Baldwin, K.J., Hunter, D.M., Batchelder, D.N. and Pitt, G.D. [1995] Diamond & Relat. Mater., **4**, 617.

Janseen, K.T.F. and Boudewijn, P.R. [1991] "Analysis of Microelectronics Materials and Devices", John Wiley & Sons, New York, 407.

Leeds, S.M., Davis, T.J., May, P.W., Pickard, C.D.O. and Ashfold, M.N.R. [1998] Diamond & Relat. Mater., **7**, 233.

Morgan, A.E., de Grefte, H.A.M., Tolle, H.J., Warmoltz, N. and Werner, H.W. [1980] Proc. of 4th Conference on Solid Surfaces, p 1238.

Pankove, J.I. [1975] "Optical Processes in Semiconductors", Dover, NewYork.

Quinn, J.J. [1962] Phys. Rev., **126**, 1453.

Raman, C.V. and Krishna, K.S. [1928] Nature, **121**, 501.

Raptis, J., Liarokapis, E. and Anastassakis, E., [1983] Appl. Phys. Lett., **44**, 125.

Sails, S.R., Gardiner, D.J., Bowden, M., Savage, J. and Rodway, D. [1996] Diamond Relat. Mater. **5**, 589.

Schroder, D.K., [1990] "Semiconductor Materials and Device Characterisation", John Wiley & Sons, New York, 494.

Schroder, D.K., [1998] "Semiconductor Materials and Device Characterisation", John Wiley & Sons, New York, 651.

Siegbahn, K., Nordling, C. and Hagstrom, S. [1964] Z. Phys., **178**, 433.

Sigmund, [1969] Phys. Rev., **184**, 383.

Stevie, F.A., Kahora, P.M., Simons, D.S. and Chi, P. [1988] J. Vac. Sci. Technol., **A6**, 76.

Stingeder, G. [1988] Anal. Chem., **60**, 1524.

Turner, J., Amano, J., Gronet, C.M. and Gibbons, J.F. [1987] Appl. Phys. Lett., **50**, 1601.

van der Pauw, L.J. [1956] Phil. Tech. Rev., **20**, 220.

van der Pauw, L.J. [1956] Phil. Res. Rep., **13**, 1.

Wada, N. and Solin, S.A., [1981] Physica B, **105**, 353.

Wagner, C.D., Riggs, W.M., Davies, L.E., Moulder, J.F. and Muilenberg, G.E. [1979] "Handbook of X-Ray Photoelectron Spectroscopy", Perkin Elmer, Eden Prairie, MN.

Wagner, J., Ramsteiner, M., Wild, C. and Koidl, P. [1989] Phys. Rev. **B40**, 1817.

Wagner, J., Wild, C., Muller-Sebert, W. and Koidl, P. [1992] Appl. Phys. Lett. **61**, 1284.

Werner, H.W. and Boudewijn, P.R. [1984] Vacuum, **34**, 83.

Wittmaack, K. [1984] Vacuum, **34**, 119.

Yoshikawa, M., Katagiri, G., Ishida, H., Ishitani, A., Ono, M. and Matsumura K. [1989] Appl. Phys. Lett., **55**, 2608.

Young, R.A. and Kalin, R.V. [1986] "Scanning Electron Microscpoic Techniques for Characterisation of Semiconductor Materials" in Microelectronic Processing Inorganic Material Characterisation. America Chem. Soc. Symp. Series **295**, Washington DC, 49.

Chapter 6

Characterisation of Surface Conductive Layer on Thin Film Diamond

Contents

Section 6.1 Introduction

Atomic hydrogen plays an important role in the CVD deposition of diamond. It suppresses the formation of sp^2 material and at the same time enhances the formation of sp^3 bonds during growth. As a result, the growth of diamond favours the kinetic mechanism in the CVD method rather than the thermodynamic processes. The surface of diamond at which growth occurs is terminated by a mono-layer of hydrogen. This stabilises the dangling bonds of carbon at the surface and allows the addition of radical groups such as methyls through hydrogen abstraction. The presence of this layer of hydrogen has been confirmed through the use of thermal desorption spectroscopy (TDS) [Chua, 1994], secondary ion mass spectroscopy (SIMS) [Hayashi, 1996] and elastic recoil detection analysis (ERDA) using a 2.4 MeV He ion beam

[Kimura, 1999]. The orientation of the hydrogen on the different surfaces have been confirmed by Low energy electron diffraction (LEED) [Bobrov, 1998]. Kawarada *et. al.* [1995] have suggested the (100) plane of CVD diamond was reconstructed in the form of a 2 x 1. Exposure to atomic hydrogen results in hydrogen termination of these dangling bonds. Reconstruction of the surface and the desorption of the hydrogen terminated layer can occur at temperature above 1000°C in vacuum [Bobrov, 1998]. Under the presence of oxygen, this can occur at a much lower temperature.

It is well known that this form of termination is responsible for the NEA properties on diamond. Surface science characterisation methods such as XPS and UPS have been used to study the properties of various metal contacts (thickness < 1nm) deposited on these surfaces[Baumann, 1998]. An NEA peak is often observed for metal contacts deposited on hydrogen terminated diamond. On the other hand, the NEA peak disappears if similar surfaces are oxidised and these surfaces give the largest Schottky barrier height. In addition, electrical characterisation of the metallisation contact on oxidised surfaces revealed that the experimentally determined Schottky barrier height is independent of the work function and the electronegativity of the metallisation contact and is pinned by the high defect density at the surfaces i.e. the barrier is Bardeen limited [Bardeen, 1947].

Apart from the NEA properties, an intriguing observation is that undoped hydrogen terminated diamond can display much lower resistivity than natural diamond. Landstrass and Ravi [1989] first demonstrated that the low conductivity is related to a hydrogen layer. Heating the diamond in nitrogen ambient at temperatures above 600°C reduces its conductivity to the natural intrinsic level. However, a subsequent exposure to a hydrogen plasma restored the original high conductivity. Others have also observed similar trend [Shirafuji, 1995]. Stallcup *et al.* [1995] observed that approximately 20% of the CVD diamond surface was covered with non diamond carbon and Jiang *et al.* [1999] speculated that these might contribute to the surface electrical conductivity. In addition, Mori *et al.* [1995] detected a non diamond carbon layer on the surface on diamond films grown by the CVD method using ESR measurements. Using a 4 point probe, Gildenblat *et al.* [1991] recorded a sheet resistivity of approximately 8kΩ/square for undoped hydrogen terminated homoepitaxial diamond. The sheet resistivity of as-grown diamond films were almost independent of the amount of boron incorporated in the bulk. The author suggested that the high conductivity was caused by the non diamond carbon layer on the surface. Furthermore, the author demonstrated that this non diamond conductive layer can be removed in a strong oxidising etch comprising a mixture of H_2SO_4 and CrO_3 at 170°C for 3 min followed by a rinse in boiling mixture of 1:1 H_2O_2 and NH_4OH. Unfortunately, the conductive layer is also believed to be the source of leakage current encountered in the electronic devices fabricated from diamond and similar treatment have often been used by many workers to clean the diamond surfaces before metallisation contacts are deposited [Gildenblat, 1991].

Until recently, the usefulness of this conductive layer was not realised. Kawarada *et al.* [1994] first utilised the conductive layer on a hydrogen terminated {100} homoepitaxial CVD

diamond to fabricate Schottky diodes and MESFETs. Metallisation contacts deposited on this conductive layer showed dependency on the electronegativity of the metal. Al formed Schottky contacts (ϕ_b = 0.8 eV) while Au displayed ohmic properties on similar surfaces [Gluche, 1997]. Hayashi *et al.* [1996] carried out a Hall assessment on these surfaces and obtained p-type properties which revealed a sheet charge density of $10^{13}cm^{-2}$ with a corresponding Hall mobility of 28 cm^2/Vs.

Section 6.2 Experimental Aims

The aim of the experimental work described in this chapter was to study the electrical properties of hydrogen terminated surface conductive layers on PCD films. This information is vital as the presence of the conductive layer to date is only confirmed on (100) homoepitaxial CVD diamond by Hall measurement. Its properties on other types of CVD diamond film remain unexplored. For this purpose, this study employed one of the most reliable electrical characterisation techniques, the van-der-Pauw [1956] Hall characterisation method to probe the sheet resistivity, Hall mobility and sheet carrier density without interference from the contact properties (see Chapter 5). Changes which occur to this conductive layer after subsequent heat treatments are presented to monitor the stability of this layer. Furthermore, resistivity changes in this layer observed by many workers after heat treatments in different environments were not properly explained in terms of carrier concentration and transport properties. This well known experimental observation has made this dopant unique compared to other conventional impurity dopant in semiconductors and may provide the clue to explain the formation of this layer. In addition, similar measurements conducted at high temperature after stabilisation would provide information to determine the transport properties of the carriers.

Raman spectroscopy and scanning electron microscopy (SEM) have been used to clarify the quality and the morphology of the PCD used here. Secondary ion mass spectroscopy (SIMS) was used to determine the atomic species present in the material. Ultra-violet photoelectron spectroscopy (UPS) and X-ray photoelectron spectroscopy (XPS) were used to reveal modifications to the chemistry of the surface caused by heat treatment. The photoelectron spectra will determine if changes to the chemistry on the surface or shifts in the spectrum peaks after heat treatment could be responsible or related to the modification in the conductivity of the layer as observed from the Hall measurement. Finally, I-V measurements under high vacuum were used to monitor changes in the resistivity caused by the effect of annealing on the surface conductive layer in PCD films. These experimental results are compared with the existing reports by others in the literature and the usefulness of this conductive layer is discussed. Numerous mechanisms which were proposed by many workers appeared to be controversial and this work aimed to solve the confusion. Lastly, a simple mechanism which might explain the origin of carriers measured is presented.

Section 6.3 Experimental Methods

Free standing polycrystalline CVD diamond grown by the technique of microwave plasma enhanced CVD were used throughout. Following growth, the samples were cooled whilst being exposed to a pure hydrogen plasma. Diamond cooled under this condition is believed to be terminated by a monolayer of hydrogen [Sun, 1993]. Two different types of diamond films were used throughout this chapter. BD8 is a free standing diamond wafer about 300μm thick with randomly aligned grains about 30 - 60μm in size while WM60 is a slightly thinner film roughly 100μm thick with a smaller grain size approximately 10 - 30μm. Both of these materials were grown under the same condition. The CVD chamber used for growing these films has been purposely used for only producing intrinsic films hence the conductivity measured in these films could not have resulted from the memory effects of boron contamination. The SEM and optical picture of both of these film are shown in Figure 6.1(a) and Figure 6.2(b). The Raman spectrum for both of these films are displayed in Figure 6.2(a) and Figure 6.2(b). The spectrum was obtained using a Renishaw system 2000 with red (He-Ne) laser excitation.

All samples were degreased according to the method described in Appendix 1 before any form of metallisation contact was placed on the sample. The Hall measurements conducted at room temperature were performed with a BioRad HL5200 with a magnetic field strength of 0.32T. The equipment set up and sample preparation for the Hall measurement is given in Appendix 2. The metallisation contacts were placed at the circumference of the sample. I-V characteristics of the contacts were checked to ensure that they were ohmic before the actual Hall measurement. The high temperature Hall measurement was performed in a manually designed kit with a thermocouple temperature controller, Keithley multimeter 2000 to measure a Hall voltage, a constant current source and the magnetic field strength is about 0.3T. The setup for this high temperature Hall equipment kit and the sample preparation is given in Appendix 6. Semiconductor parameter analyser HP4145B and HP4061A were used to probe the I-V characteristic of the samples with metal contacts. Metallisation contacts were deposited by means of thermal evaporation using the Edwards 306 evaporator with a base pressure lower than 10^{-6}mbar. Shadow masking was used to position the metallisation contacts at the 4 corners of the sample as described in Appendix 6. The photoelectron spectra were recorded using a VG ESCLAB fitted with Al Kα centered around 1486.6eV and Helium (I) centered around 21.2eV. A thin (200nm) gold layer deposited near the edge of each sample was used for calibration purposes. The SIMS measurement were made by bombarding the surface with O_2^+ primary ions with an energy of 15keV.

Section 6.4.1 Experimental Results :- Raman and SEM

SEM and optical micrographs of the growth surface of BD8 and WM60 are shown in figure 6.01(a) and figure 6.01(b) respectively. The picture revealed that on both of these films all the grains were randomly aligned and mainly comprised of {110} and {111} facets. On average,

the thicker material BD8 (~300μm) has larger grains compared with the thinner (~100μm) material WM60. The grains on BD8 ranged from 30 - 60μm while on WM60 10 - 30μm.

Figure 6.01(a)

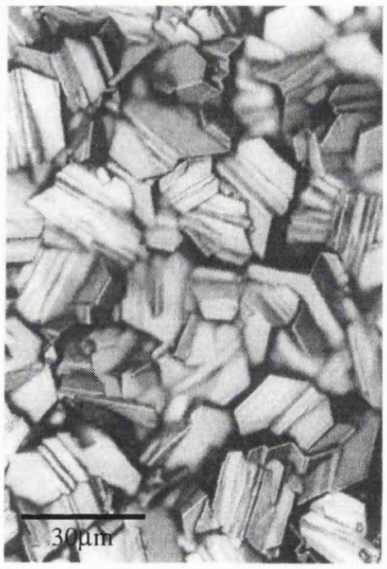

Figure 6.01(b)

Figure 6.01(a) shows the SEM of PCD material BD8 while Figure 6.01(b) shows an optical micrograph of PCD material WM60

All the electrical characterisation and surface science methods were performed on the growth side of the material where the conductive layer is present. The growth side of both films were hydrogen terminated. The PCD samples used in the experiments had a clean 'white' appearance and did not have any black graphitic spots on the surface or at the edge after inspection under the microscope.

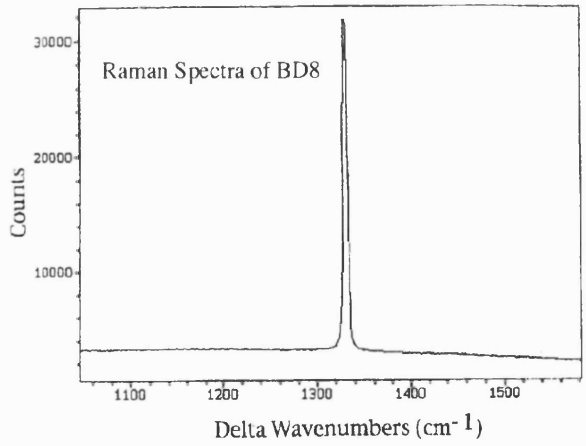

Figure 6.02(a)

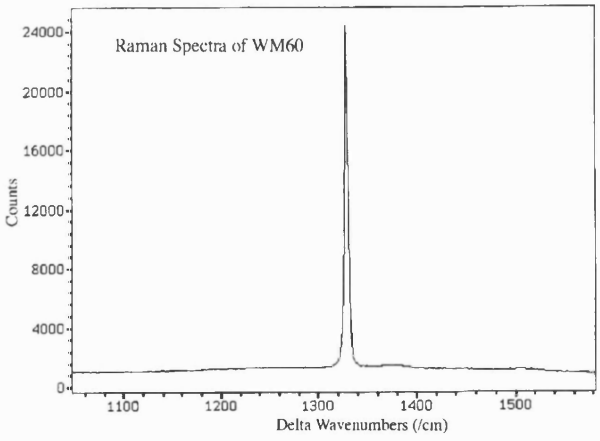

Figure 6.02(b)

Figure 6.02(a) and Figure 6.02(b) shows the Raman Spectra of the material BD8 and WM60 respectively taken using a red He-Ne laser at a wavelength of 633nm.

The Raman Spectrum for both of these films are displayed in figure 6.02(a) and figure 6.02(b). The spectra for both films are quite similar; this is expected as both films were grown under similar conditions. Both spectra reveal only a sharp peak at 1332cm^{-1} with no other

apparent structure. The He-Ne laser excitation used (633 nm) here is very sensitive to the presence of non diamond carbon indicating that the diamond films used were of high quality and relativity free of any sp^2 phase in the bulk.

Section 6.4.2 Experimental Results :- I-V and Hall Measurements

Aluminium and gold contacts were deposited on these surfaces by means of shadow masking. These metals were chosen as they have different electronegative values. Ohmic properties were recorded for the case of Au-Au contacts and rectifying properties for the case of Al-Au. (The properties of the rectifying Schottky contact are discussed in chapter 7 while the ohmic properties are elaborated in chapter 8.) For Au-Au contacts, current levels in the range of mA (at ± 10V) were recorded for rectangular shaped contact pads (2 x 3 mm) separated by about 0.5mm deposited on wafer BD8 as displayed in figure 6.03. This was unexpectedly high as the intrinsic PCD films used here were relatively high quality and almost free from graphitic phases in the bulk and therefore should not have displayed these properties. A rectification ratio of 6 orders of magnitude was recorded at ±10V for the Al-Au Schottky diode. Hence, the high conductivity recorded here can be attributed to the hydrogen terminated surface conductive layer that has previously been demonstrated on homoepitaxial diamond by other workers.

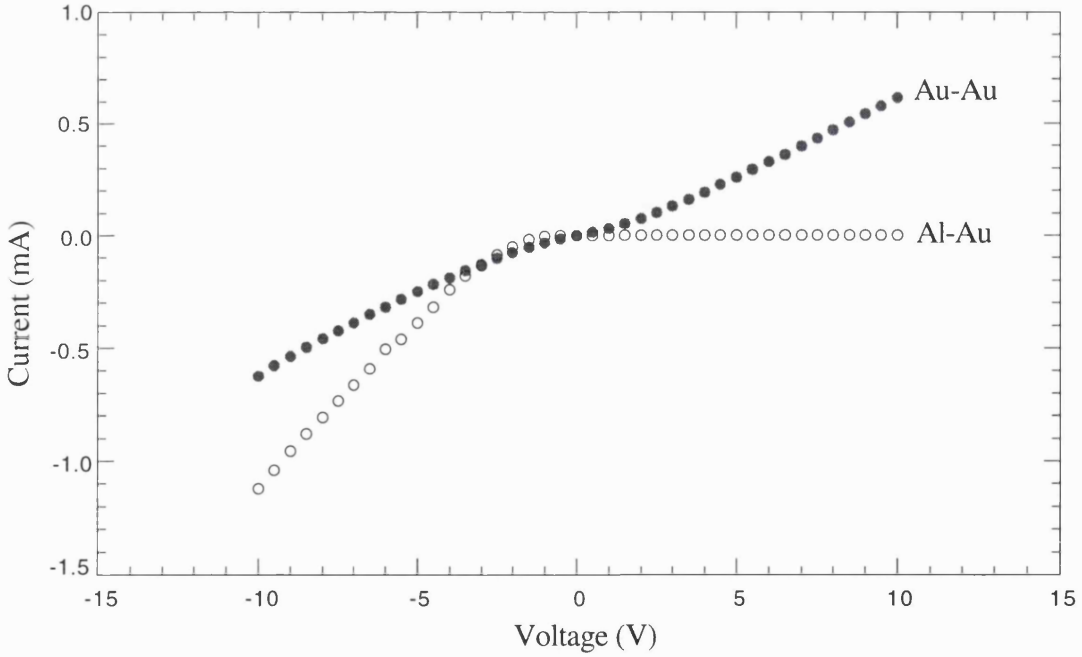

Figure 6.03 The I-V characteristic of metallisation contacts on as grown PCD diamond indicating the dependency of electrical properties on the metallisation scheme.

In order to investigate the nature of the carriers, Hall measurements using the 4 point van der Pauw configuration were carried out to confirm the p-type properties of the surface carriers and provide other useful information such as the sheet resistivity, sheet charge density and Hall mobility of the carriers. For this purpose, low resistive electrical contacts are required. Ag conductive paint contacts were placed carefully at the 4 corners of the almost square sample from

wafer BD8. The contacts were significantly smaller than the active area of sample to reduce the error during the measurement. In this section, the Hall measurements were made using the BioRad HL5200. A brief description on the set up of this system and sample preparation are given in Appendix 2. The effect of an air anneal on these films was also investigated. In this case, Hall measurements were performed at room temperature for films that had been heated previously to 60°C, 100°C, 150°C and 200°C for increasing periods of time in air. The heating was carried out on a hotplate. Immediately after the heating, the samples were placed on a large metal block kept at room temperature for several minutes to allow rapid cooling before Hall measurements were performed at room temperature.

Figure 6.04 shows the changes in sheet resistivity which occurred for a number of samples that were either as-grown or had undergone annealing in air at temperatures up to 200°C. The trends presented were typical of that obtained for all the samples of the PCD wafer, BD8. Following annealing at 60°C little variation was apparent in measurements taken over a prolonged period. However, if the film was annealed at higher temperatures the sheet resistivity increased with time, although a stable value was eventually reached after a given period for 100°C, 150°C and 200°C respectively.

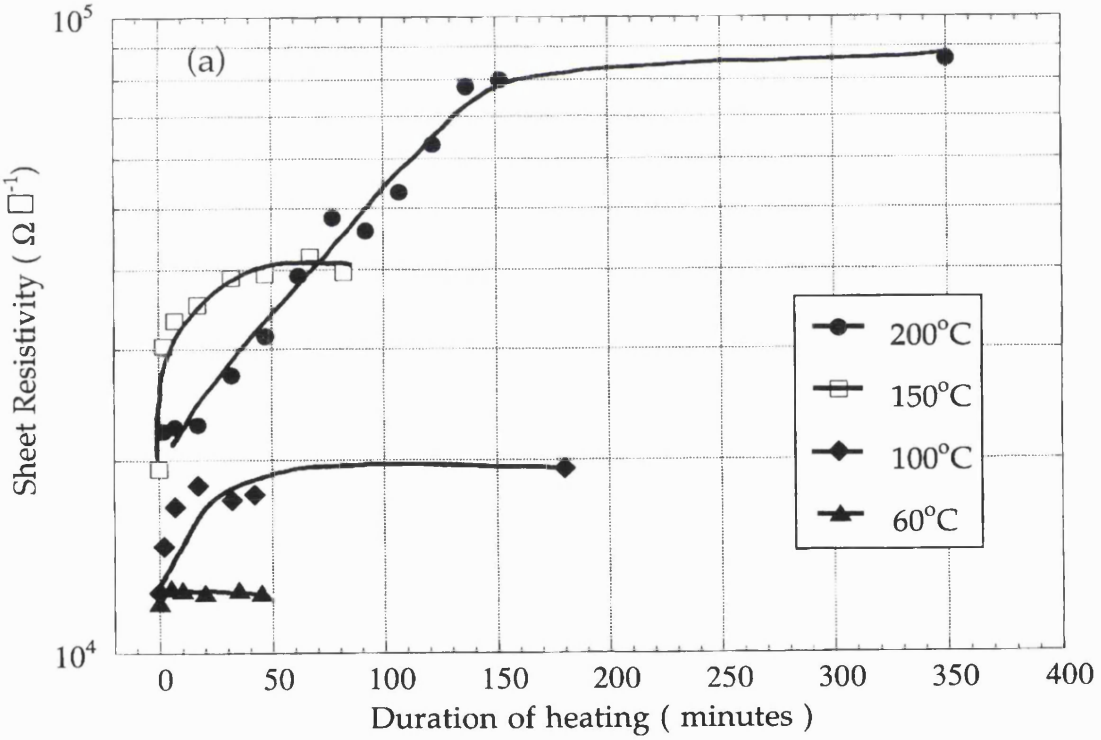

Figure 6.04 The van der Pauw measurements of sheet resistivity for samples from BD8 after being subjected to heat treatment in air at different temperatures for a varying duration of time.

Figure 6.05 shows the change in sheet carrier concentration measured under similar conditions. In general, annealing the samples in air reduced the sheet carrier concentration in the conductive layer. Only small changes were measured for samples which were annealed at 60°C. However, at higher temperatures, for example at 200°C, more significant changes were

recorded. During the early stages of heating, the sheet carrier density decreased rapidly. Then the rapid decrease began to saturate and finally a stable value was achieved. This behaviour was observed for heating at 100°C, 150°C and 200°C. For experiments which involved heating at 60°C, the changes were too small to be certain of the trend.

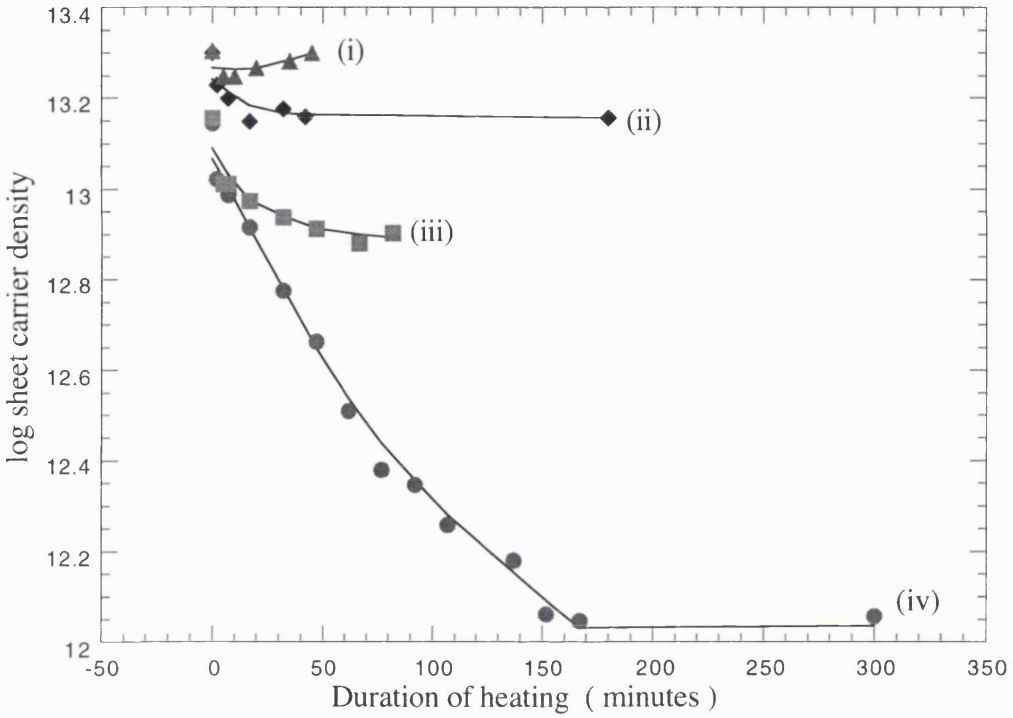

Figure 6.05 Changes in the sheet carrier density against the duration of heating for samples which have been subjected to (i) heat treatment in air at 60°C (ii) heat treatment in air at 100°C (iii) heat treatment in air at 150°C (iv) heat treatment in air at 200°C.

Figure 6.06 shows the corresponding Hall mobility values recorded at room temperature, following heating at different temperatures for increasing periods. Generally, there were few changes in the recorded Hall mobilities except for the sample annealed at 200°C which displayed an unusual characteristic. In this case, an initial drop in mobility from 27 to 20cm^2/Vs was followed by a rise, saturating at values of about 70cm^2/Vs for heating more than 160 minutes. The values recorded following annealing at other temperatures are shown as traces (i) - (iii) for 60°C, 100°C and 150°C respectively. Interestingly, the trend observed for these temperatures are different, with only modest changes in Hall mobility values being apparent. Figure 6.07 shows the increase in the Hall mobility values for a reduction in the carrier concentration. The reduction of carrier concentration (obtained by assuming a 20nm wide channel [Hayashi, 1997]) was provoked by heating the sample in air at 200°C.

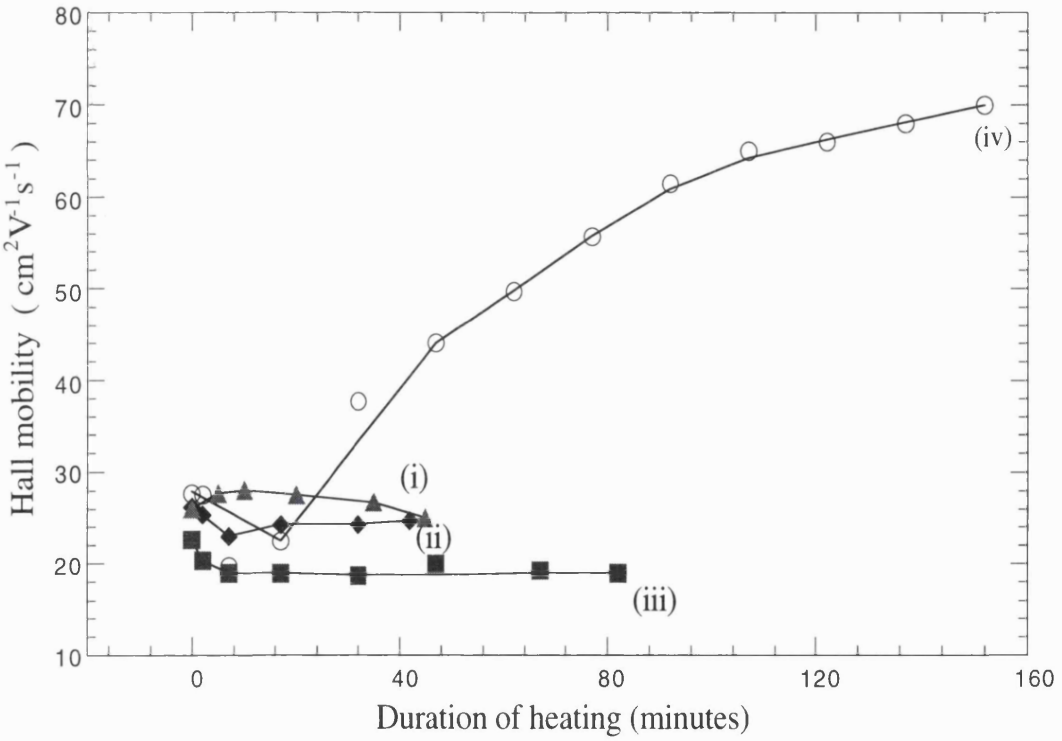

Figure 6.06 Corresponding modification of the Hall mobility for samples which have undergone treatment according to (i) heat treatment in air at 60°C (ii) heat treatment in air at 100°C (iii) heat treatment in air at 150°C (iv) heat treatment in air at 200°C.

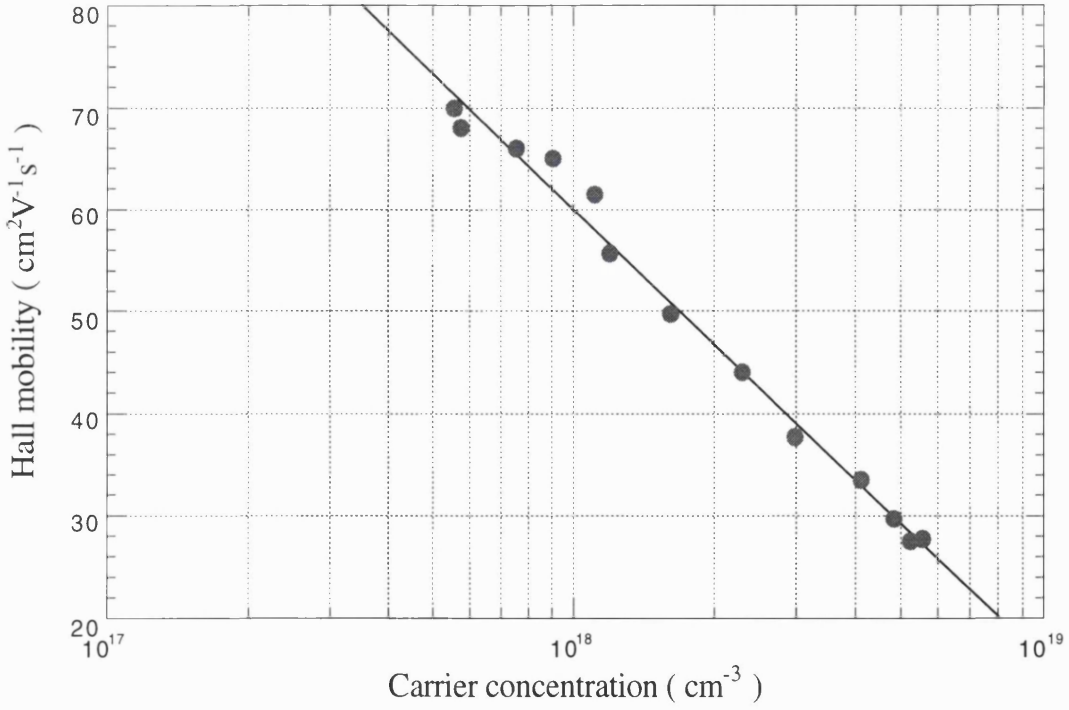

Figure 6.07 The changes in the Hall mobility recorded against carrier concentration for a sample from BD8 caused by the loss of carriers during the 200°C anneal.

In order to investigate if oxidation of the surface and the amount of water vapour in the air were affecting the properties of this layer, I-V measurements and heat treatments were conducted in an environment where both of these properties were minimised. This was achieved by performing the measurements and treatments under high vacuum. The BioRad Hall equipment described previously was not setup for high vacuum characterisation therefore only a simple resistance measurement based on two rectangular Au contacts (2 x 4mm) separated by 0.5mm was carried out. An as-grown sample from wafer BD8 was used for this measurement. The pressure in the chamber throughout the experiment was maintained at about 10^{-6}mbar. The heating in this system was provided by passing a large current through the molydenum sheet where the sample was resting. The temperature was monitored by means of a type K (Alummel-Chromel) thermocouple. After each subsequent heating the sample was allowed to cool down to room temperature before the I-V measurements were conducted. Unlike the 4 contacts van der Pauw configuration, the contact resistance for Au would be present in the 2 contact measurement, fortunately these values were small for the large Au pads used here (calculation of contact resistance is given in chapter 8) and can be assumed to be negligible. Figure 6.08 revealed the plot of resistance (measured from taking the best fit of the I-V curves) against the total duration of heating. For annealing at 60°C and below, only small resistance changes were recorded in contrast to higher temperature annealed especially at 150°C and 200°C. Interestingly, for the same heating temperature and after a certain duration of heating the resistance appeared to saturate. These results were consistent with the trends observed from the sheet resistivity measurement from the Hall method. This set of experiments demonstrate that changes to the resistance in the conductive layer can also occur where the effect of oxidation and water vapour is significantly reduced.

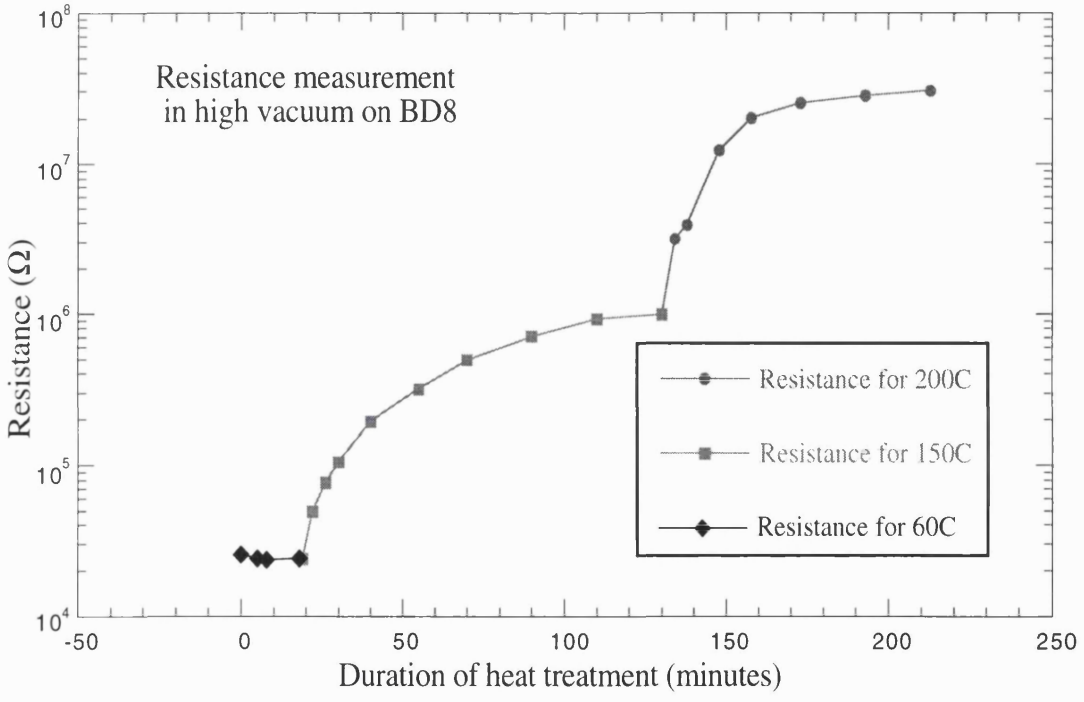

Figure 6.08 Changes in the resistance of material BD8 measured between two Au contact pads for heat treatments conducted in high vacuum.

Section 6.4.3 Experimental results:- High Temperature Hall

In order to fully investigate the transport properties of the carriers, Hall measurements performed over a wide range of temperatures are necessary. A different Hall setup was used in this experiment as high temperature measurements were not possible on the previous Hall kit (BioRad HL5200). In this section the samples were taken from as grown PCD films WM60. Au electrical contacts were placed at the circumference of the rectangular samples. These contacts were then bonded to the legs on a sample mount to facilitate measurement. The schematic setup of the equipment and the positioning of samples on the mount is given in Appendix 2. The results from the previous section indicated that when the conductive layer was heated in air above room temperature a reduction in sheet carrier concentration occurred. Figure 6.07 also revealed that changes in the level of carrier concentration can cause variation in the measured Hall mobility. Hence, for high temperature measurements, to ensure that the changes obtained from the Hall mobility are due to the temperature change and not influenced by the reduction in carrier concentration, the sheet carrier density must be stabilised first.

The conclusion from the last section revealed that prolonged annealing of the surface conductive layer in air results in stabilisation of the sheet carrier concentration. In this case, it was performed by heating the samples in air for a prolonged period of approximately 2 hours. Two samples were prepared, one of them was heated at 235°C while the other at 200°C. It should be noted that these measurements were conducted in air. The measured sheet carrier density shown in figure 6.09 (a) and (b) revealed only small changes over a temperature range of 310K to 470K. This confirmed the stability of the sheet density after the treatment at a level around $10^{13}cm^{-2}$ for these two samples.

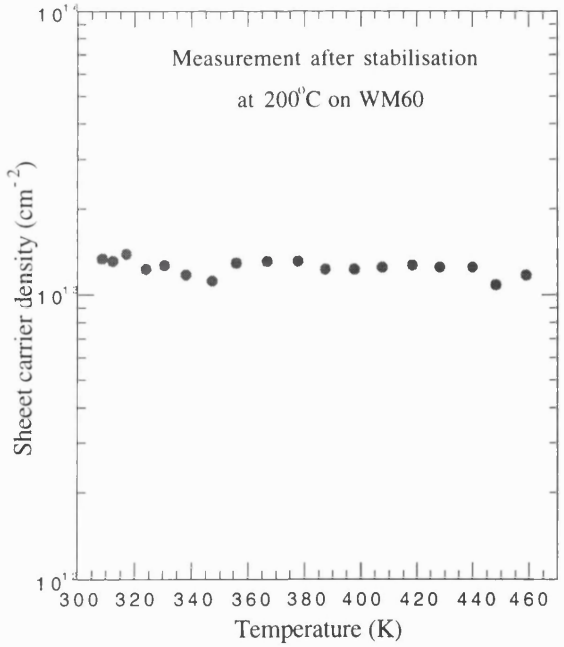

Figure 6.09(a)

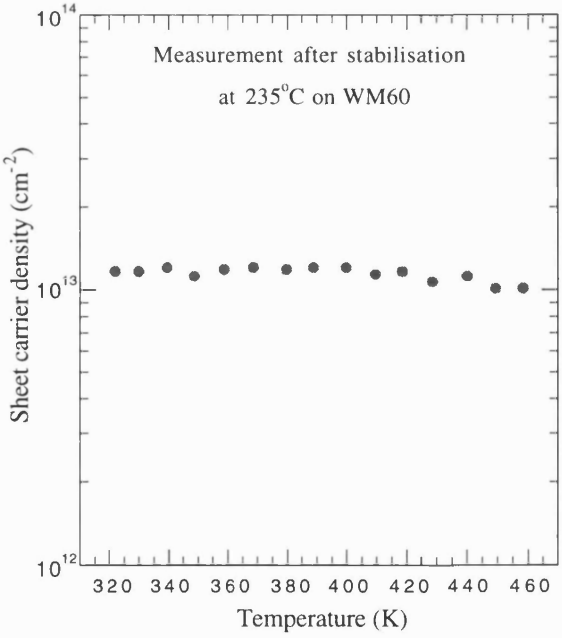

Figure 6.09(b)

Figure 6.09(a) and 6.09(b) show plots of sheet carrier density measured across a temperature range in air for WM60 after heat treatment in air at 200°C and 235°C respectively to stabilse the carriers.

The experimental values measured here are comparable with those reported by others on homoepitaxial films [Jiang, 1999; Hayashi, 1997]. Unlike the sheet carrier density, the sheet resistivity decreases exponentially with the temperature. At room temperature a value around 65 to 75 kΩ/square was recorded. This value decreased to only about 35 to 40 kΩ/square at 180°C.

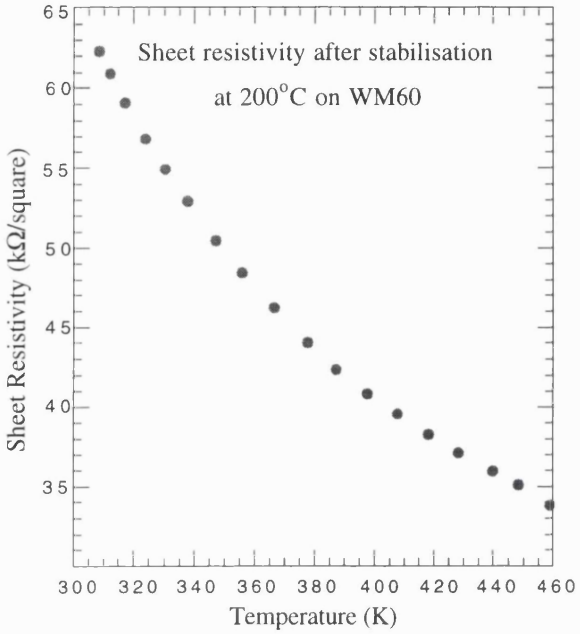

Figure 6.10(a)

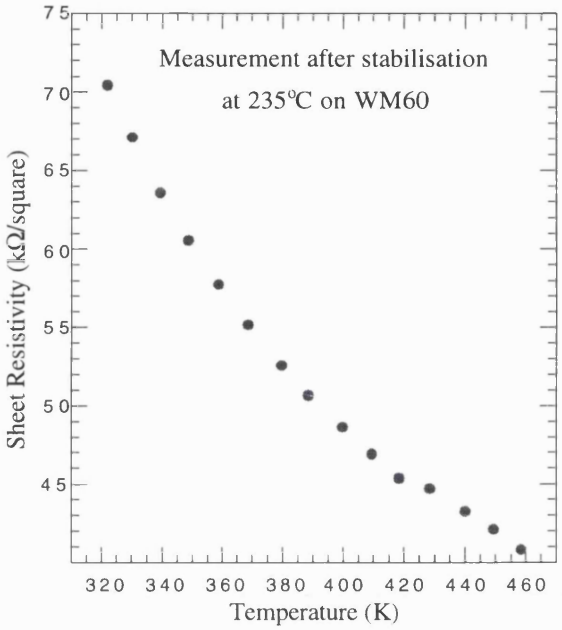

Figure 6.10(b)

Figure 6.10(a) and (b) show the variation of sheet resistivity with temperature after stabilisation

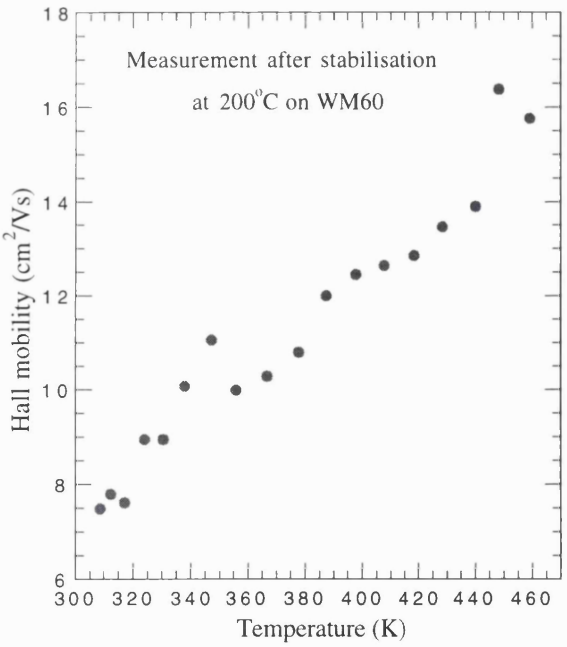

Figure 6.11(a)

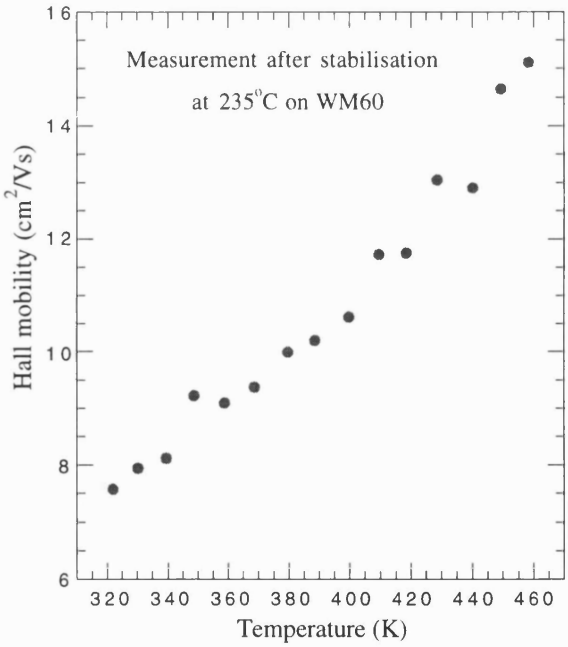

Figure 6.11(b)

Figure 6.11(a) and Figure 6.11(b) reveal the data of Hall mobility against temperature. The increase in Hall mobilities with temperature were not effected by changes in the carrier density as the carriers have been stabilised by heat treatment shown in figure 6.09(a) and (b).

The sheet resistivity of the sample annealed at 200°C was higher than at 235°C as shown in figure 6.10(a) and 6.10(b). Figure 6.09(a) and 6.09(b) showed there was almost no variation in the sheet carrier density throughout the temperature range investigated here. This implies that the carriers were totally activated above room temperature. In addition, after stabilisation in air, almost no loss of carriers was recorded. However, a consistent exponential-like reduction in the sheet resistivity was observed on both samples as temperature increased. The data in figure 6.11(a) and 6.11(b) shows that changes in the Hall mobility of carriers are likely to account for this observation. In fact, these results also explain and support the experimental observation of the reduction in the forward bias current for the Al-Au Schottky diodes at high temperature described in Chapter 7, Section 7.5 in this thesis. The mobility in figure 6.11(a) and (b) increases with temperature. These trends strongly suggest that ionised impurity scattering is dominating in the conductive layer.

The Hall mobility of both samples from WM60 annealed at 235°C and 200°C recorded almost similar values from 320K to 460K. On the other hand, the Hall mobility recorded for the larger grain size material, BD8 was much higher (30cm^2/Vs) at room temperature compared to the smaller grain size material WM60 (8cm^2/Vs). After being subjected to heating at 200°C, the Hall mobility of BD8 increased further to about 70 cm^2/Vs presumably due to the reduction of impurity scattering caused by the loss of carriers. In general, the highest sheet carrier density measured on these as-grown surfaces was approximately 2 x 10^{13}cm^{-2}. The sheet resistance may vary from 10 to 20 kΩ/square on as grown PCD films. These values were consistent with those reported on homoepitaxial CVD films [Hayashi, 1997; Jiang, 1999].

Section 6.4.4 Experimental Results:- UPS, XPS and SIMS

This section describes experiments carried out to monitor the chemical changes which might occur to the surface of hydrogen terminated PCD films. Samples from the wafer BD8 were used for all the experiments described in this section. The previous electrical characterisation conducted by the Hall technique revealed that modification to the electronic properties of the surface conductive layer can occur at temperatures as low as 150°C. Following this observation, this main focus of this section is to monitor changes in the surface binding species which might occur to the surface conductive layer caused by the heat treatment conducted in air. The conclusion from this section could provide an insight to explain the electronic properties of the material. As the conductive layer may be related to the surface terminating species, techniques which were sensitive to the surface were employed to detect possible modification to the chemical content.

Two samples from wafer BD8 were prepared for SIMS. These consist of an as-grown sample and the other heat-treated at 200°C in air for a sufficient period to stabilise the I-V characteristic of the film. The SIMS signals recorded at 1 atomic mass unit for hydrogen are plotted in figure 6.12 as function of sputter depth. The SIMS measurements were made by

bombarding the surface with O_2^+ primary ions with an energy of 15keV. Boron were not detected by the SIMS hence confirming that the p-type conduction cannot be due to other dopants. The as-grown film produced a strong hydrogen signal over the first 20nm of diamond with a significant tail persisting to depths greater than 60nm. This tail maybe contributed by hydrogen in the grains, at the grain boundary, the background level or it could be due to re-adsorption of sputtered hydrogen. In contrast, the heated film reveals little hydrogen presence at depths greater than around 10nm. The data in figure 6.12 should only be taken as an approximate guide to the depth of hydrogen as the rough polycrystalline CVD diamond surface may distort the SIMS signal. However, the data do indicate that there is high concentration of hydrogen near the surface.

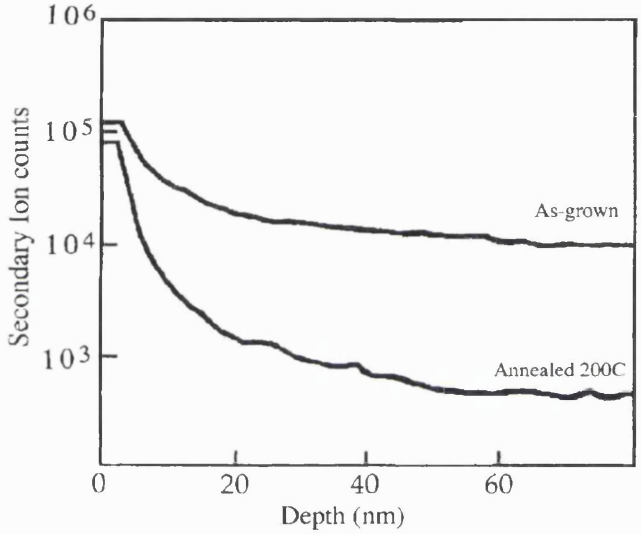

Figure 6.12 shows the hydrogen depth profile measured by SIMS on the growth side BD8.

UPS and XPS were employed to investigate the chemical and electrical condition of the surface itself. The curves presented in figure 6.13(a) and 6.13(b) are XPS spectra obtained for the surface of as grown BD8. The curves presented in figure 6.13(a) can be used for monitoring the degree of oxidation which might be occurring on the surface. Initially, a weak O 1s peak is visible on the as-grown sample located at 534eV as shown in figure 6.13(a). This weak peak in trace (i) indicates that the as grown PCD surface has little oxygen bonded to the carbon on the surface. After the sample has undergone the heat treatment in air at 100°C and 200°C, for a prolonged period, there is a slight increase (<15%) in the intensity of the peak located at 534eV shown as traces (ii) and (iii) in figure 6.13(a). However, the O/C peak ratio remains at ~0.1 for all the 3 traces suggesting that significant oxidation of the surfaces is not occurring at these temperatures. Electrical measurements detected more than an order of magnitude change in the conductivity of the film at these temperatures. In addition, the heat treatments conducted in high vacuum where oxidation was minimised also display a similar trend. These experimental results suggest that the changes in the conductivity due to the heat treatments were not caused by oxidation of the as grown diamond surfaces.

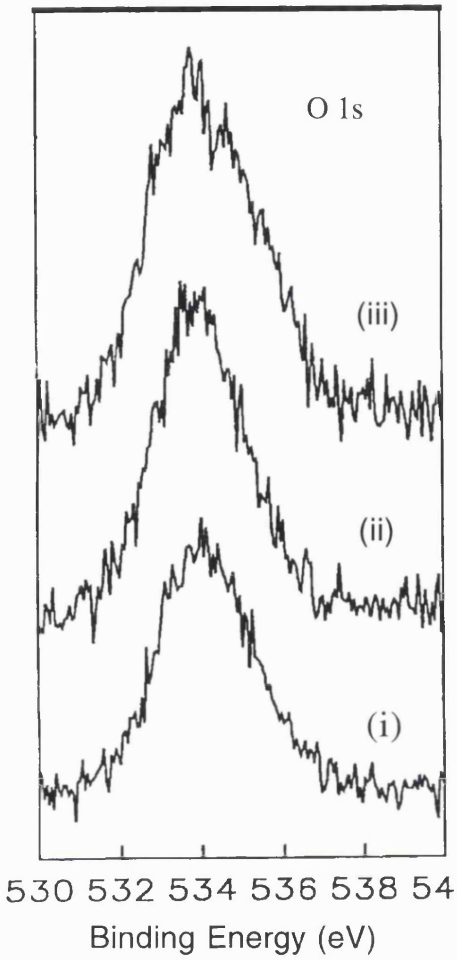

Figure 6.13(a)

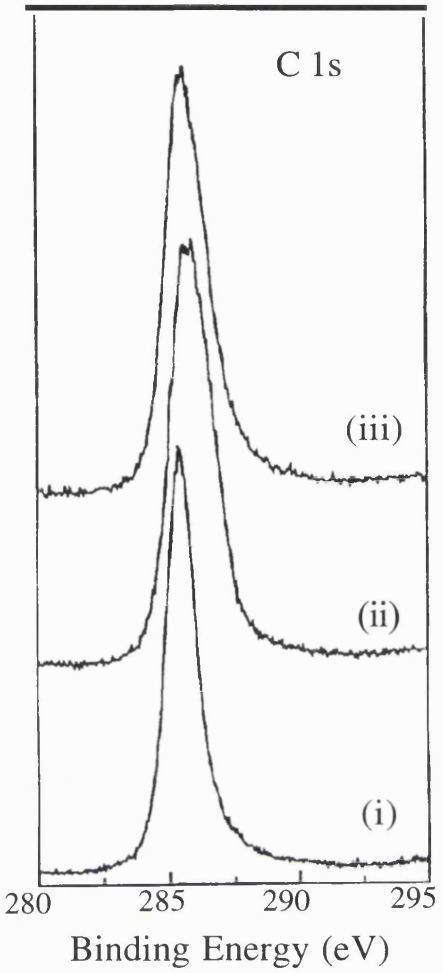

Figure 6.13(b)

Figure 6.13(a) shows XPS spectra for O 1s and figure 6.13(b) shows the XPS spectrum for C 1s of the same samples for which have been subjected to different heat treatment as follows :- (i) samples were as-grown. (ii) samples were annealed in air at 100°C for 2 hours while (iii) samples were annealed in air at 200°C for 2 hours.

Figure 6.13(b) shows the curves of the carbon (C) 1s peak, the peak is initially located at 285.4eV binding energy and is fairly sharp with a FWHM of 1.25 eV. During heating at 100°C the peak broadens to 1.75eV with shift initially to 285.8eV. However, heating at 200°C causes shifting back to 285.5eV further heating at 200°C caused no more changes as shown in figure 6.13(b). On the whole the heating has caused the peak to broaden. A curve fitting program was used to investigate the origin of the shoulder on the C 1s peak. The result is shown in Figure 6.13(c). It was assumed that the peak present for the carbon surface as grown is the standard carbon 1s energy for the CVD diamond. A Gaussian curve was fitted to this peak. The position was found to be 285.5eV. The first peak (full lines) was held at 285.5eV while the second peak (dotted lines) was allowed to move in order to best fit the data. The second peak centered around 286.2eV. This second peak could be attributed to surface alcohol groups.

The ultra-violet photoelectron spectroscopy (UPS) data recorded with He(I) radiation is shown in figure 6.13(d). In this case, the UPS was used as a fingerprint to identify any changes

in the state of the surface. The intensity of all three peaks in figure 6.13(d) at 15eV were unchanged and there is little modification or appearance of any new structure. The as-grown sample shows a broad band centered at 15eV. Upon heating, the band narrows by ~0.2eV and shifts to lower kinetic energies becoming centered at ~14eV. The shoulder detected at 9.5eV did not shift but decreased in intensity and was most probably due to secondary electron emission. The He(I) spectra confirmed that the sample was not heated sufficiently to drive much of the hydrogen from the surface. If hydrogen was significantly desorbed from the surface then there will be significant change on the UPS spectra.

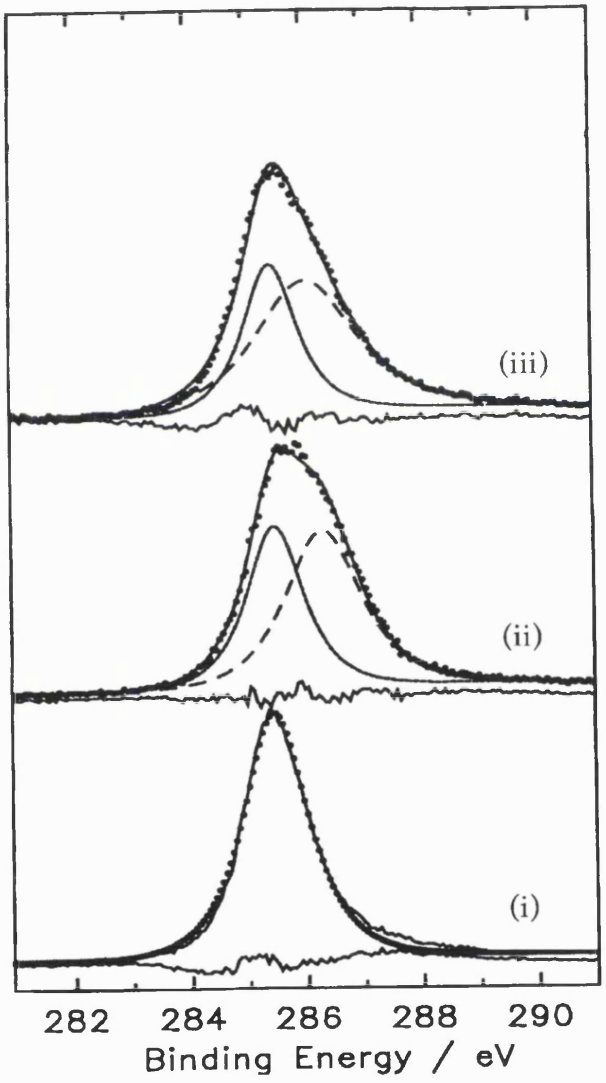

Figure 6.13(c)

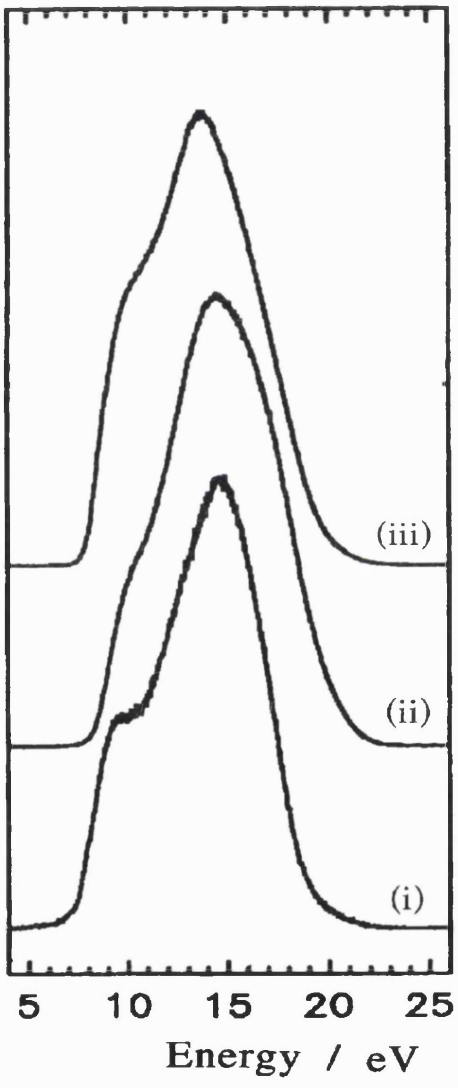

Figure 6.13(d)

Figure 6.13(c) shows XPS spectra for C 1s fitted with a fixed main C 1s peak at 285.4eV and figure 6.13(d) shows the UPS spectrum of the samples which have been subjected to different heat treatment. (i) for as-grown samples. (ii) for samples which were annealed in air at 100°C for 2 hours while (iii) for samples which were annealed in air at 200°C for 2 hours.

Section 6.5 Analysis

The Hall measurements presented earlier provide direct evidence that hydrogen terminated as-grown PCD films can support high hole concentration in the surface region. The SEM and the optical micro graph presented in figure 6.01(a) and (b), show that the diamond films used here were predominantly {110} and {111} facets. The Raman spectra of both films in figure 6.02(a) and (b) indicate that the diamond used is of high quality and relatively free of graphitic phase in the bulk and surface. The sheet carrier concentration of approximately 2 x $10^{13}cm^{-2}$ obtained from the Hall measurements was comparable with values measured by Hayashi *et al* [1997] and Jiang *et al.* [1999] on homoepitaxial {100} diamond surfaces. The morphology of the PCD films used here indicate that the carriers in this conductive layer are not only confined to the homoepitaxial {100} surfaces, as is widely reported in the literature, but can also be supported by other types of surface.

Landstrass *et al.* [1989] previously suggested that the annealing in air will remove the conductive layer. Grot *et al.* [1990] showed that cleaning the diamond films in a strong acid mixture of H_2SO_4 and CrO_3 at 170°C restored the original bulk diamond resistivity. Little insight into the effect of temperature on the actual sheet carrier concentration and the Hall mobilities within the p-type layer has previously been presented. From the experimental results presented in figure 6.06 and 6.08, it is clear that annealing in air at 100°C increases the sheet resistivity and decreases the sheet carrier concentration but does not alter the carrier mobility value on wafer BD8. The changes occur within the first 30 minutes, after which all measured values remained constant following prolonged heating. The increase in resistivity after annealing could either be due to the loss of carriers from the surface or the generation of more scattering centers. Since mobility is not significantly altered, the former case appears more likely. Similar observations can be made for annealing at 150°C where again carrier mobility values remain rather constant whilst the sheet resistivity changes considerably. In this case, all the measured quantities stabilise after around 50 minutes of annealing. Annealing at 200°C gives a rather different result, the sheet resistivity and sheet carrier concentration increase and decrease as before, but the Hall mobility increases after a small initial fall. This suggests that a reduction in the concentration of scattering centres is occurring

SIMS was used to determine the depth profile of hydrogen on homoepitaxial films [Hayashi, 1996]. A high density of hydrogen over the first 20nm of the surface was observed and was absent on oxidised surfaces. Hayashi *et al.* [1996] assumed that carriers were distributed over this depth. Similar SIMS performed on as grown PCD films were presented here. Although quite similar profile was recorded, the determination of hydrogen depth profile by using SIMS was not an accurate method especially on a large grain PCD films. The small cross section of the SIMS primary ion beam compared with the roughness of the surface may introduce large errors. Nevertheless, the profile also showed approximately 20nm hydrogen rich layer near the surface consistent with the result obtained by Hayashi. However, the use of 20nm as the depth of the conductive layer also assumes that the hydrogen is directly responsible for the

conductive layer, a fact which is still unclear at the moment. A more reliable and useful experimental method to estimate the actual depth of the carriers from the MESFET transfer characteristic will be presented in chapter 8. Nevertheless, the quantitative conclusion that there is a relatively higher concentration of hydrogen near the surface rather than in the bulk itself can be drawn.

The loss of chemisorbed hydrogen from diamond surfaces require temperatures of ~1000°C to occur with any significant rate[Bodrov, 1998] so the simple loss of surface hydrogen would not appear to account for the observations made by the Hall and resistance measurement after heat treatments. Oxidation can occur at a relatively lower temperature, although heating a CVD diamond film in air at 400°C for an hour leads to the formation of significantly less than a monolayer of surface oxide [Chan, 1997]. As the change in electrical properties of the CVD diamond surfaces appear to be limited at a given temperature a simple thermal loss of hydrogen or thermal oxidation on their own seem unlikely to be the cause of the modification measured. If near surface shallow acceptor states are responsible for the carriers, then annealing at high temperatures could lead to a change in the number of activated states, resulting in a modified carrier concentration but a similar number of scattering centers. This would account for the relatively unchanged mobility values for the lower temperature annealing processes. At 200°C, when the loss of near surface (not chemisorbed) hydrogen became more significant, a further reduction in carrier concentration would be accompanied by a decrease in scattering centers and hence a significant rise in carrier mobility. Heat treatments and I-V measurements conducted under high vacuum also display a same trend. The base pressure was maintained at about 10^{-6} mbar hence the effect of oxidation should be significantly reduced. The experimental results showed that after each anneal at a fixed temperature, there was an increase in the resistance measured between the two electrodes which saturate after longer anneal times. However, if a higher temperature anneal is performed, the resistance will increase and saturate at a higher level.

After stabilising the samples from WM60 in air at 235°C for 3 hours, Hall measurements were performed on the sample from room temperature up to 200°C. Throughout this temperature range stabilisation in the sheet carrier concentration around $10^{13}cm^{-2}$ was obtained on samples from WM60. The Hall mobility of carriers showed positive power dependence on temperature as shown in both the plots in figure 6.14(a) and (b).

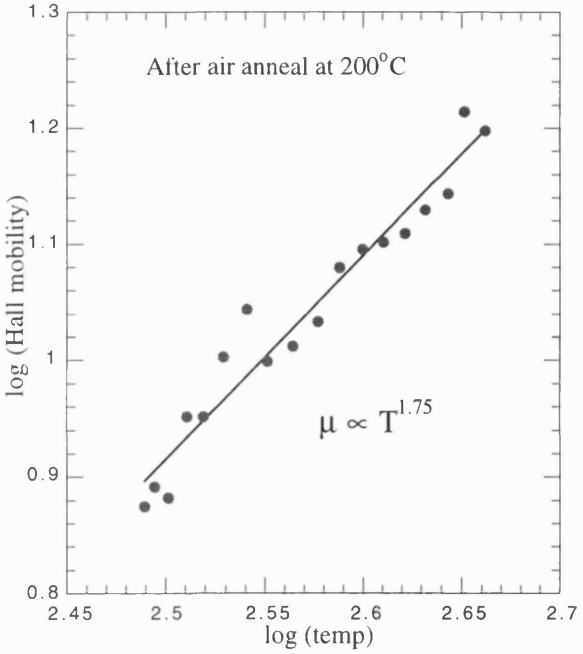

Figure 6.14(a)

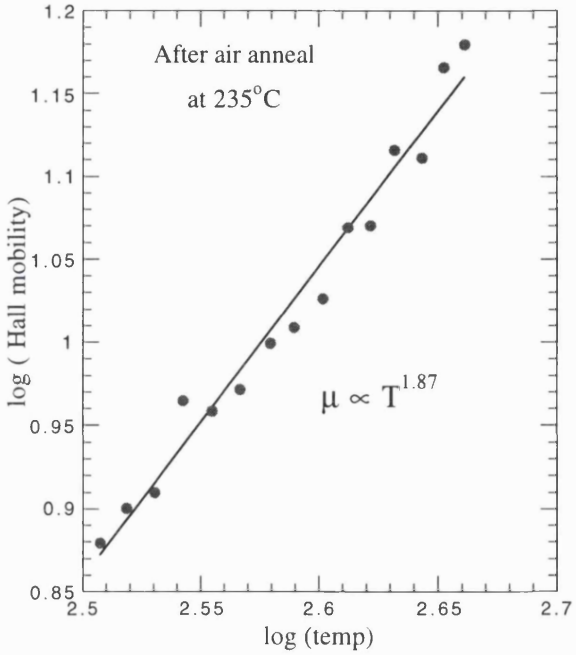

Figure 6.14(b)

Figure 6.14(a) and (b) are plots of log mobility against log temperature in which the dependency of Hall mobility with the power of temperature were determined.

Theory suggests that the mobility is proportional to $T^{1.5}$ for the ionized impurity scattering mechanism and $T^{-1.5}$ for phonon scattering mechanism [Streetman, 1995]. From figure 6.14(a) and 6.14(b), values of $T^{1.75}$ and $T^{1.87}$ were determined; the positive index indicates that the ionised impurity mechanism is dominating in these films. For the case of impurity doping on other semiconductors, ionised impurity scattering normally dominates at low temperatures. On hydrogen terminated PCD surfaces, ionised impurity scattering recorded at higher temperatures indicates that the carriers in this conductive layer deviate from most conventional doping methods. In contrast to this behaviour, the Hall mobility for holes generated by boron doping, for example, will decrease with increasing temperature for the same temperature range used here most probably due to lattice scattering. Fox *et al.* [1995] and others obtained this relation experimentally for homoepitaxial, highly oriented and randomly oriented polycrystalline diamond. The plot of mobility against carrier concentration in figure 6.07 for BD8 also supported the ionised impurity scattering mechanism, showing a decrease in mobility for larger carrier concentration. However, no significant increase in the Hall mobility was recorded for the samples from wafer WM60 after an air anneal at 200°C and 235°C unlike on BD8. The higher mobility recorded for the larger grain size material could indicate the influence of scattering mechanisms at the grain boundaries or the quality of the film on the transport properties of carriers.

Section 6.6 Discussion

It has been known for some time that the electrical properties of diamond surfaces are strongly modified by the presence of hydrogen. Hydrogenation leads to a decrease in resistivity through increased hole conduction. This has been confirmed on homoepitaxial films [Hayashi, 1996] through Hall measurement. In addition, some electronic devices have been successfully fabricated using this layer where unreliable and poorer device performance would have resulted had an oxdised boron doped material been used. Despite the success of fabricating devices, the origin of this surface effect has remained controversial. Hence, much effort has been focused on the characterisation of the highly conductive surfaces of CVD diamond and many useful observations have been obtained. A number of reports have proposed that the carriers arise through the formation of shallow acceptor states beneath the surface when hydrogen is present [Maki, 1993; Jiang, 1999; Hayashi, 1996]. Other studies suggested that it is surface band bending caused by surface termination of hydrogen leading to an accumulation of holes in this region [Shirafuji, 1996]. In the case of polycrystalline diamond films, several groups have also claimed that changes to the sp^2 (non-diamond) carbon may be responsible for variations in surface conductivity rather than directly or indirectly to the presence of hydrogen itself [Kulkarni, 1994; Muto, 1991]. To complicate the picture further, in the absence of surface hydrogen metal-diamond surfaces suffer from a 'pinned' Fermi level leading to Schottky barrier heights that are insensitive to both the work function and the electronegativity of the metal used [Gildenblat, 1991]. When hydrogenated, this pinning effect is removed and near ideal interfacial characteristics have been measured [Kawarada, 1994; Kiyota, 1996]. By selecting the appropriate metals, both Schottky (Al) and ohmic contacts (Au) can be realised on the similar surfaces as shown in figure 6.03.

The dependence of the room temperature conductivity on heat treatments on hydrogenated films has been observed previously. Landstrass *et al.* [1989] found that heating hydrogenated natural diamond and polycrystalline CVD material up to 360°C in a nitrogen ambient considerably increased the resistivity; the authors attributed this effect to changes in the type of gap states present in the material. However, Muto *et. al* [1991] suggested that the increase in resistivity when thin film (1μm) hydrogenated PCD was annealed results from the removal of disordered graphite. Changes in Raman spectra were presented to support their argument. However, in the current study no changes to the Raman spectrum could be detected and the removal of disordered sp^2 carbon seems unlikely to be the origin of the I-V modification seen here.

Adsorbed hydrogen is not expected to thermally desorb at the temperatures investigated here (< 200°C) [Chua, 1994]. This assertion is supported by the absence of significant new structures in the UPS spectrum as the sample is heated as shown in figure 6.13. The primary C1s and O 1s XPS peaks do not shift significantly upon heating, indicating that major changes to any band bending cannot be taking place. The small shifts in the XPS cannot be correlated to the the degree of oxidation on the surface as during the air anneal very little change in oxidation is occurring. The appearance of a high binding energy component to the C 1s peak can be attributed

to surface alcohol groups [Haasz, 1996]. The shoulder to the O 1s peak can be attributed to C-O species. If near surface shallow acceptor states are responsible for the carriers, then a more plausible explanation would involve thermally promoted redistribution of hydrogen and/or oxygen within the surface region. This could lead to a change in the number of activated states, resulting in a modified carrier concentration. The constant O/C ratio indicates that air annealing at these temperatures (<200°C) is not leading to significant oxidation of the diamond surface. The similarity in the I-V changes recorded when annealing was carried out in air and vacuum further support this assertion. The fact that the films became highly resistive, suggesting that the carrier concentration had decreased by many orders of magnitude once heated above 350°C (where adsorbed hydrogen would not be lost), further emphasises that band bending cannot explain the disappearance of the majority carriers measured in these films.

Shirafuji *et al.* [1995] and Kawarada *et al.* [1994] have proposed the band bending model to explain the accumulation of holes on the surface. They explained that hydrogen terminated diamond causes the energy of the valence and conduction band to bend upwards. The upwards band bending of the valence band at the surface is sufficient enough to dip above the Fermi level resulting in the accumulation of holes. However, the band bending reported by other workers on hydrogen terminated diamond appeared to be in the opposite direction which is downwards [Bachmann, 1996]. This clearly does not favour the accumulation of holes. The conduction and valence band for hydrogen terminated surfaces actually bend downwards, presumably due to the difference between the electronegativity of hydrogen and carbon, this model is also applied to describe the NEA properties which can be observed on these surfaces. Oxidised surfaces will promote upwards band bending and hence removing the effective NEA properties from the diamond surfaces [Baumann, 1998]. Conductivity measurements on oxidised diamond (homoepitaxial or polycrystalline) surfaces indicate near intrinsic resistivity hence band bending model cannot explained the origin of holes. Experimental results in section 6.4.4 did not show significant changes in the XPS or UPS spectra after the sample was annealed when changes in the conductivity is apparent. This enables the conclusion to be drawn that the band bending model was not the origin of the conductivity that was measured here.

On the other hand, experimental results in this study are consistent with the model proposed by Hayashi *et al.* [1996] based on the original suggestions of Landstrass *et al.* [1989]. They observed a near-surface hydrogen in SIMS and were able to associate this phase with a peak at 540nm in Cathodoluminescence studies [Hayashi, 1997]; this implied that the hydrogen was promoting the formation of gap states, some of which act as shallow acceptors leading to p-type diamond. The correlation found between the sheet resistance and carrier concentration with a reduction in near surface hydrogen from the SIMS profile in the absence of band bending measured here would appear to confirm that this is the primary origin of the hole concentration observed. Furthermore, Hall measurement indicate that ionised impurity scattering is dominating in this layer. SIMS and Schottky barrier height measurements indicate that the presence of adsorbed hydrogen on the surface is vital to improve the electrical quality of the electrical contacts by reducing Fermi level pinning and leakage currents. The nature of how hydrogen at the near surface can promote shallow acceptor states in diamond is an interesting

issue and worthy of further investigation.

Gi *et al.* [1995] suggested that the origin of the conductivity could be related to acidic and alkali environment. Under the acidic conditions, the conductivity was enhanced. On the contrary, the conductivity was reduced under alkali environment. The conductivity of the samples used in this experimental chapter could not be modified in the similar manner as suggested by Gi *et al.* [1995], provided that the experiment was carried out at room temperature. Furthermore, once the conductivity was lost, it could only be restored by exposing the surface to hydrogen plasma.

In order to clarify the mechanism of surface conductivity, the first step is to determine if hydrogen leads indirectly or directly to the formation of holes. On diamond surfaces, hydrogen forms a single strong covalent bond with carbon, as it has only a single electron and is paired up with the valence electron of the carbon. Hence, hydrogen does not have any free electrons left. C-H bonds are very strong and hydrogen is expected to desorb from the surface at temperatures exceeding 1000°C in a vacuum. At room temperature it is unlikely that these bonds can directly contribute to the formation of holes. Furthermore, if hydrogen is directly causing the formation of holes, then ion implantation of hydrogen ions into the diamond lattice should cause a considerable reduction in the resistivity. This is not the situation as implantation of large doses of hydrogen on a type IIa diamond causes disappearance of p-type characteristic [Kalish, 1997] most probably caused by radiation damage [Mainwood, 1998]. Therefore, it is more likely that hydrogen indirectly leads to the formation of acceptor states.

Another important point is that the p-type conductive layer only appears to exist at or near the surface not deep in the bulk and this is true regardless of the thickness of the diamond film. Device simulations by Noda *et al.* [1998] and Tsugawa *et al.* [1999] on homoepitaxial film and calculations from the transfer characteristic of the MESFET carried out for PCD (in Chapter 8) estimate the thickness of the channel to be less than 10nm. Hayashi *et al.* [1997] proposed a thickness of 20nm from their hydrogen SIMS profile. Using C-V measurements, Kiyota *et al.* [1996] suggested a thickness less than 50nm. Shirafuji *et al.* [1996] suggested it was around 2nm. Without the exact knowledge of how or what causes the conduction, at present it is difficult to accurately determine the thickness of this conductive layer. It is still not known how the thickness of this layer will vary with surface morphology, quality or for a material undergoing hydrogen plasma treatments under different conditions. The threshold voltages recorded from the MESFETs fabricated on two PCD films showed variations from -0.87V (300μm film) and +0.6V (100μm film) appear to support that different materials will lead to slightly different carrier profile or channel thickness (see Chapter 9).

A mechanism which leads to the generation of near surface holes should satisfy the following experimental observations :-

(a) The conduction is present on diamond which is grown using the CVD method but can be removed by heat treatments alone (this work).

(b) It occurs at or near the surface (<10nm) however not in the bulk [Tsugawa, 1998;

Noda, 1997] (see Chapter 9).

(c) Carriers are lost at temperatures as low as 150°C but this is not high enough to remove the hydrogen layer from the surface or cause significant oxidation (see section 6.4.4)

(d) Carriers are lost during anneal in high vacuum (see section 6.4.2)

(e) Carrier transport properties of holes are governed by ionised impurity scattering at low [Jiang, 1999] and high temperature (up to 200°C) (see section 6.4.2)

(f) Schottky barrier height measured on these surfaces were dependent on the electronegativity of the metal deposited [Kawarada, 1994; Mori, 1991] (see chapter 7)

(g) An exposure to hydrogen plasma following heated oxidation will restore the conductivity (see chapter 8).

(h) The conduction indirectly related to hydrogen as type IIa diamond implanted with hydrogen show a decrease in conductivity [Kalish, 1997].

The surface conductive layer exists on the growth surface of the diamond grown under the CVD process and is more prominent for samples grown using the microwave plasma method. In addition, it is very thin (<10nm), exists on the top surface regardless of the thickness of the bulk material. This suggests that it could be related to the way the diamond is grown. Hydrogen plays an important role in the kinetic growth of diamond in the CVD process. It stabilises the dangling bonds of carbon on the surface and at the same time allows the addition of methyl groups. The carbon atom from these groups will have to rearrange, loses all its hydrogen and eventually transform into bulk crystalline diamond. Throughout this process, hydrogen also plays an important role by suppressing the formation of sp^2 phase. During the transformation into diamond and restriction caused by steric hindrance, it is possible that some of these dangling bonds are unable to be terminated by hydrogen atom. The incomplete diamond layer will always exist on and near the surface. It could be this layer where the carriers originate from. The partially formed diamond structure with uncompensated dangling bonds may give rise to shallow surface states which supply the holes detected by Hall effect measurements. The more complete diamond structure exists in the bulk. With a growth temperature around 900°C and without the supply of atomic hydrogen from the plasma some of the C-H bonds will recombine with a dangling bonds releasing the hydrogen atom to the surface. The incomplete diamond structure has rearranged to form diamond. Hence, as diamond is formed from the intermediate carbon atoms, the dangling bonds recombine, removing the surface states which could result in the disappearance of holes. This satisfies the reasoning that the conductive layer has to be thin, always exists on the surface and at the same time requires high temperature plus an atomic rich hydrogen atmosphere to produce. At high temperature, without a hydrogen plasma, the dangling bonds near or at the surface are encouraged to recombine with a dangling bond or a C-H. Once this occurs, there is no atomic hydrogen to reverse the process hence carriers are gradually lost. After growth, the structure of carbon atoms on and near the surface is unlike those in the bulk. It could be the thickness of this layer which is related to the thickness of the surface conductive layer. The stabilisation of the carrier concentration at each temperature level may suggest that there are certain states which are more susceptible to heat and prone to restructuring or modification at lower temperatures and others which are more stable will require a higher temperature anneal. Nevertheless, as the temperature is increased the rate of loss of carriers

decreases with an exponential trend. The presence of this layer was indicated by Mori *et al.* [1993] using an electron spin resonance (ESR) method. In addition, Won *et. al.* [1996] have employed photoluminescene to study CVD films subsurface regions (~4nm). They found that the subsurface contains a substantially higher density of intrinsic point defects. On the diamond surface, oxygen will require 2 covalent bonds to be stable. Hence, terminating the diamond surface with oxygen could remove the dangling bonds which are available at the surface or subsurface. The mechanism proposed here is also in agreement with model proposed by Jiang *et al.* [1999] which speculates that this conduction is closely related to the complexes of the hydrogen atoms with the carbon-dangling bonds in the diamond subsurface region.

Section 6.7 Conclusion

A wide range of scientific techniques have been used simultaneously to study the properties of the p-type hydrogen related surface conduction on as-grown PCD films. SIMS results indicate that as-grown PCD has a relatively high near surface concentration of hydrogen, presumably due to the way in which the CVD growth is typically terminated. Raman spectra showed that these films were of high quality and the conduction detected can not be due to graphitic phases in the surface or at the bulk. Hall measurements indicate that polycrystalline material can also support holes in which the levels of sheet carrier concentration is similar to those recorded on homoepitaxial material. Heating the film to 200°C provoked some loss of carriers from the surface. Prolonged treatment in air ceased to cause further changes and the carriers appear to be stabilised. Similar trends were observed for samples treated and characterised in high vacuum. The sheet carrier concentration in these as grown films were approximately $10^{13}cm^{-2}$ with a Hall mobility of around $15cm^2/Vs$ for WM60 and $30cm^2/Vs$ on BD8. The transport properties in these films were governed by the ionised impurity scattering mechanism with a Hall mobility depending on the positive power of temperature ($\sim T^{1.8}$). The current study shows that it is hydrogen within the diamond that indirectly gives rise to the carriers, shallow acceptor states and possibly other deeper gap states. It is not possible to determine the activation energy of the carriers from the temperature range used during the Hall measurement indicating that it is very small. A simple mechanism based on surface states or holes indirectly related to hydrogen which arise through an incomplete diamond structure at the surface which may include dangling bonds and lone pairs of electrons have been proposed. The proposal is just a hypothesis which might explain observations from experimental results. However, the exact nature of these shallow acceptor states remain unresolved and more research is necessary.

The Hall measurement confirmed the existence of holes on the near surface of hydrogen terminated PCD films with good mobility values and complete ionisation at room temperature. More importantly, there is a new source of carriers which can be utilised apart from the conventional impurity dopant, boron. The next few chapters will concentrate on exploiting the conductive layer for electronic device applications. There is a possibility that the performance of electronic devices fabricated on polycrystalline films can be improved.

References:-

Bachmann, P.K., Eberhardt, W., Kessler, B., Lade, H., Radermacher, K., Wiecher, D.U. and Wilson, H. [1996] Diamond & Relat. Mater., **5**, 1378.

Bardeen, J. [1947] Phys. Rev. **71**, 717.

Baumann, P.K. and Nemanich, R.J. [1998] Diamond & Relat. Mater., **7**, 612.

Bobrov, K., Shechter, H., Folman, M. and Hoffman, A. [1998] Diamond & Relat. Mater., **7**, 170.

Chan, S.S.M. [1996] Ph.D. Thesis University of London, chapter 5.

Chua, L.H., Jackman, R.B., Foord, J.S., Chalker, P.R., Johnston, C. and Romani, S. [1994] J. Vac. Sci. Tech., **12**, 3033.

Diederich, L., Kuttel, O.M., Schaller, E. and Schlapbach, L. [1996] Surf. Sci., **349**, 176.

Fox, B.A., Hartsell, M.L., Malta, D.M., Wynands, H.A., Kao, C.-T., Plano, l.S., Tessmer, G.J., Henard, R.B., Holmes, J.S., Tessmer, A.J. and Dreifus, D.L. [1995] Diamond & Relat. Mater., **4**, 622.

Gi, R.S., Mizumasa, T., Akiba, Y., Hirose, Y., Kurose, T. and Iida, M. [1995] Jpn. J. Appl. Phys., **34**, 5550.

Gildenblat, S.Sh., Grot, S.A. and Badzian, A., [1991] Proceedings of the IEEE, **79**, 647.

Gluche, P., Aleksov, A., Vescan, A., Ebert, W. and Kohn, E. [1997] IEEE Electron Device Lett., **18**, 54

Grot, S.A., Gildenblat, G.Sh., Hatfield, C.W., Wronski, C.R., Badzian, A.R., Badzian, T. and Messier, R. [1990] IEEE Electron Device Lett., **11**, 100.

Haasz, K. et al. [1996] J. Vac. Sci. Tech., **A 14**, 189.

Hayashi, K., Yamanaka, S., Okushi, H. and Kajimura, K. [1996] Appl. Phys. Lett., **68**, 376.

Hayashi, H., Watanabe, H., Yamanaka, S., Sekiguchi, T., Okushi, H., and Kajimura, K. [1997] Diamond & Relat. Mater., **6**, 303.

Hokazono, A., Ishikura, T., Nakamura, K., Yamashita, S. and Kawarada, H. [1997] Diamond & Relat. Mater., **6**, 339.

Jiang, N. and Ito, T. [1999] J. Appl. Phys., **85**, 8267.

Kalish, R., Uzan-Saguy, C., Philosoph, B. and Richter, V. [1997] Appl. Phys. Lett., **70**, 999.

Kawarada, H., Aoki, M., Sasaki, H. and Tsugawa, T., [1994] Diamond & Relat. Mater., **3**, 961.

Kawarada, H., Sasaki, H. and Sato, A. (1995) Phys. Rev. B **52**, 11351.

Kimura, A., Nakatani, Y., Yamanada, K. and Suzuki, T. [1999] Diamond & Relat. Mater., **8**, 37.

Kiyota, H., Okushi, H., Ando, T., Kamo, M., Sato, Y. [1996] Diamond & Relat. Mater., **5**, 718.

Kulkarni, A.K., Shrotriya, A., Cheng, P., Rodrigo, H., Bashyam, P. and Keeble, D.J. [1994] Thin Solid Films, **253**, 141.

Landstrass, K.I., and Ravi, K.V., [1989] Appl. Phys. Lett., **55**, 1391.

Maki, T., Shikama, S., Komori, M., Sakaguchi, Y., Sakuta, K. and Kobayashi, T. [1992] Jpn. J. Appl. Phys., **31**, 1363.

Mainwood, A. [1998] Diamond & Relat. Mater., **7**, 504.

Mori, Y., Kawarada, H. and Hiraki, A. [1991] Appl. Phys. Lett., **58**, 940.

Mori, Y., Show, T., Deguchi, M., Yagi, H., Yaghu, H., Eimori, N., Okada, T., Hatta, A., Nishimura, K., Kitabatake, M., Ito, T., Hirao, T., Izumi, T., Sasaki, T. and Hiraki, A. [1993] Jpn. J. Appl. Phys., **32**, 987.

Muto, Y., Sugino, T., Shirafuji, J. and Kobashi K. [1991] Appl. Phys. Lett., **59**, 843.

van der Pauw, L.J. [1958] Philips Res. Rep **13**, 1

Shiomi, H., Nishibayashi, Y. and Fujimori, N., [1991] Jpn. J. Appl. Phys., **30**, 1363

Shirafuji, J. and Sugino, T. [1996] Diamond Relat. Mater., **5**, 706.

Stallcup, R.E., Aviles, A.F. and Perez, J.M. [1995] Appl. Phys. Lett., **66**, 2331.

Streetman, B.G. [1995] "Solid State Electronic Devices", Prentice Hall Int. Ed., New Jersey, Chapter 3.

Sun, B., Zhang, X., Zhang, Q. and Lin, Z., [1993] Appl. Phys. Lett., **62**, 31.

van der Pauw, L.J. [1956] Phil. Tech. Rev., **20**, 220.

Won, J.H., hatta, A., Ito, T., Sasaki, S. and Hiraki, A. [1996] Appl. Phys. Lett., **69**, 4179.

Yun, Y., Maki, T. and Kobayashi, T. [1997] J. Appl. Phys., **82**, 3422.

Chapter 7

The Properties of Metal-Semiconductor Contacts on Polycrystalline CVD Diamond

Contents

Section 7.1 Introduction

The properties of metal-semiconductor contacts have been extensively studied on natural [Mead, 1976; Humpreys, 1991], homoepitaxial [Gildenblat, 1991] and CVD diamond [Hicks, 1989; McKeag, 1995]. Metal contacts deposited on single crystal diamond (natural and homoepitaxial) normally display better Schottky characteristics in terms of a lower ideality factor and a higher rectification ratio [Vescan, 1997; Gildenblat, 1990; Kiyota, 1995] compared to polycrystalline material [Miyata, 1991; Chan, 1995]. The large defect density associated with irregular grains was believed to be responsible for the degradation of Schottky characteristic. On the other hand, it is easier to fabricate low resistivity ohmic contacts on polycrystalline films. The defective film coupled with sharp peaks promote regions of high electric field which favour

tunneling of carriers. In addition, the formation of a defective interface between the metallisation contacts and semiconducting diamond were useful for realising ohmic contacts due to the Schottky barrier height (SBH) lowering of the metallisation contact [Tachibana, 1992; Werner, 1996].

The use of an insulating layer in the form of a thin intrinsic diamond layer (MIS) or SiO_2 (MOS) layer sandwich between the metal contacts and semiconductor have shown to enhance the rectification ratio of a diode by significantly reducing the reverse bias leakage current [Miyata, 1992]. However, this inevitably reduces the forward current as well. Boron is currently the only established dopant on both polycrystalline diamond and single crystal diamond [Malta, 1993]. Prototype boron doped devices on homoepitaxial and natural diamond operate effectively at temperatures up to 700K [Fox, 1995]. Device performances degrade progressively at lower temperature as the dopant has a large activation energy (E_A = 0.37eV). Recently with the introduction of a delta doped channel, the performance of devices on homoepitaxial films in the lower temperature region have been improved [Ebert, 1998].

The effectiveness of boron doping on the more commercially available material, polycrystalline CVD diamond, remains very poor in terms of success in fabricating electronic devices. Schottky devices fabricated from this material suffer from large leakage current [Hicks, 1989]. Devices fabricated normally require an insulating layer to partially overcome the problem. The large leakage current prevents accurate assessment of the Schottky barrier height and ideality factor through electrical characterisation methods. Tachibana *et al.* [1992] and Baumann *et al.* [1998] have used XPS and UPS measurements to determine the Schottky barrier height of metallisation contacts on these films. However, this method can only be conducted under an ultra high vacuum environment (UHV) with a metallisation of thickness less than 1nm. The difficulty in fabricating simple devices explains the lack of interest in this material which is cheaper and offers the advantage of availability over a large area for active diamond electronics. This situation was further aggravated by the low mobility of carriers on PCD films caused by scattering centers especially at the grain boundaries [Fox, 1994].

A new approach to doping diamond using a surface conductive p-type layer has emerged [Kawarada, 1994(b); Hayashi, 1997] as discussed in chapter 6. Point and thermally deposited metal contacts on this doping layer for homoepitaxial diamond films display good room temperature characteristics [Kawarada, 1994(a)]. The Schottky barrier height of point Schottky contacts on these films showed dependency on the electronegativity of the metal points used. For example aluminium and lead contacts form a good Schottky characteristic while Au forms a near ohmic contact [Kawarada, 1994(a)]. These combinations have been used to fabricate Schottky diodes which display an ideality factor of 1.1 and operate effectively at room temperature. Boron doped diamonds which were cleaned in a strong oxidising mixture of H_2SO_4 and CrO_3 do not display this characteristic [Kiyota, 1995]. Schottky characteristics of oxidised boron doped films suffer from Fermi level pinning, as a result a typical barrier height of 1.0 to 2.0eV had been reported for Au depending on the measurement techniques and quality of material. In contrast, Au consistently formed good ohmic characteristics on hydrogenated surfaces although the actual

barrier height of Au is not available through electrical characterisation in the literature on as-grown PCD films. Some workers assumed that it could be close to zero based on extrapolation[Kawarada, 1994]. Thermally deposited metal contacts do not display the dependency of metal electronegativity nor work function on oxidised, hydrogenated nor on surfaces which are free of foreign terminating species as pointed out by Baunmann *et al.* [1998]. The Schottky barrier height obtained through UPS measurement indicates the barrier height is the lowest on cleaned surfaces followed by hydrogen terminated surfaces and is the highest on oxidised surfaces [Baunmann, 1998].

The electrical properties of metal-semiconductor contacts on hydrogen related p-type layers has not been thoroughly investigated on polycrystalline CVD diamond (PCD). It will be an advantage if this form of conductive layer can be introduced as the current device performance is poor on this material. This alternative dopant may turn out to be more reliable than the only one that is currently available.

Section 7.2 Experimental Aims

In the previous chapter, the Hall measurements revealed that the surface conductive layer exists on polycrystalline CVD diamond and is p-type in nature. In addition, a sheet carrier concentration of 2 x 10^{13} holes/cm^2 with a Hall mobility of around 30 cm^2/Vs have been measured at room temperature. In this chapter, on samples obtained from the same wafer, the rectification properties of different metallisation contacts thermally deposited on as grown surfaces were investigated. The six different types of metal which were deposited are Al, Ti, Au, Sn, Ag and Ni. Electrical characterisation in the form of current-voltage (I-V) testing was employed to determine the properties of these contacts. In addition, high temperature operation of Al Schottky diodes on samples which have been stabilised in air will be presented at room temperature and in steps of temperature up to 200°C. The electrical properties of Al Schottky contacts for a range of temperature will be assessed and correlated with the data from the Hall measurements conducted under similar conditions.

Section 7.3 Formation & Current Injection Mechanism of Schottky Contacts

Metal-semiconductor contacts can achieve many of the useful rectification properties of a p-n junction. This type of contact offers simplicity in fabrication steps as only a single type of dopant is required (either p or an n-type), it has lower turn on voltage and much faster switching speed due to the reduction of the charge storage effect. This method is well suited for diamond electronics as n-type doping has not been well established. However, this device has a larger reverse bias leakage current compared to a p-n junction. Furthermore, the leakage characteristics normally depend on the quality of the metal semiconductor interface and the doping level in the semiconductor.

The energy band diagram of a metal and an n-type semiconductor are shown in Figure 7.01(a). The Fermi level of the n-type semiconductor is much higher than the Fermi level of the metal. According to the Schottky Mott theory [Rhoderick, 1988], neglecting the presence of interface surface states, when the metal and semiconductor are connected, electrons will diffuse from the conduction band in the semiconductor into the metal until the two Fermi levels coincide. The net flow of electrons is caused by the presence of empty lower energy states in the metal. The negative charge on the surface of the metal will be balanced by the uncompensated positive donors ions in the semiconductor. The equilibrium contact potential V_o will prevent further net diffusion of electrons into the metal. The potential experienced by the electrons from the metal injecting into the semiconductor is known as the Schottky barrier height. When a forward bias voltage V is applied to the Schottky barrier the contact potential V_o is reduced to V_o - V. The electrons from the n-type region will see a smaller barrier, this will give rise to a forward current. Conversely, when a reverse bias is applied the contact potential is increased to $V_o + V_r$ and the electrons in the semiconductor will experience a bigger barrier and current will not flow. The height of the Schottky barrier is not affected by the application of a bias prohibiting electrons diffusing from the metal to the semiconductor. The electron flow dominates the current in either direction and these majority carrier devices are known as unipolar devices.

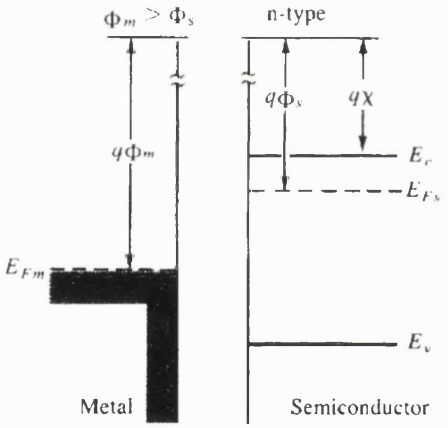

Figure 7.01(a)

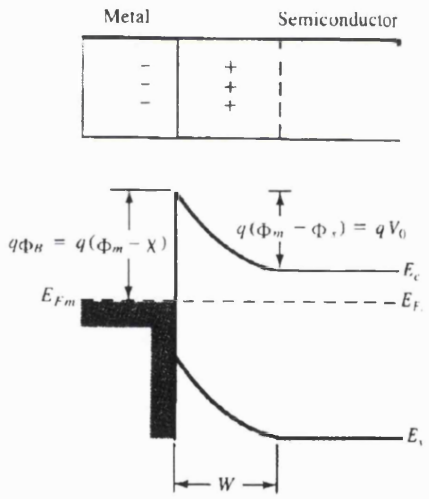

Figure 7.01(b)

Figure 7.01(a) shows the band diagram of the metal and n-type semiconductor separated by a distance and Figure 17.01(b) shows the band diagram when both are in contact.

The Schottky barrier height of a p-type semiconductor is given by

$$\phi_b = E_g - (\phi_m - \chi)$$

while for the n-type is

$$\phi_b = \phi_m - \chi$$

where

χ is the electron affinity of the semiconductor
ϕ_b is the Schottky barrier height
ϕ_m is the work function of the metal

The maximum electric field strength in an abrupt junction is given by

$$E_{max} = \frac{qN_A x_p}{\varepsilon_s}$$

where $N_A.x_p$ can be replaced by the sheet carrier concentration

Under forward bias, there are various ways that electrons can be transported across a metal-semiconductor junction. The mechanisms are :-

(a) Emission of electrons from the semiconductor over the top of the barrier into the metal
(b) Quantum mechanical tunneling through the barrier
(c) Recombination in the space charge region
(d) Recombination in the neutral region.

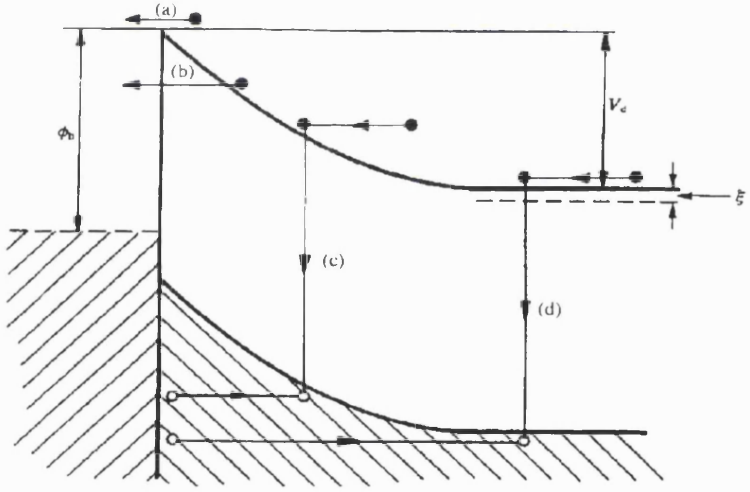

Figure 7.02 Electrons emission across the metal-semiconductor interface [Schroder, 1990].

Under the normal operation mode, if current flows this occurs only because of mechanism (a), and such diodes are generally referred to as nearly ideal. In this chapter, this mechanism is the dominating one which governs most of the flow of current under forward bias. However, under reverse bias mechanism (b) was sometimes observed especially at high carrier concentration and high electric field. Mechanism (a) is in accordance to Bethe's thermionic emission theory, which states that the current limiting process in a metal semiconductor interface is the actual transfer of electrons across the interface [Bethe, 1947]. The inverse process, under reverse bias is analogous to the injection of electrons from the metal into the vacuum but with the barrier height replacing the metal work function. Based on this basic principle, for a semiconductor with a spherical constant-energy surface, the current density due to electrons

passing from the semiconductor into the metal is given by :-

$$J_{sm} = \frac{pqN_c\bar{v}}{4} \exp\{ -q(\phi_b - V)/kT \} \quad \text{.....(equation 7.1)}$$

where $\bar{v}$ is the average thermal velocity of electrons in the semiconductor

p is the fraction of electrons which can tunnel into the metal

ϕ_b is the Schottky barrier height

k is the Boltzman constant

V is the external bias applied

N_c is the effective density of states in the conduction band

T is the temperature in K

J is the current density

Another component of current consists of electrons flowing from the metal to the semiconductor which is unaffected by the application of a bias is given by :-

$$J_{ms} = \frac{pqN_c\bar{v}}{4} \exp(-q\phi_b/kT) \quad \text{.....(equation 7.2)}$$

For zero bias, the current flow from both directions must balance out hence :-

$$J = J_{sm} - J_{ms}$$

$$= \frac{pqN_c\bar{v}}{4} \exp(-q\phi_b/kT) \{ \exp(qV/kT) - 1 \}$$

assuming that $p = 1$, and $N_c = 2(2\pi m^* kT/h^2)^{3/2}$, substituting into the equation above gives the current-voltage characteristic according to the thermionic-emission theory as :-

$$J = A^* T^2 \exp(-q\phi_b/kT) \{\exp(qV/kT) - 1\} \quad \text{.....(equation 7.3)}$$

where $A^* = 4\pi m^* qk^2/h^3$

$= 1.2 \times 10^6 (m^*/m_e)$ $Am^{-2}K^{-2}$

m^* is the effective electron mass in the semiconductor

A^* is also known as the Richardson constant

h is the Planck constant

m_e is the mass of an electron

Equation 7.3 is normally written in the form of

$$J = J_o \{ \exp\left(\frac{qV}{nkT}\right) - 1 \} \quad \text{.....(equation 7.4)}$$

where n is often called the 'ideality factor'. Equation 3 ignores the effect of image force lowering of the Schottky barrier height [Rhoderick, 1988]. Under ideal conditions, n has a value of 1. Normally, the metal semiconductor interface deviates from the ideal conditions, in this case, n will be larger than 1.

The Schottky barrier height of the metal semiconductor interface can be measured by a number of different methods. One of the simplest method is to determine the leakage saturation current (I_s). This value can be obtained by extrapolating the ln I versus V curve to V = 0. The Schottky barrier height ϕ_b can then be calculated from the equation given below :-

$$\phi_b = \frac{kT}{q} \ln\left(\frac{AA^*T^2}{I_s}\right) \qquad \text{.....(equation 7.5)}$$

Section 7.4 Experimental Methods

The free standing PCD films used for this experiment were grown by a standard microwave enhanced CVD reactor with a microwave power of about 4kW. The film was deposited on top of a silicon substrate. Later, the silicon substrate was removed using a hydrofluoric solution. The growth chamber has been used only for growing intrinsic diamond, hence there would not be any memory effects cause by residual traces of boron which is left in the chamber. Three types of diamond films were used here, BD8 which is approximately 300μm thick , WM60 is about 100μm thick and WM40 which was laser cut and then rehydrogenated. All the films were grown under similar condition. BD8 comprised of randomly aligned grains with an average grain size of about 30 - 60μm while WM60 and WM40 were oriented in the same manner but with a smaller grain size of about 10 - 30μm. The Raman spectra of these films displayed a sharp single peak at 1332cm^{-1} with undetectable structures in regions which are associated with non diamond carbon. This indicates a relatively good quality diamond film. The Raman spectra were obtained using a red He-Ne laser at a wavelength of 632.8nm. The red laser is very sensitive to the presence of non diamond carbon bonds.

The BD8 and WM60 films were not subjected to heat treatment or cleaned in strong oxidising solution which may modify the as-deposited surface conductive properties. Prior to metal deposition, the samples were de-greased according to the method described in Appendix 1. This degreasing step served only to remove contamination caused by poor handling and atmospheric contaminants when the material was outside the clean room. Metal deposition was performed by using a resistive thermal evaporator (Edwards 306). The pressure of the chamber before evaporation was below 10^{-6} mbar. In the preliminary study, the rectangular metallisation structures on the sample were defined by shadow masking with a clean wire. Later, a proper metal mask was designed and used instead. The method employed for defining the metallisation structure will not affect the electrical properties of the device. The typical contact dimension was 3.5 x 0.7mm separated by about 0.5mm. Current-voltage (I-V) measurements were performed in

a probe station using HP 4145B semiconductor parameter analyser.

Section 7.5.1 Experimental Results : Metallisation contacts on as-grown surfaces.

In the preliminary study, Au contacts were thermally deposited on the growth side of an as grown sample and an acid cleaned sample from wafer BD8. This experiment was performed to compare the conductivity of the material when it is as grown and acid treated. I-V tests were carried out at room temperature between adjacent Au contacts. The curves in figure 7.03 reveal near linear characteristics for the as grown sample with current levels in the mA range indicating the formation of ohmic contacts. However, current in level of pA was detected when similar Au contacts were tested on the samples which had been acid cleaned as described in Appendix 1. Hence, a current variation of almost 9 orders of magnitude was obtained for Au contacts between the as grown and the acid cleaned samples. The properties of Au contacts on this surface conductive layer had not been thoroughly investigated in the literature; a more comprehensive study of Au contacts will be presented in chapter 8.

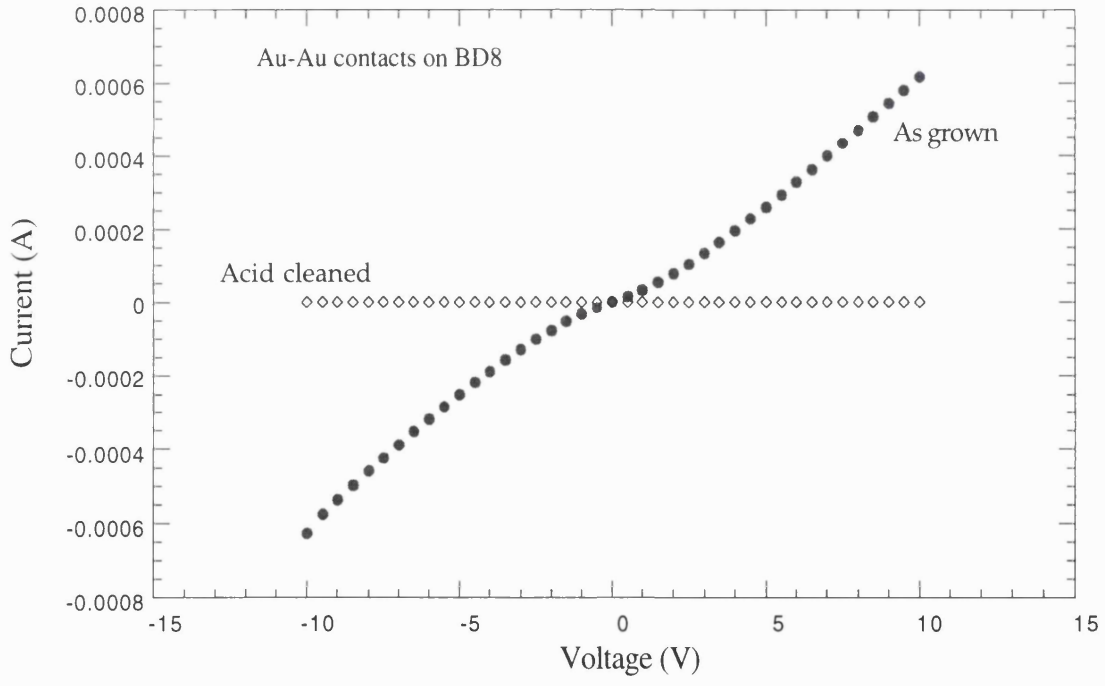

Figure 7.03 The I-V characteristics between Au contacts on as grown and acid cleaned BD8

Later, Al contacts were thermally deposited adjacent to the Au contacts on the as grown samples. The I-V curves of the Al-Au contacts are shown in figure 7.04. Application of negative voltage on the Al contact (Schottky) with respect to Au (ohmic) results in current level of mA. However, current level less than 1nA was recorded if a positive voltage is applied instead. This can be explained using Bethe's thermionic field emission theory. As the surface conductive layer

is p-type, applying a negative potential on the Al contact with respect to the ohmic (Au) reduced the built in potential at the Al | diamond interface seen by the holes in the conductive channel. At a higher negative bias, the built in potential will be lowered to a point where the holes from the channel will have enough energy to diffuse across the barrier resulting in a large forward bias current. This occurred when the bias was about -0.7V. If a positive voltage is applied on the Al contact, the height of the built in barrier will be increased. The holes in the channel will not have sufficient energy to jump cross this barrier. As a result, very little current will flow and the device is operating in the reverse bias mode.

The voltages shown in all the plots were applied on the Schottky contact itself measured with respect to the ohmic contact. Hence, in this situation, a negative bias applied on the Schottky contact is necessary to switch on the Schottky diode fabricated from a p-type semiconductor.

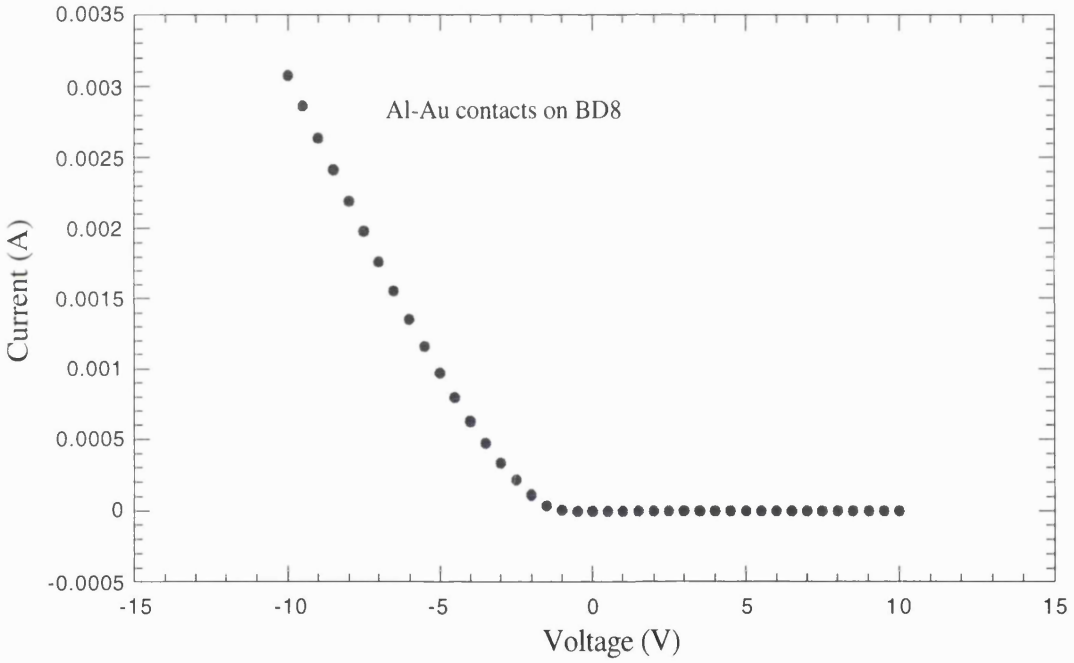

Figure 7.04 Rectification I-V characteristic between Al-Au contacts on as grown BD8.

By just placing Au and Al contacts adjacent to each other on the growth side, a simple planar Schottky diode has been fabricated. Similar structures were then tested at higher voltages to measure the reverse bias voltage blocking capability of this diode.

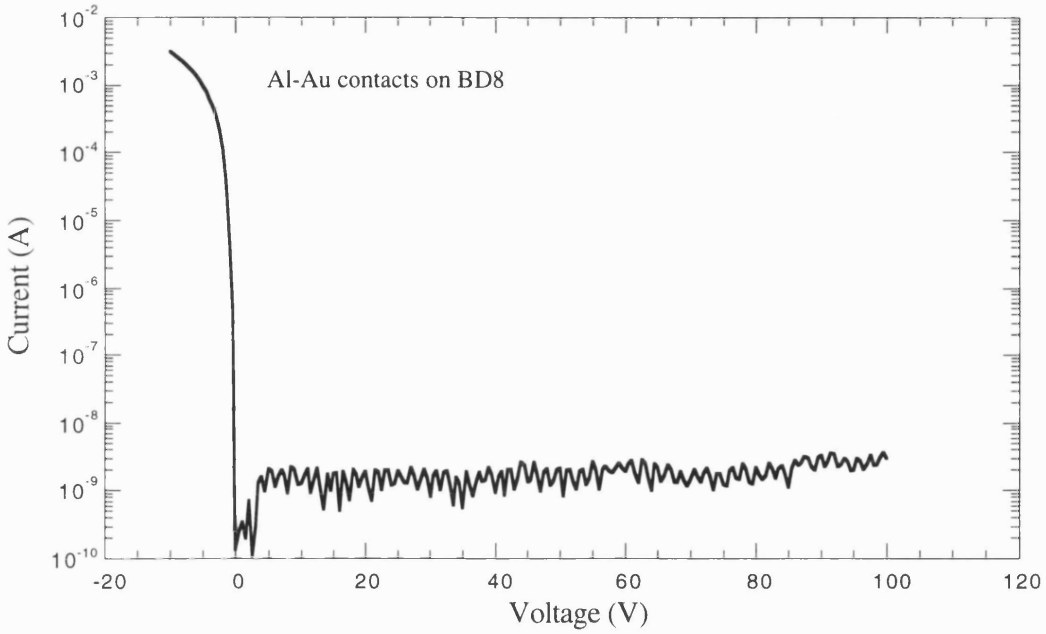

Figure 7.05 Log current against voltage plot of Al-Au contact on BD8 indicating the reverse bias leakage current and its blocking capability.

In figure 7.05, the plot of I against V shows that this diode has a blocking capability of more than 100V without any apparent sign of breakdown. The leakage current was within the nA region with a forward current in the mA levels at 10V.

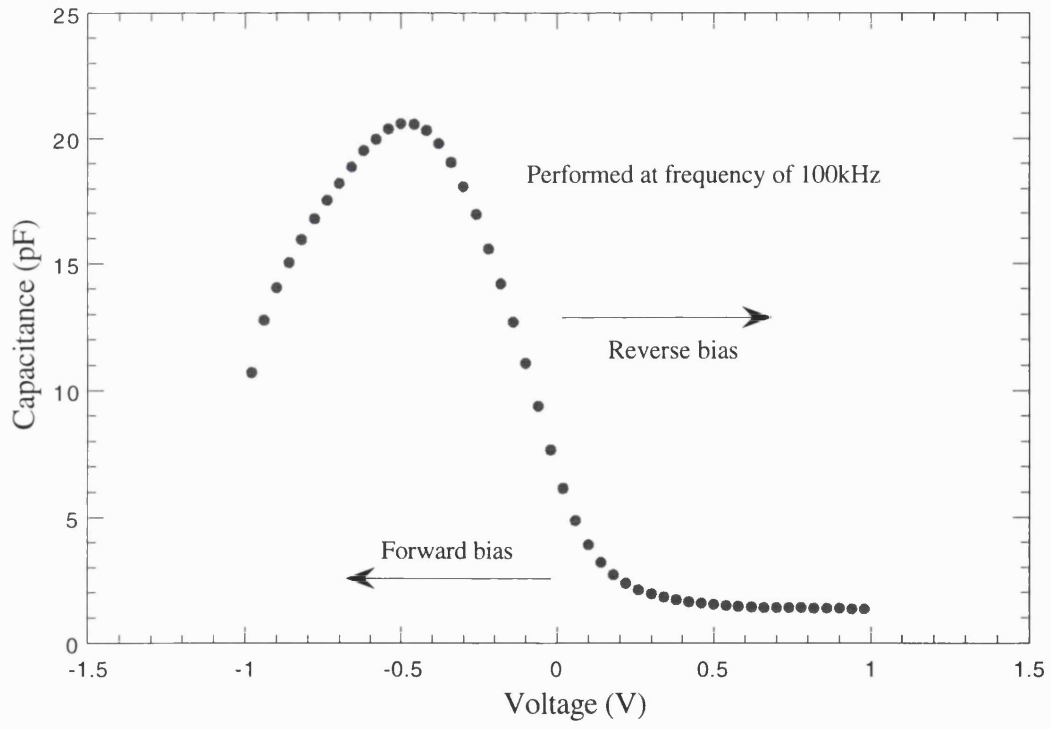

Figure 7.06 The capacitance voltage curve of the Al-Au diodes on as grown BD8 taken at a frequency of 100kHz

The capacitance against voltage plot in figure 7.06 showed changes in the depletion region width when the bias on the sample was swept from positive to negative. For a p type channel, the Schottky diode will be under forward bias if the Schottky contact (Al) is negatively biased with respect to the ohmic (Au). From the C-V plot, the capacitance under forward bias is larger than when under reverse bias. The depletion width under the Al contact will decrease with increasing negative bias (forward bias). The decrease in the depletion width will result in an increase in the capacitance as capacitance is inversely proportional to the width of the depletion region. However, from the plot the capacitance ceased to increase further at about -0.5V. At this point the large forward bias current flowing across the device may cause the reverse bias capacitance to be very leaky. It is difficult to determine the doping profile from this C-V curve as the Schottky diode tested here is in a planar configuration and fabricated on a polycrystalline material where the surface roughness is a few orders of magnitude larger than the thickness of the doping layer. Furthermore, the electric field strength and its direction will not be uniform on a randomly oriented surface. For increasing positive bias, the capacitance appeared to saturate above 1.0V. As the carrier concentration in the channel is high (~5 x $10^{18}cm^{-3}$), the lateral spread of the depletion is very small compared to the area of the Al contact therefore only a small decrease in capacitance in recorded.

The tungsten probes on the probe station formed low resistive contacts on the as grown BD8 and WM60. Although there were numerous studies which showed good rectifying characteristic using point Schottky contacts made from different metal, the I-V characteristics of the probes in figure 7.07 showed otherwise. This result proved to be beneficial especially when the probes can be readily used as a rough and quick assessment to inspect the current levels in this conductive layer.

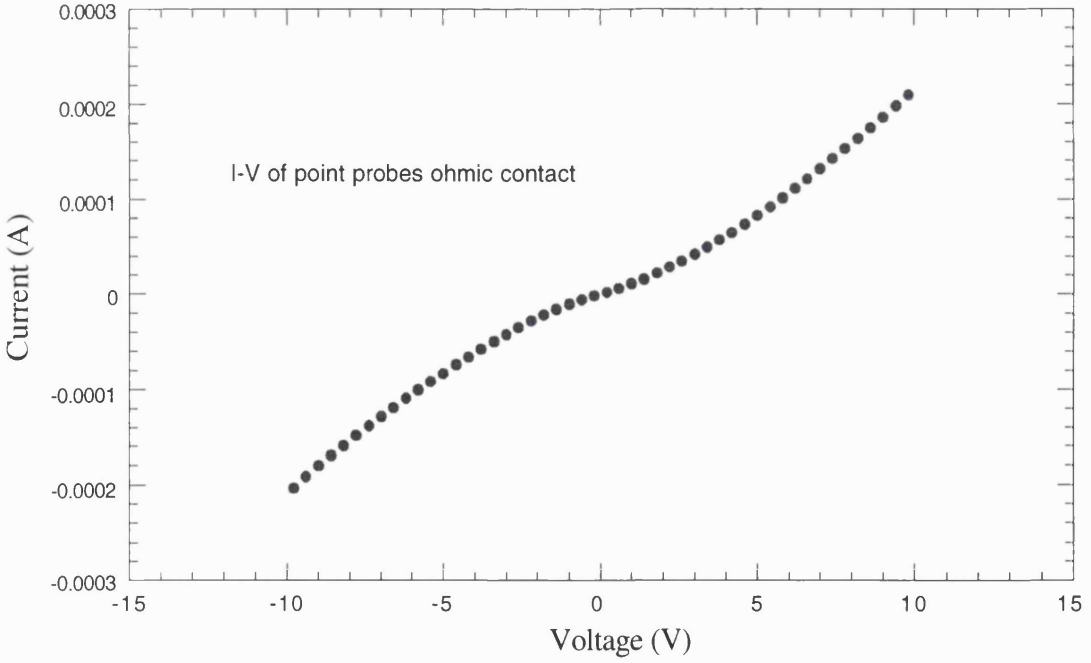

Figure 7.07 I-V plot of point probes on as grown BD8

Al and Au contacts were deposited on another free standing smaller grain size wafer WM60. Good rectification characteristics were recorded at low voltages, however at higher voltages the I-V curves in figure 7.08 revealed evidence of reverse breakdown occurring at 40V and another one at 80V. This could imply that the breakdown was occurring at different regions on the metal semiconductor interface. This observation is most probably caused by the high electric field strength at sharp peaks which will lead to field emission currents. An early work by Gildenblat *et al.* [1991] also revealed the presence of a non uniform defective sites in the PCD film which explained the non uniform leakage current in their Schottky diodes.

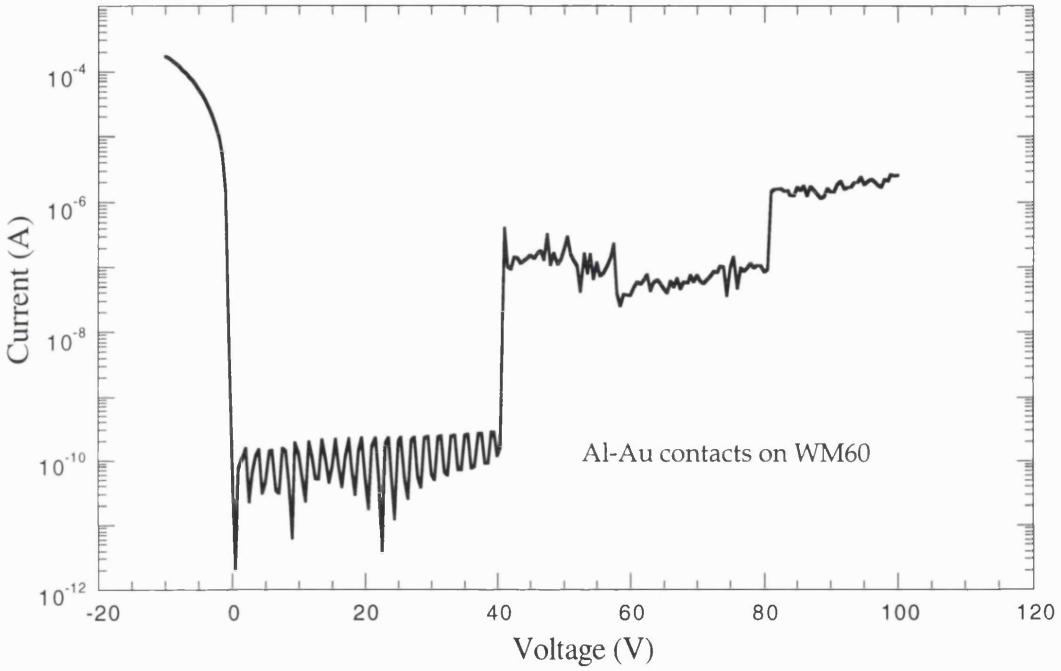

Figure 7.08 The forward and breakdown characteristics of Al-Au contact on as grown WM60

The properties of other metallisation contacts on hydrogen terminated diamond were next investigated. In general, the reverse leakage current of these Schottky diodes were much higher compared to the Al diodes. The use of point contacts as the ohmic results in the high series resistance observed under forward bias. However, under reverse bias, the I-V characteristics will be dominated by the properties of the Schottky contact.

Ni contacts displayed the second best rectification characteristic on WM60. Ni was chosen as it has a work function which is quite similar to Au. In addition, Ni has a much lower electronegativity compared to Au [Rhoderick, 1988]. Rectification characteristics of nickel contacts on oxidised boron doped polycrystalline CVD diamond have been reported [McKeag, 1995]. The I-V measurements in figure 7.09 show strong rectification properties with a leakage current of less than 10nA and a rectification ratio of about 4 orders of magnitude taken at ±10V.

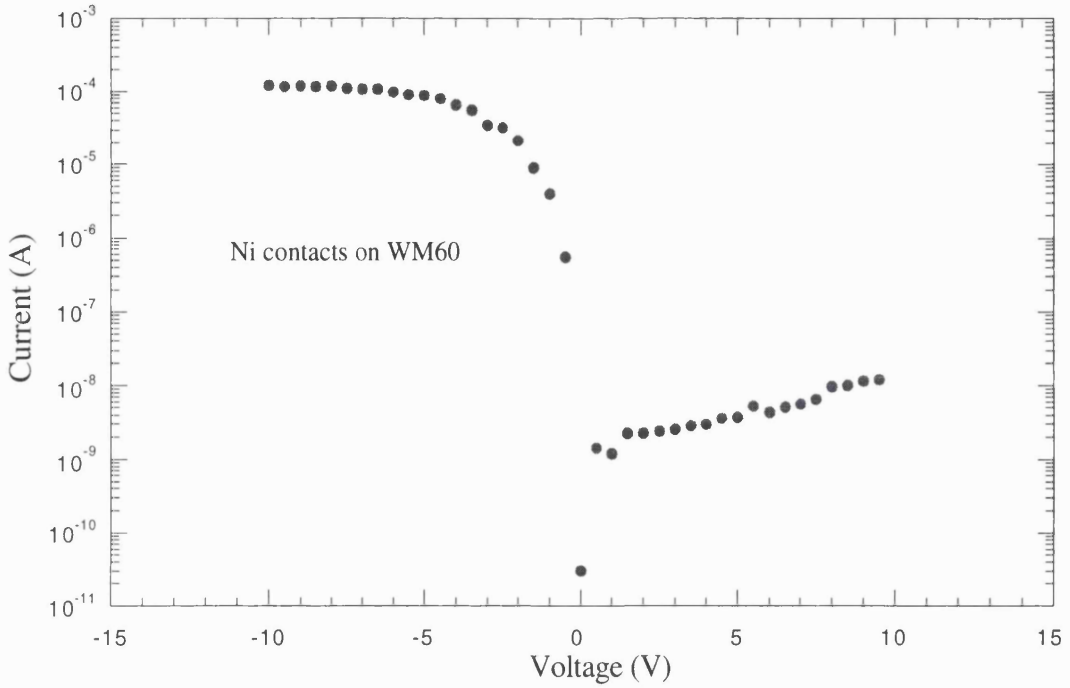

Figure 7.09 I-V characteristics of Ni-Au contacts on as grown WM60.

The rectification characteristics obtained from tin contacts were displayed in figure 7.10. Mild reverse breakdowns were observed at 18V, 33V and 45V. The breakdown characteristic was similar to the one observed for Al contacts except that it occurs at different voltages.

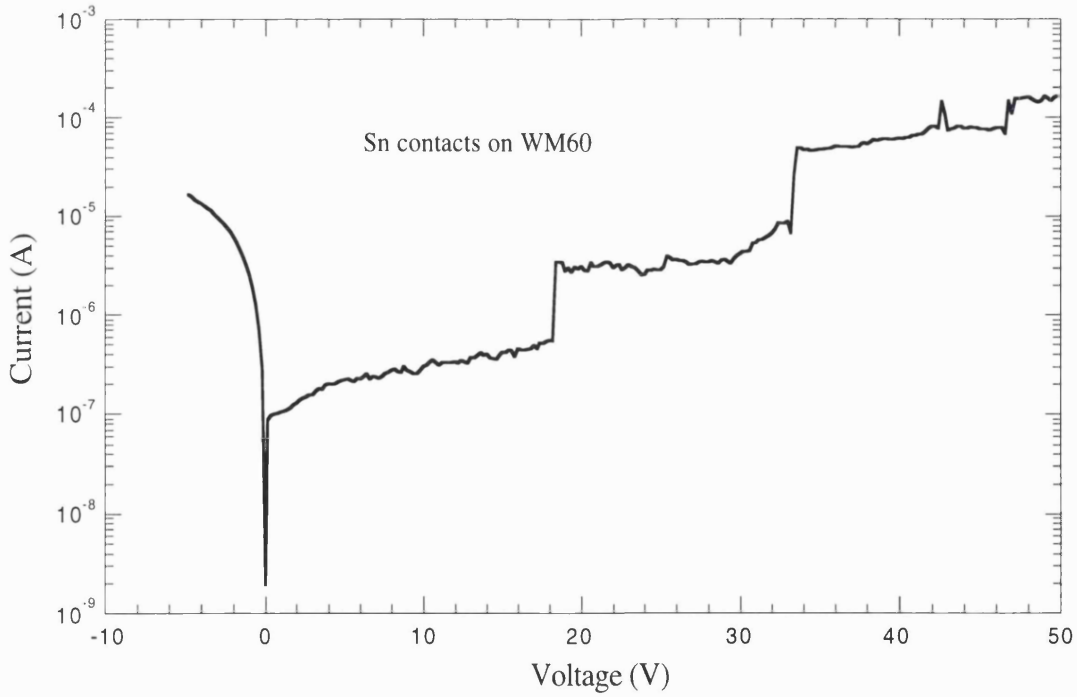

Figure 7.10 I-V characteristics of Sn contacts on WM60

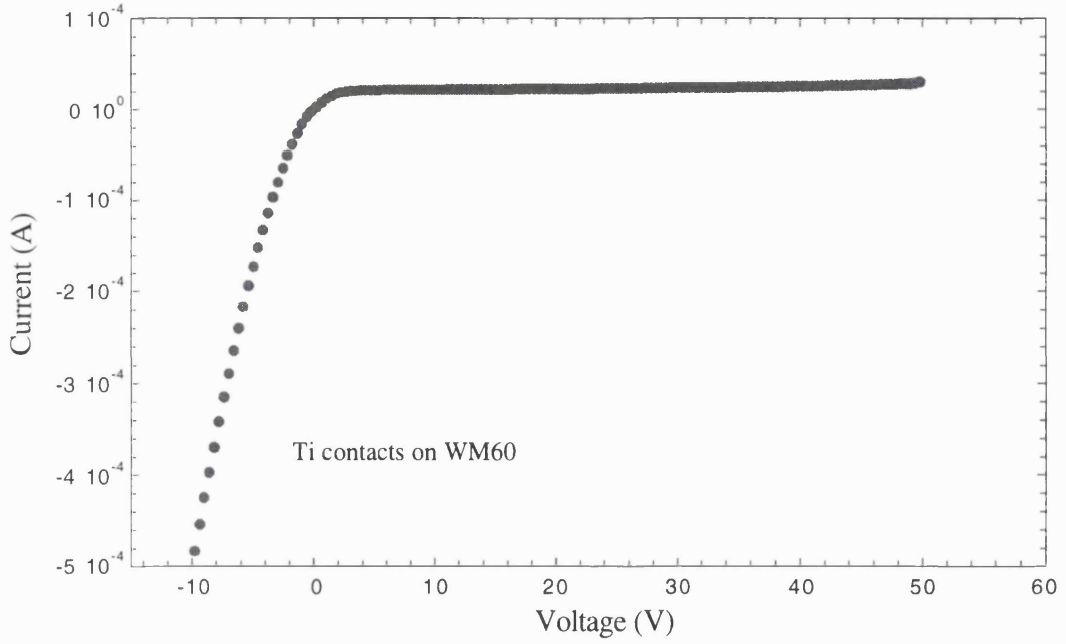

Figure 7.11 I-V characteristics of Ti on WM60 displaying a blocking ability of 50V

Ti is a carbide forming metal and has been routinely used to promote a reacted interface which displays good ohmic characteristic on boron doped diamond. However, Ti contacts on WM60 displayed rectifying properties. Typical I-V characteristics are shown in figure 7.11. The reverse leakage current is high in this case compared to other metallisation contacts, nevertheless it is capable of blocking up to 50V. The properties of a Ti | diamond reacted interface on re-hydrogenated surfaces will be presented in the next chapter.

Silver, a non carbide forming material was also thermally deposited on WM60. Figure 7.12 reveals a Schottky characteristic with a rectification ratio of 2 orders of magnitude at ±10V. All the electrical characterisation in this section were carried out at room temperature. Apart from Au, the other metals deposited on the surface conductive layer displayed rectification properties.

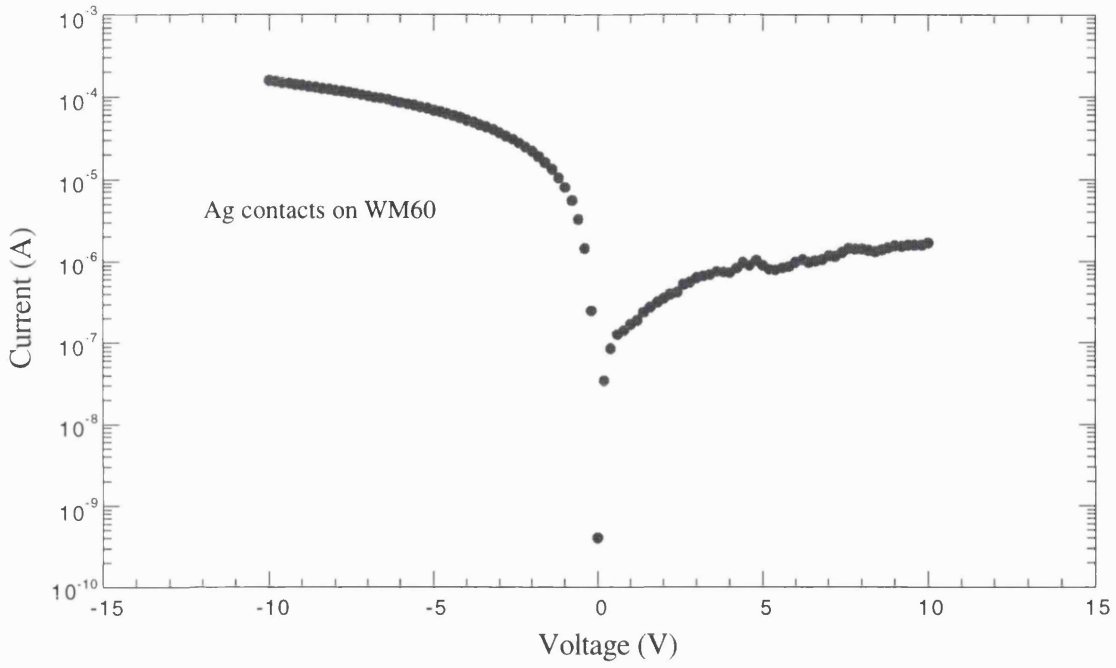

Figure 7.12 I-V plot of Ag contacts on WM60

Section 7.5.2 Experimental Results: High Temperature Measurements

In order to investigate the properties of metal contacts on this conductive layer at higher temperatures, it is necessary to anneal the material in air for a prolonged period before the metallisation contacts are deposited. This procedure is essential because above room temperature the conductivity of the material will decrease with time and the current-voltage characteristic will will be governed by the dynamic changes in the resistivity of the conductive layer. Figure 7.13 reveals the high temperature I-V plots of Al diodes deposited without the anneal treatment. Although, the I-V characteristic shows good rectification up to 200°C, the forward bias current is not stable with changes in time and temperature. A stabilisation anneal at high temperature (235°C) in air is necessary, as this will prevent further loss of carriers from the material as demonstrated in Chapter 6. After stabilisation by prolonged heating in air, Hall measurements have confirmed that the carrier transport properties will be governed by ionised impurity scattering.

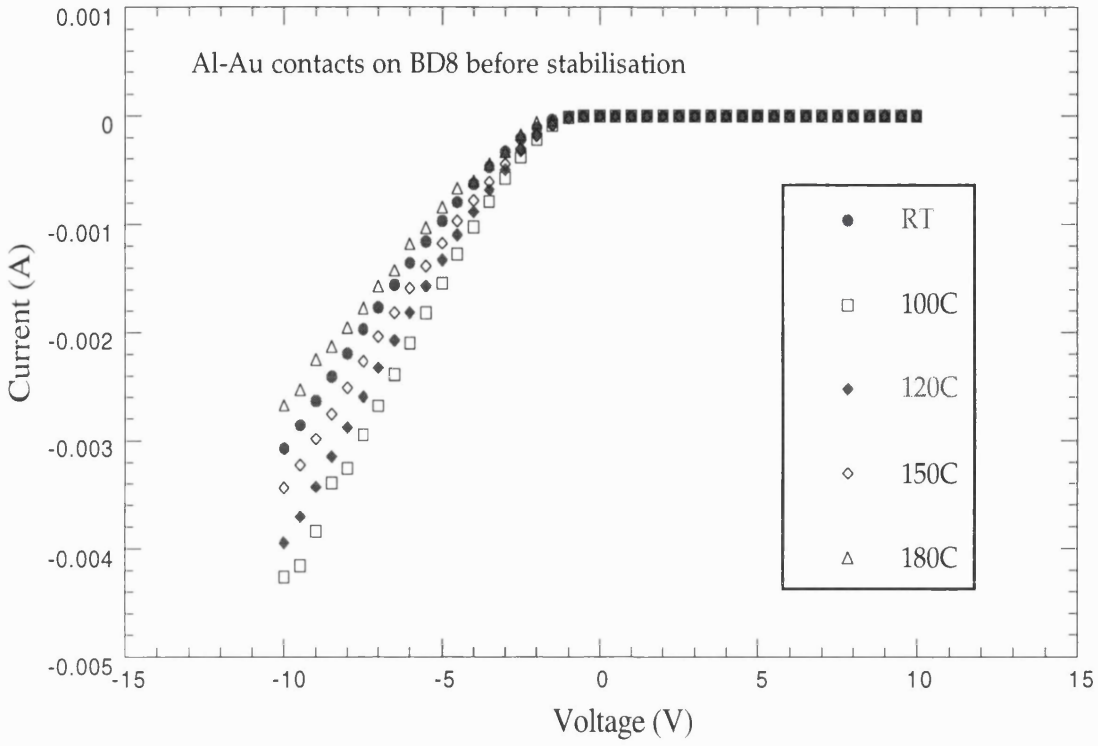

Figure 7.13 I-V characteristics of Al-Au contacts above room temperature on as grown BD8.

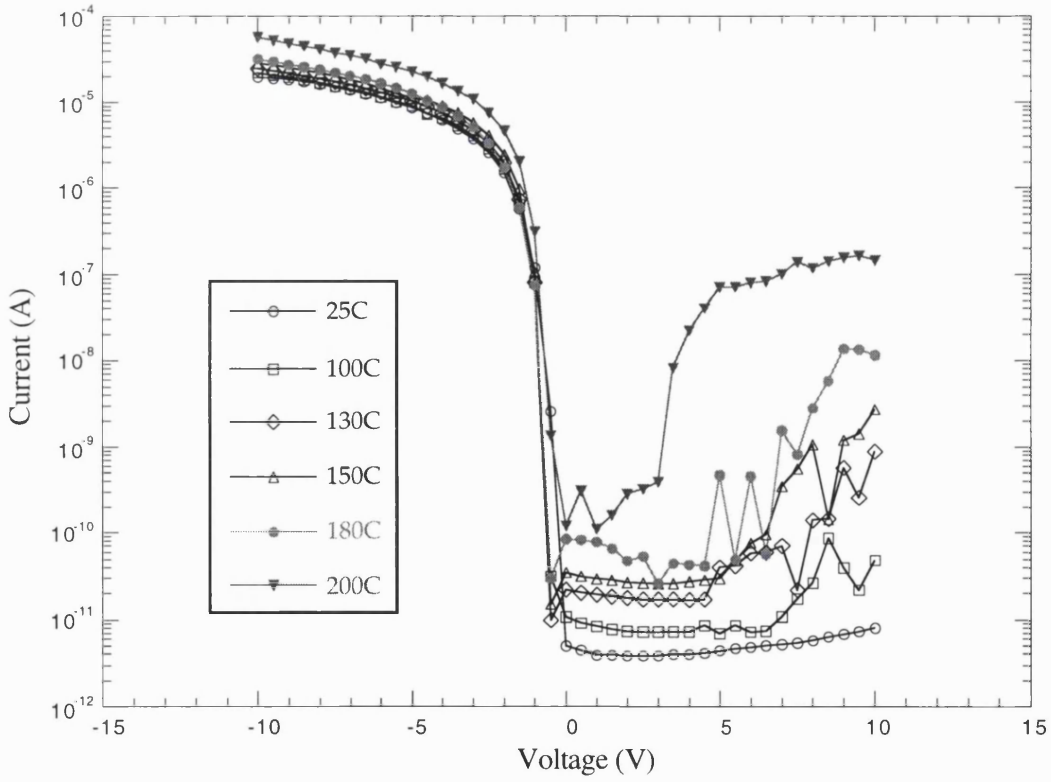

Figure 7.14 I-V characteristics of Al-Au contacts from room temperature to 200°C on air annealed BD8

Figure 7.14 shows the performance of the Al-Au Schottky diode at different temperature after the material was stabilised using an air anneal at 220°C for 3 hours, before the Al and Au contacts were deposited. The forward bias current is more stable and consistent, it increases with temperature. At higher temperatures the leakage current increases with temperature in a non uniform manner. At 200°C, these diodes still exhibit a rectification ratio of about 3 orders of magnitude taken between +10 and -10 V.

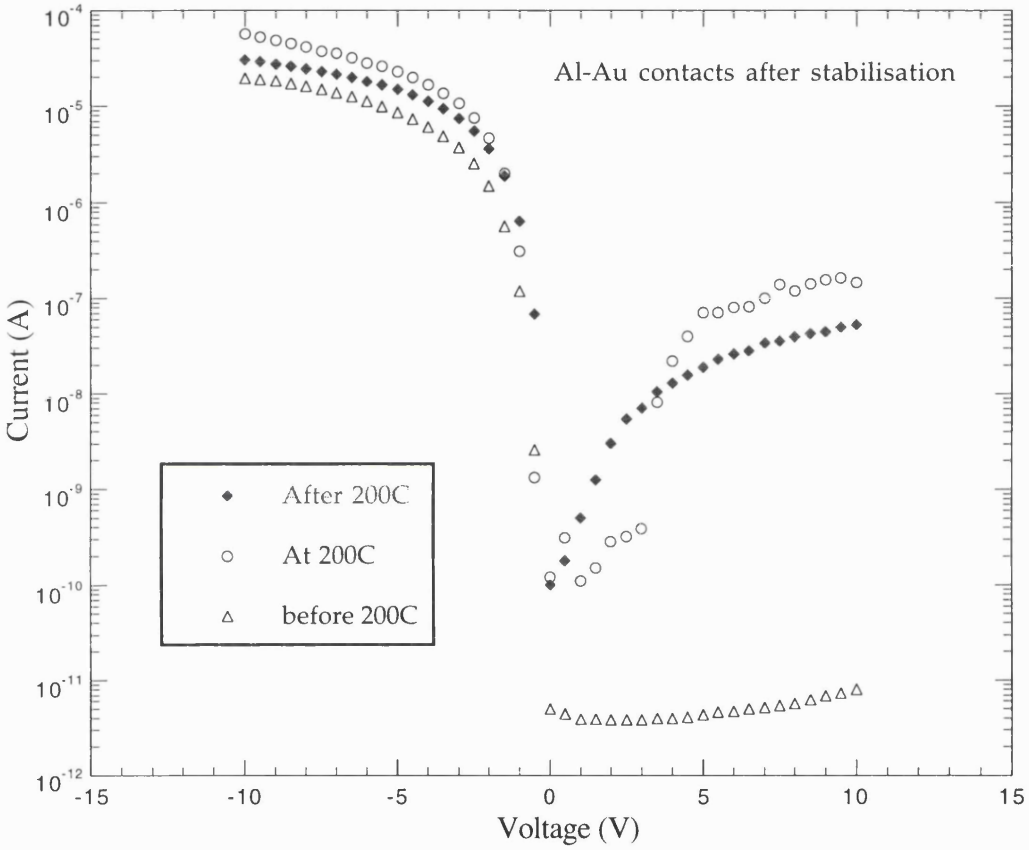

Figure 7.15 I-V curves of Al-Au contacts before and after heating.

Figure 7.15 shows the performance of Schottky diodes before heating (room temperature), during heating at 200°C and after heating (room temperature). The graphs reveal that heating up to 200°C increases the leakage current of this device. Once cooled to room temperature the leakage current was slightly lower compared the level at 200°C and did not recover to its original low level before the heating; heating has caused damage to the Al Schottky contact.

Section 7.6 Analysis

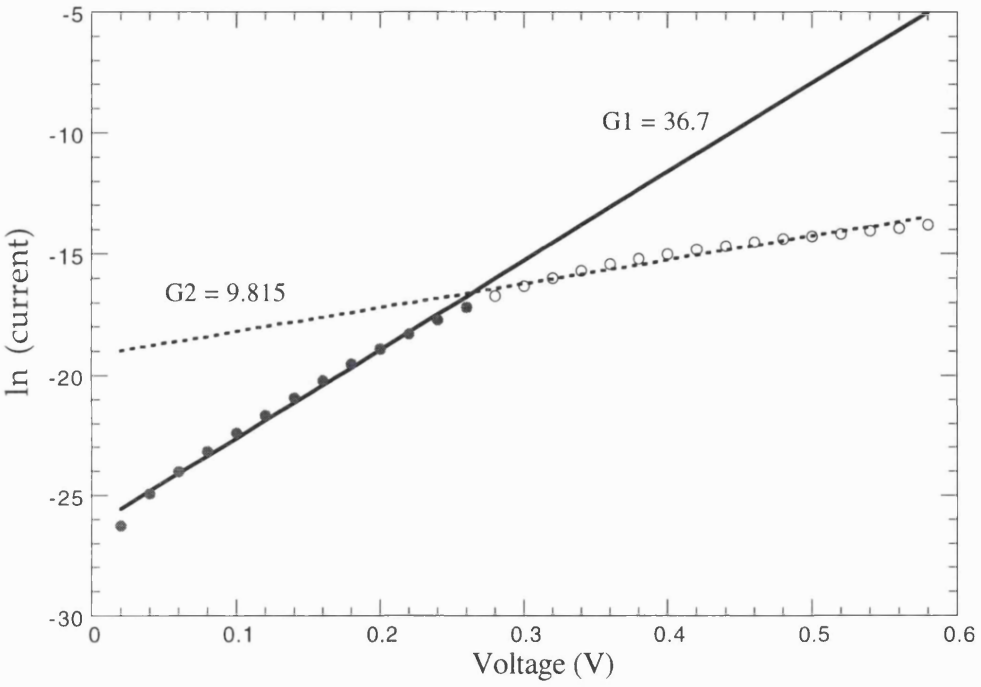

Figure 7.16 Ln I against V plot for Al-Au Schottky diode at small voltage

The ideality factor for these devices is determined by taking the best linear fit of the ln current against voltage plot shown in figure 7.16. The current at 0V is omitted due to the inaccuracy involved during the measurements when no voltage is applied. In addition, a higher voltage range is not used here as this diode suffered from a large series resistance as the ohmics were not situated close enough to the Schottky contact. From figure 7.16, taking the voltage between 0.02V and 0.28V, a gradient of 36.7 is measured from the linear fit G1 with a correlation of 0.995 between the data points and the fit. Applying equation 7.4, an ideality factor of 1.1 is obtained for the Al-Au Schottky diode on as grown BD8. The best linear fit taken between 0.3 and 0.6V results in a lower gradient of 9.82 indicating the effect of series resistance on the ideality factor of this device.

The Schottky barrier height can also be determined from this plot. Firstly, the reverse leakage current needs to be measured. Extrapolating the ln current plot to 0V gives a reverse leakage current of 3.4pA. Applying equation 7.5 and assuming thermionic emission current flow, a Schottky barrier height of 0.98eV is calculated for these Al contacts. A relative hole effective mass of 0.7 was used in this calculation. This value was chosen by Kiyota *et al.* [1995] to determine the Schottky barrier height of Al on homoepitaxial hydrogenated surfaces.

The methods described above were used to determine the electrical properties of all the other Schottky diodes fabricated including those Al diodes which have been stabilised and characterised from room temperature to 200°C. Details of the calculations will not be shown

here. But the outcome of the calculations will be summarised in table 7.1 and table 7.2.

Metals	Saturated Leakage Current (A)	Rectification Ratio (±5V)	Series Resistance (Ω)	Ideality Factor	Barrier Height (eV)	Material Type & Pre Treatment
	3.4×10^{-12}	4.7×10^{6}	2.6	1.1	1.0	BD8 300um as-grown
	1.8×10^{-12}	3.2×10^{6}	42	1.5	1.0	WM60 100um as-grown
Al	1.7×10^{-8}	310	180	2.7	0.8	WM40 100um re-Hydrogenated air anneal
	9.0×10^{-14}	2.0×10^{6}	420	1.2	1.1	BD8 300um as-grown air anneal
Ni	2.1×10^{-9}	2.0×10^{6}	80	1.8	0.8	WM60 100um as-grown
Ag	4.7×10^{-9}	920 (1V)	17	1.4	0.8	WM60 100um as-grown
	3.4×10^{-8}	96 (10V)	56		0.7	WM40 100um re-Hydrogenated air anneal
Sn	4.7×10^{-8}	76	570	3.6	0.7	WM60 100um as-grown

Table 7.1 Properties of metallisation contacts deposited on diamond undergoing different treatments.

Schottky diodes which display the best I-V characteristic were fabricated from the combination of Al-Au contacts. These contacts deposited on as-grown BD8 display a Schottky barrier height of 0.98eV with an ideality factor of 1.1. The rectification ratio is approximately 6 orders of magnitude taken at ±5V. The other 4 types of metals form Schottky contacts as well, however with a much lower barrier height and larger ideality factor. Au consistently displays near ohmic characteristics on all the material investigated. Amongst the materials used, the best results were obtained from Schottky diodes fabricated on BD8. This material is the thickest polycrystalline film used in this set of experiment, being approximately 300μm thick and consisting of the an average grain size between 30 - 60μm. This was followed by WM60 which is a thinner film of about 100μm and with a smaller average grain size between 10 - 30μm. The poorest results were contacts deposited on WM40 which consists of 4.2 x 4.2 mm laser cut tiles. After being cut, the tiles displayed intrinsic diamond resistivity. These tiles were then exposed to a pure hydrogen plasma for 30min in the same growth chamber and under the same conditions to when it was grown. Metal contacts which previously showed Schottky characteristic deposited on these re-hydrogenated surfaces on other material did not show any sign of rectification characteristic although the conductivity on these surfaces were similar level to BD8 and WM60. However, after an air anneal at 250°C for 3 hours, the contacts deposited on the more resistive surfaces (lower carrier concentration) displayed a modest improvement. At this point, it is

difficult to identify the problem as there were still lack of study in the literature regarding the re-hydrogenation effect on polycrystalline films of different grain size and quality.

Temperature (K)	Leakage Current (A) at 0.0V	Leakage Current (A) at 10.0V	Rectification Ratio (5V)	Ideality Factor	Barrier Height (eV)	Diode Series R(kΩ)
295	9.0×10^{-14}	8.0×10^{-12}	2.0×10^{6}	1.2	1.1	420
373	2.8×10^{-11}	4.8×10^{-11}	1.3×10^{6}	1.5	1.2	390
403	6.9×10^{-12}	8.8×10^{-10}	2.2×10^{5}	1.5	1.3	360
423	1.8×10^{-11}	2.7×10^{-9}	3.8×10^{5}	1.7	1.4	310
453	3.0×10^{-11}	1.1×10^{-8}	2.7×10^{5}	2.0	1.4	270
473	9.0×10^{-11}	1.5×10^{-7}	3.2×10^{2}	2.2	1.5	160
Back to 295	9.0×10^{-12}	5.4×10^{8}	7.7×10^{2}	1.7	0.9	300

Table 7.2 Properties of Al-Au contacts at higher temperature on air annealed BD8

After stabilisation in air at 220°C for about 3 hours, the material is expected to be slightly more resistive resulting from the loss of carriers. Al-Au contacts deposited on BD8 after the anneal still exhibit good rectification properties. Leakage currents in the pA levels were detected at about 10V with a rectification ratio of 6 orders of magnitude at ±10V and an ideality factor of 1.24. The Schottky barrier height is about 1.1eV at room temperature, slightly higher than 0.98eV for similar contacts deposited before the annealing procedure.

As the ambient temperature of this diode is increased from room temperature, the properties of this diode began to change. Firstly, the series resistance of this diode decreases with increasing temperature. Hall measurements conducted under similar conditions showed that after the carriers in the channel were stabilised by a 250°C anneal, the Hall mobility displayed a positive power dependency on the temperature. The increase in conductance of the substrate was caused by the increase in Hall mobility at higher temperature. Sheet carrier concentration from the Hall data reveals that there is no change in the carrier level throughout this temperature range.

Further, the ideality factor increases with temperature and is at its maximum at 200°C. Recombination of carriers and degradation of the metal semiconductor interface maybe occurring. When the device was cooled to room temperature, the ideality factor decreased but was not restored to its original level before the heating. This indicates that the metal-semiconductor interface has degraded. In addition, the barrier height is lower after heating and

the leakage current at 0 and 10V has increased by a few orders of magnitude. The I-V curves in figure 7.15 indicate signs of breakdown occurring. Other workers have shown that the barrier height is generally sensitive to pre-deposition and post deposition heat treatments. As the material used for this experiment is far from ideal, the increase in leakage current could be caused by metallic spikes [Andrews, 1974]. The tendency for this to occur increases especially at high temperatures where Al, which has a low melting point, may migrate into the cracks at the grain boundaries. This is a common phenomena and has been observed with other semiconductors [Hiraki, 1977]. A very strong electric field strength in the cracks within the grain boundary favours breakdown and tunneling. The barrier height measurement above 473K has a larger degree of inaccuracy compared to lower temperature measurements. This is because the current values recorded at voltages near to zero suffer from the effect of noise. Nevertheless at 473K, a Schottky diode with a rectification ratio of 3 orders of magnitude at 10V and 5 orders at 3V has been demonstrated on the surface conductive layer.

Section 7.7 Discussion

On the whole, the experimental results revealed that this new form of dopant can be utilised on polycrystalline CVD diamond to form high performance Schottky diodes that operate satisfactorily at room and higher temperatures. The Al-Au Schottky diode fabricated displays an ideality factor of 1.1 (measured between 0.02V and 0.28V), the closest to unity ever reported on this type of material over this voltage range. Apart from Au, other metals which have been investigated had good rectification characteristics as well. The success of fabricating simple Schottky diodes using this form of conductive layer will lead to the possibility of fabricating more advanced devices from this cheaper form of diamond.

Ideally, the barrier height of a metal-semiconductor contact is dependent of the metal work function, ϕ_m according to equation 7.1. In practice this relation is far from true. Typically, it has been shown experimentally that the barrier height is a less sensitive function of ϕ_m than predicted. This situation is true and applicable for diamond as well. In the literature there were reports where the dependency was not observed particularly on oxidised diamond surfaces. A few experimental reports exists which show dependency on the electronegativity rather than ϕ_m [Mori, 1991; Kawarada, 1994]. Experimental results which displayed these dependency were normally point Schottky contacts placed on the surface conductive layer of homoepitaxial grown diamond films.

Bardeen [1947] put forward an explanation for the weak dependency of ϕ_b on ϕ_m. He suggested that the discrepancy may be due to the effect of surface states present in the metal-semiconductor interface. For an n-type semiconductor, in the absence of surface states, the negative charge on the surface of the metal must be balanced by the positive charge on the uncompensated donor so that on the whole the junction remains neutral. When a thin insulating layer is present giving rise to surface states then the occupation level of the surface states is determined by the Fermi level which is constant throughout the barrier region in the absence of a

bias. If the neutral level ϕ_o is above the Fermi level then the surface states will have a net positive charge and vice versa. This means that the positive charge on the semiconductor will be reduced as part of charge is being taken by the surface states instead. Smaller positive charge on the semiconductor reduces the depletion width and band bending resulting in a smaller barrier height. For a metal-semiconductor interface which is separated by a thick oxide layer this dependency may disappear altogether. The same thing would happen if the density of states becomes very large. In both cases the barrier height is said to be pinned by the surface states and barrier height will be given by $\phi_b = E_g - \phi_o$. This is known as the Bardeen limit.

Table 7.3 shows the relation between the electronegativity values, work function of metals, the Schottky barrier height and ideality factor. The work functions in table 3 are obtained for polycrystalline metals which resemble more closely the nature of metal contacts thermally deposited on the polycrystalline diamond surface [Rhoderick, 1988(a)]. The metallisation contacts investigated here display a reasonable dependency of Schottky barrier height on electronegativity of metal as shown in figure 7.16. However, the dependency on the work function of the metal was not observed in this work. The barrier height for Au (0.39eV) is determined from chapter 8.

Metals	Electronegativity of metals	Work Function (eV)	Experimental Barrier Height (eV)	Ideality Factor
Au	2.4	5.1	0.39	-
Sn	1.8	4.4	0.73	3.6
Ag	1.9	4.3	0.78	1.4
Al	1.5	4.3	0.98	1.1
Ni	1.8	5.2	0.81	1.8

Table 7.3 Properties of metals contacts deposited on surface conductive polycrystalline CVD diamond.

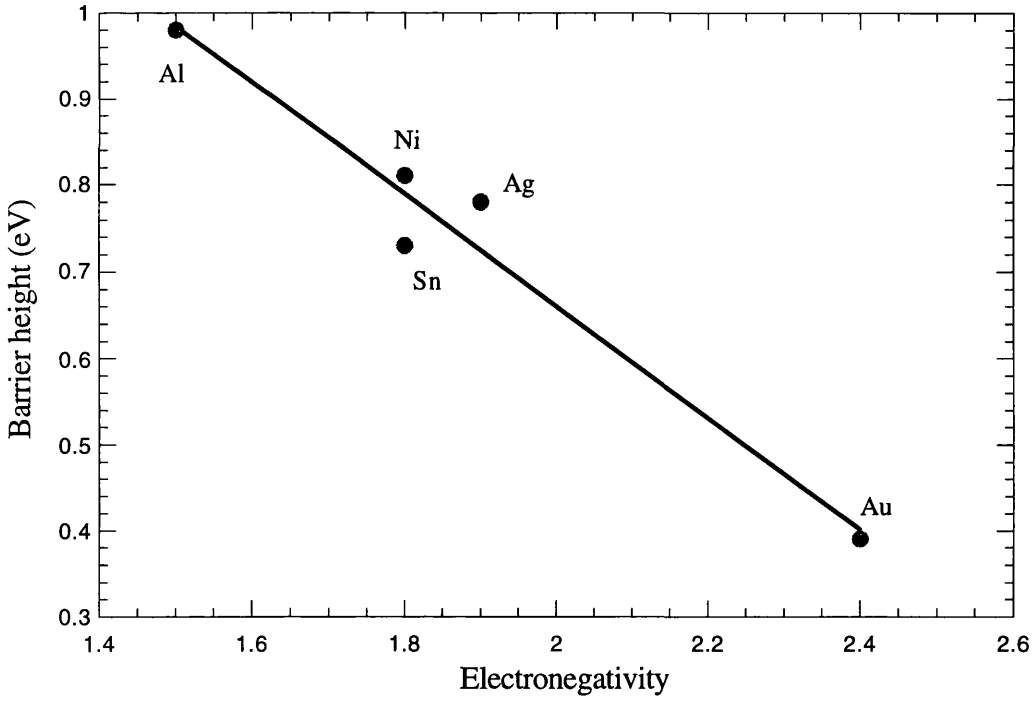

Figure 7.17 The dependency of barrier height with electronegativity.

Low temperature (77K) I-V measurements on diodes deposited on homoepitaxial diamond revealed that a thermionic emission current was the dominant current injection mechanism [Hayashi, 1997]. An Al barrier height of 1.2eV on hydrogen terminated boron doped homoepitaxial diamond was measured by Kiyota *et al.* [1995]. They attributed the difference of barrier height obtained between Au and Al to be caused by the difference in electronegativity or work function of these metals. In figure 7.5, similar I-V characteristic was obtained for Al and Au in this work. However, there are no available data in the literature to compare the result of thermally deposited Ag, Sn and Ni. Kawarada *et al.* [1994(a)] demonstrated the correlation between metal electronegativity and Schottky barrier height for point Schottky contacts on hydrogen terminated homoepitaxial diamond. The experimental results displayed in figure 7.17 here support Kawarada's findings. The correlation between ϕ_m and SBH was not demonstrated by the experimental results obtain in this work as nickel, which is expected to have similar work function to Au, showed rectification characteristics. In most cases the work function of a metal will vary under different conditions. When metal and semiconductor make intimate contact, the precise atomic position and charge distribution at the solid surfaces in contact will be different from when the metal is clean. Hence, the true work function of a metal may have been modified once deposited on the surface on a semiconductor [Rhoderick, 1988(a)]. The variation of metal work function on polycrystalline material is difficult to understand. The Schottky barrier height measured by XPS on diamond (111) and (100) surfaces for Al, Au and Ti on hydrogen terminated surfaces do not show any correlation with the work function or the electronegativity [Tachibana, 1993]. However, the authors indicated that the XPS measurements were made on insulating single crystal diamond which may be different from the surface conductive sample studied here. Other methods such as the internal photoemission spectroscopy (IPS) measurement

of ϕ_b for Al and Au contacts on p-type polycrystalline CVD diamond shows a value of 1.13 ± 0.03eV for both contacts [Hicks, 1989]. The author attributed the high density of surface states to be responsible for this pinning effect.

Breakdown was observed on some of the Schottky devices fabricated. It became more prominent when the diodes were tested at the higher voltage ranges. Two examples which clearly demonstrate this effect are shown in Figure 7.8 for Al-Au Schottky contacts on WM60 and in Figure 7.10 for Sn contacts on WM60. There are two main mechanism which describe the breakdown behaviour in the reverse bias region applicable for almost all semiconductors. They are quantum mechanical tunneling and avalanche multiplication breakdown. Normally, it is easy to separate the two. Quantum mechanical tunneling occurs at a much lower voltage compared to avalanche breakdown. It is more common on devices which are fabricated on a material which has a high carrier concentration ($>10^{18}cm^{-3}$). Generally the breakdown mechanism favours tunneling for breakdown occurring at voltages less than $4\ E_g / q$. On the other hand, it favours avalanche multiplication for voltages exceeding $6\ E_g / q$ [Sze, 1993]. As for diamond with an E_g of 5.5eV, the threshold voltage for tunneling is less than 22V, while breakdown voltages exceeding 33V favours avalanche multiplication. On the as grown surfaces where the carrier density is the highest, there are devices which do not show any breakdown even bias up to 100V. Furthermore, the evidence of breakdown in Figure 7.8 and 7.10 exceeds 22V, which favours avalanche. A more probable explanation for the breakdown mechanism that is observed here is the non uniform distribution of electric field strength. The field strength is the highest at the peaks of the grains or it can be near or at the grain boundary where the Schottky metals form sharp spikes. Breakdown does not occur at the same reverse bias voltage even for devices fabricated on the same sample. The microscopic uniformity of the doping layer on polycrystalline material is still unclear.

Section 7.8 Conclusion

The properties of thermally deposited metal-semiconductor contacts has been investigated. The diamond used here is commercially available and can be grown over a large area on non diamond substrates. Experimental results demonstrate that the surface conductive layer on polycrystalline diamond can also be used to fabricate simple Schottky diodes. Six different metals (Al, Au, Ti, Sn, Ni and Ag) have been deposited on these surfaces. Apart from Au, all the other metals showed strong rectification characteristics. The best rectification characteristic is obtained using a combination of Al and Au. The best Schottky diodes were fabricated from as grown BD8 which is the largest grain size material used in this investigation. The Al-Au Schottky diodes displayed over 6 orders of rectification ratio, an ideality factor of 1.1 (measured between 0.02V and 0.28V), a breakdown capability of more than 100V with a leakage current in the nA level throughout this voltage range and a forward current in the mA range at room temperature. On average these Schottky diodes turned on at about -0.7V.

The high temperature operation of these diodes has also been investigated. Al-Au diodes

operate satisfactorily from room temperature up to 200°C with an ideality factor within the range of 1.6 to 2. Throughout this temperature range a rectification ratio of 3 and 5 orders of magnitude measured at 3V and 5V respectively was demonstrated. After a stabilisation step, the forward current of these devices does not vary much throughout this temperature range. This characteristic cannot be achieved using a boron doped channel as it suffers from a high activation energy of 0.37eV [Collins, 1971]. Hall measurements confirmed that the slight increase in forward bias current throughout this temperature range was caused by the dependency of mobility with temperature. Sheet carrier density measurements at high temperature (chapter 6), showed that the carriers have a low activation energy and the carriers are fully ionised at room temperature.

The Schottky barrier height of the metals investigated here do not show a strong dependency on the work function of the metal contacts. However, a weak dependency on the metal electronegativity was demonstrated instead. It should be pointed out that this correlation is difficult to achieve on thermally deposited metal contact as the contact covers a large area. More often there will be defects on the polycrystalline film prohibiting the best possible condition to be achieved. The breakdown occurring in these diodes has also been presented. Based on the argument given in the discussion section, the breakdown is most probably caused by high electric field strength at a particular spot in the metal-semiconductor interface especially near the peaks and in the grain boundaries where metallic spikes may be present.

The success of fabricating simple Schottky diodes will lead to the possibility that more complex devices can be fabricated using this conductive layer. This prospect of utilising the surface conductive layer on polycrystalline CVD diamond for other type of electronic application will be addressed in chapters 9 and 10.

References :-

Andrews, J.M. [1974] J. Vac. Sci. Technol., **11**, 972.

Bardeen, J. [1947] Phys. Rev. **71**, 717.

Baumann, P.K., and Nemanich, R.J. [1998] J. Appl. Phys., **83**, 2072.

Bethe, H.A. [1942] MIT Radiation Lab. Rep. 43-12.

Chan, S.S.M., Peucheret, C., McKeag, R.D., Jackman, R.B., Johnston, C. and Chalker, P.R. [1995] J. Appl. Phys., **78**, 2877.

Collins, A.T. and Williams, A.W.S. [1971] J. Phys. C **4**, 1789.

Ebert, W., Vescan, A., Gluche, P., Borst, T. and Kohn, E. [1998] Diamond & Relat. Mater., **6**, 329.

Fox, B.A., Stoner, B.R., Malta, D.M., Ellis, P.J., Glass, R.C. and Sivazlian, F.R., [1994] Diamond & Relat. Mater., **3**, 382.

Fox, B.A., Hartsell, M.L., Malta, D.M., Wynands, H.A., Kao, C.-T., Plano, I.S., Tessmer, G.J., Henard, R.B., Holmes, J.S., Tessmer, A.J. and Dreifus, D.L. [1995] Diamond & Relat. Mater., **4**, 622.

Gildenblat, G.Sh., Grot, S.A., Badzian, A.R. Hatfield, C.W. and Badzian, T. [1990] IEEE Electron Dev. Lett., **11**, 371.

Gildenblat, S.Sh., Grot, S.A. and Badzian, A., [1991 (b)] Proceedings of the IEEE, **79**,647.

Hayashi, K., Yamanaka, S., Watanabe, H., Sekiguchi, T., Okushi, H. and Kajimura, K. [1997] J. Appl. Phys., **81**, 744.

Hicks, M.C., Wronski, C.R., Grot, S.A., Gildenblat, G.Sh., Badzian, A.R., Badzian, T. and Messier, R. [1989]
J. Appl. Phys., **65**, 2139.

Hiraki, A., Shuto, K., Kim, S., Kamamura, W. and Iwami, M. [1977] Appl. Phys. Lett., **31**, 611

Humpreys, T.P., LaBrasca, J.V., Nemanich, R.J., Das, K. and Posthill, J.B. [1991] Electron Lett., **27**, 1515.

Kawarada, H., Aoki, M., Sasaki, H. and Tusgawa, K. [1994 (a)] Diamond & Relat. Mater., **3**, 961.

Kawarada, H., Aoki, M. and Ito, M. [1994 (b)] Appl. Phys. Lett., **65**, 1563.

Kiyota, H., matsushima, E., Sato, K., Okushi, H., Ando, T., Kamo, M., Sato, Y. and Masamori, I. [1995] Appl. Phys. Lett., **67**, 3596.

Malta, D.M., Windheim, J.A. and Fox, B.A. [1993] Appl. Phys. Lett., **62**, 2926.

McKeag, R.D., Chan, S.S.M. and Jackman, R.B. [1995] Mater. Science. Eng., **B29**, 223.

Mead, C.A. and McGill, T.C. [1976] Phys. Lett., **58A(4)**, 249.

Miyata, K., Matsui, Y., Kumagai, K., Miyauchi, S., Kobashi, K. and Nakaue, A. [1991] Proc. of 2nd Int. Conference New Diamond Science and Technol. Materials Research Society, Pittsburg, 981.

Miyata, K., Dreifus, D.L. and Kobashi, K. [1992] Appl. Phys. Lett., **60**, 480.

Mori, Y., Kawarada, H. and Hiraki, A. [1991] Appl. Phys. Lett., **58**, 940.

Rhoderick, E.H. and Williams, R.H. [1988(a)] "Metal-Semoconductor Contacts", Claredon Press, Oxford, page 47.

Schroder, D.K., [1990] "Semiconductor Materials and Device Characterisation", John Wiley & Sons, New York.

Streetman, B.G. [1990] "Solid State Electronic Device 3rd Ed.", Prentice Hall Inc., USA.

Sze, S.M. [1993] "Physics of Semiconductor Devices 2nd Ed.", John wiley & Sons, Canada.

Tachibana, T. and Glass, J.T. [1992] J. Appl. Phys., **72**, 5912.

Tachibana, T., Glass, J.T. and Nemanich, R.J. [1993] J. Appl. Phys., **73**, 835.

Vescan, A., Daumiller, I., Gluche, P., Ebert, W. and Kohn, E. [1997] Diamond & Relat. Mater., **7**, 581.

Werner, M., Job, R., Denisenko, A., Zaitsev, A., Fahrren, W.R., Johnston, C., Chalker, P.R. and Buckley-Golder, I.M. [1996] Diamond & Relat. Mater., **5**, 723.

Chapter 8

Characterisation of Ohmic Contacts on Surface Conductive Diamond Films

Contents

Section 8.1 Introduction

In general, a potential barrier is developed at the metal-semiconductor interface due to either the difference between the work function of the 2 materials or to the presence of interface states which pin the Fermi level. An ohmic contact is defined as a metal-semiconductor interface that has a negligible contact resistance relative to the bulk. The voltage drop across this contact should be sufficiently small compared with the voltage drop across the active region of the device. This allows useful electrical properties of the device to be utilised.

Diamond does not have a native oxide. Therefore, the properties of metal contacts on

diamond are heavily dependent on the surface terminating species [Kiyota, 1996; Mori, 1991]. By modifying the properties and chemistry of diamond surfaces, metal contacts which are normally rectifying can be turned into ohmic [Gildenblat, 1991; Aoki, 1994]. As a result, the surface pretreatment [Mori, 1991], doping level [Iwasaki, 1993] and the quality of diamond are critical factors determining the properties of metal contacts. It is difficult to fabricate good ohmic contacts on moderately doped diamond surfaces which normally form Schottky contacts. Therefore it is necessary to modify surfaces and then selectively deposit ohmic contacts at places which are desired. In general, there are 3 methods through which this can be achieved.

(a) Selective ion-implantation at high doses exceeding $10^{20}cm^{-3}$ [Kalish, 1999].

(b) Lowering of barrier height by forming a defective interface [Moazed, 1988; Yokoba, 1997].

(c) Lowering of barrier height by choosing the appropriate metallisation scheme [Aoki, 1994].

Method (a) is the standard technique and has been widely used on diamond and other semiconductors. On diamond this is normally achieved by heavily doping the region beneath the contact with boron [Zeisse, 1991]. Once the implantation dosage exceeds a critical level of 10^{22} vacancies/cm^3 graphitisation will occur and a low resistance contact can be realised [Uzan-Saguy, 1995]. Formation of ohmic contacts in this manner is caused by the mechanism of field emission current tunneling through the barrier. This method can be improved by incorporating method (b). A combination of both method (a) and (b) reliably produces ohmic contacts with a specific contact resistance in the order of 10^{-5} Ωcm^2 [Tachibana, 1992; Werner, 1995]. The metallisation scheme which are normally used in (b) are carbide forming metals such as Ti and Mo capped by Au to protect the contact from oxidation during high temperature annealing. The annealing step is necessary to enhance the formation of a leaky reactive interface [Nakanishi, 1997; Miller, 1997]. Annealing is normally carried out above 400°C for a duration of 30 minutes [Yokoba, 1997].

Formation of ohmic contacts using method (c) is not very common on most semiconductors due to Fermi level pinning. On diamond surfaces which are acid cleaned or oxygen terminated method (c) is not possible. On the other hand, the dependency of Schottky barrier height on the electronegativity of metals observed on hydrogen terminated diamond surfaces enables method (c) to be explored and used effectively to form ohmic contacts [Tsugawa, 1999] on both homoepitaxial and PCD films. Au and Pt having a high electronegativity form ohmic contact on hydrogen terminated diamond. These have been used satisfactory as the metallisation contact for defining the source and drain in MESFET's and as ohmic contacts for Schottky diodes which are capable of operating up to 200°C. In addition, it has been used as the electrical contact for high power devices. There is no thorough study in the literature regarding the properties of Au contacts deposited on hydrogen terminated polycrystalline surfaces. Furthermore, on these surfaces, other alternative methods of obtaining low resistance contacts, such as method (b), have not been explored.

Section 8.2 Experimental Aims

The properties of metal contacts on p-type PCD surface conductive layers have been investigated using Shockley's transfer length method (TLM) [Schroder, 1998] and the circular transmission line model (c-TLM) developed by Reeves [1980]. The metal contacts investigated here are Au, Ti | Au and Ti | Al. These metal schemes were chosen with the intention of investigating the formation of low resistive contacts using method (b) and (c) described earlier. Au being an inert and a non carbide forming metal is suitable for investigating formation of low resistive contacts under mechanism (c) while Ti a reactive carbide forming metal will favour mechanism (b). In addition, different surface pretreatments have been carried out to assess the performance of these metal contacts on PCD films. The pretreatment is carried out to seek the optimised conditions for realising an ohmic contact. The pretreatments that are introduced before and after contacts deposition are

(i) Acid cleaned (Appendix 1) :- with the intention to oxidise the surface.
(ii) High temperature anneal :- to form a leaky TiC interface
(iii) Exposure to hydrogen plasma :- to create a surface conductive layer.

The following experiments were set up to achieve the objective :-

Experiment 1 :- characterisation of Au contacts on as grown WM60 at room temperature after subsequent heat treatments of 80°C, 200°C and 280°C.
Experiment 2 :- fabrication of a leaky low resistive contact on as grown WM60 and finding the optimum annealing condition. Ti|Al contact is used for this investigation.
Experiment 3 :- characterisation of Ti|Au, Ti|Al and Au on as grown and acid treated WM60 using the annealing procedure from Experiment 2.
Experiment 4 :- characterisation of contacts in Exp 2, 3 and 4 after 4 hours anneal at 250°C. This is to investigate modification that occur after the anneal.

The main conclusion from the experiment will reveal the best metallisation scheme and the most optimised treatment for engineering low resistive contacts. In addition, a simple equivalent circuit which consists of resistors representing the test structure will be included.

Section 8.3 Contact Resistance and Measurement Technique

When two ohmic metallisation contacts are placed on a semiconductor, the total resistance between the two contacts can be divided into 3 components:-
(a) the resistance of the metallic conductor R_m
(b) the contact resistance R_c
(c) the semiconductor resistance R_s

The contact resistance includes the resistance of the metal-semiconductor contact, a portion of the

metal immediately above the metal-semiconductor interface, a part of the semiconductor below the interface, current crowding effects, spreading resistance under the contact and any interfacial oxide that may be present between the metal and the semiconductor. The contact resistance for a unit area is known as the 'specific contact resistance' ρ_c (Ωcm^2). This is a more useful form which is independent of contact area and is a convenient parameter for comparison. There are various methods for measuring this quantity and this section will concentrate on two of the standard techniques.

The first measurement technique is called the transfer length method (TLM) introduced by Shockley [Schroder, 1998]. This technique requires the deposition of a number of rectangular parallel contacts which are separated from each other by an increasingly spaced distance as shown in figure 8.01(a)

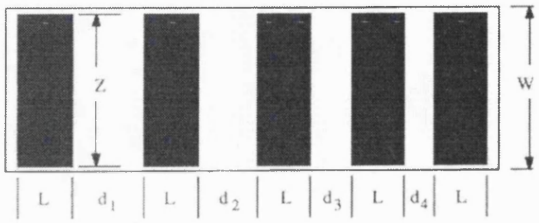

Figure 8.01 (a)

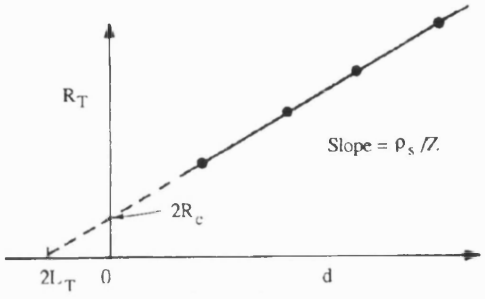

Figure 8.01(b)

For contacts with $L > 1.5L_T$ and for a front contact resistance measurement, the total resistance between any two contacts is given by

$$R_T = \frac{\rho_s d}{Z} + 2R_c \approx \frac{\rho_s d}{Z} + 2\frac{\rho_s L_T}{Z} \qquad R_c \approx \frac{\rho_c}{L_T Z}$$

where

L_T is the transfer length
ρ_s is the sheet resistance of the material
ρ_c is the specific contact resistance

L_T is defined as the length where the voltage due to the current transferring from the semiconductor to the metal or vice versa has dropped to 1/e of its maximum value. R_T is calculated from the gradient (resistance) of the I-V plot between two adjacent contacts. The procedure is repeated to determine R_T for each of the contacts pairs separated by different spacings. The corresponding R_T for each spacing d is plotted against d itself. The gradient of the slope, intercept at $d = 0$ and at $R_T = 0$ will give the necessary information to determine ρ_c, ρ_s and L_T. The transfer length method gives a complete characterisation of the ohmic contact by providing the sheet resistance, contact resistance and specific contact resistance. However, it assumes that the sheet resistance under the contact is the same as the bulk sheet resistance which will introduce inaccuracy, as this is not always the case in practical contacts [Reeves, 1980]. For this test structure, it is important that W = Z. It can be achieved by a mesa etch structure to isolate the test structure. If this condition is not

satisfied the non parallel current path at the edge will introduce errors when calculating ρ_c .

The second measurement method is known as circular transmission line model (c-TLM). It avoids the need of a mesa etch to isolate the test structure hence simplifying the processing step. This test pattern consists of a central dot contact surrounded by two outer concentric circular ring structures as shown in figure 8.02(a). By definition the specific contact resistance includes the resistance of the actual interface and the region just above and below the interface. Unlike the front end resistance measurement, Reeves introduces an additional measurement to the circular structure known as the contact end resistance measurement. It allows the determination of the 'sheet resistance beneath the contact' ρ_{sk} and the 'true sheet resistance of the bulk' ρ_s separately. This gives a more precise determination of ρ_c. In addition, this method provides a model of the test structure in the form of a simple equivalent circuit which consists of resistors representing properties which are related to the bulk material and the contact interface. The equivalent circuit is given in figure 8.02(b) together with the resistors

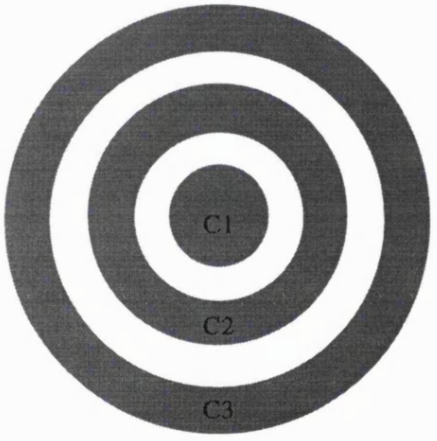

Figure 8.02(a)

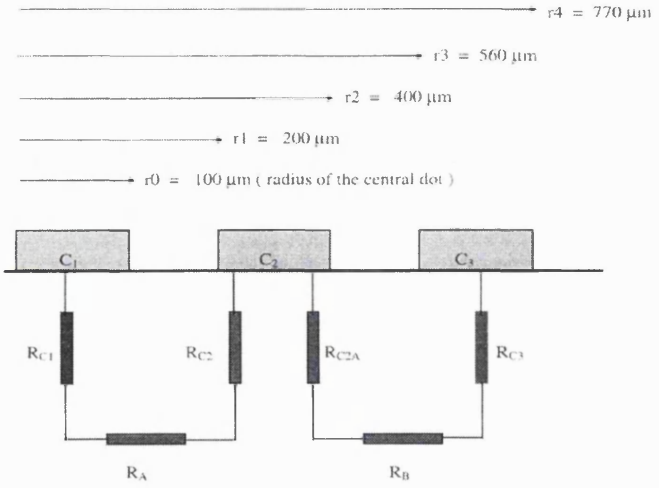

Figure 8.02(b)

The dimension of the test structure used in this chapter is given in Figure 8.02(b). The solution to the transmission line model is complicated and calculations cannot be performed manually [Reeves, 1980]. This problem can be overcome by applying computational numerical solution using the mathematical package Matlab. The numerical solution is divided into two parts for simplicity. The first part of the formulae in Appendix 3 is used to solve ρ_s. The second part of the formulae given in Appendix 4 provide solutions to other important parameters and the resistors in the equivalent circuit. The spreading resistance R_{SP} of the middle spherical point contact can be estimated from the relation :-

$$R_{sp} = \frac{\rho}{4r}$$

where ρ is the resistivity of the substrate

r is the radius of the circular contact

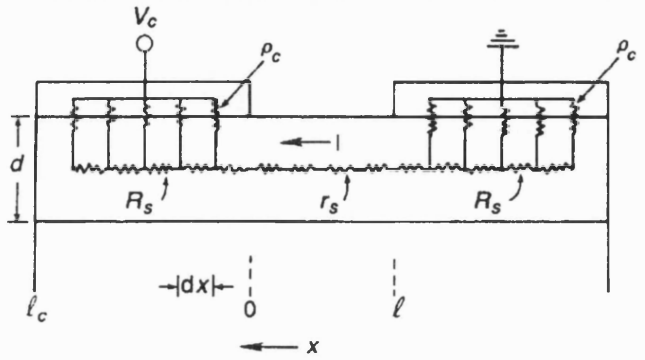

Figure 8.03 The transmission line mode of planar ohmic contact on a semiconductor

The current path flowing out from a planar contact generally would not be uniform throughout the entire metal contact area, but would crowd towards the edge nearest to the other contact. This description of the actual current path can be modeled in terms of a transmission line as shown by Berger and Widmann as in Figure 8.03. In addition, from this model

$$L_T = \sqrt{\frac{\rho_c}{\rho_S}}$$

Hence, the effective area for a planar contact is actually the product of L_T and Z instead of the product of the Z and the actual length of the contact (L).

The determination of Schottky barrier height (ϕ_b) in this chapter is based on the equation [Sze, 1993] :-

$$\rho_c = \frac{k}{qA^* T} \exp\left(\frac{q\phi_b}{kT}\right) \quad \text{(equation 8.1)}$$

where ρ_c is the specific contact resistance.
k is the boltzman constant.
A^* is the Richardson constant assuming a relative effective mass of 0.7 as described in chapter 7.
T is the temperature in K.
q is the electronic charge.

The following assumptions were made while applying this equation

(a) Current injection mechanism in the contact is assumed to be thermionic emission. This is a reasonable assumption as Al contacts deposited on this surface show very low leakage currents (nA) over 40V. In addition other workers have shown this mechanism is the dominating current transport in these devices [Hayashi, 1997].

(b) The effective mass of holes used in this chapter is 0.7. This value is chosen to show consistency from the last chapter. In addition, Kiyota *et al.* have used similar values for their calculation of barrier height in the surface conductive layer [Kiyota, 1996].

(c) The contact resistance is dominated by the actual resistance of the interface. Other components which may be present are assumed to make a negligible contribution.

Section 8.4 Experimental Methods

In order to investigate the properties of ohmic contacts, as grown randomly oriented free standing thin film PCD WM60 with an average grain size of about 10 - 30μm was chosen. Previously Schottky diodes have been successfully fabricated on this wafer. The Raman spectra measured by a He-Ne laser at 633nm on this material reveal a sharp peak at 1332cm^{-1} with no other apparent structure. Details of the Raman spectra and the optical micrograph of this film is given in Figure 6.1(a) and (b) (see Chapter 6). The circular (c-TLM) and rectangular (TLM) test structures were fabricated by using photolithography. The contact metallisation was approximately 200nm thick. The deposition technique is conducted by means of a resistive thermal evaporation using an Edwards E306 at a base pressure lower than 10^{-6} mbar. During lithography the sample was inevitably baked at a temperature not higher than 85°C to assist in the development of the photoresist. The mask aligner used here is a Karl Suss powered by a UV enhanced mercury-helium lamp. The high temperature anneal to form a reactive titanium carbide interface is carried out in a carbolite furnace at atmospheric pressure under a constant flow of nitrogen. Lower temperature annealing was performed on a hot plate. A hydrogen plasma is useful for restoring the conductive layer on the diamond surface. The hydrogen plasma was generated by a 0.8kW microwave at 2.45GHz. The diamond samples were treated in this plasma without a bias. The pressure in the chamber was kept at about 30torr with a hydrogen flow rate of 100sccm. The graphite heater beneath the sample controls the temperature of the sample during the hydrogen plasma treatment. I-V testing was carried out in a probe station with the assistance of testing instrument HP 4145B, Keithley 2000 multimeter and Keithley Picoammeter.

Section 8.5 Fabrication of Test Pattern on PCD

The test patterns were defined on the surfaces of PCD using a photolithographic lift-off technique. However, defining the test pattern cannot be performed using the standard lithography techniques as the surface on the PCD material used in this experiment is too rough. Details of the processing parameters developed to overcome this problem are given in Appendix 3 and below.

The diamond samples were de-greased according to Appendix 1 to remove organic contamination due to poor handling outside the clean room. The samples have a surface roughness of approximately 25μm. If a normal photoresist is spun on these surfaces, the region at the peaks will not be properly covered by the photoresist. To avoid this problem, a thick positive resist AZ4652 was used to planarise the rough surface. Unfortunately, this leaves places where the resist is more than 25μm thick and at the peaks it will be much thinner. During exposure, the resist at the thickest region will require a longer time to develop and the resist just covering the peaks will be over exposed. A non isotropic etch will result during the development stage. This problem can be overcome by spinning a double layer of photoresist.

(a) The first resist layer is spun at high speed to form a thin coating. This layer is baked in the oven to harden the resist. Then the entire layer is exposed to UV.

(b) The second layer of resist is spun at a lower speed on top of the first layer. This is to ensure the peaks are properly covered. It is baked at the same temperature as the first and then exposed to UV through a dark field mask defining the desired contact pattern on the resist.

During the developing stage, the 2nd layer will be etched at a region which is weakened by the UV. Once this layer is removed the developer will begin to etch the 1st layer. As the 1st layer is entirely exposed to UV, the etch will be in all directions. This will create under cutting which will assist in the lift off. By carefully optimising the spin speed and the exposure duration, the 2nd layer will determine the device structure and the 1st will assist in the lift off process. In addition, longer exposure time will not be required to reach the thickest region and the top layer will not be over exposed. An optical microscopy picture of the under cutting in the resist profile of the c-TLM structure is presented in figure 8.04(a) and (b).

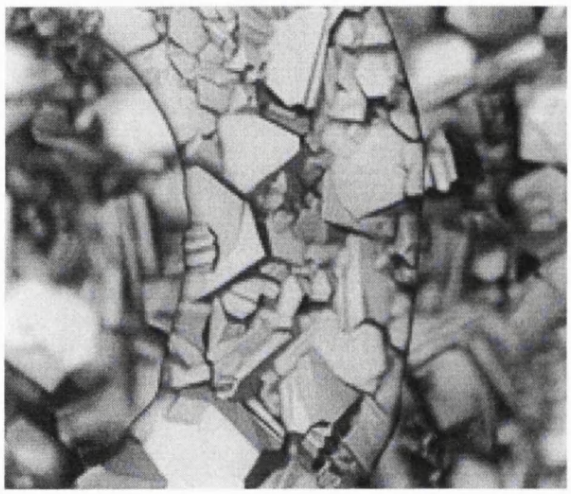

Figure 8.04(a)

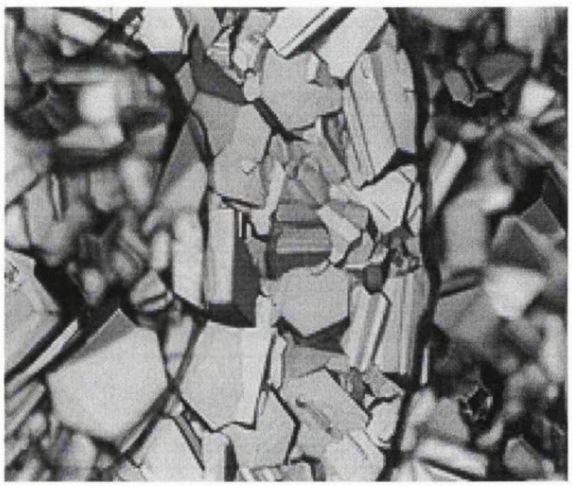

Figure 8.04(b)

Figure 8.04(a) shows little undercutting in the photoresist pattern. However, in figure 8.04(b) increased undercutting occur indicated by the thicker boundary at the edge of the photoresist.

Section 8.6 Testing Procedure of TLM and c-TLM

This section describes the testing procedure for the rectangular test structure. Characterisation of the TLM structure with a front contact resistance measurement is straight forward. The I-V characteristics are measured between the contact pads placed adjacent to each other. The gradient of the best fit line through the plot will give the total resistance between the two contact pads. This is repeated for other adjacent pairs of contact which is spaced at different separation. The plot of R_T against the spacing d will provide sufficient information to calculate ρ_s, ρ_c and L_T.

For testing the c-TLM structure, I-V characterisation was performed between contact C_1 and C_2 using HP 4145B semiconductor parameter analyser from -4.0V to 4.0V. A small step size

of 0.05V was used as this allows to monitor the small changes in the I-V curves if any non linear current flows are present. This was then repeated for contact pads between C_2 and C_3.

R_{in} is the total resistance between C_1 and C_2
R_{out} is the total resistance between C_2 and C_3

The end resistance R_{END} is experimentally determined from the following method. Firstly, a current I_{12} is injected between contact C_1 and C_2, at the same time the open circuit voltage between contact C_2 and C_3 (V_{23}) is measured. The end resistance is defined as

$$R_{END23} = V_{23} / I_{12}$$

The measurement is repeated for the other pair of contact. If the current is injected between C_2 and C_3 and the voltage is measured across C_1 and C_2, then

$$R_{END12} = V_{12} / I_{23}$$

The open circuit voltage (V_{23}) is directly dependent on the current flowing between C_1 and C_2. Varying the current injected into C_1 and C_2 with a corresponding measurement of open circuit voltage will yield a plot shown in the inset of Figure 8.08. Normally, a linear dependency is observed between the measured open circuit voltage and the injected current. The end resistance can be obtained from the best fit line through all the data points. The current I_{12} was measured and supplied by Keithley 487 voltage source / picoammeter while the open circuit voltage was measured by Keithley 2000 multimeter. Precise measurement is critical as the open circuit voltage will be in the mV range.

Section 8.7.1 Experimental Results : TLM for Au contacts

This section will reveal the experimental results obtained from the rectangular Au contacts deposited on as grown WM60 using the lithography method described earlier. The optical micrograph of the successfully fabricated rectangular Au contact pattern on WM60 is given in the figure 8.05. A total of six rectangular strips is defined on the material. Each of these strips has a length of 600 μm and a width of 76μm. The closest separation *d* between the adjacent contacts is 40μm and the largest spacing *d* is 240μm.

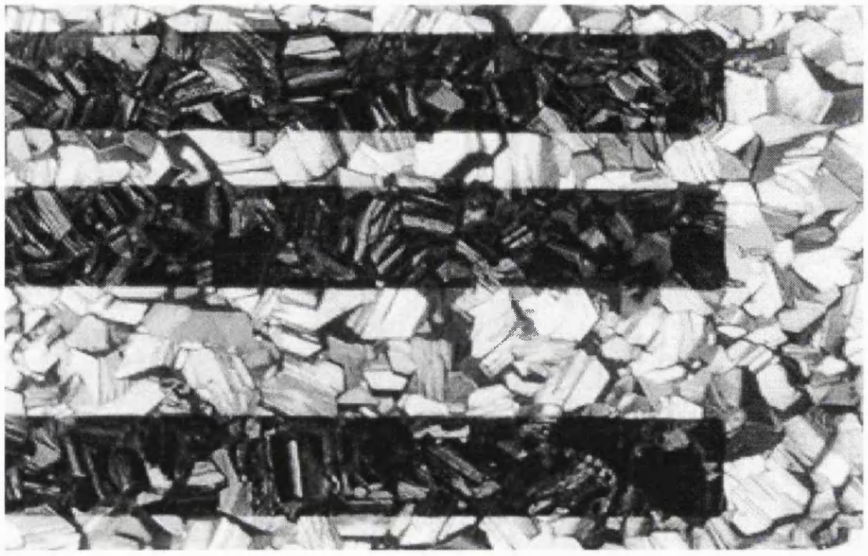

Figure 8.05 TLM test pattern on WM60

Figure 8.06(a) shows R_T plotted against spacing d for each of the adjacent Au contacts on WM60. A linear relation is obtained between R_T and d. As the spacing between the contacts is increased, the resistance between the contacts will increase proportionately. However, the graph in figure 8.06(b) has a negative R_T for intersection at $d = 0$. Calculation which is vital to determine ρ_c cannot be performed as negative resistances practically will not occur here. This is most probably caused by additional current flowing at the edge of the contact. The correction for this component is not included in the equation used to determine ρ_c. Accurate measurement of ρ_c cannot be determined using this test structure. The gradient of the straight line provides a reasonable estimate of the sheet resistance ρ_s as it is less affected by the current at the edge.

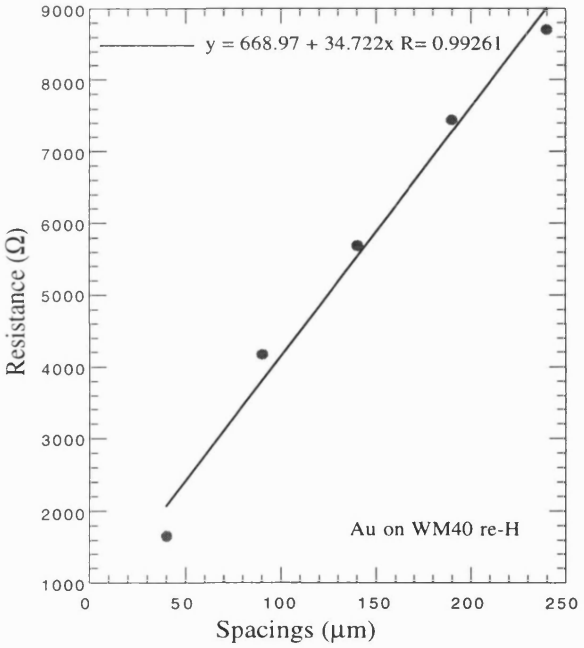

Figure 8.06(a)

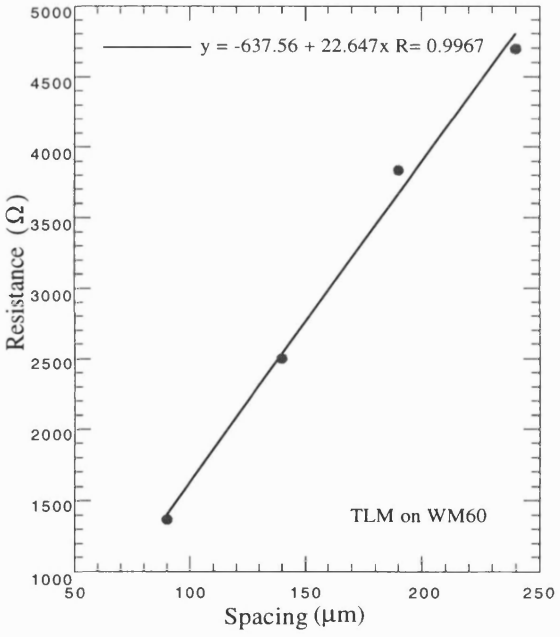

Figure 8.06(b)

Figure 8.06(a) and figure 8.06(b) shows the R_T against d plot for the TLM structure on WM40 and WM60

For figure 8.06(a) ρ_s = 20.8 kΩ/□
For figure 8.06(b) ρ_s = 13.5 kΩ/□

The problem can be solved by proper isolation of the test structure. But it require an additional step of mesa etching the structure in a reactive ion etching (RIE) system. The Reeves c-TLM test structure does not require the mesa etch to isolate the structure. Due to its simplicity, it is therefore used for the rest of the experiments in this chapter.

Section 8.7.2 Experimental results : c-TLM for Au contacts

This section describes the experimental results for the Au c-TLM test pattern. Using the photolithography method described in Section 8.3, concentric circular Au contacts were defined on WM60. One of the circular test pattern is shown in figure 8.07.

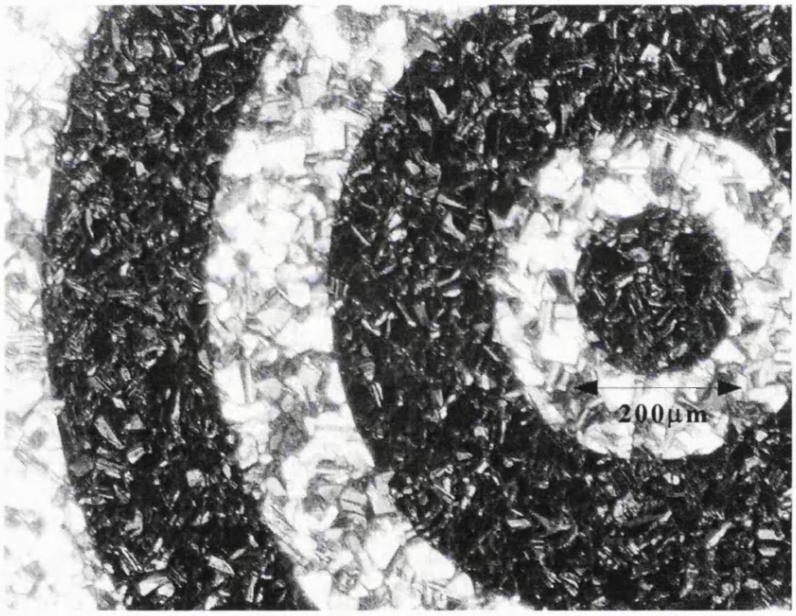

Figure 8.07 The optical micrograph of the c-TLM test structure

Figure 8.08 shows the I-V plot of the Au test structure at room temperature performed using the HP4145B. Current levels in the mA range were recorded between ±4.0V. Comparing the best linear fit of the data and the actual data itself, the data are not entirely linear indicated by the soft bending of the current characteristic. The conductivity between the two contacts is slightly voltage dependent. If the voltage range for the linear fit is taken between ±1.0V, then the gradient of the fit will be larger than when it is taken between ±2.5V. The inset of figure 8.08 shows the I-V plot to determine the end resistance. The experimental measurements required to construct this plot were explained in section 8.6. The respective position of contacts C_1, C_2 and C_3 are displayed in Figure 8.02(a).

$\mathbf{R_{in}}$ is the inverse gradient of the linear fit between the I-V data points measured across two inner contact (C_1 and C_2)

$\mathbf{R_{out}}$ is the inverse gradient of the linear fit between the I-V data points measured across two outer contact (C_2 and C_3)

The end resistance measurement is based on R_{END23} . A R_{END23} value of 2.0 Ω is obtained from the gradient of the linear fit as shown in the inset in figure 8.08.

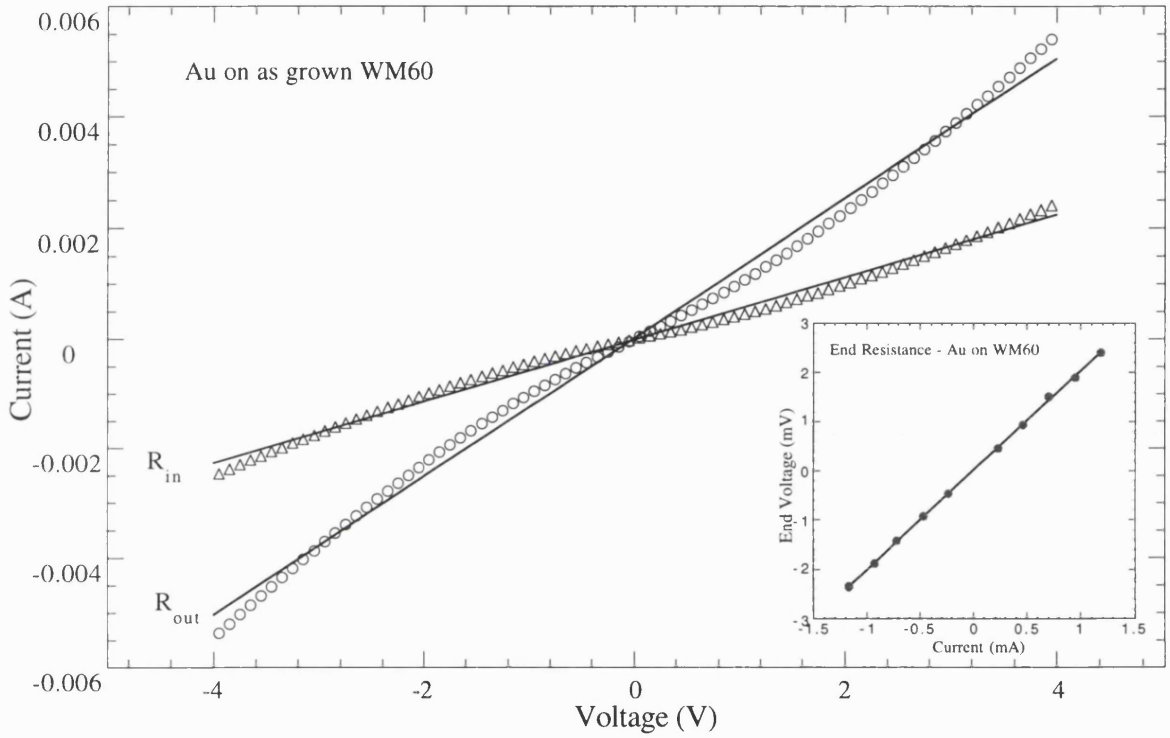

Figure 8.08 The I-V plot of Au contact with the end resistance measurement inset.

The values of R_{in} and R_{out} along with R_{END2} were determined experimentally from the I-V plots. These values are required by the formula in Appendix 4. Appendix 5 provides solutions to the resistor components to complete the representation of the concentric circles in the form of an equivalent circuit as shown in figure 8.02(b). The formulae in Appendix 4 and 5 are written in Matlab to facilitate the calculations. They are based on the equations introduced by Reeves [1980].

The sample was then annealed at higher temperatures to investigate the change in the specific contact resistance which may occur due to modification of the sheet resistance. The temperatures used to investigate this effect were 200°C and 280°C. An anneal time of 3 hours was carried out at these chosen temperatures. Figure 8.09 shows the I-V characteristics of the Au contact after an anneal at 280°C with the end resistance measurement inset.

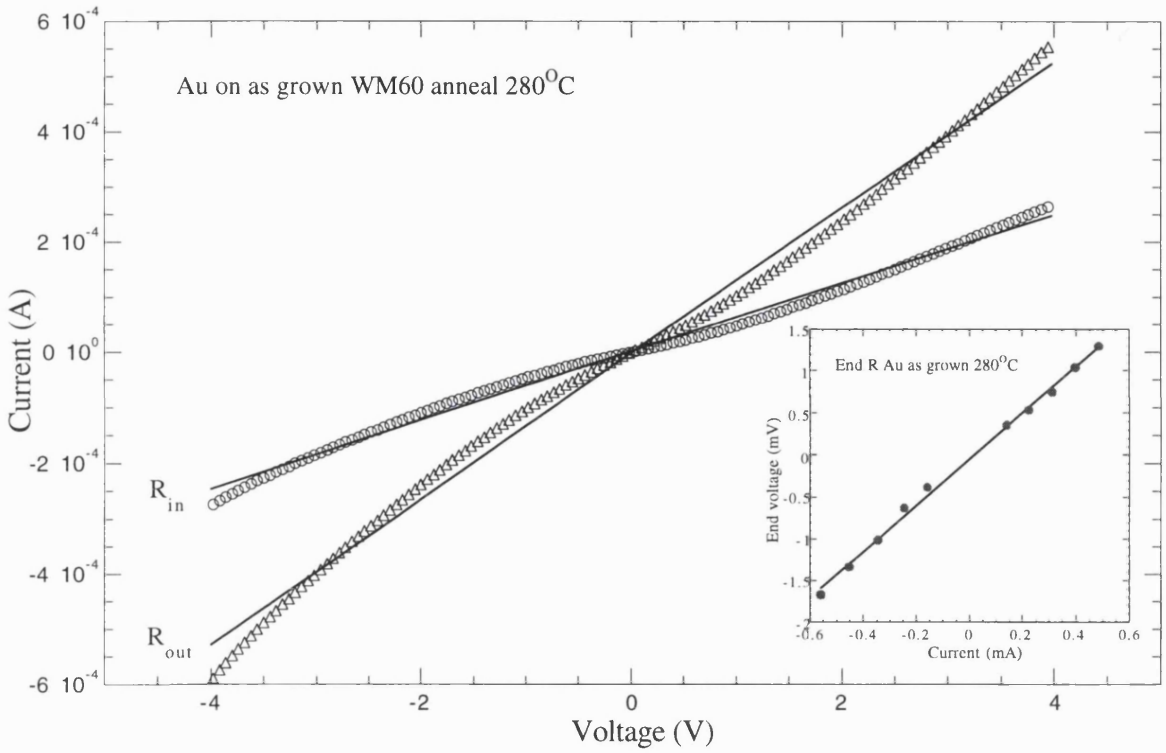

Figure 8.09 The I-V plot of Au test structure after an 280°C anneal for 30 min.

Comparing figures 8.09 and figure 8.08, annealing the test structure at 280°C for 3 hours caused the current levels to decrease by about an order of magnitude. The value of the end resistance has increased by 50% indicating that modification has occurred at the interface.

Section 8.7.3 Experimental results : c-TLM for Ti|Al contacts

The fabrication of ohmic contacts using a reactive interface on the surface conductive layer will require a hydrogen plasma treatment. This is because the formation of a reacted interface requires an anneal at a temperature exceeding 400°C. The anneal will result in the loss of carriers from the surface. The plasma treatment is important to restore the original level of conductivity on the PCD film. The annealing step is critical as Ti forms a good Schottky contact on hydrogen terminated surfaces. This property is expected to change once the annealing is performed.

Titanium contacts deposited on the as grown WM60 showed rectification characteristics (see chapter 7). In the first set of contacts deposited, the metallisation scheme of Ti|Al was chosen. Al is chosen to cap the Ti layer instead of Au. This is to prevent Au from dominating the I-V characteristic in case the deposition of Ti was not uniform. In addition, during the anneal, the Au might diffuse into the material shunting the Ti contact, this will provide difficulty in assessing the performance of the TiC interface and finding the optimum anneal condition. C-TLM measurements cannot be performed for contacts which exhibit strong rectification properties. In order to transform the Ti contact to ohmic behaviour the sample is annealed at 430°C for 30 minutes. After the annealing procedure, a 400°C treatment in a hydrogen plasma for 5 minutes is

necessary to restore the conductive layer. The I-V characteristics of the Ti|Al contacts before and after treatment are shown in figure 8.10.

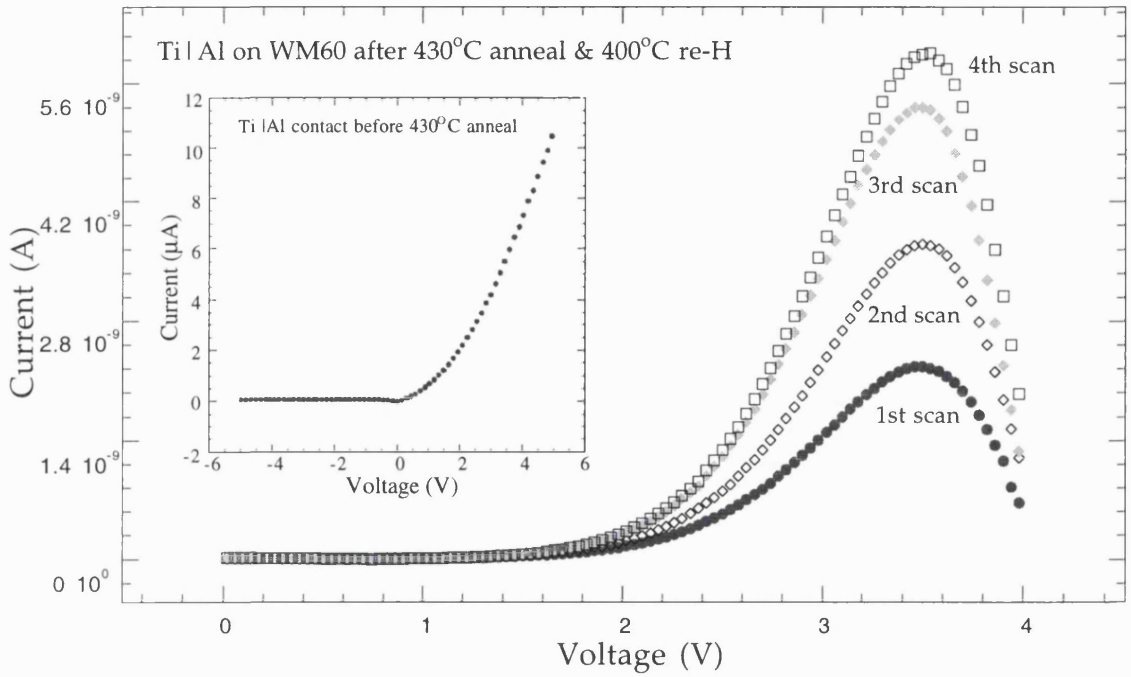

Figure 8.10 The I-V plot of Ti |Al contacts after a 430°C anneal for 30 min. Current level is dependent on the number of scan times indicating charging up at the interface and the existence of shallow traps. The inset shows rectification properties of this contact before the anneal.

The inset shows the properties of the Ti|Al contacts before the anneal, a good rectification characteristic is obtained. After the 430°C anneal followed by hydrogen plasma exposure for 5 minutes at 400°C, the rectification properties of the contacts disappeared. However, the contacts are unstable. The I-V curves shown above are obtained by doing a scan from 4.0V down to 0.0V. Immediately after the 1st scan, a 2nd similar scan was conducted followed by the 3rd and 4th. The current recorded increases after each subsequent scan. The result shows that charging up could be occurring at Ti|Al and PCD interface. The charging occurring at the interface is dominating the I-V characteristic giving a poor and unreliable performance of the ohmic contact.

The same test structure was then annealed at a much higher temperature (600°C for 20 minutes). After this annealing step, the test structure was again treated in a hydrogen plasma at 600°C for 5 minutes. The I-V characteristics of the same test structure are shown in figure 8.11. The result shows that after the 600°C anneal for 20 minutes the Ti|Al contacts are more stable compared to the 430°C anneal for 30 minutes. The I-V characteristics of the contact after the higher temperature anneal are more consistent and do not depend on the number of scans. The inset in figure 8.11 shows the end resistance measurement. A current in the region of mA is recorded at ±4.0V after this treatment compared to a level of around μA before the treatment. This result is consistent with the current levels recorded for Au contacts on the same material. The properties of this contact can now be analysed using the c-TLM method.

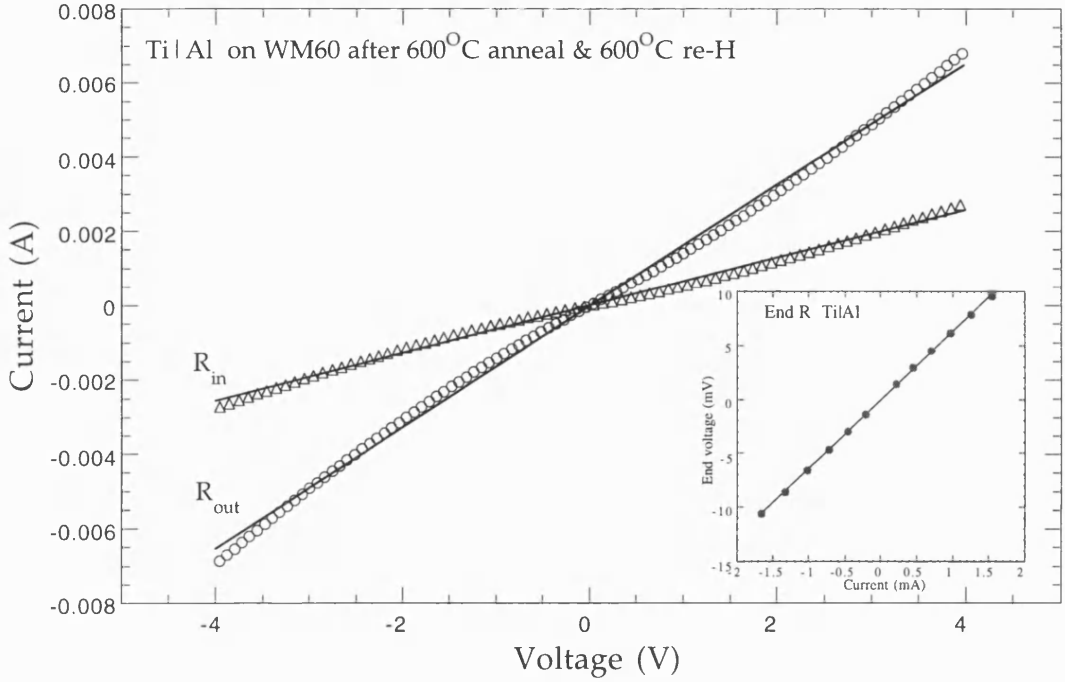

Figure 8.11 The I-V plot of TilAl contact after an anneal at 600°C for 20 minutes.

After this experimental observation, the annealing procedure at 600°C in a constant flow of nitrogen at atmospheric pressure for 30 minutes followed by hydrogen plasma treatment at 600°C for 5 minutes was adopted throughout this chapter for the formation of ohmic contacts using a reacted interface of Ti metals.

Section 8.7.4 Experimental results : c-TLM for TilAl, TilAu and Au contacts

In this experimental section, the properties of TilAu and TilAl metallisation scheme were investigated on different surfaces with Au contacts as a control. Three sample sets were prepared :-

(a) TilAu scheme on WM60 acid cleaned (oxidised) surface
(b) TilAu scheme on WM60 as grown surface
(c) Au contacts on WM60 as grown surface

The thickness of the metallisation schemes in these sample sets were as follows :-
(a) All titanium contacts were 110nm thick
(b) All the gold contacts were 200nm thick

The test structures were subjected to the same annealing and hydrogen plasma treatment described earlier. If this procedure is not carried out then the TilAu contacts on the oxidised surface will be highly resistive as there are no carriers for conduction. However, on the as grown

surfaces TilAu contacts will be highly resistive due to the rectifying (Schottky) nature of Ti contacts.

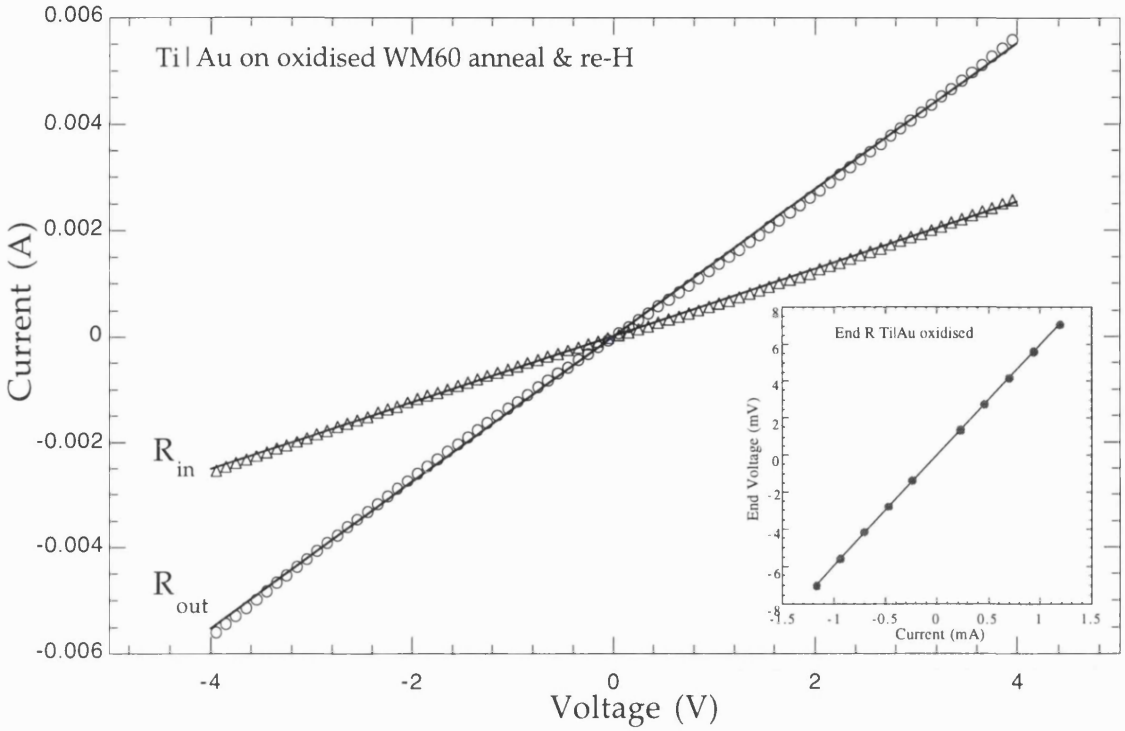

Figure 8.12 The I-V plot of the TilAu on oxidised surface after treatment.

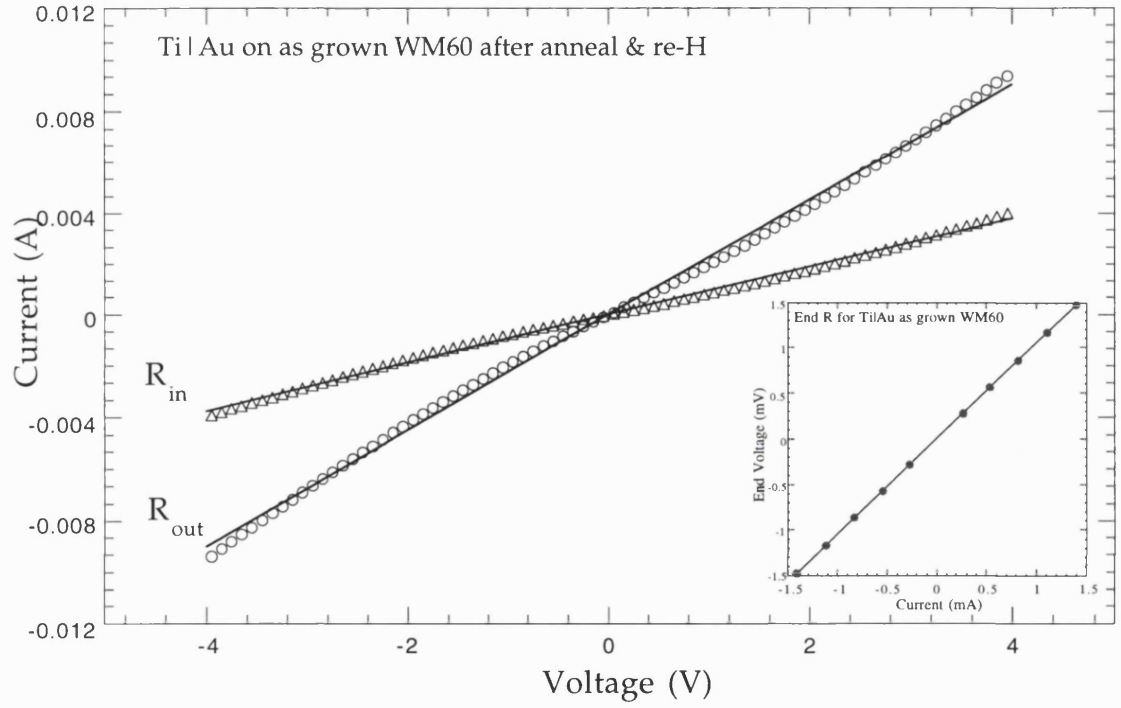

Figure 8.13 I-V plot of the TilAu contact after anneal and re-H.

The I-V characteristics of the TilAu metallisation scheme deposited on the as grown and oxidised surfaces were displayed in figure 8.12 and figure 8.13. The results from the I-V curves show that there are no significant differences in the current level for TilAu contacts deposited on oxidised and as grown surfaces provided both the annealing and plasma treatment are carried out.

The Au test structures after undergoing the same treatment displayed similar characteristics. The deviation of the I-V curves from the linear characteristic after the treatment becomes less prominent as shown in figure 8.14.

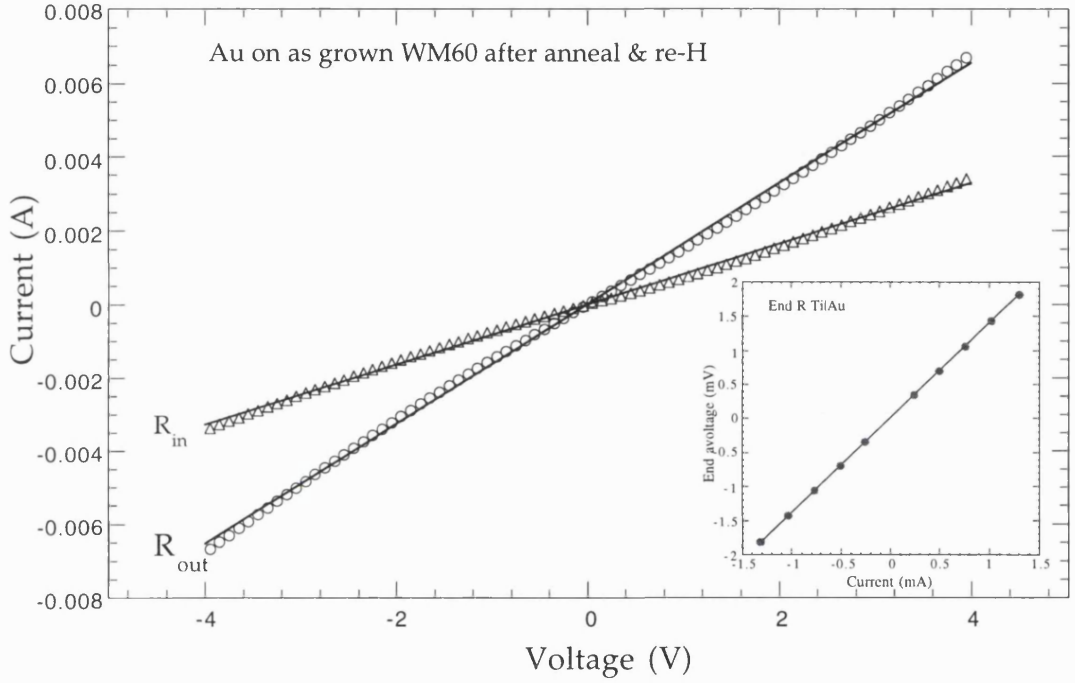

Figure 8.14 I-V plot of Au on as-grown WM60 after the treatment

The 3 samples were then heated on a hot plate to 250°C for 4 hours. This is to investigate the effect of prolonged heat treatment on the specific contact resistance. After the treatment the test structures were characterised at room temperature. The I-V plot will not be shown here. After the 250°C anneal, the current levels measured between the contacts were reduced by approximately an order of magnitude. The shape of the I-V curves was still similar to those shown in this section. The reduction of current was caused by the loss of carriers from the surface. In order to gain more insight on the changes in the surface conductive layer, the analysis section will deconvolute the effect of the various resistances in the test structure.

Section 8.8 Analysis

The experimental results obtained in this chapter may suffer from a 10% error under the worst condition caused by deviation in the measuring instruments. The results of the analysis from Appendix 3 and 4 are summarised in table 8.1 for Au contacts on as grown surfaces without

undergoing a series of 600°C treatments. A specific contact resistance of $0.038\Omega cm^2$ was measured by taking the I-V plot at ±1.5V. By comparing the data points and the best fit line, the I-V plot in figure 8.08 is not perfectly linear. A slightly different result will be obtained if the best fit for the I-V plot is taken between ±2.5V instead of ±1.5 to determine R_{in} and R_{out}. In addition, experimental results revealed that the sheet resistivity of the bulk increases after the samples have been annealed at a higher temperature. The corresponding value for the specific contact resistance shows the same trend. The sheet resistivity below the contact is lower than the sheet resistivity of the bulk (ρ_s). In order to validate the calculation presented here, the value of ρ_s is compared with the experimental results determined from the transfer length method and the van der Pauw measurements using 4 contacts as described in chapter 6. The measurement presented here is within reasonable range from those obtained by these methods. The transfer length (L_T) of the Au contacts on as deposited surfaces ranged from 7 - 14μm. Hence, not the entire contact length of Au used here (150μm) is effective for current injection into the material. This parameter is essential for high power applications as it determines the current density flowing into the ohmic contact and the degree of current crowding. The barrier height in this chapter is determined from equation 8.1. The assumptions made were given in section 8.3.

Contacts Scheme	Material Treatment	Voltage Range (V)	Bulk Sheet R (kΩ/ □)	Sheet R contact(Ω/□)	Specific C R (Ωcm^2)	Transfer Length (μm)	Barrier Height (eV)
Au	as grown	±1.5	17 19	1200	0.04	14	0.41
Au	as grown heat 200°C 30 min	±1.5	35 33	1460	0.06	13	0.42
		±2.5	31 30	750	0.05	12	0.41
Au	as grown heat 280°C 30min	±1.5	180 170	7800	0.13	9	0.44
		±2.5	160 150	7100	0.07	7	0.42

Table 8.1 The properties of Au contacts on as grown WM60

The plots in figure 8.15 show the variation in the specific contact resistance calculated from the R_{in} and R_{out} taken at different bias voltages. The graph revealed that at higher voltages the specific contact resistance is lower than at small voltages. This observation may be explained by the image force which is present in the metal when carriers are injected across the interface. At a higher voltage, more carriers are injected into the metal, the image force experienced by these

carriers will be stronger, hence reducing the barrier height at the interface. An alternative explanation could be the lowering of small individual potential barriers at the grain boundaries that the carriers need to surmount before they can drift in the direction of the applied field. At higher voltages, some of the barriers could be lower and hence more current will flow. The best fit line for R_{in} and R_{out} in figure 8.15 is taken at ±0.2V at the particular voltage where ρ_s is determined. This is further confirmed as the reduction of specific contact resistance displays a natural logarithmic relationship with voltage. A similar relation is expected for lowering of the barrier height by the image force or lowering of potential barriers at the grains.

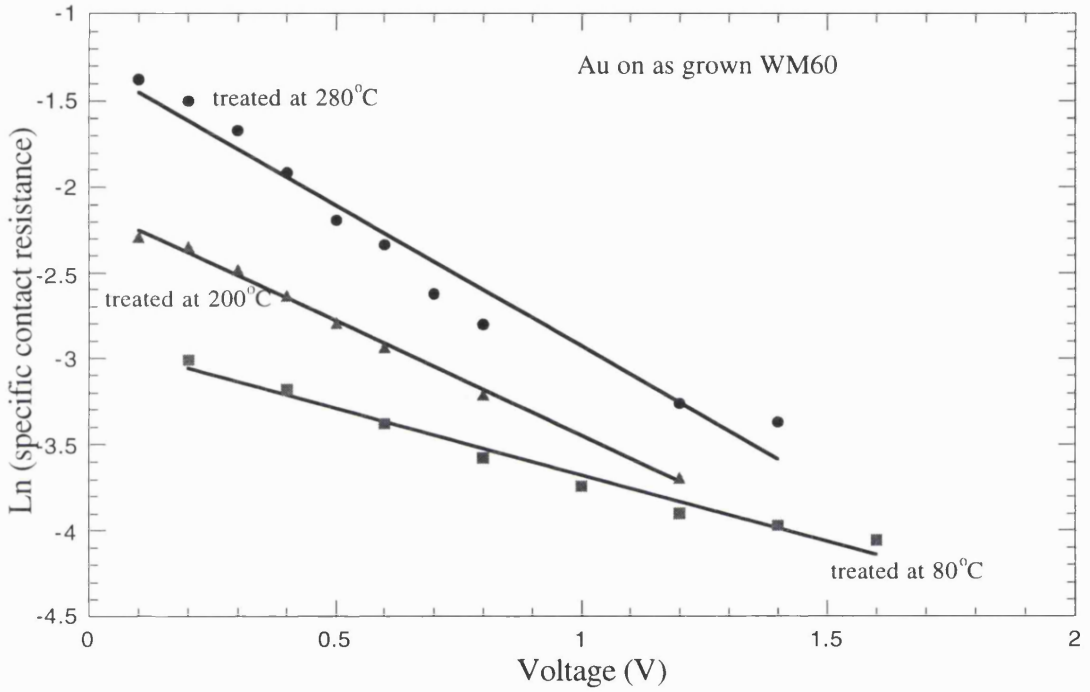

Figure 8.15 The dependency of ρ_c on the bias voltage for the as grown Au contact

The performance of Ti capped with Al test structures (table 8.2) are quite similar to Au (table 8.1) apart from a lower sheet resistivity on the substrate. The process of hardening the photoresist by baking (conducted at 80°C for 20 minutes) reduced the conductivity of the material while the H plasma treatment for the Ti/Al contact restored the original conductivity of the as grown surface.

Contacts Scheme	Material Treatment	Voltage Range (V)	Bulk Sheet R (kΩ/ □)	Contact Sheet R (Ω/ □)	Specific C R (Ωcm^2)	Transfer Length (μm)	Barrier Height (eV)
Ti | Au 3	oxidised						
	annealed	±1.5	14	77	0.028	14	0.40
	re-H		14				
		±2.5	14	66	0.027	14	0.40
			14				
Ti | Au 2	as grown						
	annealed	±1.5	10	120	0.026	16	0.39
	re-H		10				
		±2.5	9.7	45	0.022	15	0.39
			9.3				
Ti | Au 1	as grown						
	annealed	±1.5	9.2	770	0.022	15	0.39
	re-H		8.2				
Ti | Al	as grown						
	annealed	±1.5	14	1300	0.068	22	0.42
	re-H		12				
		±2.5	13	960	0.06	21	0.42
			11				
Au	as grown						
	annealed	±1.5	12	15	0.006	7.2	0.36
	re-H		12				

Table 8.2 The properties of the material and different contacts deposited after the metallisation contact were annealed at 600°C for 20 minutes, followed by re-Hydrogenation at 600°C for 5 minutes.

Table 8.2 also shows experimental results for Ti contacts where Au was used as the cap layer. Comparing between Al and Au capping layer, Au performed better than Al indicated by the lower ρ_c. During the high temperature anneal, oxidation of Al may be occurring. Furthermore, Al has a lower melting point and may not be fully protecting the Ti layer beneath. Au being more inert, will resist oxidation. In addition, it has a larger atomic radius and a higher melting point. The lowest value of ρ_s is obtained for the test structure fabricated using Au on an as grown surface. Immediately after deposition, the Au contact is annealed at 600°C for 20 minutes followed by a re-hydrogenation step to restore the conductivity of the material. A ρ_c value of 6 x $10^{-3}\Omega cm^2$ is measured. On the whole, after a series of treatment, the ρ_s and ρ_c have improved compared to the result in table 8.1. The transfer length of the contacts ranges from 7 to 22μm. However, the sheet resistivity of the material beneath the Au contact (ρ_{ssk}) after the anneal appears

to be much lower than the other metallisation scheme. Comparing a value of only 15.1 kΩ/square for Au contacts after treatment and a value of 1200 kΩ/square for Au contacts without treatment. As Au is inert and do not react chemically with diamond, the possible explanation for a decrease of ρ_{ssk} by 3 orders of magnitude could be the migration of Au into the grain boundaries, hence providing a better contact with the diamond surface.

Contacts Scheme	Voltage Range (V)	Bulk Sheet R (kΩ/□)	Contact Sheet R (Ω/□)	Specific C R (Ωcm^2)	Transfer Length (μm)	Barrier Height (eV)
Au	±1.5	210 180	53	0.39	13	0.47
	±2.5	210 180	43	0.33	13	0.46
Ti / Au 1	±1.5	95 65	45	0.35	19	0.47
	±2.5	88 61	41	0.32	19	0.46
Ti / Au 2	±1.5	97 61	56	0.42	21	0.47
	±2.5	92 59	49	0.39	21	0.47
Ti / Au 3	±1.5	330 270	91	0.80	16	0.49
	±2.5	320 260	83	0.74	15	0.48

Table 8.3 The properties of metallisation scheme after a 4 hour anneal at 250°C

Table 8.3 shows the properties of the contact after a prolonged anneal at 250°C for 4 hours. After the anneal the conductivity level of the doping layer has decreased. The ρ_s has increased by about 20 times. The same trend is observed for Au contacts listed in table 8.1. The specific contact resistance has degraded as well. This demonstrates the importance of the doping concentration on the properties of metal contacts in terms of their specific contact resistance. The increase in the sheet resistance was caused by the loss of carriers from the surface provoked by the high temperature anneal as indicated in Chapter 6.

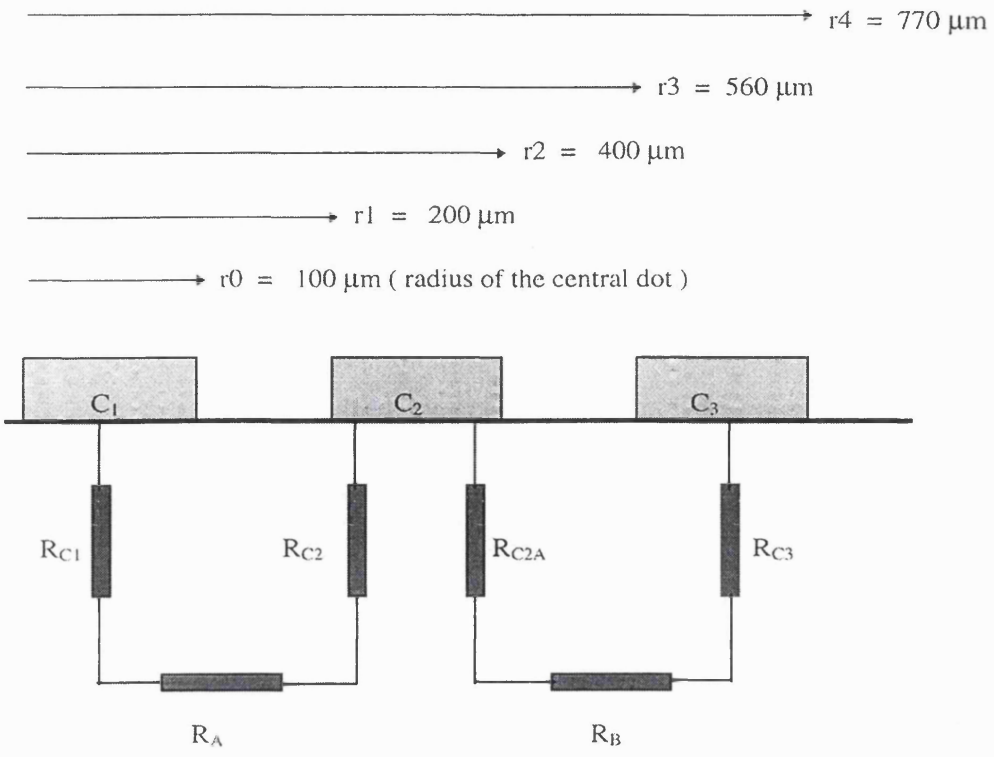

Figure 8.16 The equivalent circuit of the c-TLM test structure

Solving the rest of the parameters in the c-TLM method allows a simple equivalent circuit representation of the entire test structure by six resistors. The equivalent circuit and dimension of the test structure are shown in figure 8.16. C_1 is the central spherical contact surrounded by two other outer concentric contact. R_A and R_B represent the resistance contributed by the bulk while the rest represent the interface resistance. This model is useful as it indicates approximately the distribution of resistance across the ohmic contact and semiconductor. In general from the test structure $R_A > R_B$ because the outer concentric circles have a larger diameter and hence lower resistance contribution. The interface resistance should vary according to the order $R_{C1} > R_{C2} > R_{C2A} > R_{C3}$, as the interface resistance will be dependent on the area of the contact, smaller area will lead to higher resistance. The values that have been calculated should follow this general trend. R_{C2} represents the resistor seen by the current flowing in or out from contact C_2 to C_1 while R_{C2A} represents the resistor seen by the current flowing in or out from contact C_2 to C_3.

Contact Scheme	Material pre-Treatment	Voltage Range (V)	R_{C1} (Ω)	R_A (Ω)	R_{C2} (Ω)	R_{C2A} (Ω)	R_B (Ω)	R_{C3} (Ω)
Au	as grown	±1.5	160	2100	48	29	920	18
Au	200°C	±1.5	250	3900	66	42	1800	26
		±2.5	180	3400	40	26	1600	16
Au	280°C	±1.5	680	20000	230	140	9300	88
		±2.5	440	18000	170	93	8400	62

Table 8.4 Magnitude of resistors in the equivalent circuit for Au c-TLM structure on as grown surfaces.

Table 8.4 displays the magnitude of resistors in the equivalent circuit for the results presented in table 8.1; the magnitude of resistors follow the general trend described in the previous paragraph. The interface resistance is much lower compared to the resistance contributed by the bulk. Hence the formation of an ohmic contact is confirmed in this structure. Comparing the bulk resistance (R_A and R_B) and interface resistance (R_{C1}, R_{C12}, R_{C2A} and R_{C3}), the total interface resistance contributes about 5% of the total resistance. After heat treatment in air at 280°C, all the interface resistances and the bulk resistance degraded. Modification to both of these properties are caused by the loss of carriers from the surface. The dependency of contact resistance on the carrier concentration in diamond has been reported previously [Yokoba, 1998]. Heat treatment at 280°C was conducted as at this temperature significant changes were occurring to the resistance of the hydrogenated surfaces. Furthermore, Al Schottky diodes fabricated on hydrogen doped layer are capable of operating up to 200°C (see chapter 7), therefore it would be interesting to investigate the changes to the ohmic contact after the treatment. Heating at higher temperature will increase the resistance of the surface to a level where it would not be advantageous for electronic applications.

Table 8.5 shows the magnitude of resistors in the equivalent circuit for metal contacts after undergoing a 600°C anneal for 20 minutes followed by a hydrogen plasma treatment at 600°C for 5 minutes. Apart from the Ti/Al contacts, all the other metallisation schemes display lower interface and bulk resistance. The lowest interface resistance (< 3Ω) is obtained using Au after undergoing 600°C anneal and plasma treatments. Ti/Al contacts display slightly higher interface resistance probably because of the inefficiency of Al which is used to cap the Ti layer on diamond. During the high temperature anneal, Al might have oxidised or diffused on to the surface of the diamond itself prohibiting a formation of low resistance contact.

Contact Scheme	Material pre-Treatment	Voltage Range (V)	R_{C1} (Ω)	R_A (Ω)	R_{C2} (Ω)	R_{C2A} (Ω)	R_B (Ω)	R_{C3} (Ω)
Au	as grown	±1.5	21	1300	2	2	656	1
TiAu 1	as grown	±1.5	96	1000	29	18	446	11
TiAu 2	as grown	±1.5	85	1700	12	10	527	5
		±2.5	72	1500	8	7	509	3
TiAu 3	oxidised	±1.5	91	1600	11	9	752	4
		±2.5	87	1500	10	9	735	4
TiAl	as grown	±1.5	270	1500	65	42	635	25
TiAl	as grown	±2.5	230	1400	52	34	607	20

Table 8.5 Magnitude of resistors in the equivalent circuit for different contact schemes after an anneal at 600°C for 20 minutes and re-Hydrogenation at 600°C for 5 minutes.

Contact Scheme	Material pre-Treatment	Voltage Range (V)	R_{C1} (Ω)	R_A (Ω)	R_{C2} (Ω)	R_{C2A} (Ω)	R_B (Ω)	R_{C3} (Ω)
Au	as grown	±1.5	2700	23720	1100	590	9800	400
		±2.5	2200	22830	880	490	9700	330
TiAu 1	as grown	±1.5	2400	10000	940	520	3500	350
		±2.5	2200	9800	860	480	3300	320
TiAu 2	as grown	±1.5	2900	11000	1100	630	3300	420
		±2.5	2600	10000	1000	570	3200	380
TiAu 3	oxidised	±1.5	5100	36000	2000	1100	14000	740
		±2.5	4700	35000	1800	1000	14000	680

Table 8.6 Resistors value in the equivalent circuit for similar contacts as in table 8.5 but after heat treatment at 250°C for 4 hours.

After the heat treatment and hydrogen plasma exposure at 600°C, the test structures in table 8.5 were annealed in air at 250°C for 4 hours. Comparing table 8.5 and 8.6, on the whole, all the properties have degraded after the annealing at 250°C for 4 hours. The total interface resistance for Ti/Au contributes less than 10% of the total bulk resistance indicating that the contacts are still able to perform satisfactory as an ohmic.

Section 8.9 Discussion

Shockley [1964] proposed the idea of specific contact resistance. This theory has been used successfully to explain the current transport mechanism in metal/ silicon contact by Yu *et al.* [1970]. It is well known that the difference between the work function of the metal and semiconductor should determine whether linear or nonlinear I-V characteristic occurs. Linear or ohmic is obtained when the difference is small. However, under practical conditions, this particular property is seldom observed due to the high defect density on the surface mainly caused by natural oxide layers and the Schottky barrier height is said to be pinned [Bardeen, 1947]. Interestingly, Schottky barrier heights on hydrogen terminated diamond show more dependency on the electronegativity of the metal

Among all the metallisation contacts deposited on diamond, Au shows the most material dependent properties. In early reports Au contacts formed Schottky barrier height of 1.5 to 2.0eV on oxidised boron doped homoepitaxial material [Gildenblat, 1991]. Fermi level pinning caused by the high density of surface states on the oxygen terminated diamond was believed to be responsible. Later, on surface conductive hydrogen terminated diamond, it formed reasonable ohmic characteristics. There are literature reports which regard that the formation of ohmic properties of Au is linked to its high electronegativity value. In this case, the barrier height for Au is regarded to be 0eV for contacts deposited on homoepitaxial diamond. There is no proper study based on the specific contact resistance method to assess the actual performance of Au contacts on diamond.

The results presented in this chapter give an insight into the properties of Au deposited on the surface conductive layer based on the method developed by Reeves [1980]. In addition, Schottky barrier height measurements of Au deposited on hydrogen terminated homoepitaxial diamond by UPS conducted in UHV do not obtain a zero barrier height [Tachibana, 1993] but instead is within the range of the values we measured here. The barrier height measurement for Au in this chapter fell within the range of 0.36 to 0.47eV based on the assumptions in Section 8.05 with approximately 15% experimental error. The specific contact resistance of Au is approximately 0.006 Ωcm^2, the lowest obtained in this study. The resistor components in the equivalent circuit show that the interface resistance is less than 5% of total bulk resistance. This indicates that Au contacts should perform satisfactorily as ohmic contacts for the dimension of test structures used here. However, if the bulk resistance is reduced then the percentage contributed by the Au contact will change. This will occur if the separation between the Au contacts is approximately within the μm range. The I-V characteristics of Au contact pads on polycrystalline

diamond reveal slight non linearity, the situation becomes worse as the sample is heated; it is difficult at this point to assume a near 0eV barrier for this metal.

Nakanishi *et al.* [1994] have investigated the optimum conditions for the formation of low resistance contacts using Ti, Mo and Cr on oxidised boron doped diamond films. The authors suggested an anneal at 400°C for 5 minutes for Ti in an evacuated quartz tube. On hydrogenated surface conductive layers, the current study shows that Ti deposited on as grown surface displayed good Schottky characteristic, similar to that reported by [Tachibana, 1992]. Upon annealing at 430°C for 20 minutes, followed by a 400°C exposure to hydrogen plasma, the Schottky characteristic disappeared. However, a poor ohmic property was observed presumably due to charging occurring at the interface. However, a good ohmic resulted from a 600°C anneal for 30 minutes with a 5 minutes 600°C exposure to hydrogen plasma on the same sample. This was at a higher temperature compared to the conditions suggested by Nakanishi *et al.* [1994] on oxidised surfaces.

Miller *et al.* [1997] have performed a careful study of phase transformation of metallic titanium into TiC_x using X-ray photoelectron spectroscopy (XPS) for annealing ranging from room temperature to 700°C on oxidised natural diamond. The authors concluded that, with increasing temperature, the formation of $TiC_{0.56}$ increases until at 430°C, all former metallic Ti will be transformed to $TiC_{0.56}$. Between 430°C and 900°C, the value x depended nearly linearly on temperature. For the annealing temperature of 600°C used in this study, according to Miller's data, an x value of 0.7 is extracted. However, as Ti does not react with hydrogen as easily as oxygen a higher temperature is required by the Ti to surpass the activation energy of the mono hydride structure to reach the carbon atoms beneath.

Yokoba *et al.* [1997] have conducted a detailed study of ohmic contacts to boron doped polycrystalline diamond for films with varying acceptor concentrations. They suggested that the mechanism of field emission (FM) was dominating the transport properties across the ohmic contact for acceptor concentrations (N_A) exceeding $10^{20}cm^{-3}$ and thermionic field emission (TFE) for diamond with N_A ~3 x $10^{18}cm^{-3}$. In addition, they obtained a barrier height measurement of ϕ_b ~ 0.5eV for the annealed Ti, Mo and Cr contacts. They also suggested the similarity between these values is caused by the pinned Fermi level related to the carbidisation. The experimental results from the study showed a Ti barrier height ranged between 0.4 - 0.5eV. This was in good agreement with the values measured by Yokoba *et al.* [1997]. However, the carriers from the diamond film used here originate from surface conductivity rather than impurity boron dopants. Yokoba's experimental results also revealed that in general, for diamond films, specific contact resistance lower than $10^{-4}\Omega cm^2$ can be achieved for doping levels exceeding $10^{20}cm^{-3}$, as displayed in figure 8.16(a). In fact, if the depth of the carriers within the surface conductive layer is assumed to lie within 10nm from the surface, the specific contact resistance that is calculated here is in good agreement with values reported by Yokoba *et al.* [1997]. Their study revealed a value of around 10^{-1} to $10^{-3}\ \Omega cm^2$ for carrier concentrations of 10^{18} to $10^{19}\ cm^{-3}$.

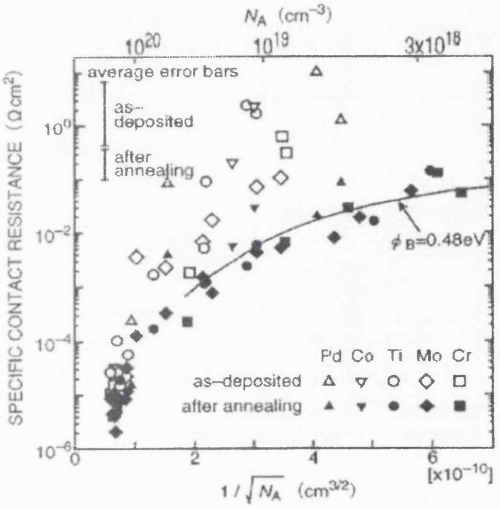

Figure 8.16(a)

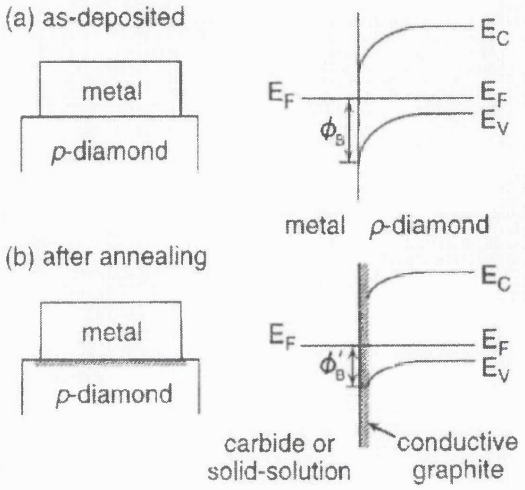

Figure 8.16(b)

Figure 8.16 shows the specific contact resistance measured on diamond films with different carrier concentration and figure 8.16 (b) shows the formation of a low resistive interface caused by conductive graphite [Yokoba, 1997].

The properties of TilAu contacts have been investigated by many workers on boron doped diamond films. The formation of TiC is the main reason for the leaky ohmic behavior of this metallisation scheme. The experimental results in this chapter, showed a similar trend. If the contacts are not properly annealed ohmic properties will not be achieved. No significant difference is observed whether the TilAu contacts are deposited on oxidised or hydrogen terminated surfaces. The leaky interface could result from a damaged layer of non diamond carbon [Tachibana, 1992]. A conductive graphite layer formed beneath the annealed contact could also be responsible [Yokoba, 1997] as shown in figure 8.16(b). The formation of this interface will proceed for both types of termination and once this occur the terminating species will be destroyed. An active hole concentration exceeding 10^{20}cm^{-3} can not be achieved at the moment on the surface conductive layer to allow the field emission mechanism (FE) transport properties. In order to obtain a contact resistance lower than 10^{-4} Ωcm^2, additional carriers must be supplied. This can be achieved by selectively implanting high doses of boron at region where an ohmic contact is desired.

Section 8.10 Conclusion

The properties of ohmic contacts on surface conductive layers have been investigated using c-TLM method. Different metallisation schemes have been explored to find alternative to Au. Experimental results show that it is possible to find an alternative choice of metallisation contact other than Au on these surfaces without resorting to ion implantation at selective site. Although implantation by boron provides a low resistive contact, however it requires an additional processing step and increases the cost of device fabrication. The method which is introduced here

offers the advantage of a cheaper and simpler processing step.

The properties of Au contacts have been improved by annealing the test structure at 600°C for 30 minutes followed by a re-hydrogenation at 600°C for 5 minutes. This metallisation scheme and treatment provide the lowest possible specific contact resistance achieved. The formation of ohmic contacts via Ti has also been investigated. Experimental results shows that without any treatment Ti forms a highly rectifying contact. From the I-V curves, an anneal at 430°C for 30 minutes is not sufficient to form an ohmic contact. A higher temperature anneal at 600°C for 30 minutes improved contact performance. A re-hydrogenation after the anneal is necessary to restore the high conductivity of the material. After this process, a low resistive contact with performance ($\rho_c = 0.02\ \Omega cm^2$) matching those obtained from Au is achieved. The metal which is used to protect Ti from oxidation has some effect on the contact properties. Comparing Al with Au as the protective layer on surfaces which possessed the same degree of resistivity (sheet resistance), Au displayed a lower contact resistance. Oxidation of the Al could be occurring during the 600°C anneal and hence degrading the contact.

References :-

Aleksov, A., Vescan, A., Kunze, M., Gluche,P., Ebert, W., Kohn, E., Bergmaier, A. and Dollinger, G. [1999] Diaond & Relat. Mater., **8**,941.

Aoki, M. and Kawarada, H. [1994] Jpn. J. Appl. Phys., **33**, 708.

Bardeen, J. [1947] Phys. Rev. **71**, 717.

Collins, A.T., and Williams, A.S.W. [1971] J. Phys. C Solid State Phys. **4**, 1789.

Gildenblat, G. Sh. Grot, S.A. and Badzian, A. [1991] Proc. IEEE **79**, 647.

Gluche, P., Aleksov, A., Vescan, A., Ebert, W. and Kohn, E [1997] IEEE Electron Device Lett., **18**, 547.

Hayashi, K., Yamanaka, S., watanabe, H., Sekiguchi, T., Okushi, H. and Kajimura, K. [1997] J. Appl. Phys, **81**, 744.

Iwasaki, T., Okano, K., Matsumate, Y., Matsushima, E., maekawa, H., Kiyota, H., Kurosu, T. and Iida, M. [1993] Diamond & Relat. Mater., **3**, 30.

Kalish, R., Uzan-Saguy, C., Ran, B., Ferber, H., Guettler, H. and Zachai, R. [1998] Diamond & Relat. Mater., **8**, 877.

Kiyota, H., Okushi, H., Ando, T., Kamo, M. and Sato, Y. [1996] Diamond & Relat. Mater., **5**, 718.

Miller, S., Fischer, R., Plank, H., Roth, J. and Dose, V. [1997] J. Appl. Phys., **82**, 3314.

Moazed, K.L., Nyugen, R. and Zeidler, J.R. [1988] IEEE Electron Device Lett., **9**, 350.

Mori, Y., Kawarada, H. and Hiraki, A. [1991] Appl. Phys. Lett., **58**, 647.

Nakanishi, J., Otsuki, A., Oku, T., Ishiwata, O. and Murakami, M. [1997] J. Appl. Phys., **76**, 2293.

Reeves, G.K. [1980] Solid State Electron, **23**, 487.

Schroder, D.K. [1998] 'Semiconductor Device and Material Characterisation', John Wiley & Sons, New York, Chapter 3.

Sze, S.M. [1993] Physics of Semiconductor Devices II, New York, Chapter 5.

Tachibana, T., Williams, B.E. and Glass, J.T. [1992] Phys. Rev. B, **45**, 1975.

Tachibana, T., glass, J.T. and Nemanichj, R.J. [1993] J. Appl. Phys., **73**, 835.

Tsugawa, K., Kitani, K., Noda, H., Hokazono, A., Kirose, K., Tajima, M. and Kawarada, H. [1999] Diamond & Relat. Mater., **8**, 927.

Uzan-Saguy, C., Cyterman, C., Brebner, R., Shaanan, M. and Kalish, K. [1995] Appl. Phys. Lett., **67**, 1194.

Werner, M., Dorsch, O., Naerwind, H.U., Obermeier, E., Johnston, C., Chalker, P.R. and Romani, S. [1995] IEEE Trans. Electron Devices, **42**, 1344.

Yokoba, M., Koide, Y., otsuki, A. and Murakami, M. [1997] J. Appl. Phys., **81**, 6815.

Yu, A.C.Y. [1970] Solid State Electron., **12**, 239.

Zeisse, C.R., Hewett, C.A., Nguyen, R., Zeidler, J.R. and Wilson, R.G. [1991] IEEE Electron Device Lett., **12**, 602.

Chapter 9

Metal Semiconductor Field Effect Transistors from Thin Film Diamond

Contents

Section 9.1 Introduction

Previously many attempts have been carried out to fabricate active electronic devices on diamond. A very early example was a bipolar transistor fabricated on a naturally p-type doped diamond by Prins [1981]. The emitter and collector regions were formed from natural p-type diamond, while the n-type for the base was formed by implanting carbon ions. N-type conduction is believed to be caused by shallow defect states near the conduction band in the crystal. Since then, many attempts to fabricate transistors have been carried out, most of them being field effect transistors (FETs) depending on p-type channels from boron doping. Due to the large leakage current of the Schottky contact most of these devices require an insulating dielectric to isolate the channel and the gate. Diamond MISFETs rely on an intrinsic diamond layer as the insulator dielectric for the gate contact while for diamond MOSFET's SiO_2 is used instead [Gildenblat, 1991]. In general, transistors which utilise natural diamond and homoepitaxial CVD diamond as the substrate display much better performance compared to

heteroepitaxial PCD film.

Boron doping for the FET's channel using both ion implantation and in-situ doping methods have been performed on single crystal diamond [Zeisse, 1991]. Both of these methods have reliably produced MOSFETs which show current pinch off and saturation of drain current. In addition these devices are capable of operating in excess of 500°C. Logic circuits have been fabricated using a combination of these devices and high temperature operation of these circuits have been confirmed. The lower defect density in the material and better CVD deposition technique have lead to improvements compared with the poor device performance reported in the early 90's [Fox, 1995].

Boron forms a p-type dopant with a high activation energy at 0.37eV above the valence band [Collins, 1971]. As a result, for moderately doped film, transistors which are fabricated normally display low current levels at room temperature. However, the activation energy decreases with increasing boron concentration in the diamond. Therefore delta doping of the boron channel might improve device performance, for example boron delta doped MESFET on homoepitaxial films[Shiomi, 1995; Vescan, 1997]. Doping using this method has been carried out by incorporating a boron rod in the chamber during the CVD growth process[Aleksov, 1998]. The memory effects in the chamber, however, produced a tail once the boron source was removed. The tail can be eliminated by implanting nitrogen to compensate for the p-type carriers. Devices which display higher transconductance and operate satisfactory at 200°C have been realised.

A metal semiconductor field effect transistor (MESFET) offers the advantage of simplicity in terms of fabrication process and a faster response compared with a MISFET or MOSFET. However, MESFET devices rely heavily on the formation of a good Schottky contact which has a low level of leakage current. The leakage current in a Schottky contact depends heavily on the doping level and the defect density in the diamond film. Although MESFETs with boron doped channels showing saturation and pinch off have been fabricated [Vescan, 1997], these devices are still poor compared with the performance of MISFETs [Aleksov, 1999; Fox, 1995].

A fully ionised dopant utilising conduction from the hydrogen terminated surfaces has been realised on homoepitaxial diamond films. Kawarada *et al.* [1994] successfully fabricated MESFETs which performed satisfactory at room temperature. These devices were capable of withstanding potentials up to 200V without suffering from breakdown [Tsugawa, 1999]. The transconductance measured at room temperature is the highest ever recorded on diamond, out performing the characteristic of boron doped transistors at room temperature. A combination of these MESFETs produced a logic circuit which displayed satisfactory switching operation at 100kHz. Other than MESFETs, MISFETs using CaF_2 as the gate insulator have also been realised on homoepitaxial CVD diamond [Yun, 1997].

Transistors which are fabricated on PCD diamond display poor characteristics and suffer

from large leakage currents. MISFETs and MOSFETs using boron doped channels on PCD film display current levels in the nA and μA range respectively. The highest transconductance recorded was only 174 μS/mm (300°C) [Pang, 1997]. Transistors fabricated on these materials do not show current pinch off or saturation. As a result, there were few attempts to fabricate active electronic devices using this substrate. The surface roughness of the material coupled with highly defective film and grain boundary scattering make this material difficult to handle in terms of device processing and carrier transport properties. Fabrication of a MESFET has not been previously reported on this material.

Section 9.2 Experimental Aims

In the previous chapter, Hall measurements confirmed the presence of a p-type surface conductive layer on PCD. Also in chapter 7, the operation of Schottky diodes has been demonstrated with 5 different metal contacts. Al contacts displayed the most rectifying properties and Au being nearest to ohmic. The main experimental aim in this chapter is to demonstrate the operation of a MESFET using the surface channel as grown on PCD. Al was chosen as the metallisation contact for the gate as Schottky diodes previously fabricated using this metal displayed the lowest reverse leakage current. This will be useful to prevent excessive current from flowing into the gate. Furthermore, a MESFET requires a good depletion region to control the current flow between the source and drain.

The transfer characteristics of these transistors will be presented and their operational mechanism discussed. In addition, the difficulty which is associated with processing and fabricating MESFETs on PCD will be reviewed. In the discussion section, the performance of the transistors will be compared with the performance of similar MESFETs deposited on homoepitaxial material. The properties which influence the FET characteristics on PCD and performance enhancing device designs will be presented.

Section 9.3 Experimental Methods

The metal contacts were deposited by thermal evaporation using an Edwards E306 evaporator. The pressure during evaporation was maintained at approximately 10^{-6}mbar. Two PCD films, BD8 and WM60, were used as substrates for fabricating the MESFETs. Both the PCD films with randomly aligned grains were grown using the MPECVD method. All the samples were degreased according to Appendix 1 before metal contacts were deposited.

BD8 is approximately 300μm thick with average grain size 30-60μm
WM60 is approximately 100μm thick with average grain size 10-30μm

The Raman spectra recorded using a red He-Ne laser (633nm) for both of these films was shown in Chapter 5. A single sharp peak is present at 1332cm^{-1} with no other signal in the

non diamond carbon region indicating that the diamond film used here is of high quality and almost free of graphitic phases. Shadow masking was used to define the gate metallisation contact on the larger grain material BD8, while photolithography was employed on the smaller grain material WM60. I-V characteristics of the MESFETs were ascertained using HP4145B semiconductor parameter analyser. The characterisation of MESFETs in this chapter was performed only at room temperature.

Section 9.4 Device Fabrication

Initially, shadow masking was used to define structures on both of the PCD samples. Later, a chrome mask was designed using the software Wavemaker and photolithography was used to define the FET structure. However, photolithography cannot be performed on BD8 due to the surface roughness of the material and so shadow masking was always employed. Fortunately, photolithography is successful on the smaller grain size material WM60. Shadow masking was performed by using clean Al wire (0.5mm diameter) which acts as a mask. Samples from the wafer were cut manually and placed on the glass slide. They were attached on the glass slide with double sided adhesive tape on the substrate side. Strips of Al wire were placed carefully across the sample. They were positioned as close as possible without touching each other. After the deposition of metal, the wires were carefully removed. Rectangular strips of Al from the evaporation remained on the sample. The width of the Al strips deposited is dependent on the separation between the wires. This is critical as the area of Al strip will influence the leakage current in the MESFET.

Photolithography is carried out in the clean room using the Karl Suss mask aligner equipped with a 10W He-mercury lamp. The lamp generates ultra-violet (UV) light which is required to project the image of the mask on to the photoresist coated sample. To planarise the rough surface, a positive thick photoresist AZ4652 is used. The photoresist is spun twice. The parameters for the process are given in Appendix 3. An etching technique is used to define the metallisation structure on the sample. Firstly, Al is deposited on the entire sample to a thickness of 200nm. A layer of photoresist is spun on top of the Al layer and baked in order to harden it. A light field mask which contains the image of the gate metallisation contact is placed between the UV source and the sample during exposure. After exposure, the weakened photoresist is removed in a (1:3) mixture of developer and deionised water. Once the unwanted photoresist is completely removed from the sample, it is placed in an aluminium etch solution. The Al layer which is not protected by the photoresist will be etched away. Once this process is complete, the layer of photoresist protecting the Al is removed using acetone. An example of the completed gate metallisation structure taken from the optical microscope is displayed in the figure 9.01. The gate length in the figure is approximately 30 μm.

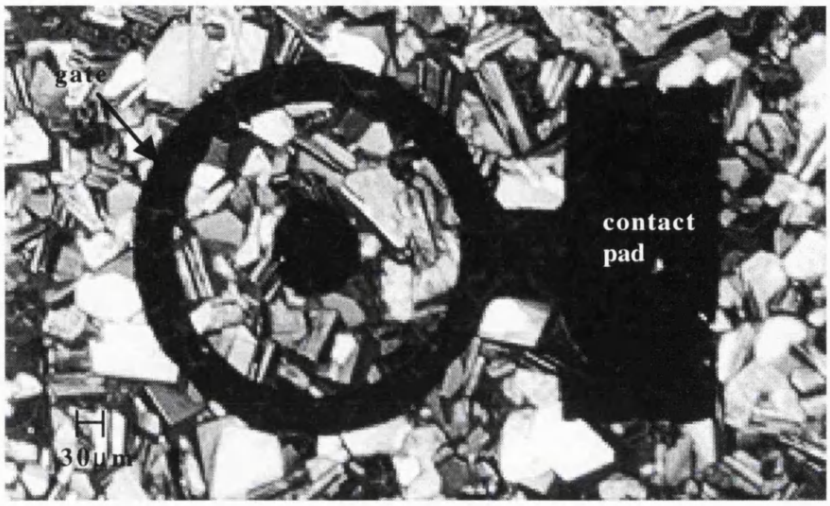

Figure 9.01 The Al gate of the MESFET defined by photolithography on WM60

Section 9.5.1 Experimental Results: MESFETs from BD8 (shadow masking)

The first set of results presented here were obtained from rectangular strips of Al deposited on BD8 by means of shadow masking. Point contacts from the probes were used as ohmic contacts for the drain and source in this MESFET. The I-V characteristic of the point ohmic contacts on the sample is shown in figure 9.02(a). A near linear relation between the current and voltage is recorded for the point probe contact. This indicates that reasonably good ohmic contact can be obtained in this manner.

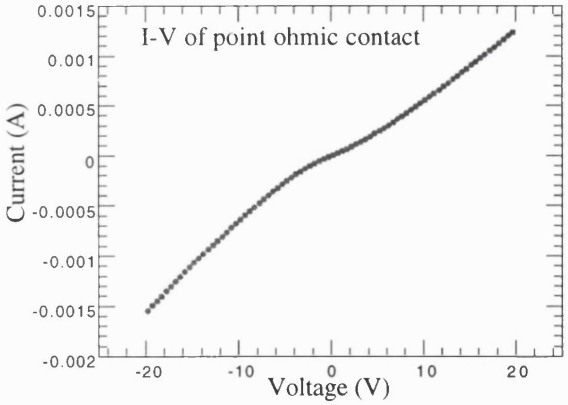

Figure 9.02(a)

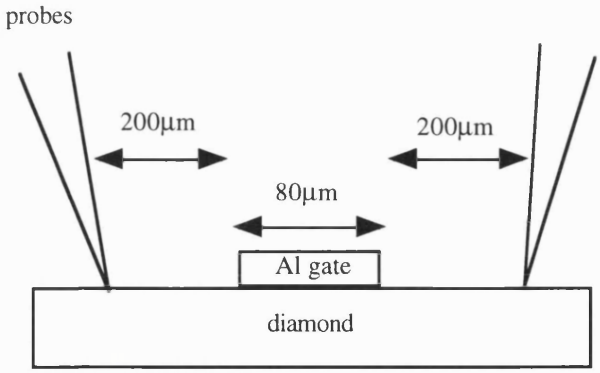

Figure 9.02(b)

Figure 9.02(a) The I-V plot of the point probe ohmic contacts on the surface of PCD films and figure 9.02(b) reveal the positioning of the probes on the MESFET structure.

The voltage given in the transistor transfer characteristic plotted in this chapter is measured with respect to the source. The I-V characteristics of the first MESFET fabricated on PCD material is shown below in figure 9.03. Point ohmic contacts are used as the source and

drain respectively. When zero bias is applied to the Al gate, current in the nA scale is flowing between the drain and the source. As the gate is biased more negatively with respect to the source, the source to drain (I_{DS}) current increases rapidly. At about V_{GS} = -1.0V, the MESFET is turned on. Significant changes in current level are recorded between the drain and source (I_{DS}) for step changes in gate bias applied above the threshold voltage. The operation of a MESFET is confirmed on a thin film PCD. MESFET's operating in this manner are known as enhancement mode (normally off) transistors. An application of a negative bias at the gate is required to switch this transistor on. The Al gate generates a depletion region which is wide enough to totally deplete the conducting p-type channel beneath it. No carriers will be available for current conduction in this region.

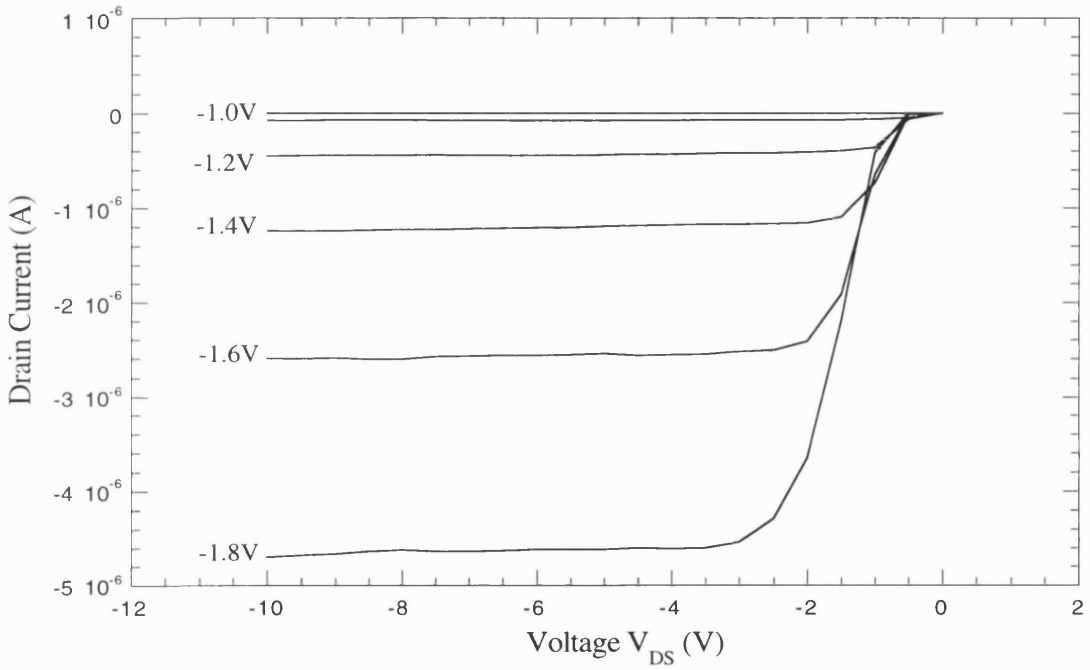

Figure 9.03 The transfer characteristics of a MESFET (Device 1) first obtained on BD8.

The plot in figure 9.03 shows current saturation of I_{DS} for V_{DS} of greater than -2.0V. The gate length of this device is about 80μm while the separation between the point source and drain is about 200μm as shown in figure 9.02(b). In addition, good modulation of I_{DS} with V_{GS} is obtained. Previously, Al Schottky diodes fabricated on this material displayed a reverse breakdown capability of more than 100V. This indicates that the MESFET fabricated here should be capable of withstanding a bias of similar magnitude applied between the source and drain (V_{DS}).

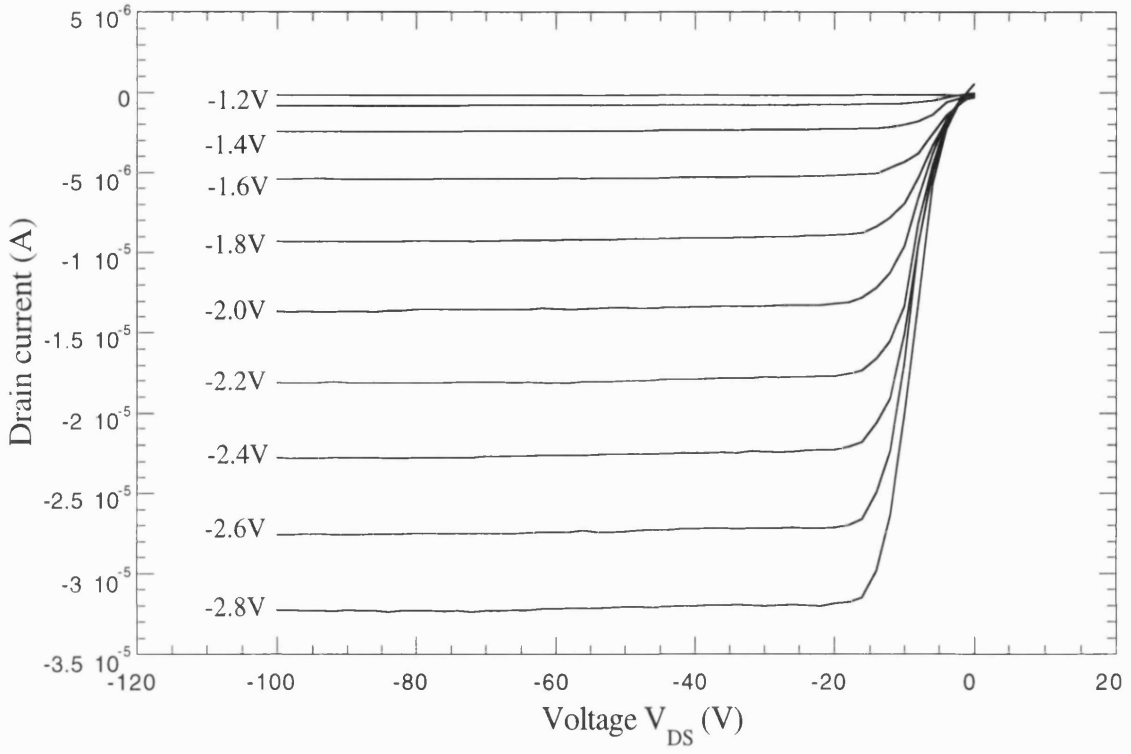

Figure 9.04 The transfer characteristics of a MESFET (Device 2) on BD8 with a breakdown > 100V.

Figure 9.04 shows the I-V characteristic of a PCD MESFET with a breakdown capability of more than 100V. There is no indication of breakdown across the entire voltage range. The turn on voltage for this particular device is at V_{GS} = -1.0V similar to the one previously recorded. The I-V plot shows current saturation of I_{DS} and good modulation with V_{GS}. The maximum range of 100V in this plot is caused by the limitation of the testing instrument, a higher breakdown voltage should be possible for this device.

The plot of leakage current (I_G) for this particular device against V_{DS} at different V_{GS} is given in Figure 9.05. At V_{DS} = 0.0V the leakage current is highest for a particular gate bias. However, as V_{DS} is increased, the leakage current decreases sharply and saturates at approximately V_{DS} > 8.0V. In addition, the leakage current is dependent on the gate bias V_{GS}. The more negative the gate bias the greater the leakage current at V_{DS} = 0.0V. The same relation was observed for the saturation of leakage current, it will saturate at a higher value for a larger V_{GS}.

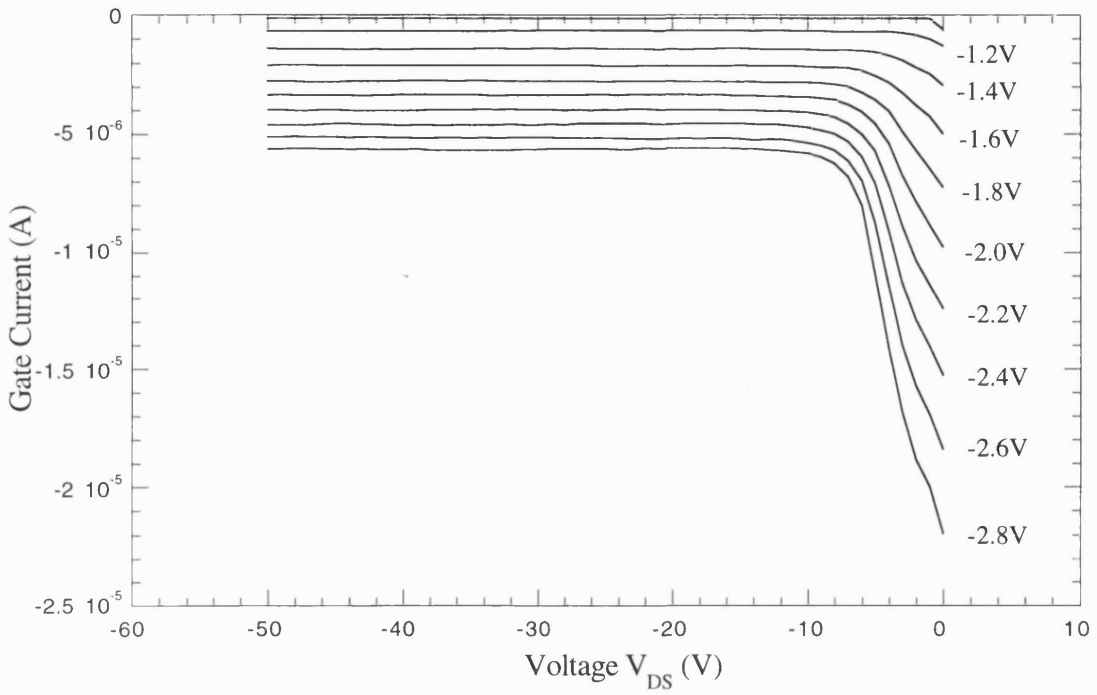

Figure 9.05 The plot of I_G against V_{DS} at different V_{GS}.

However, not all the devices fabricated on BD8 displayed characteristics as described in figure 9.04. Devices which displayed breakdown at a potential smaller than 100V have been observed. This results from the breakdown of the reverse biased Al Schottky contact between the gate and drain. Excessive leakage current (I_G) was also recorded. As shown in Figure 9.05, this is significant when zero bias is applied at the drain and the source. Under this condition both the source and drain will be under forward bias with respect to the gate. This form of leakage current can be reduced by biasing the gate at a smaller negative potential and more importantly by decreasing the total area of the gate. This also effectively decreases the probability that the gate metallisation contact will be deposited over a defective region of the diamond film. This is vital especially on a PCD surfaces. In order to fabricate a good MESFET, a smaller gate length is also essential to allow positioning of the drain contact closer to the source. In order to achieve a smaller gate area by reducing the gate length, fabrication of devices through the use photolithography is required.

Section 9.5.2 Experimental Results: MESFET on WM60 (photolithography)

Photolithography cannot be performed on the large grain size PCD BD8. In this section, smaller grain material (10 - 30 μm) WM60 was used for the fabrication of MESFETs. The Al gate metallisation structure can be defined successfully by photolithography. Unfortunately due to the surface roughness it is not possible to perform an alignment to define the source and drain contacts. The depth of field in the microscope, the non uniform thickness of the photoresist and the reflection of light from each grain obscures the alignment marks on the diamond surface.

With the gate structure well defined by photolithography, point probe contacts were again used as the ohmic contacts for the source and drain respectively. The gate length of the MESFET was about 30μm while the gate width was approximately 550μm as shown in figure 9.01. The separation between the two probes (source and drain) was approximately 200μm. The I-V characteristic of the device shown in figure 9.07 indicate the typical transfer curves for a reasonable operating MESFET. The source to drain current increases rapidly for $V_{DS} < -5V$ when negative bias is applied at the gate with respect to the source. At higher potentials, current saturation of I_{DS} was observed indicating that the conducting channel was successfully pinched off at each step of gate bias.

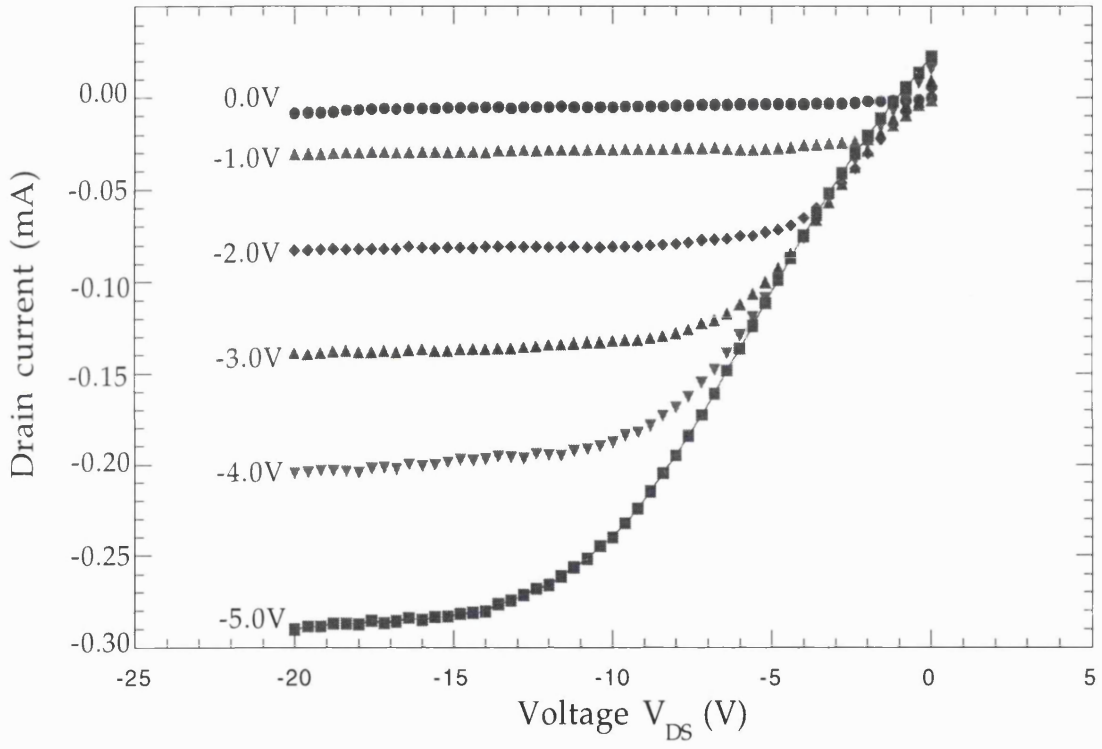

Figure 9.07 The transfer characteristics of the MESFET on WM60 at large gate bias

A small gate bias was applied to inspect the changes of current level close to the threshold voltage. Figure 9.08 reveals that a current of approximately 90μA is flowing between the drain and the source at $V_{GS} = 0.0V$. The drain current of the MESFET displayed here is not totally pinched off compared with the same device on BD8 which required a V_{GS} of at least -1.0V to switch the device on.

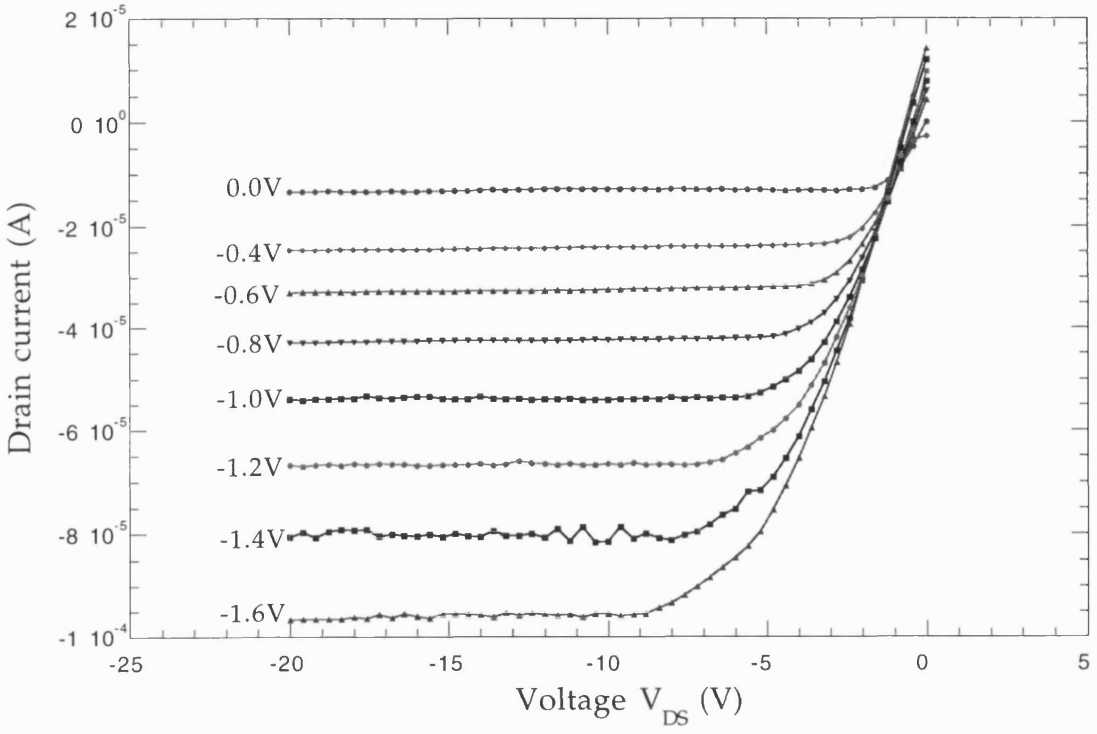

Figure 9.08 The transfer characteristics of MESFET (Device 3) on WM60 at small gate bias.

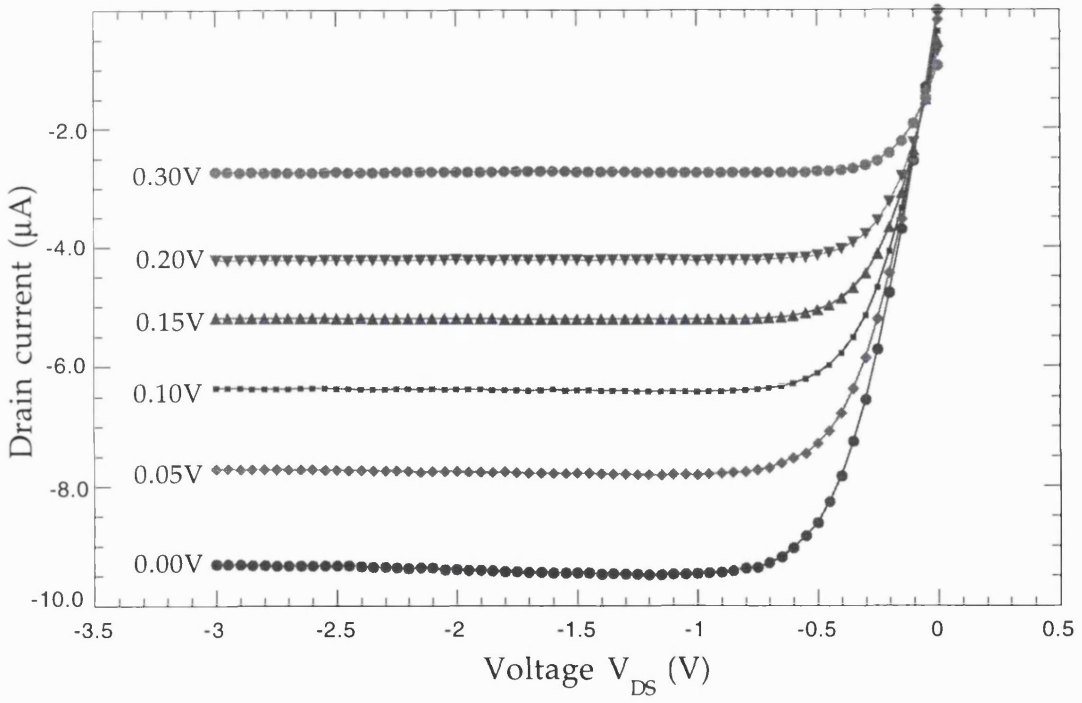

Figure 9.09 The I-V plot shows depletion mode action of MESFET (Device 4) on WM60

If a positive bias is applied to the gate of the MESFET whose transfer characteristics are displayed in figure 9.08, the current flowing in the conductive channel I_{DS} can reduced. A depletion mode operation of the MESFET is demonstrated as shown in figure 9.09. This arises

because the Al gate on WM60 is insufficient to deplete the entire channel beneath the contact. This was not the case for MESFET fabricated on BD8.

Section 9.6 Analysis of MESFETs

For a MESFET to operate in enhancement mode, the gate metallisation contact must be able to deplete the entire channel beneath it under zero bias conditions. This can be achieved with a very thin channel on the surface. Normally a delta doped channel will be necessary to obtain this condition. For a p-type channel, to switch the device on, a negative bias must be applied between the gate with respect to the source. The bias will reduce the width of the depletion region beneath the gate resulting in a thin undepleted channel which will allow current to flow. Once this is achieved the bias between the source and the drain will inject current through this conductive path. In order to prevent forward bias leakage current flowing between the gate and the drain, the drain has to be biased negatively with respect to the gate. This will cause a reverse bias junction between the drain and the gate hence only a small reverse bias leakage current (I_{GD}) will flow. The larger the negative bias applied on the gate, the wider the undepleted channel and consequently the higher the source to drain current.

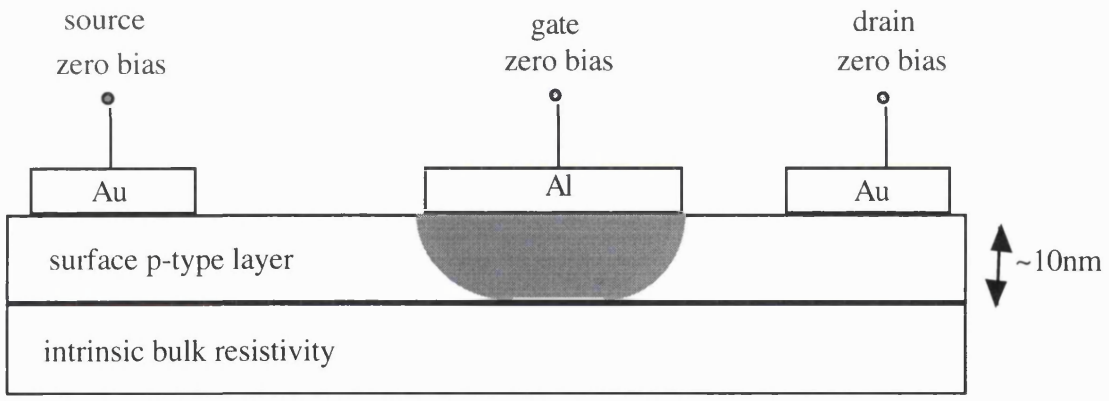

Figure 9.10 shows the depletion region of an enhancement mode MESFET under zero bias. The gate is placed closer to the drain to increase the series resistance between the gate and the source reducing the leakage current in the device.

In a depletion mode MESFET, the gate metallisation contact must leave a section of undepleted channel large enough for current to flow between the drain and the source under zero gate bias. For a p-type channel biasing the gate positively with respect to the source will increase the width of the depletion region beneath the gate thus reducing the width of the remaining useful channel. As a result, the source to drain current driven by the negative bias applied at the drain will be smaller than before. Again the drain has to be biased negatively with respect to the source to only allow a small reverse leakage current to flow between the gate and the drain. If a large enough positive voltage is applied at the gate, the conducting channel will be pinched off.

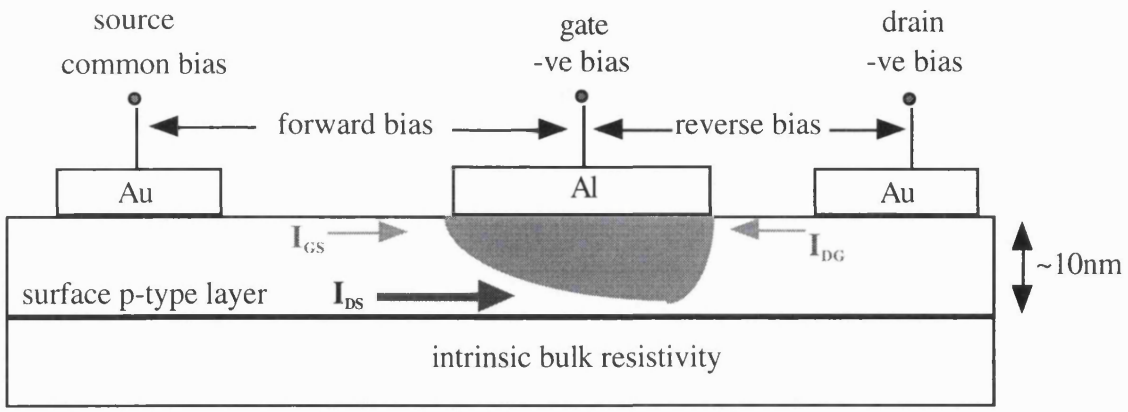

Figure 9.11 shows the current path in the MESFET when a negative bias is applied at the gate with an even larger negative bias applied on the drain. I_{DS} is the main useful current component while I_{GS} and I_{DG} are leakage currents flowing into the gate.

The inevitable forward bias between the gate and the source produced a large forward bias leakage current flowing into the gate (I_{GS}). The more negatively the gate is biased the larger this current will be. The I_{GS} will remain as long the gate has to be in forward bias to allow the injection of I_{DS}. The magnitude of I_{GS} is strongly dependent on the effective area of the gate and the ohmic contact of the source. Smaller total gate area will reduce this forward bias leakage current injected into the gate. However, the presence of a negative potential on the drain reduces the active area of the gate for this form of current injection. This is because the reverse bias between the gate and the drain will deplete the channel on the side of the gate which is adjacent to the drain. Hence only the gate region near to the source will be active for this form of current injection. This is the main form of leakage current encountered in this mode of operation. However, in the depletion mode the leakage current through the gate is less severe. This is because with a positive bias applied on the gate and negative bias on the drain, both the source and the drain will be in reverse bias hence the leakage current in the gate will only constitute the small leakage current from the reverse bias of the Schottky Al gate contact.

For an improved device design the gate area will need to be small which is best achieved by reducing the gate length as a large gate width is required to obtain a large I_{DS}. A smaller gate length will reduce the effective area and therefore the depletion capacitance which leads to a faster switching device. The gate has to be long enough to allow control of the channel which can be approximated to the thickness of the conducting channel. At these dimensions, the short channel effect and the saturation of drift velocity will dominate the characteristics of the FET. In addition, a shorter gate length allows the drain and source to be closer thus reducing the series resistance contributed by the conductive channel. This is the most significant design parameter which determines the normalised experimental transconductance of the device.

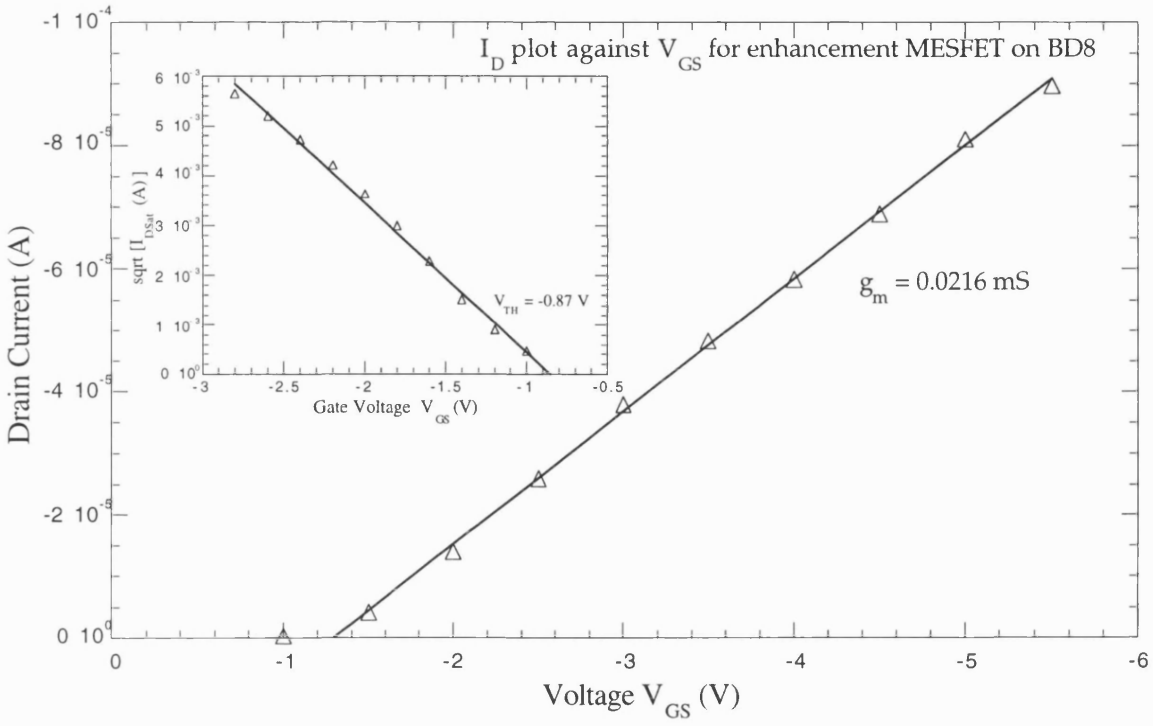

Figure 9.12 The plot of I_D against V_{GS} for enhancement MESFET (device 2) on BD8 with the g_m of 0.022mS and V_{TH} of -0.87V shown inset.

The transconductance of a MESFET is defined as

$$g_m = \frac{\partial I_{DSat}}{\partial V_{GS}}$$

where ∂I_{DSat} is the change in the saturated source to drain current.

∂V_{GS} is the change in the gate to source voltage.

This quantity indicates the ability of the gate voltage to control the source to drain current.

The plot of $(I_{Dsat})^{0.5}$ against V_{GS} can be applied to determine the threshold voltage (V_{TH}) of the MESFET as displayed in the inset of figure 9.12. The intercept at the V_{GS} axis by extrapolating the linear region of the plot will give the value of this quantity. The threshold voltage for the MESFET fabricated on both of these films were different. The calculated V_{TH} for the MESFET on BD8 was about -0.87V (figure 9.12) while the MESFET on the smaller grain WM60 displayed a V_{TH} of 0.68V (figure 9.13). A linear relation was obtained for the dependency of drain current with V_{GS} in figure 9.12. The gradient of the best fit line revealed a transconductance of 0.022mS.

An upper estimate for the potential transconductance of the device structure fabricated here can be obtained from [Sze, 1993] :-

$$g_{max} = \frac{2qN_A Z\mu a}{L} \quad \text{..... (Equation 9.1)}$$

where L is the length of the gate structure (cm)

Z is the width of the gate structure (cm)

N_A is the active acceptor concentration (cm^{-3})

a is the thickness of the channel (cm)

μ is the carrier mobility (cm^2/Vs)

$(N_A.a)$ in this case, is assumed to be the sheet carrier concentration (cm^{-2})

As shown in equation 9.1, g_{max} is inversely proportional to the gate length (L_T). It is also directly dependent on the mobility of carriers and sheet carrier concentration. These two quantities are material dependent, the other parameters are either constant or a function of the device dimension. Hence, given the same device design the sheet resistivity and mobility of the carriers in the material are important in determining g_{max}. Applying equation 9.1 on the MESFET whose characteristics are displayed in figure 9.12 and assuming the following values :-

$\mu = 28\ cm^2/Vs$ $N_{sh} = 2 \times 10^{13}\ cm^{-2}$ $L = 80\mu m$

a theoretical normalised g_{max} of 2.4mS/mm was obtained. This value is much higher than the experimentally determined value of g_m = 0.022/1.5mm (gate width) = 0.015mS/mm. The reason for this large discrepancy is due to the series resistance between the drain and source as point ohmic contacts were used. In addition, equation 9.1 assumes that under ideal conditions the separation of the drain to source is equal to the gate length, which cannot be achieved practically.

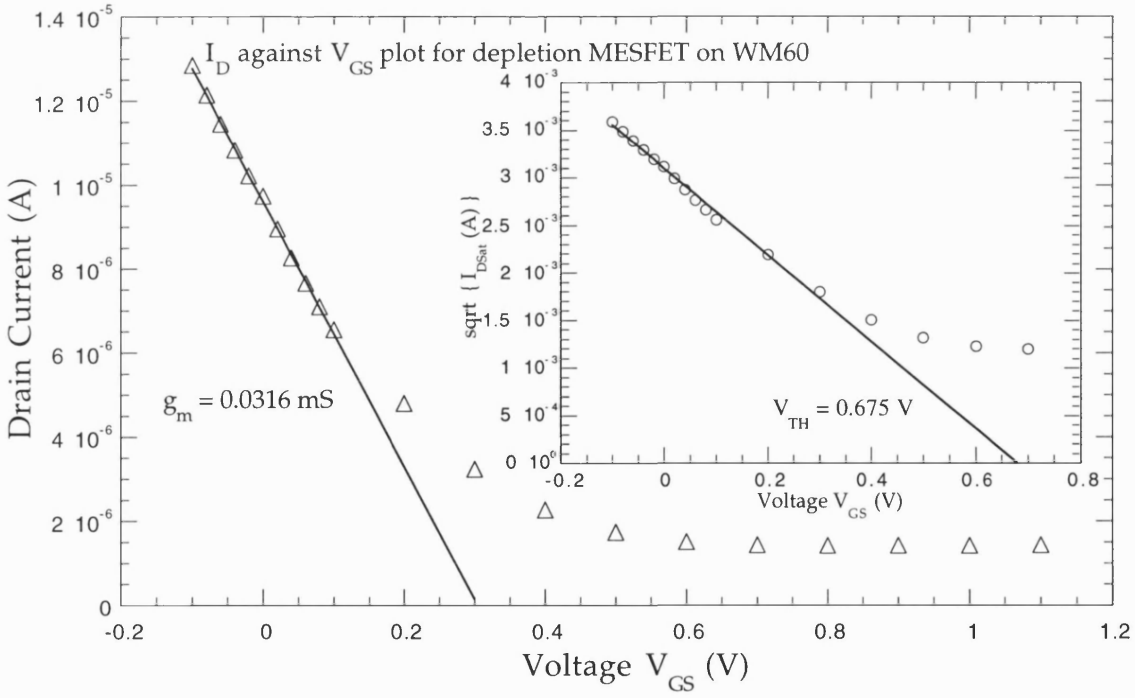

Figure 9.13 The I_D against V_{GS} plot for depletion mode MESFET on WM60.

Figure 9.13 shows the plot of I_{Dsat} against V_{GS} for the depletion mode MESFET fabricated on WM60. The linear fit displayed a transconductance of 0.032mS. Figure 9.14 shows similar plot for the enhancement mode MESFET on the same material with a higher transconductance of 0.064mS. Both of these modes were achieved by biasing the gate contact of the device in the opposite direction. As a result of this biasing condition, comparing both the graphs, the I_{Dsat} for the depletion mode is much lower than the enhancement mode device. The experimental results for these plots are summarised in table 9.1

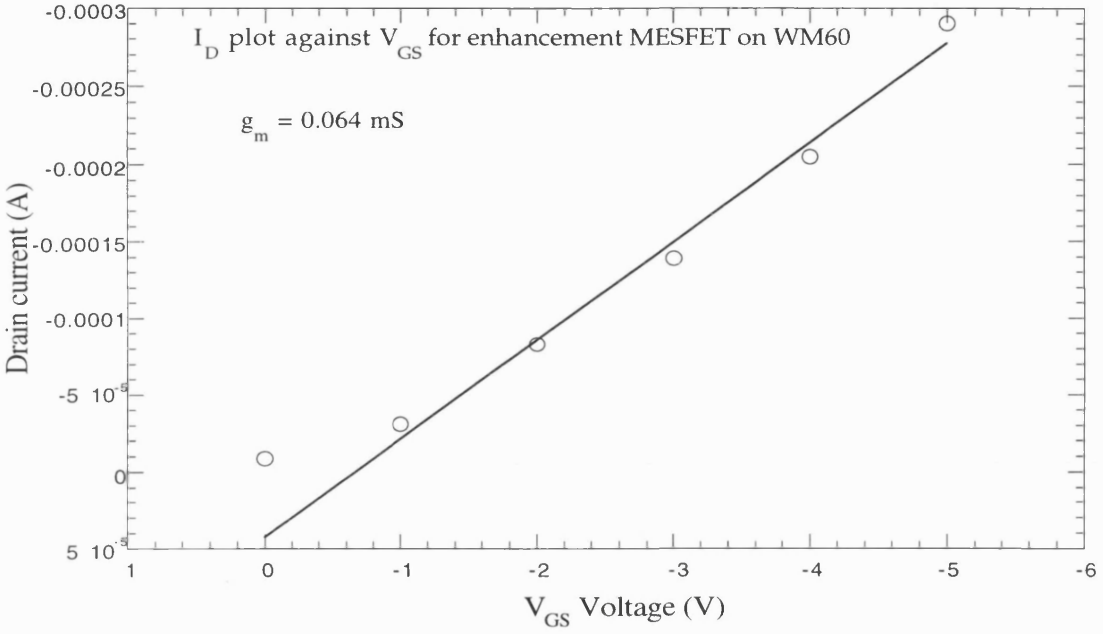

Figure 9.14 The I_D against V_{GS} plot for MESFET on WM60 in enhancement mode.

As point probes were again used as the electrical contacts for the source and drain in figure 9.14, the current will be severely limited by the small area of the probe. Had dedicated Au contacts been used instead, a higher current injection from source to drain would have been expected from these MESFETs. A summary of the threshold voltage (V_{TH}) and transconductance measurement of MESFETs in this chapter is given in the table 9.1.

Device	Material	Gate Type	Device mode	Transconductance g_m (mS)	V_{TH} (V)
1	BD8	shadow masking rectangular	enhancement	0.016	-0.60V
2	BD8	shadow masking rectangular	enhancement	0.022	-0.87V
3	WM60	photolithography conc. circle	enhancement	0.064	0.68V
4	WM60	photolithography conc. circle	depletion	0.032	0.68V

Table 9.1 The transconductance g_m and the V_{TH} of the devices when point ohmic contact are used

It is possible to approximate the channel depth of the conductive layer from the transfer characteristic of these MESFETs. Due to the surface roughness and the randomly aligned grains of this material, it is not possible to do a simulation of the FET characteristics fabricated on these surfaces. Two methods have been introduced to estimate the thickness of the channel called method 1 and method 2. However, both methods assume that the FETs are fabricated on an ideal smooth surface which clearly deviates from the actual condition. So in this case the term effective channel depth, a_{eff} was used for results obtained from both of these methods.

Method 1

The actual channel depth can be approximated from the equation below :-

$$V_P = \frac{qN_A a_{eff}^2}{2\varepsilon_s} \quad \text{..... (equation 9.2)}$$

where V_P is the pinch off voltage (V)

a_{eff} is the channel depth (m)

ε_s is the permittivity of free space (F/m)

The saturation voltage V_{Dsat} is given by the equation below :-

$$V_{Dsat} = V_P + V_{GS} - V_{bi} \quad \text{..... (equation 9.3)}$$

where V_{bi} is the built in potential at the gate junction (V)

V_{GS} is the gate to source voltage (V)

V_{Dsat} is the drain to source voltage the point when I_{DS} is just saturating (V)

In equation 9.3, V_P will be the sum of V_{Dsat} and V_{bi} minus V_{GS}. This is because the pinch off condition will be enhanced by the voltage contributed by V_{Dsat} and V_{bi}. However, a more negative value of V_{GS} will have the tendency to open the channel and hence reduce the pinch off condition. The value of V_{bi} is about 0.7V, obtained from the I-V curves of the Al Schottky diode. In addition, $N_A \, . \, a_{eff} = N_{sh}$ assumes a uniform carrier profile.

Rearranging and combining equation 9.2 and 9.3 the following expression is derived :-

$$V_{Dsat} = \frac{qN_A a_{eff}^2}{2\varepsilon_s} + V_{GS} - V_{bi}$$

$$\frac{V_{Dsat} - V_{bi}}{V_{GS}} = \frac{qN_{sh} a_{eff}}{2\varepsilon_s} \frac{1}{V_{GS}} + 1 \quad \text{..... (equation 9.4)}$$

A plot of $\frac{V_{Dsat} - V_{bi}}{V_{GS}}$ against $\frac{1}{V_{GS}}$ will give a linear line with the gradient $\frac{qN_{sh}a_{eff}}{2\varepsilon_s}$, and as the other parameters in the gradient are constant or can be experimentally determined, the channel depth can be calculated. The built in potential (V_{bi}) of the junction can be determined from the forward characteristic of the diode.

assuming N_{sh} = 2 x 10^{13}cm^{-2} (from Hall measurements)
ε_s = 5.5 x 8.85 x 10^{-12} F/m

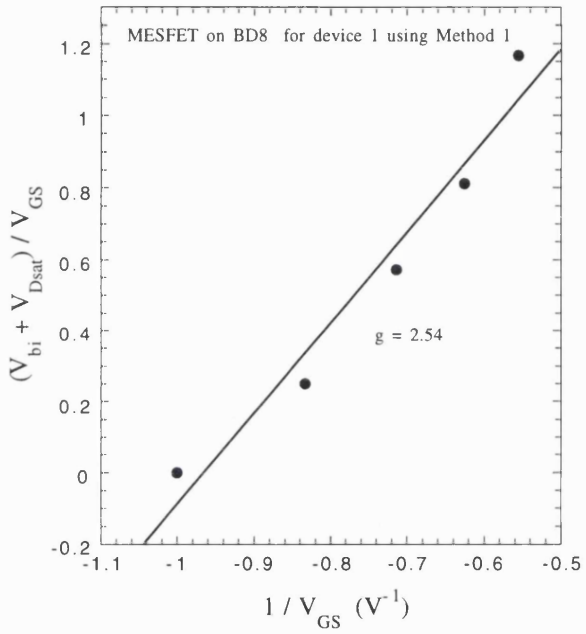

Figure 9.15(a) The plot which reveals the determination of channel depth based on method 1.

An a_{eff} value of 7.7nm is extracted from figure 9.15(a). As for other MESFETs, it is difficult to determine the exact position where the drain current begins to saturate and the plots do not show a linear relation hence the results of the calculation are not included.

Method 2

Besides the method above the channel depth can also be estimated from the expression below :-

$$I_{Dsat} = \frac{Z\mu\varepsilon_s}{2a_{eff}L}(V_G - V_{TH})^2 \quad \text{..... (equation 9.5)}$$

where I_{Dsat} is the saturated drain current (A)
V_{TH} is the threshold voltage (V)
a_{eff} is the effective channel depth (m)
ε_s is the permitivity of the semiconductor (F/m)

plotting a graph of I_{Dsat} against $(V_G - V_{TH})^2$ will yield a linear line where the positive gradient g will be as :-

$$g = \frac{Z\mu\varepsilon_s}{2a_{eff}L} \quad \text{..... (equation 9.6)}$$

from here the effective channel depth a_{eff} can be estimated.On WM60, assuming μ = 17 cm^2/Vs, L = 30 μm and Z = 71 μm while on BD8 assuming μ = 28 cm^2/Vs, L = 80 μm and Z = 80 μm.

Strictly, method 2 requires that the value of V_{GS} approaching that of V_{TH} is used for equation 9.5 to be valid. Hence the product of $(V_{GS} - V_{TH})^2$ of less than 1 is chosen to reduce the error.

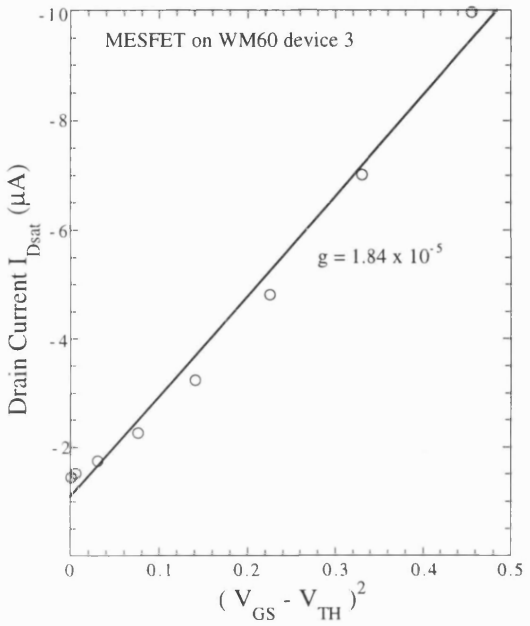

Figure 9.15(b)

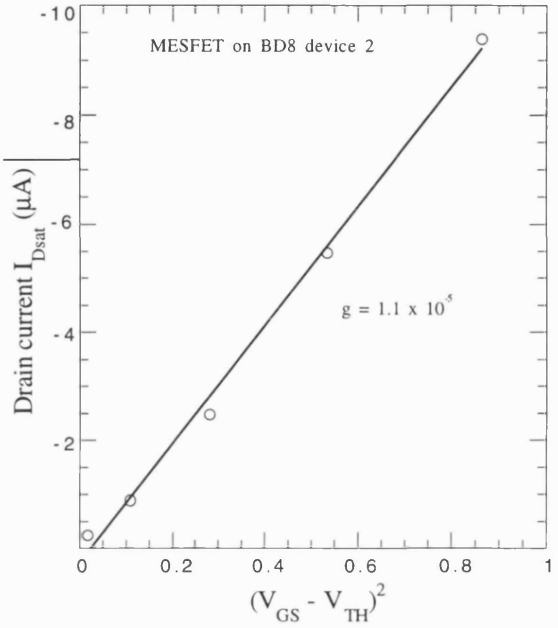

Figure 9.15(c)

Figure 9.15(b) and (c) show the I_{Dsat} plot against $(V_{GS} - V_{TH})^2$ to estimate the channel depth based on method 2

The results of estimating the channel depth based on method 1 and method 2 are given in table 9.2. The methods used here are only an estimation as the MESFET transfer characteristics of these transistors are not ideal. In addition for method 1, it is difficult to accurately determine the exact value of V_{DS} when I_{DS} begins to saturate. Nevertheless, for most of the devices tested, the channel depth falls within the region of 5-10nm. It is very difficult to determine the actual profile of the carriers as the origin of these carriers is still unknown. Moreover, the determination of the carrier profile which is based on the concentration of hydrogen in the bulk from SIMS is not accurate as hydrogen is not directly related to this conductivity. The actual carrier profile is more likely to follow a Gaussian distribution with peak concentration near the surface, decreasing rapidly into the bulk as determined from the simulation data presented by Tsugawa *et al.* [1999].

Device	Material	Device mode	Method 1 Channel depth a_{eff} (nm)	Method 2 Channel depth a_{eff} (nm)
1	BD8	Enhancement	7	6
2	BD8	Enhancement	-	6
3	WM60	Enhancement	-	5

Table 9.2 Estimated channel depth using method 1 and method 2 for the MESFET fabricated on different material

Section 9.7 Discussion

Using point probe ohmic contacts as the source and drain, MESFETs fabricated from hydrogen doped PCD display a g_m of 0.64mS at room temperature. Higher value should be expected if proper Au contacts are used for the source and drain. The theoretical maximum normalised g_m is 2.4mS/mm (for a gate length of 80μm) on these material. These carriers offer the advantage of being fully ionised at room temperature. As a result, it is possible that devices fabricated on rough surfaced PCD can display transconductance values of the same order of magnitude as a homoepitaxial boron channel FET (1.3 mS/mm) if improvement in fabrication technique can be achieved. Additionally, MESFETs fabricated on hydrogen doped heteroepitaxial highly oriented diamond (HOD) on β-SiC had already achieved performances similar to the homoepitaxial hydrogen doped FET [Kawarada, 1998]. It is therefore not surprising that device performance on PCD can exceed that of boron doped homoepitaxial diamond. This result is further supported by the Hall mobility measurements [see Chapter 6] which show that the sheet carrier concentration and mobility values recorded are quite close to those reported on hydrogen doped homoepitaxial material around $30cm^2/Vs$ [Hayashi, 1996]. If device structures of similar dimensions to those fabricated by Kawarada *et al.* [1998] can be realised on PCD material the MESFETs should show similar transconductance values. In Kawarada's homoepitaxial MESFET, Al/Cu contacts were used for the gate and an ohmic Au contact for the source and drain. Depletion mode operation was obtained from Cu as it is more electronegative than Al. The Cu gate MESFET has a transconductance of 7.5mS/mm. The sheet carrier density on these surfaces was $\sim 10^{13} cm^{-2}$ with a surface Hall mobility of approximately 30 - $40cm^2/Vs$.

The performance of the PCD MESFET fabricated here is limited by the series resistance between the drain and the source. If the 200μm between the drain and source is reduced to 20μm then there will be approximately ten times decrease of series resistance. In this case, the normalised transconductance will increase from 1 to 10 mS/mm which closely matches results reported by Kawarada *et al.* [1998], Gluche *et al.* [1997] and Tsugawa *et al.* [1999] for homoepitaxial material.

MOSFETs operating at 773K were demonstrated on homoepitaxial CVD film with a normalised maximum g_m of 1.3 mS/mm [Fox, 1995]. The holes in the channel have a mobility of 1370 cm^2/Vs (5.9 x $10^{16}cm^{-3}$ active carriers) at room temperature. Improvement in carrier mobility is attributed to higher quality CVD layer and lower doner level compensation. However, the dopants used here has an activation energy of 0.37eV resulting in less than 0.1% of ionised carriers at room temperature. Even with a high carrier mobility, the overall device performance is controlled by the limitation on active carriers. At 773K, the Hall mobility decreases to approximately $300cm^2/Vs$. The resulting large increase in conductivity over the desired temperature range (300 to 777K) causes difficulty in optimising the device performance. In-situ boron delta doped homoepitaxial diamond MISFETs and back gate IGFETs have been demonstrated [Aleksov, 1999]. The use of a delta doped channel will reduce the effective activation energy of boron, a value of 0.1 - 0.14eV was reported by Aleksov *et al.* [1999]. This will result in higher current conduction along the channel. These devices operate satisfactory at 200°C with a normalised transconductance of 7.5mS/mm, one of the highest yet reported on a boron channel FET.

Applying equation 9.1 to the device structures fabricated on WM60 and BD8, the respective g_{max} can be calculated as in table 9.1. If, however, boron had been used in the current devices, taking a 1% activation level for acceptors states and a consequent reduction in mobility to around 3 cm^2/Vs for PCD, the transconductance value at room temperature would have been 3 orders of magnitude smaller than those reported here. Nishimura *et al.* [1991], for example, obtained a value of 5μS/mm on a PCD MISFET at room temperature and Tessemer *et al.* [1993] reported a transconductance g_m of 330mS/mm for PCD MISFET at 285°C. Later, Pang *et al.* [1997] demonstrated PCD MISFET operating at 300°C with a normalised transconductance of 174μS/mm. However, saturation and pinch off of drain current is difficult to achieve on this material. The leaky and unreproducible Schottky contact on oxidised boron doped PCD films prevents the realisation of useful MESFET characteristics on these films.

The MESFET shown in figure 9.05 displays a gate to drain breakdown exceeding 100V. The breakdown voltage here compares well with others. For example, a similar planar diamond MESFET fabricated by Gluche *et al.* [1997] showed a gate to drain breakdown at 196V on hydrogen terminated CVD homoepitaxial diamond using Al for gate control and Au for both the drain and source contact. The sheet resistance of a homoepitaxial channel is 7 kΩ/square, less than half that of ~20kΩ/square on the PCD material used in this experiment. A normalised maximum g_m of 25mS/mm was reported for a gate length of 3μm. The authors [Gluche, 1997] attributed the large breakdown capability to a thin insulating layer between the gate metal and the channel. Similar breakdown voltages were also reported by others [Tsugawa, 1999]. However, not all the PCD MESFETs fabricated here display breakdown at similar voltages. Breakdown occuring at lower voltages has been observed but in general, the magnitudes are not consistent, even for devices fabricated on the same wafer. The irregular grains and defective sites in the PCD film may be responsible for this effect and improvement in these areas are essential for enhanced performance.

Device modeling has been employed to provide further insight into the operating mechanism of MESFETs on homoepitaxial diamond [Tsugawa, 1999]. MESFET simulation was carried out based on 2 different channel carrier profiles assuming a sheet carrier density of $10^{13}cm^{-2}$ for both. Results from simulations suggest carrier confinement to within 10nm from the surface to maintain an enhancement mode operation for the MESFET. Device simulation by Noda *et al.* [1997] includes an ultra thin 0.5nm insulating dielectric. Without the addition of this insulating layer, simulated MESFET characteristics close to experimental data cannot be achieved. In addition, carrier profiles which are deeper than 10nm do not produce device characteristics similar to the experimental results. Unfortunately, device modeling is not possible on polycrystalline material. Nevertheless, two different methods have been employed to estimate the thickness of the conductive channel on polycrystalline films from the transfer characteristics of the MESFET. However, as the grain size in these films is significantly larger than the channel depth the term effective channel depth (a_{eff}) as the channel thickness will be more appropriate comparison. The values obtained from both of these methods compared well with the simulation results of Tsugawa *et al.* [1999]. Others have used conventional methods. For example, Kiyota *et al.* [1996] from their C-V measurement (from the capacitance of the Schottky diode) estimated about 50nm while Hayashi *et al.* [1997] from their SIMS measurement estimated a region approximately 20nm or less; these measurements were conducted on homoepitaxial diamond. The value calculated here using the methods described in the previous section assume a uniform profile up to the channel thickness followed by a sharp cut off. This may not be representative of the doping profile but it does provide a rough insight into the channel dimension.

Hokazono *et al.* [1997] reported the formation of a depletion mode MESFET using a Cu gate contact. The low electronegativity of Cu is not sufficient to deplete the entire channel beneath the gate. On PCD, a variation of MESFETs' threshold voltages (V_{TH}) ranging from +0.6V to -0.9V were observed for the same Al gate deposited on samples from different wafers. These variations especially allow the fabrication of a depletion mode MESFET. The effect of grain size, quality of material and hydrogen plasma treatment on the carrier distribution in the surface conductive layer is still not understood and there are few detailed studies of the impact of grains and grain boundaries on the performance of 'hydrogen doped' devices [Kawarada, 1998]. A comprehensive study in these areas may provide useful information to explain the distribution of carriers and the performance of electronic devices on PCD film.

Section 9.8 Conclusion

MESFETs which rely on hydrogen terminated diamond have been demonstrated on polycrystalline CVD diamond. These devices are capable of operating in both depletion and enhancement mode. The I-V characteristics reveal a better performance in terms of higher transconductance, full pinch off and drain current saturation compared to MISFET or MOSFET previously fabricated on similar material using boron doped channels. Surfaces of this nature exhibit a near ideal characteristic when metal contacts are deposited. A reliable depletion region

beneath the gate contact enables good control over the conductivity of the channel. The primary origin of this dramatic improvement is the use of near surface hydrogen to produce an ultra thin p-type layer on the surface of the diamond. Carriers which are generated by this conduction mechanism appear to be fully ionised at room temperature. In addition, the carrier mobility and sheet carrier concentration obtained from Hall measurements are remarkably close to values reported for hydrogen doped homoepitaxial CVD films. It is predicted that given a proper and careful device design, MESFET characteristics which are comparable to single crystal diamond can be developed on PCD films. The PCD used here offers the advantage of commercial availability at low cost and can be deposited over large areas on non diamond substrates.

There remain few studies on the electronic properties of the surface conductive layer on PCD film in the literature and their viability for other types of device application. In addition, improvement in the breakdown voltages of the Schottky contact is essential to enhance the performance of these devices. The growth of smoother diamond films (Highly Oriented & Textured Diamond) on non diamond substrate preferably with low graphitic or non diamond carbon phases and ultra low levels of nitrogen is important in realising a p-type diamond film with low compensation. Nitrogen and a high sp^2 content in the diamond film were known to compensate the acceptors [Kawarada, 1996; Jiang, 1999].

References :-

Aleksov, A., Vescan, A., Kunze, M., Gluche,P., Ebert, W., Kohn, E., Bergmaier, A. and Dollinger, G. [1999] Diamond & Relat. Mater., **8**,941.

Collins, A.T. and Williams, A.W.S. [1971] J. Phys. C Solid State Phys., **4**, 1789.

Fox, B.A., Hartsell, M.L., Malta, D.M., Wynands, H.A., Kao, C.-T., Plano, L.S., Tessmer, G.J., Henard, R.B., Holmes, J.S., Tessmer, A.J. and Dreifus, D.L. [1995] Diamond & Relat. Mater., **4**, 622.

Gildenblat, G. Sh., Grot, S.A. and Badzian, A [1991] Proc. IEEE **79**, 647.

Gluche, P., Aleksov, A., Vescan, A., Ebert, W. and Kohn, E. [1997] IEEE Electron Device Lett., **18**, 547.

Hayashi, K., Yamanaka, S., Okushi, H. and Kajimura, K. [1996] Appl. Phys. Lett., **68**, 376.

Hokazono, H., Ishikura, T., Nakamura, K., Yamashita, S. and Kawarada, H. [1997] Diamond & Relat. Mater., **6**, 339.

Kawarada, H. [1996] Surf, Sci. Rep., **26**, 205.

Kawarada, H., Wild, C., Herres, N., Koidl, P., Mizuochi, Y., Hokazono, A. and Nagasawa, H. [1998] Appl. Phys. Lett., **72**, 1878.

Jiang, N. and Ito, T. [1999] J. Appl. Phys., **85**, 8267.

Kiyota, H., Okano, K., Iwasaki, T., Izumiya, Akiba, Y., Kurosu, T. and Iida, M. [1991] Jpn. J. Appl. Phys., **30**, 2015.

Kiyota, H., Okushi, H., Ando, T., Kamo, M. and Sato, Y. [1996] Diamond & Relat. Mater., **5**, 718.

Nishimura, K., Kato, R., Miyaushi, S. and Kobashi, K. [1991] Japan New Diamond Forum, The 5th Diamond Symposium, Tsukuba, 34.

Noda, H., Hokazono, A. and Kawarada, H. [1997] Diamond & Relat. Mater., **6**, 865.

Pang, L.Y.S., Chan, S.S.M. and Jackman, R.B. [1997] Appl. Phys. Lett., **70**, 330.

Prins, J. [1982] Appl. Phys. Lett., **41**, 950.

Shiomi, H., Nishibayashi, Y., Toda, N. and Shikata, S. [1995] IEEE Electron Device Lett., **16**, 36.

Sze, S.M. [1993] Physics of Semoconductor Devices II, New York, Chapter 5.

Tessemer, A.J., Plano, L.S. and Dreifus, D.L. [1993] IEEE Electron Dev. Lett., **14**, 66.

Tsugawa, K., Kitani, K., Noda, H., Hokazono, A., Kirose, K., Tajima, M. and Kawarada, H. [1999] Diamond & Relat. Mater., **8**, 927.

Vescan, A., Gluche, P., Ebert, W. and Kohn, E. [1997] IEEE Electron Device Lett., **18**, 222.

Yun, Y., Maki, T. and Kobayashi, T. [1997] J. Appl. Phys., **82**, 3422.

Zeisse, C.R., Hewett, C.A., Nguyen, R., Zeidler, J.R. and Wilson, R.G. [1991] IEEE Electron Device Lett., **12**, 602.

Chapter 10

Electronic Devices for UV Detection :- Photodiode, MSM Photodiode and Phototransistors

Contents

Section 10.1 Introduction

Diamond possesses an indirect bandgap of 5.45eV which corresponds to a wavelength of 225nm in the electromagnetic spectrum (deep UV). Photons of wavelength (λ) less than 225nm incident on diamond are sufficiently energetic to excite electrons from the valence band to the conduction band edge. Direct transition is not possible as the indirect nature of the bandgap will require a change in the electron momentum. Once electrons are promoted to the conduction band, they will take part in current conduction if they are subjected to a potential difference or electric field. However, valence to conduction band excitation is impossible from illumination by photons of longer wavelength (λ>225nm). This implies diamond can be used to form a truly-visible blind UV detector. Excited electrons in the conduction band are unstable and will fall back

into the valence band or other electronic states in the bandgap which are normally associated with impurity levels or imperfections in the lattice. This must be followed by an emission which corresponds to the energy difference between the two levels and a change in the electron momentum if necessary. The electron transition from conduction band to valence band (recombination) is not straight forward and may occur through many different possible paths.

Mobile electrons in the conduction band have been used as the main method to detect the presence of photons. The simplest way is to apply a potential difference between two contacts on a diamond. Once a burst of photons ($\lambda < 225$nm) arrive on the surface, electrons will be excited to the conduction band and the electric field between the two contacts will drive these electrons to the electrode. Signal in the form of current will be recorded. UV photodetectors which are based on this principle have been fabricated on diamond [Binari, 1993; McKeag, 1995; Salvatori, 1998]. Under normal conditions, there are defect states in the bandgap due to imperfection in the diamond lattice. These defect states will allow electron excitation for wavelengths longer than 225nm, known as the sub-bandgap response. This has been demonstrated in both PCD and natural diamond. The defective state of natural diamond cannot be controlled and the properties of natural diamond vary from sample to sample. This problem coupled with the high cost of good quality natural diamond prompted the development of more controllable and cheaper sources such as CVD diamond. Photodetectors which show high levels of selectivity between deep UV ($\lambda<225$nm) and visible light have been reported on PCD [McKeag, 1995; Jiang, 1997].

The metal-semiconductor-metal (MSM) photodetector was proposed and demonstrated by Sugeta *et al.* [1979] on AlGaAs. This form of device utilises adjacent metal contacts which are both Schottky in nature as opposed to the ohmic and Schottky metallisations found in conventional photodiode structures [Ng, 1995; Sze, 1973].The unipolar dopant used in this form of structure increases the speed of this device as the associated charge storage time due to injection of minority carriers in a p-n junction can be avoided. In addition, a planar configuration can be adopted resulting in low capacitance offering the advantages of a high speed low noise device. Only a single fabrication step is required to form the device contacts in contrast to the p-i-n photodiode. Figueroa *et al.* [1981] reported a similar device on GaAs capable of detecting pulses with 50-60 ps of rise and fall times with DC responsivities greater than 0.3A/W when operated at 830nm incident wavelength.

Previous reports of MSM structures have been confined to those structures fabricated on undoped diamond [Jiang, 1997; Binari, 1993]. These devices are essentially photodetectors where the metallisation contacts are ohmic in nature. Salvatori *et al.* [1997] recently reported a MSM device on intrinsic diamond which exhibited rectifying behaviour. However, the device showed a very high turn on voltage (~50V) and electrical characteristics that were inconsistent with a Schottky diode mode of operation.

The goal of fabricating an effective Schottky barrier for an MSM photodetector on conventional oxidised boron doped surfaces is difficult. Most Schottky diodes on boron doped PCD film suffer from large leakage currents and inconsistent reverse bias characteristics. This is

very important for the fabrication of MSM Schottky photodetectors as the detection of light will always be conducted in reverse bias mode. In chapter 7, Schottky diodes with good rectification characteristics and consistent low reverse bias leakage current (~nA) have been demonstrated on PCD with Al as the Schottky contact. An MSM photodiode fabricated with such contacts may offer a route to simple monolithic integration of an optical detector with active electronics operating at room temperature on CVD diamond.

Transistor based switching devices which rely on the application of a bias voltage at the gate (FET) and an application of a current at the base (Bipolar) to modulate the electrical characteristic of the other two terminals have been realised on both single crystal and PCD. Both enhancement and depletion mode MESFETs have been demonstrated on PCD in the previous chapter. These devices normally operate in an active mode thus exhibiting gain unlike passive devices such as the Schottky diode. Transistor based switching devices which are modulated by electromagnetic radiation have not been reported on diamond. Phototransistors or OPFET (Optically activated field effect transistors) describe such devices [Sugeta, 1980]. These devices have several different operating mechanisms. For example in a bipolar heterojunction phototransistor, light incident at the base-collector junction generates primary electron hole pairs. The reverse bias applied at this junction will sweep the carriers out of the depletion region resulting in a secondary photocurrent flowing into the gate. It is this photocurrent which is the main component that is modulating the current in the emitter collector junction. Unfortunately, it is difficult to fabricate a bipolar phototransistor on diamond due to the lack of a reliable n-type dopant. With just a single p-type dopant, the OPFET device based on the metal semiconductor contact is currently the only alternative.

Section 10.2 Optoelectronic Detectors

To be successful as an optoelectronic detector, some property of the semiconductor device should be affected by radiation. The most commonly used property is the conversion of light into electron-hole pairs which are then detected by a carefully designed electronic circuit. Photon absorption is strongest in a semiconductor when an electron can be excited directly into the conduction band from the valence band. For an indirect bandgap semiconductor, the nearest transition (bandgap) is not situated directly above the valence band edge. Absorption of a photon with energy corresponding to the bandgap will only occur if a phonon participates in the process. As the momentum of photon is extremely small, transition will be impossible without the aid of a phonon. Hence, absorption for indirect bandgap material is generally weaker than for direct bandgap material. In addition, the absorption coefficient of an indirect bandgap semiconductor has a temperature dependent factor. As temperature increases, the lattice vibration will be stronger and hence the absorption coefficient will be higher. Besides diamond, other semiconductors such as Si and Ge have indirect bandgaps. However, it does not prevent these materials from being used as detectors. The detectors in this chapter are mainly based on the detection of radiation which corresponds to the minimum bandgap of the semiconductor. This class of detector is known as an intrinsic detector. Extrinsic detectors are based on detection of

radiation whose energy is less than the bandgap. This can be achieved by creating electronic states in the bandgap by impurity doping.

When photons impinge on a semiconductor and generate electron-hole pairs, the performance of the detector depends on the efficiency of collecting these carriers. In the absence of an electric field, these electron-hole pairs will recombine and no signal will be detected. The two most important operating parameters of a photodetectors are responsivity (R_{ph}) and quantum efficiency (ηQ). Responsivity relates the amount of current produced by a unit of optical power.

$$R_{ph} = \frac{I_L}{A}.\frac{1}{P_{op}} \qquad \text{..... (equation 10.1)}$$

where I_L is the photocurrent generated (A)

A is the area of the device illuminated (cm^2)

P_{op} is the optical intensity received by the device (W/cm^2)

The quantum efficiency (ηQ) indicates the number of carriers collected for each photon impinging on the detector. It is given as :-

$$\eta Q = \frac{J_L}{q}.\frac{h\nu}{P_{op}} \qquad \text{..... (equation 10.2)}$$

where J_L is the current density (A/cm^2)

$h\nu$ is the energy contain in each photon (J)

q is the electronic charge (C)

The photoconductor is the simplest of the detectors and consists of two electrodes across a region of semiconductor to which a bias is applied. An important property of a photoconductor is the gain as more than one electron may be collected for each photon impinging on the device. When light is absorbed the electron-hole pairs created in the semiconductor are collected at the electrodes under the influence of the applied electric field. Higher electric field improves response by increasing the drift velocity of these carriers toward the electrodes. Closely spaced electrodes are desirable as higher fields can be achieved with the application of a modest bias. Some of these carriers will recombine before they are collected. The gain in the device arises because an electron may traverse the detector circuit several times before recombination with a photo generated hole or before the hole reaches the electrode. If the electron-hole recombination time is longer than the transit time for the electron then a high gain can be achieved. The larger the difference, the higher the gain. However, the improved gain comes at the expense of speed of the detector, since this is controlled by the recombination time.

The detection of light in a Schottky diode can operate in two ways :-

(a) where $E_g > h\nu > q\phi_b$:- In this mode, carriers are excited across the Schottky barrier from the metal to the semiconductor. The impinging photons must have an energy greater than the barrier height of the Schottky contact for this to occur.

(b) where $h\nu > E_g$:- In this case, the electron hole pairs will be created in the depletion region in the semiconductor; the carriers will be swept by the electric field generating photocurrent. The photocurrent will add to the reverse bias leakage current.

Another class of metal semiconductor detectors are known as metal-semiconductor-metal (MSM) photodiodes which are based on two closely spaced Schottky barriers in a planar geometry. Interdigitated fingers are used to increase the collection efficiency of the detector. It is important that the region between the adjacent fingers is completely depleted for high speed operation. Therefore narrow finger spacing is favoured, typically between 1- 5 μm, so that a large bias is unnecessary to achieve total depletion. The substrate is usually lightly doped to ~$10^{15}cm^{-3}$. As the depletion region is not covered by the metallisation contact, light absorption will be more efficient between the electrodes.

Section 10.3 Experimental Aims

The possibility of fabricating detectors using the 'hydrogen' doped surface conductive layer has not been explored in the literature. The main experimental aim in this chapter is to demonstrate the application of this layer to fabricate devices which are useful for UV detection. Most of the UV detectors reported on diamond have been fabricated on undoped material. Their operation normally depends on the high natural intrinsic resistivity of diamond to produce a low dark current. Although these devices may show high sensitivity, they are usually slow and furthermore, it is difficult to integrate undoped devices with other active components on the same wafer. The detection of deep UV in this experiment is based on the metal semiconductor Schottky contact fabricated on a doped layer which has already been successfully used in high performance devices (chapter 9).

Three types of devices will be described in this chapter. They are the photodiode, MSM Schottky based photodiode and the OPFET. Each of these detectors has individual merits in terms of speed, gain and ease of fabrication. The electrical characterisation of these devices will be presented. The main operating mechanism in these devices will be identified, discussed and compared with the existing diamond based UV detectors. Three experiments will be described in this chapter; each will refer to a particular device :-

Experiment 1 :- Reverse bias response of a diode to UV illumination
Al contact for the Schottky contact and Au for ohmic.

Experiment 2 :- Fabrication and characterisation of MSM photodiodes based on the results of experiment 1. Only Al Schottky contact.

Experiment 3 :- Demonstration of an OPFET and identification of its operating mechanism. Al is used as the gate contact while Au for both the source and drain.

Section 10.4 Experimental Methods

Thin film intrinsic PCD, WM60, was used for the fabrication of UV detectors. Previously, Schottky diodes and MESFETs have been successfully fabricated on this wafer (see Chapter 7 and 8). An optical micrograph of the typical film is shown in figure 6.02(b) in chapter 6 indicating randomly aligned grains with an average size of 10 - 30μm. The Raman spectrum of this film in figure 6.03(b) display only a single sharp peak at 1332cm^{-1} indicative of good quality diamond. The structure for both the MSM photodiode and the OPFET is defined by means of shadow masking. All the samples were degreased according to Appendix 1 before metal contacts were deposited. The structure of the MSM photodiode is shown in figure 10.02 and the structure of the OPFET is shown in figure 10.08. The metal contacts were deposited by a thermal resistive method using an Edwards 306. Electrical characterisation was carried out using a Keithley picoammeter & voltage source along with an HP 4145B semiconductor parameter analyser. Device illumination was achieved using a Xe lamp. The output of the lamp was passed through a monochromator with order sorting filters (Amko International) offering a selection of wavelengths across the 180 - 800nm range. The optical intensity of the UV light was calibrated with reference to a silicon photodiode. The active area of the MSM devices and the phototransistors was approximately 0.3mm^2.

A UV source of variable intensity is required to test the detectors. As the lamp used was of a fixed power output the light intensity was controlled by varying the distance between the light source and the device. This was achieved by raising and lowering the probe station beneath the fixed light source. Readings were taken at 5 fixed positions and for each separation the light intensity was calibrated with a silicon photodiode.

Section 10.5.1 Experimental Results: Photodiode

In the first set of experiments, the response of the reverse bias current in a Schottky diode to UV was investigated. This was a preliminary study to observe the possible changes to reverse bias current. The diode was fabricated using Al for the Schottky contact and Au for the ohmic as this displays the best rectification properties and the lowest leakage current. The thickness of the Al contact was 150nm while the Au was 250nm. The metallisation contact was defined by shadow masking. I-V characterisation of the device was performed using an HP 4145B. Figure 10.01 reveals significant increase in the reverse leakage current of the Al-Au Schottky diode while being illuminated with 220nm light. In the dark, the Al-Au Schottky diode displayed good Schottky rectification characteristics of about 5 orders of magnification ratio

measured at ±2V and the reverse bias leakage current of the diode was less than 1nA. The same device was then exposed to deep UV(220nm) with an intensity of 0.5μW/mm^2. The I-V characteristics of this device were measured again during illumination. The reverse leakage current increased by about 3 orders of magnitude compared with the current levels in the dark. Under UV illumination, the reverse bias characteristic of the diode is strongly affected while only a small changes (10%) was recorded for the forward current. The current component contributed by the electron hole pairs swept by the electric field in the depletion region will be in the same direction as the reverse leakage current of the Schottky diode.

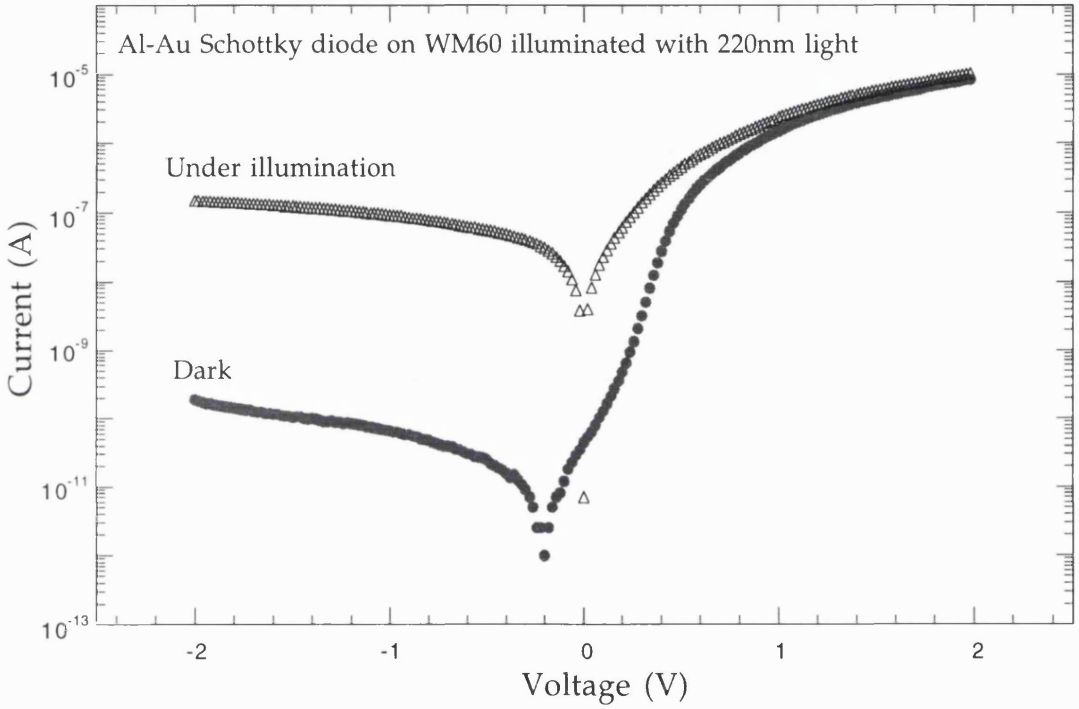

Figure 10.01 The I-V characteristics of the Schottky diode when illuminated with UV (220nm) and in the dark.

If the resistivity of the bulk is significantly affected by the UV illumination, then the forward bias characteristic of the diode should change drastically. However, experimental results indicate only about 10% increase in forward bias current levels. The diamond used in this experiment has a high sheet carrier density (~10^{13} cm^{-2}), therefore additional carriers generated by the UV should not significantly increase the original level. However, under reverse bias the depletion region beneath the contact is fully depleted of carriers. The high resistivity of this region is responsible for the low current levels at reverse bias in the dark. Hence, the photon generated electron-hole pairs are important here and therefore were responsible for the 3 orders increased in current levels recorded.

Section 10.5.2 Experimental Results: MSM Photodiode

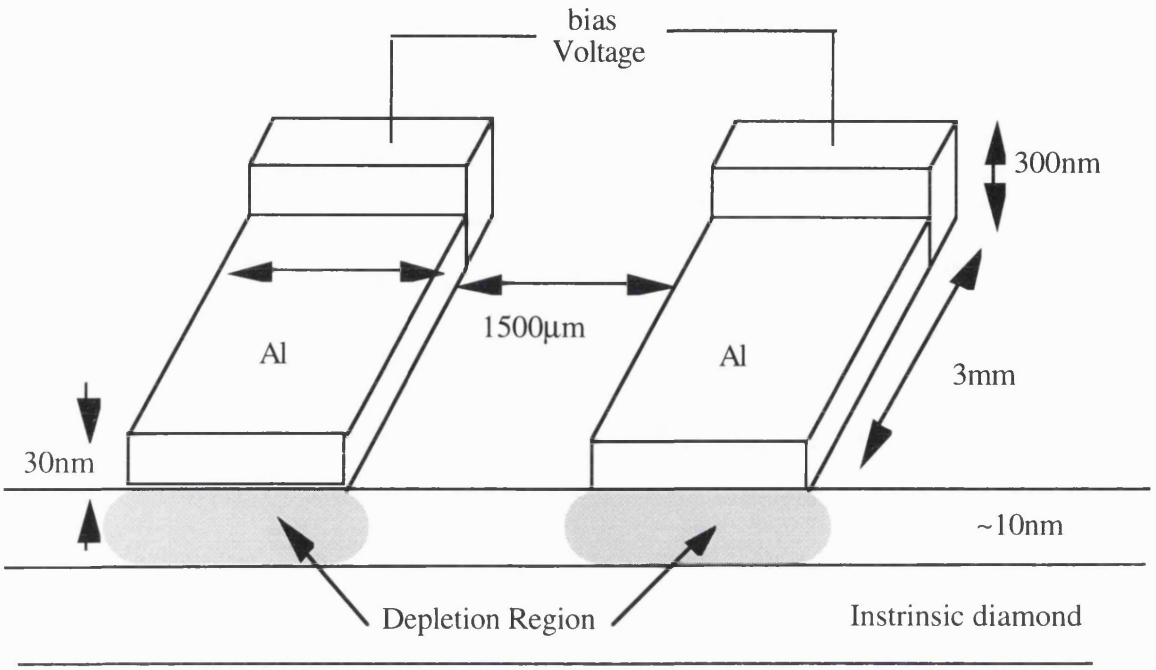

Figure 10.02 The dimension of the Al MSM structure.

The MSM photodiode is based on the detection of light in reverse bias mode in the manner of the conventional photodiode described in Section 10.4. This device offers the advantage of a simple fabrication step as the only metallisation contact required is the Schottky contact whereas a conventional photodiode requires both Schottky and ohmic contacts. The structure of the MSM photodiodes is shown in figure 10.02. The Schottky contact is kept deliberately thin (30nm) in order to minimise UV absorption. However, the ends of the contacts are made thicker (300nm) in order to withstand probing. By applying a bias voltage between the contacts one Schottky contact will be subjected to a forward bias and the other to a reverse bias.

Ideally, both of these contacts should be identical to one another. Hence, the electrical characteristic should be similar on both the positive and negative half of the bias. However, because of the nature of the PCD the two Schottky contacts are not identical. These imperfections will govern the level of leakage current recorded. In the experimental result this discrepancy is observed therefore the bias condition which produces the lowest leakage current is chosen. The dark current for the device is shown in figure 10.03

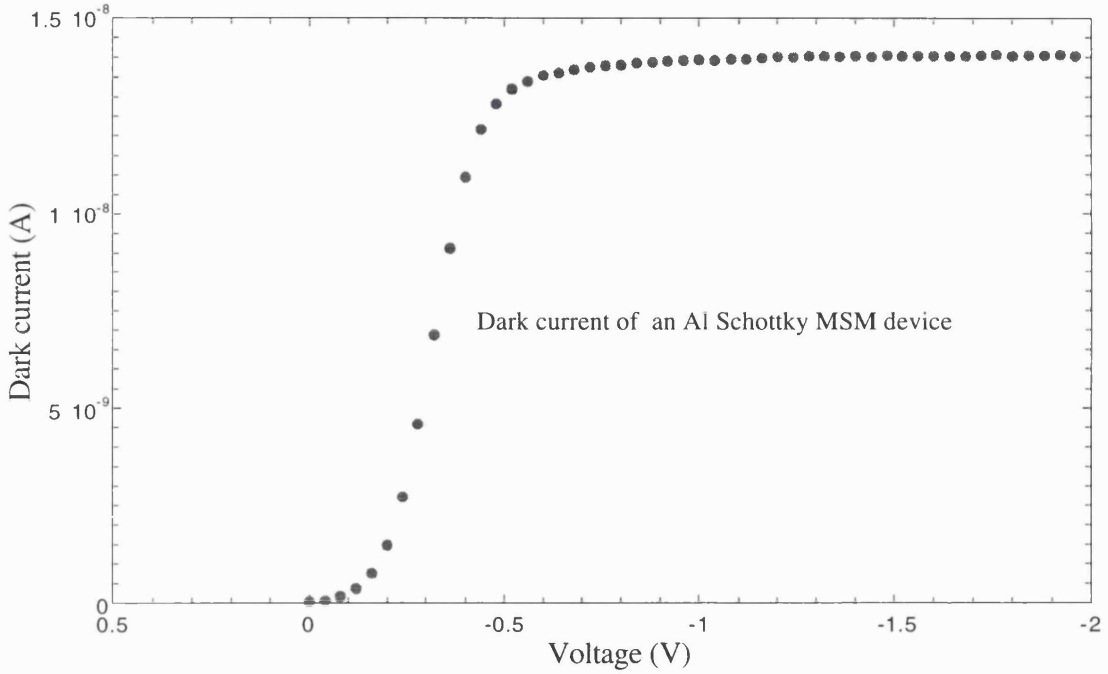

Figure 10.03 The I-V characteristic of the Al MSM contacts in the dark

The dark current increases rapidly between 0.1-0.5V and saturates at 14nA for voltages above 0.6V. At low current levels, the magnitude of the current is very sensitive to light. The high sheet carrier density on the surface and the large spacing between the Al contacts prevents total depletion of the region between the contacts for the bias levels applied here. It is to be expected that the depletion region will exist only in the area defined by the contact. The high carrier concentration in the conductive channel ($\sim 10^{19} cm^{-3}$ assuming a uniform channel thickness of 10nm) will allow a small spread of the depletion region in the lateral direction for a modest increase in bias voltage (the spread is in the nm scale for a voltage increase of 1V). This idea is supported by the capacitance-voltage measurement under reverse bias for a similar Schottky diode presented in chapter 7 figure 7.06 which also indicate the saturation of the capacitance at 1.4pF above 0.6V. As the size of the depletion region will directly govern the value of the capacitance provided other parameters remain constant, the saturation of the capacitance under reverse bias indicates that the size of the depletion region is not significantly modified.

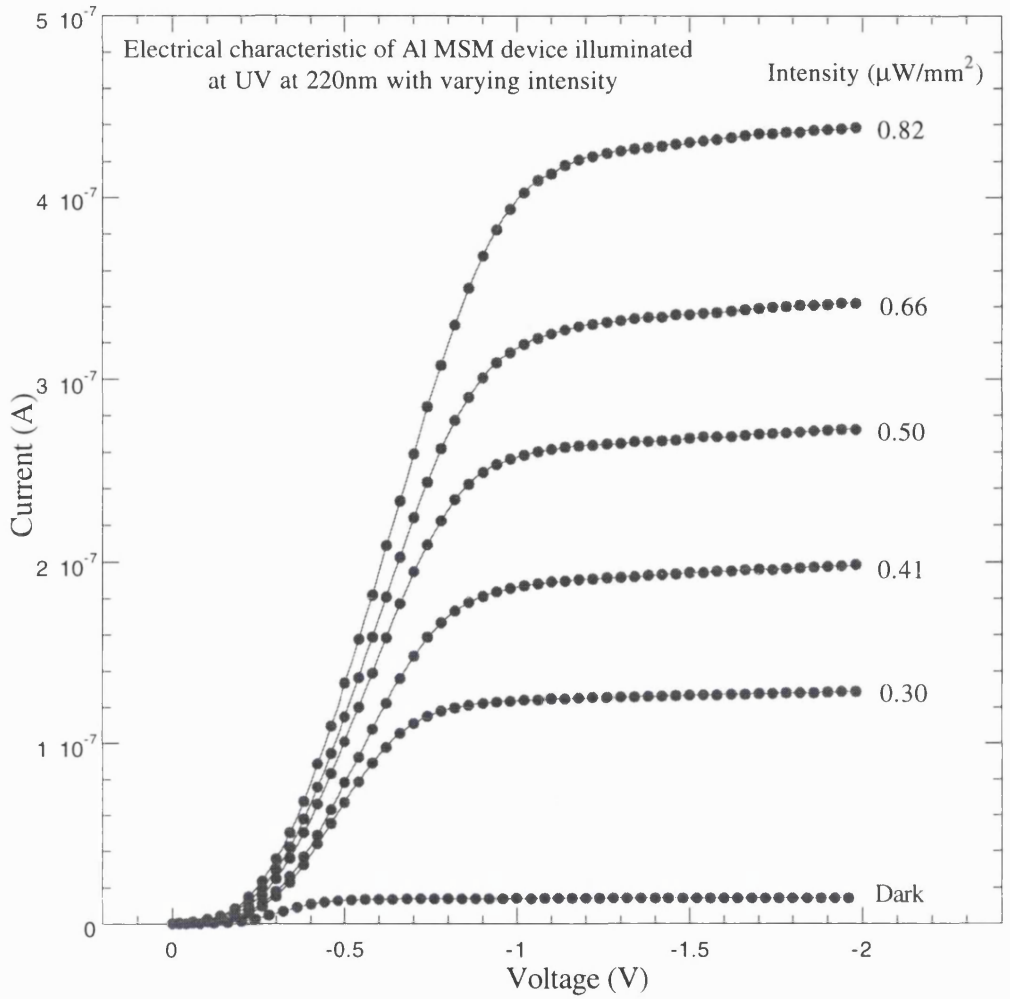

Figure 10.04 shows the I-V characteristic of an MSM device under illumination of UV light at 220nm with varying intensity.

Figure 10.04 shows the I-V characteristics of the Al MSM device exposed to deep UV (220nm) at different power intensities. The power intensity is modified by changing the distance between the output from the UV source to the surface of the device. Five levels of UV intensity were chosen for this experiment and quantified with a silicon photodiode. The electrical characteristics reveal that a significant change in the photocurrent is recorded when the device is illuminated. Under illumination, a rapid rise of photocurrent is recorded between the bias of -0.2V to -0.6V. Further increases in the bias voltage drive the photocurrent to near saturation. This occurs at V_{Dsat} ~ -0.7V although there is a slight dependence on the illuminating intensity. The E-H pairs generated by photons may have disrupted the charge equilibrium in the depletion region of the metal-semiconductor contact. In a photodetector, the photocurrent recorded will not show the tendency of saturation when bias between the electrodes is increased. Normally a linear dependency will be observed instead unless the electric field applied is strong enough to accelerate the E-H pairs to a level where they achieve their saturated drift velocity. However, for a bias of 1V and a electrode spacing of 1.5mm photoconductivity was not the dominating current component observed in the experimental curves and could not be used to explain the saturation of the photocurrent.

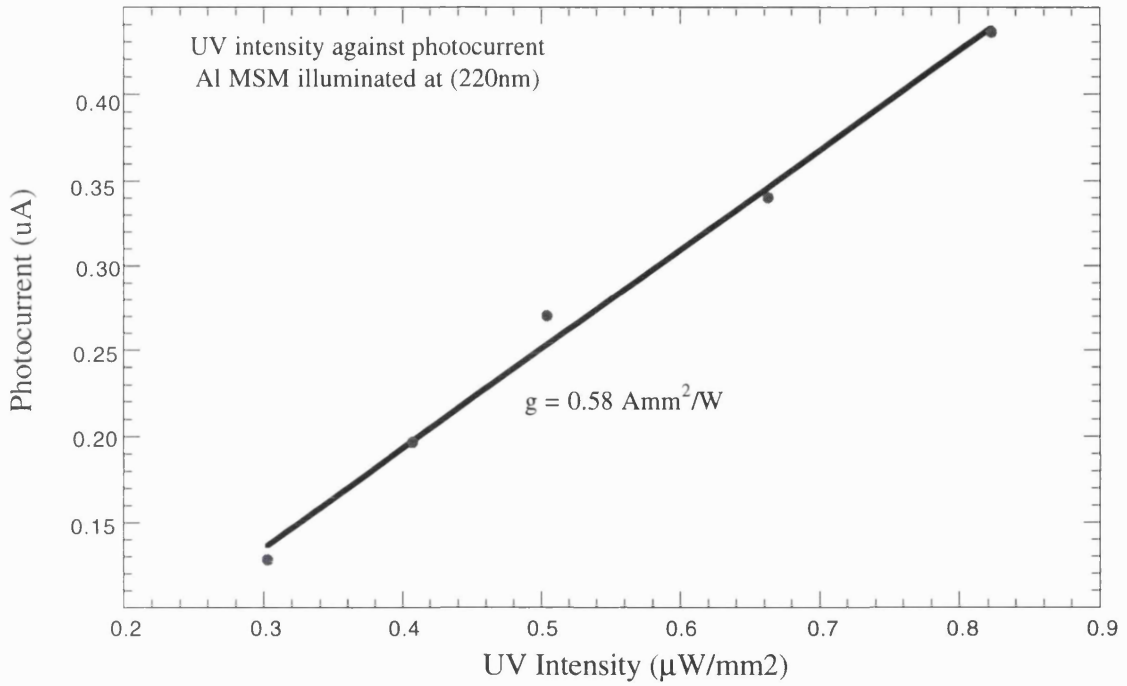

Figure 10.05 The plot of photocurrent versus UV intensity for an Al MSM

In figure 10.05, the photocurrent recorded at a bias of -1.8V is shown to increase linearly with the incident UV intensity which arises from the generation of E-H pairs. As the density of photons arriving on the detector increases, the generation of electron hole pairs will be similarly enhanced.

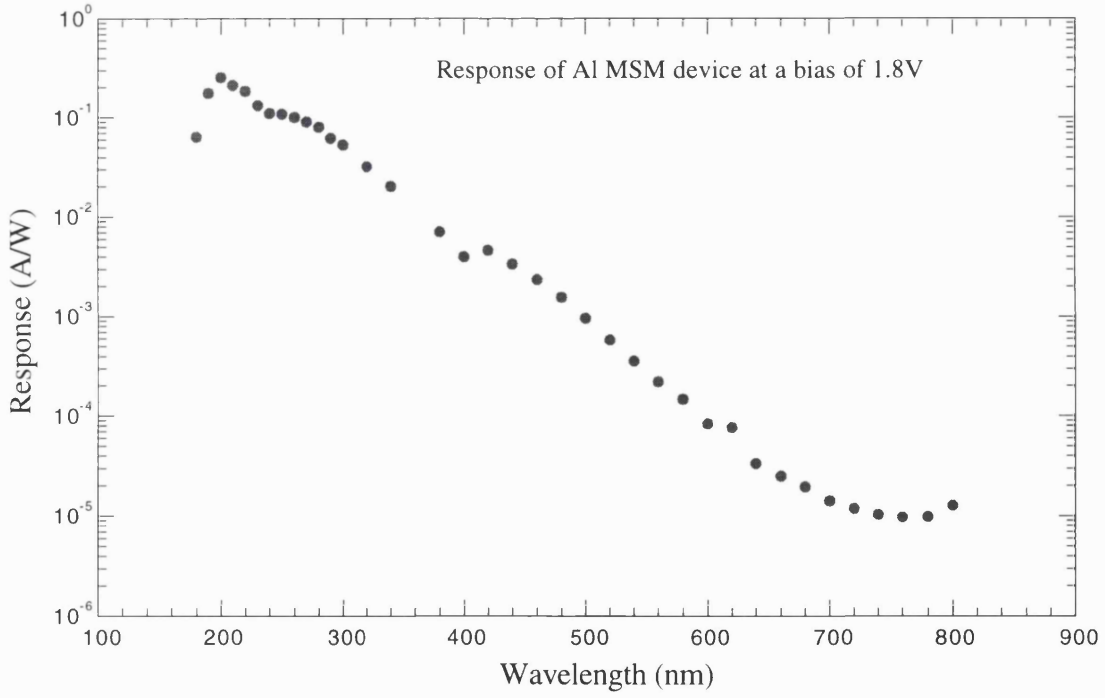

Figure 10.06 The log response of an Al MSM device illuminated at different wavelength.

The responsivity as a function of wavelength of this device plotted in log form is shown in figure 10.06. The device was illuminated from 800nm to 180nm in steps of 20nm. During the characterisation the device was illuminated for 20s at each wavelength before the photocurrent was recorded. The device was left in dark for an interval of 40s after each illumination to allow the dark current to settle down before the next measurement. The responsivity of the device increases exponentially with decreasing wavelength. This is the typical result expected for detectors fabricated on CVD diamond. The spectral response of this device is most intense at around the 200nm wavelength region. This corresponds to energy levels slightly higher than the band gap of the diamond (5.45eV). The response around the 300nm region may be due to bandgap states in the polycrystalline material. It could be also due to metal-semiconductor interface states which may be present. The response is the lowest for light at the longest wavelength 800nm which is in the infra red region.

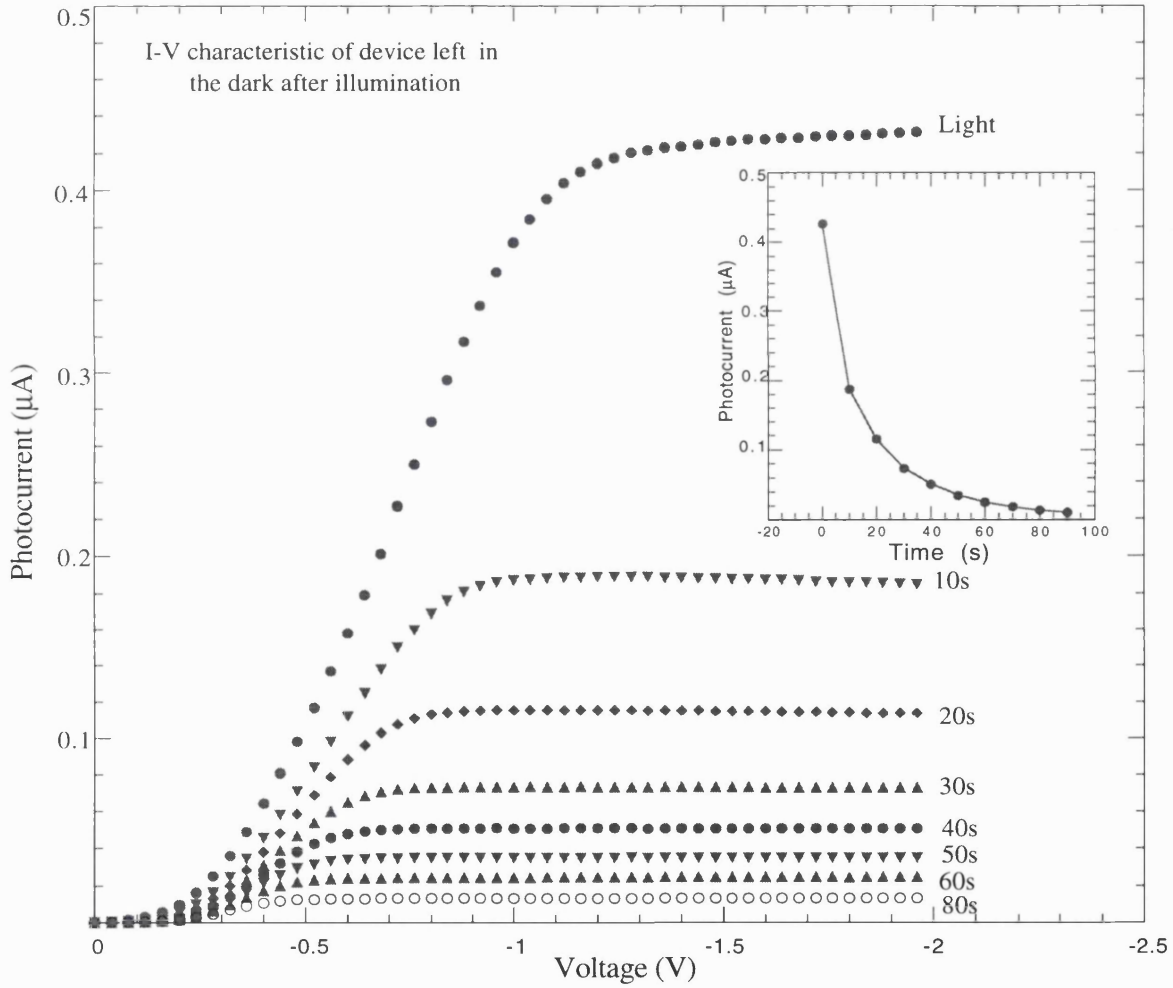

Figure 10.07 The I-V characteristic of the device every 10s after the light source is switched off.

Traps and interface states were filled by exposing the device to UV (220nm) for about five minutes. During exposure, I-V scans of the device were performed. The light source was then switched off. After every 10s, similar I-V scans were performed using the HP 4145B in the fastest scan mode. The resulting I-V curves are shown in figure 10.07. An exponential decay of the photocurrent level with time was observed. The slow decay could be caused by the release of

carriers which were trapped in the grain boundaries or trapped by deep impurity levels. The device design used here is not optimal for high speed MSM detectors and an improved geometry for fabricating a high speed device will be presented in the analysis section.

Section 10.5.3 Experimental Results: OPFET

Prior to demonstrating an OPFET which relies on the metal semiconductor Schottky contact, the operation of a MESFET for this particular device must be realised. For this purpose the structure shown in Figure 10.08 is constructed on hydrogen doped as grown PCD film.

This structure consists of two Au metallisation pads which form ohmic contacts for both the source and drain. The thickness of the Au layer is approximately 200nm. The Schottky contact is defined by performing a double Al evaporation. The first layer of Al deposited was about 30nm thick, chosen to minimise the absorption of UV. The 2nd layer of Al deposited, 300nm thick, was placed on the edge of the contact to facilitate probing of the gate.

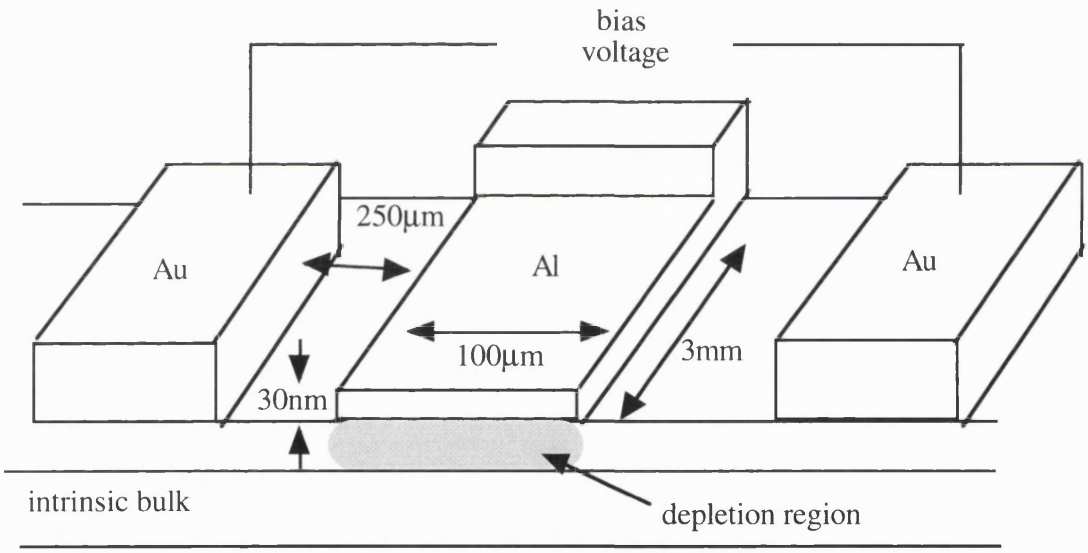

Figure 10.08 The schematic diagram of the OPFET structure (not according to scale).

The I-V characteristics of the drain to source contact were measured with an HP4145B semiconductor parameter analyser. The structure in figure 10.08 was tested for its MESFET characteristics and result is given in figure 10.09. The MESFETs fabricated on these surfaces operated in the enhancement mode. Current pinch off and saturation of I_{DS} was observed. A negative bias applied between the source and the gate switches the device on. Good modulation between the gate bias and drain current is observed. This is typical of MESFETs and quite similar to those reported in Chapter 9.

There are several methods for testing OPFETs. The open circuit gate (floating gate) configuration was chosen as it is simple in operation and compatible with enhancement mode MESFETs controlled by a Schottky gate. The I-V scan between the source and the drain was

measured in the dark. The small levels of current recorded indicated that the entire channel beneath the gate was totally depleted.

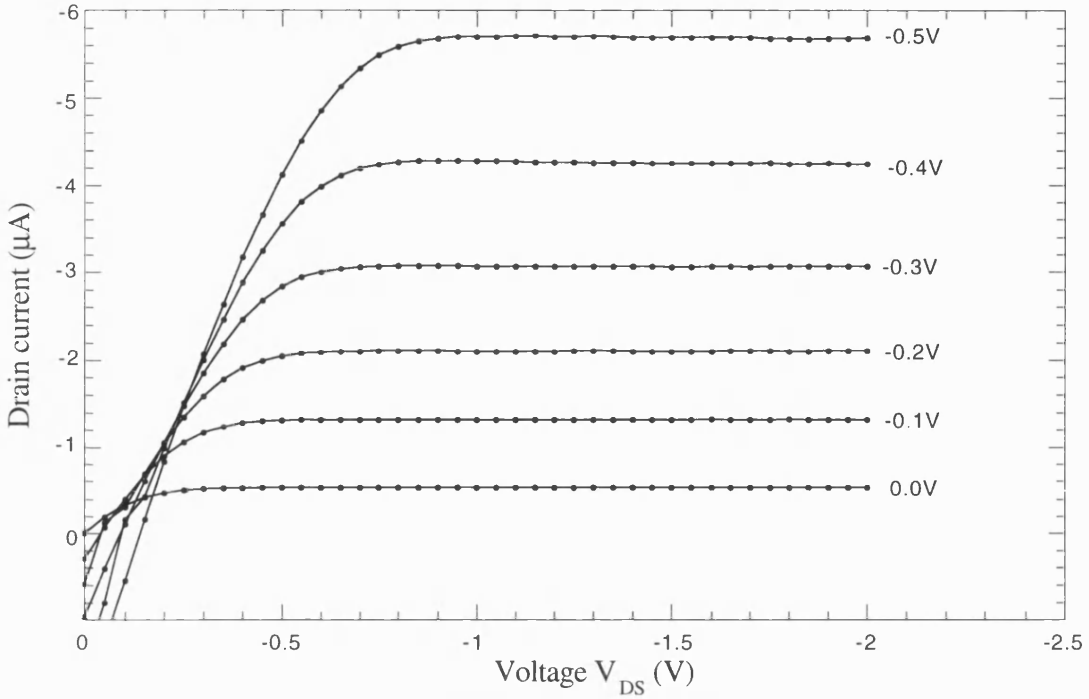

Figure 10.09 The transfer characteristic of the MESFET fabricated from Al Schottky contact with Au as both the drain and source.

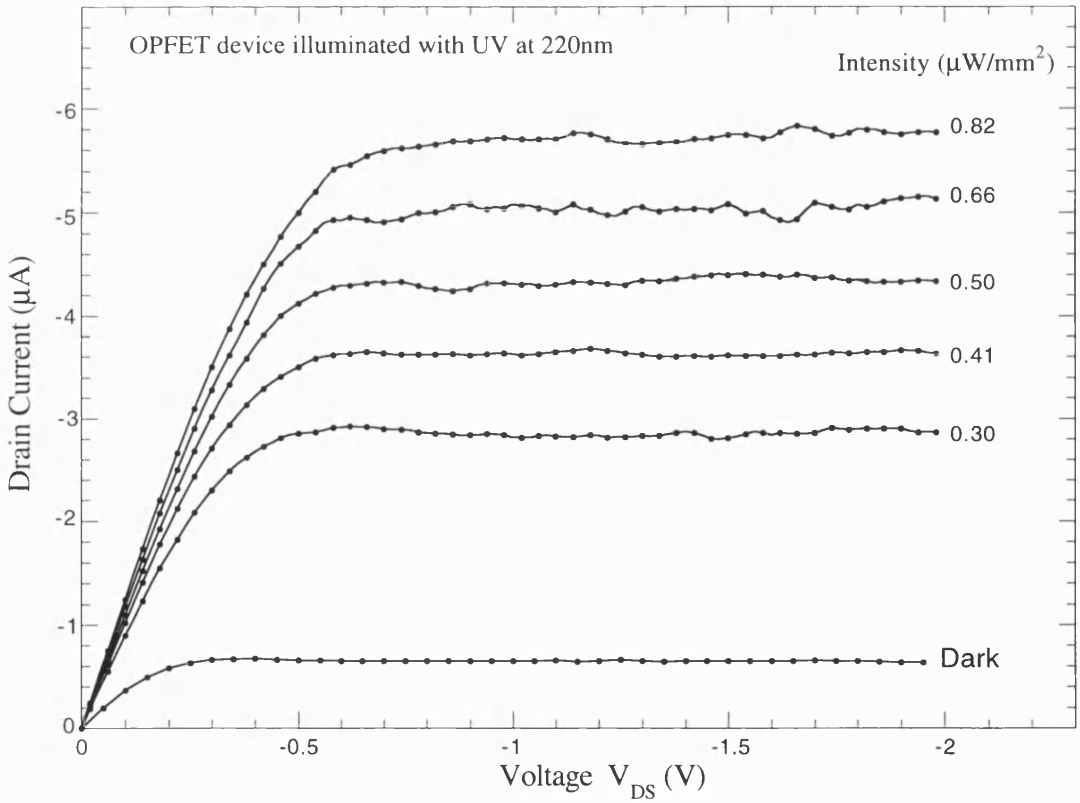

Figure 10.10 The electrical characteristic of an OPFET illuminated with UV at 220nm

The device was then exposed to UV at 220nm and the I-V scan was performed again. Significant changes in the I-V curves were observed under illumination. The current increased from less than 0.5μA to nearly 3μA between the source and the drain. The intensity of the UV incident on the device was varied by modifying the distance between the device and UV source as described in section 10.5. A corresponding variation in the I-V curves was recorded for different UV intensities; the results are given in Figure 10.10. The effect of UV is to enhance the current in the drain in the same manner as the increasingly negative gate potential for the same device shown in figure 10.09. For V_{DS} less than -0.5V, there is a very rapid rise in the drain current. However, I_{DS} begins to saturate at about -0.7V. The point (voltage) at which I_{DS} saturates (V_{Dsat}) increases slightly with UV intensity. This shows a clear sign that the UV radiation is somehow modifying the depletion region beneath the Al gate allowing increasing flow of I_{DS}. For each level of increase in intensity a higher saturation level of I_{DS} was obtained.

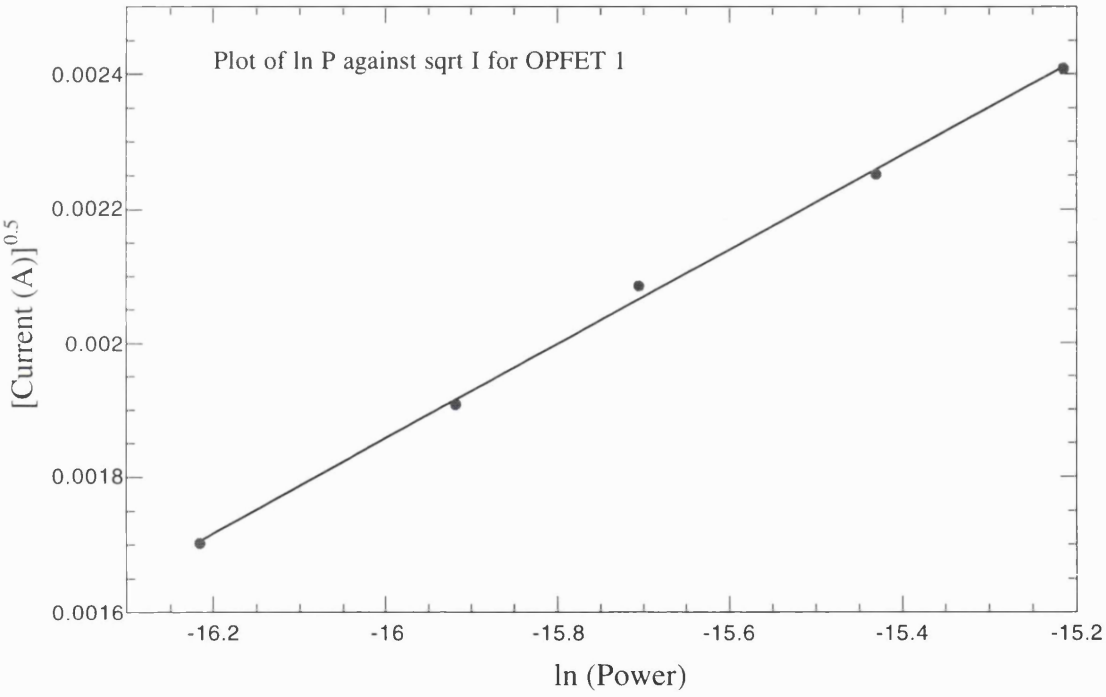

Figure 10.11 Plot of $I_{DS}^{0.5}$ against ln (Power) for I_{DS} taken at V_{DS} = -1.8V

The plot of $I_{DS}^{0.5}$ against ln (Power) shown in figure 10.11 reveals a linear relationship. The value of I_{DS} in this plot is taken at V_{DS} = -1.8V. Figure 10.12 shows the decay of the drain current with time after the UV source was removed from the sample. The sample was exposed to UV radiation for approximately 10 minutes before the source was removed. The drain current takes approximately about 120s to drop to a satisfactory level. Note that at this stage the current levels appeared to decrease slightly after the saturation point for each scan conducted at an interval of 10s. This occurs because the conductivity of the material decreases gradually during the scan. In general, the drain current decreases in an exponential manner with time.

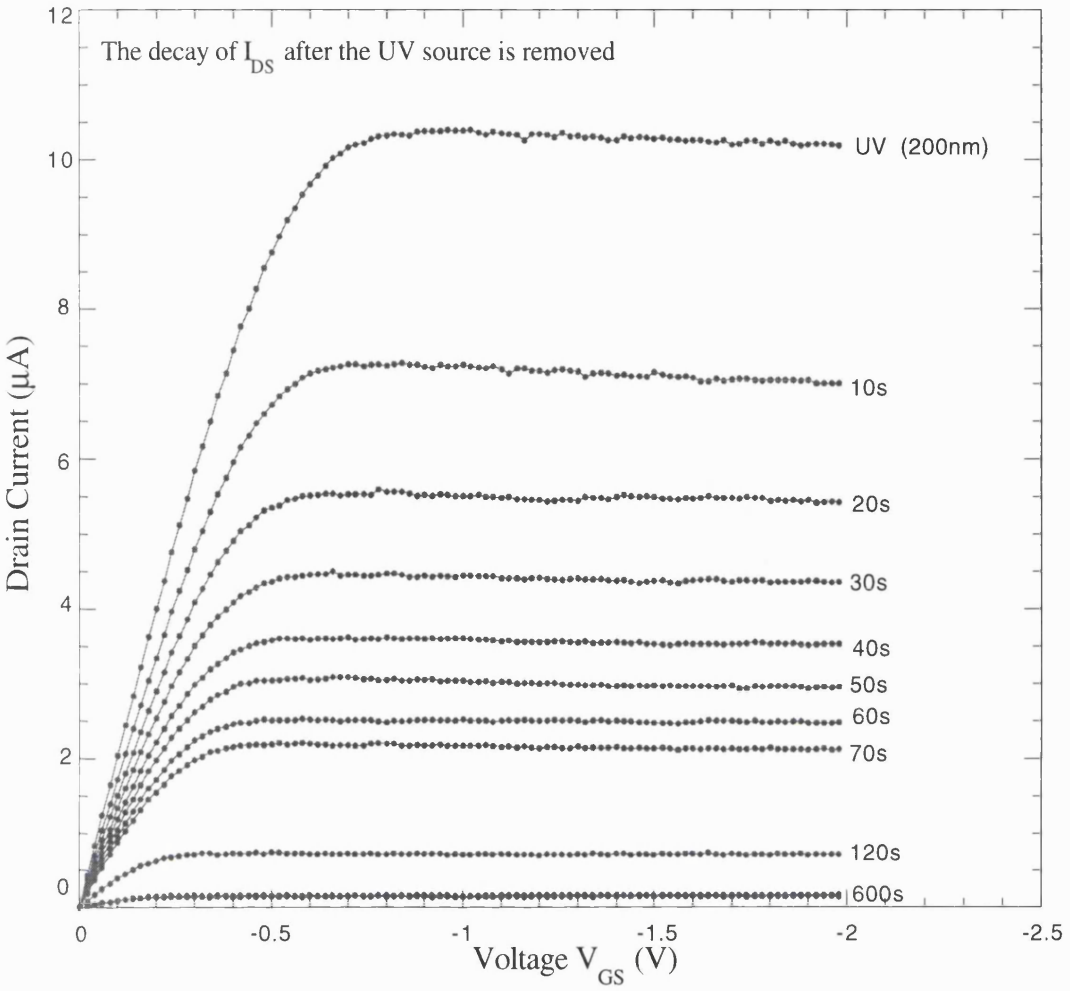

Figure 10.12 The decay of the drain current when the light source is removed. The I-V curves were obtained using the fastest scan (approximately 1s) on the test instrument.

Section 10.6.1 Analysis :- MSM Photodiodes

Previous work presented in chapter 7, revealed that aluminium contacts deposited on hydrogen terminated PCD films formed good Schottky diodes with an ideality factor of 1.5 and a Schottky barrier height of 1.0eV. More importantly, these diodes have a low (~nA) and consistent leakage current. This property enables light to be detected under reverse bias mode. The saturation of the leakage current at low voltages (<5.0V) also indicates that the device is operating under a thermionic emission regime. Detection of light will be difficult if field emission current is present as this current component (bias voltage dependent) may dominate the I-V characteristic of the device rather than the photocurrent. The MSM structure shown above consists of two back to back Schottky diodes. A bias voltage between contacts 1 and 2 will always forward bias one of the diodes and reverse the other. Reversing the bias voltage will swap the bias condition of these diodes. Figure 10.13 shows both of these biasing conditions. Unlike a single Schottky diode shown earlier, the current in such a device is comprised of two components. The first arises from thermionic hole injection from the metal to the semiconductor which forms the usual leakage current in the diode. The second current component arises from

the electron current injection from the forward biased junction into the semiconductor [Sze, 1973]. The second forward bias electron current will only be important when the depletion region of the reverse bias contact extends to the other forward bias contact. This is known as the 'reach through' condition. The large separation of the MSM device here and the high sheet carriers density will prevent this phenomenon from occurring under the modest bias voltage used here. Hence the dark current of this device is similar to the reverse-bias characteristic of a typical Schottky diode.

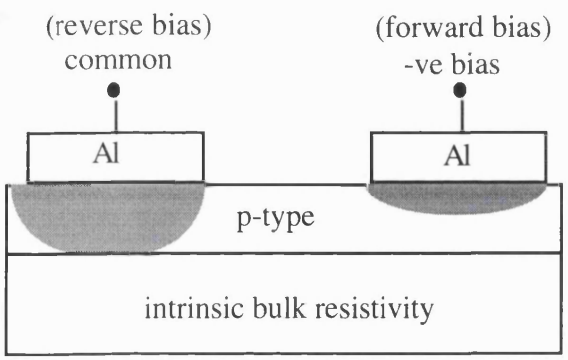

Figure 10.13(a)

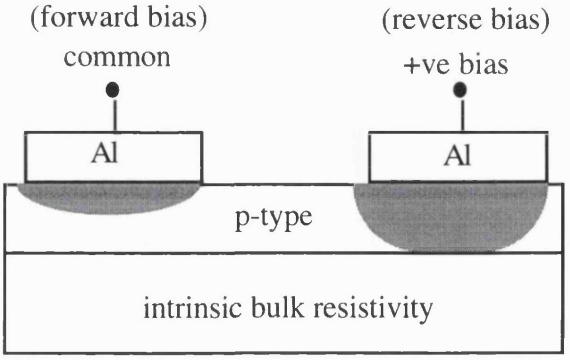

Figure 10.13(b)

Figure 10.13(a) and (b) show changes in the depletion region under the Al contact when the polarity of the bias voltage is reversed.

The dark current, which saturates around $0.05pA\mu m^{-2}$ in figure 10.03, is extremely low even compared with MSM structures fabricated on other semiconductors which utilise barrier enhancement layers to reduce the leakage [Shi, 1992]. This presumably arises through a combination of the large Schottky barriers on a wide bandgap semiconductor such as diamond together with the reduced Fermi level pinning through the use of hydrogen terminated surfaces. Other workers have also achieved current levels of similar magnitude for Schottky diodes formed on homoepitaxial diamond [Hayashi, 1997; Gluche, 1997] and attributed that the thermionic current emission is dominating in these devices.

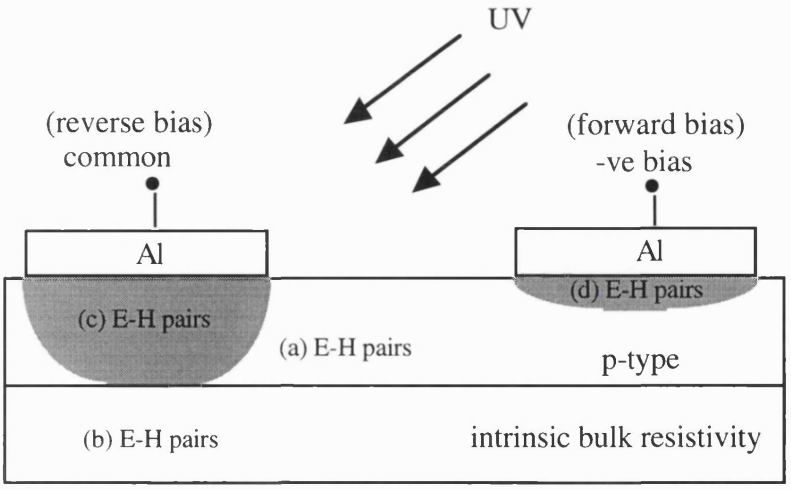

Figure 10.14 shows generation of electron hole pairs in the device at region illuminated by UV

As the entire device was illuminated by UV, E-H pairs were generated in all regions, as illustrated in figure 10.14. The carriers generated by the UV in region (c) are the most significant in this application. Electron hole pairs generated here will be swept by the strong electric field in the depletion region and constitute a photocurrent that is detectable. Carriers which are generated in region (a) are not important as there are already a high density of local carriers from the surface conduction. Furthermore, there is no high electric field in this region to sweep the carriers. Carriers which are generated at region (d) will complement the effect of E-H generated in (c). However, under increasing bias, the active volume for light detection in region (c) will become larger (reverse bias) while region (d) will shrink due to the forward bias. As a consequence, more E-H pairs can be captured in region (c) compared with (d).

The I-V curves of the MSM device show a rapid current rise in the voltage range around 0 to 0.75V. This results from the rapid decrease in the size of the depletion region in the forward direction, a moderate increase in the size of the depletion region in the reverse bias and also the forward bias contact turning more ohmic (lower Schottky barrier) resulting in a lower resistance to the photocurrent. Once this has stabilised, the photocurrent saturates. The saturation of the photocurrent can be explained by the modest increase in the volume of the reverse bias depletion region in the lateral direction. This is in contrast to the active volume of the forward bias junction which decreases vertically over the whole contact area. As a result, the net photocurrent in the devices, the sum of each of these opposing components, will increase rapidly. Experimentally this is found to occur up to a bias of ~1V, the point at which the forward bias contact is turned ohmic.

The slight positive slope observed following the onset of saturation may arise from a contribution from photoconductivity effects due to long lifetime traps in the material. The presence of long life-time traps was confirmed by the detection of high current levels in scans performed after the light source was extinguished. The presence of traps depending on whether an electron or hole is caught may affect the depletion region under the contact.

A linear relationship between the photocurrent and the incident UV radiation obtained here in figure 10.05 was also reported by Binari *et al.* [1993] who fabricated a photodetector using natural diamond. Shi *et al.* [1992] reported similar relation for an MSM photodetector fabricated on InGaAs. In addition, the authors observed the saturation of photocurrent at a bias voltage above 1.0V for different power intensity when illuminated with an incident wavelength of 860nm and 1300nm. They used an InP barrier enhancement layer to reduce the leakage current in their device. A barrier enhancement layer was not introduced here as the Al Schottky barrier on the hydrogen terminated surface is able to maintain a low leakage current.

Section 10.6.2 Analysis :- OPFET

An Optically activated Field Effect Transistor (OPFET) relies on using a light source to switch the transistor on and off instead of a current (bipolar transistors) or voltage (field effect

transistors). The enhancement mode MESFET is suitable for this purpose as the device is normally off in the absence of a bias voltage. By illuminating the device with UV light through the thin Al gate, generated carriers will modify the properties of the depletion region and hence allow a larger drain current to flow. Without the Al gate, there would be no blocking mechanism between the two ohmic Au contact pads, consequently a high current will be detected and the device would not work. In addition, the leakage current for the floating gate configuration will not be important unlike a MESFET as it is an open circuit.

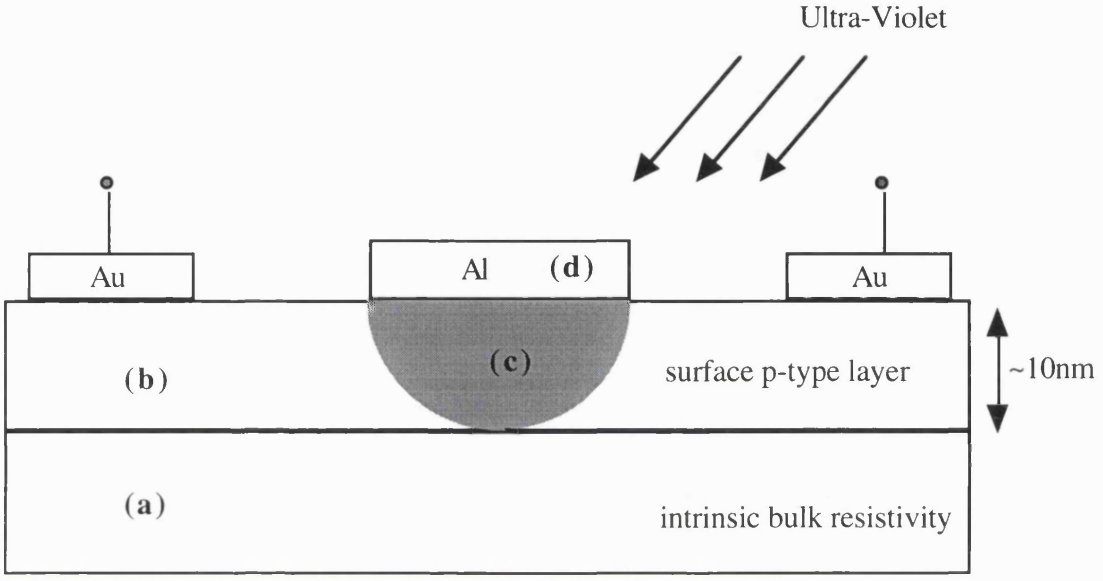

Figure 10.15 shows the cross section of the OPFET with a floating gate.

As was the case of the MSM device, the generation of E-H pairs in an OPFET will have differing influence according to the locality in which they were generated. At each different place these carriers will effect the property of the device in a different manner. Four significant regions were identified according to the diagram above. They are :-

(a) Electron hole pairs generated in the intrinsic bulk material
(b) Electron hole pairs generated in the surface channel region
(c) Electron hole pairs generated in the depletion region
(d) Electron hole pairs generated in the metal also known as photoemission from metal.

Electron hole pairs generated in region **(b)** do not contribute significantly as there are already a large number of carriers present due to the surface conductivity. Electron hole pairs generated in region **(a)** will reduce the resistivity of the intrinsic bulk region. This will affect the OPFET leakage, photocurrent and gain by forming a parallel current between the two Au contacts. Carriers generated in **(c)** will be important as they will be swept by the electric field in the depletion region. Under zero bias, holes will be repelled from the depletion region along the channel into the neutral region of semiconductor while the electrons will be swept into the metal. This will cause a new equilibrium of charge at the metal semiconductor interface which results in the reduction of depletion width which will open a wider channel available for conduction. When a voltage is applied between the two Au contacts under UV, higher current will be detected due

to the presence of this channel. As the bias is increased further, the photo current will saturate when a new pinch off condition is achieved. In the dark, the voltage required to achieve pinch off is about 0.25V but under illumination it increases to 0.7V (for a UV intensity level of $0.82\mu W/mm^2$). Comparing the actual I-V characteristics of the MESFET in figure 10.09 and the OPFET in figure 10.10 (on the same device), if a voltage is applied at the gate to switch the device on the V_{DS} which is required to pinch off the channel at a particular current level is quite similar to those recorded when UV is used in replace of the voltage at the gate. If photoconductivity at the intrinsic layer is dominating then the current in the device would not be saturating as the photocurrent in the photodetector will not saturate at the small bias used here but instead will be almost linear.

The photoemission of electrons from the Al gate in region (**d**) will tend to increase the size of the depletion region. This is unlikely to be the case here as the experimental result indicates otherwise, furthermore the potential barrier for the electron to migrate to the gate will be greater than the bandgap. However, hole emission from the gate across the Schottky barrier maybe significant as they will tend to decrease the size of the depletion region, hence switching the device on. This is known as the sub-bandgap response. Sugeta *et al.* [1980] have demonstrated an OPFET operating in this mode on n-type AlGaAs where photons of an energy corresponding to the Al Schottky barrier height (~1.0eV) gave rise to a feeble photocurrent. This phenomena may make a contribution to photocurrent in the present case of a diamond OPFET but it is not the primary mechanism for current generation.

Section 10.7 Discussion

Several mechanisms have been proposed to explain the mode of operation of OPFETs [Sugeta, 1980; Gammel, 1978; Lakshmi, 1990], the simplest of which is based upon photoconductivity. Photo generated carriers increase the conductivity of the channel region and the conduction principle is similar to that of a photodetector. Gammel and Ballantyne [1978] favoured this mechanism to explain the characteristic of GaAs OPFET's when illuminated by light with an energy greater than the bandgap. Another mechanism is where the gate to channel junction is considered as a photodiode, such that a gate current can only flow when the device is exposed to light. If the gate is connected to an external resistor, a voltage drop across the resistor will raise the gate voltage and a larger external channel current arises. This mechanism has been observed for GaAs OPFET's by Sugeta *et al.* [1980].

If, however, the MESFET gate is electrically isolated, the illumination may result in a change in charge level within the depletion region, hence modifying the channel current. Lakshmi *et al.* [1990] have explored GaAs OPFETs in this mode. They illuminated a device with above the bandgap energy light to ensure photo absorption. If this mechanism, based on the floating gate configuration, is occurring then in the square law regime it can be shown that with $V_{GS} >> V_{TH}$ the main current component will depend upon the incident light power P according to

$$(I_{DS})^{0.5} \propto \ln\left(\frac{\eta P}{h\nu}\right) \quad \text{..... (equation 10.3)}$$

where η is the quantum efficiency
$h\nu$ is the photon energy
I_{DS} is the photocurrent.
V_{TH} is the threshold voltage of the MESFET

A plot of $I_{DS}^{0.5}$ against ln P will be linear as demonstrated in figure 10.11, indicating that the OPFET is operating under the mechanism proposed by Lakshmi *et al.* [1990].

Binari *et al.* [1993] have compared photoconductivity properties of undoped natural, synthetic and PCD using the MSM structure over a wavelength range of 130 to 700nm. Their MSM structure simply consists of two Al contacts separated by a 0.35mm gap. The natural diamond displayed a quantum efficiency of 30% at 200nm with 3 orders of discrimination against visible light. However, after UV illumination the device required more than 1000s to fall by 90% of the initial current rise. This was caused by trapping of carriers in the material and the reset time was found to be proportional to the received dose of UV radiation. Salvatori *et al.* [1997] also observed a decay time greater than 1000s following long exposure to their device. The traps in these films give rise to the much extended decay time. The decay characteristics of the devices fabricated in this work display similar trends. After prolonged exposure to UV devices require approximately 80s (MSM device) and ~150s (OPFET) for the current to decay to 90% of their initial rise respectively. Using the Al layer, a discrimination of 3 orders of magnitude between UV and visible photo-response was obtained from the devices. Better performances have been reported; McKeag *et al.* [1995] demonstrated a visible-blind photodetector using interdigitated fingers on free standing PCD where the electrode separation was equivalent to the grain size. This device displayed almost 6 orders of discrimination between UV and visible light with sharp cut off near the 220nm region. The improvements in device performance are believed to result from the passivation of defect sites following annealing in various environments. Recently, Jiang *et al.* [1998] using laser writing lithography reported interdigitated photodetectors with 2 μm spaced fingers and a UV-visible discrimination of 4 orders of magnitude. Hence, their device require only a bias voltage of 5V to achieve the desired high electric field. Note that the both the MSM and OPFET fabricated here required only about 1.0V to operate effectively. The confinement of the depletion region beneath the contact coupled with the use of a thin conductive channel means that a very high electric field can be achieved with a modest bias. Salvatori *et al.* [1996] fabricated an MSM photodetector device using an Al electrode on undoped PCD 5μm thick. High discrimination was not obtained between the UV and the visible region probably due to the thin film material used. Plano *et al.* [1994] have shown that the growth side transport properties of CVD diamond improves with the thickness of the material. Whitfield *et al.* [1996] demonstrated a UV photodiode operating under reverse bias on boron doped PCD which shows very good discrimination (5 orders of magnitude) between

UV and visible. Little information was revealed regarding the Schottky diode characteristics with Au as the Schottky and Ti/Ag/Au as the ohmic. This probably arises through the difficulty in obtaining a consistent diode performance through using oxidised boron doped thin film diamond. Nevertheless, this indicated the potential for this type of application if a more reliable dopant can be found on these material.

When the same devices are exposed to short pulses of light (30ps) the decay curves show markedly different characteristics. Foulon *et al.* [1996] demonstrated this behaviour and explained that the decay curve will depend on the nature of the trapping mechanism which was excited in the material. They found a fast rise and decay time in orders of nanoseconds on a planar electrode photodetector. A short pulse of Nd:YAG laser radiation (wavelength = 266, 532 and 1064 nm with a 30ps FWHM pulse) was used. By using a short pulse length in the picosecond region, the traps which were associated with a long decay time may not be filled and excessive charging of the entire material which may modify its original conductivity (leading to the long tail mentioned earlier) did not occur. The authors also concluded that (100) textured film contain the longest carrier lifetime and thus slower response to pulse radiation and hence highest sensitivity. In addition, the authors pointed that the presence of nitrogen in the (100) textured film could reduce the device response time and sensitivity. Furthermore, depending on the trapping mechanism the rise and decay time of the photoconductivity signal may assume a different form. Salvatori *et al.* [1997] further demonstrated that for the same device which takes more than 1000s to decay after long exposure, if it is exposed to a radiation pulse of 0.3s then the decay time is only about 0.3s. This fast response actually arises from the fact that the carriers which are excited by short pulses have a small collection distance and these will be trapped before they can reach the electrode. Those which were generated close to the electrode would be collected and generate useful photocurrent. Furthermore, short pulses do not generate sufficient carriers to charge the entire device and the conductivity of the material will not dramatically changed. Once the conductivity of the diamond has changed temporarily due to charging of deep traps then the carriers close to the electrode will be masked by the long tail. However, for much longer exposures, traps which lie deep and require an indirect transition involving a phonon may be completely filled. If a voltage is applied to the devices the carriers in these traps may contribute to the conduction mechanism resulting in a greater apparent photoresponse. Gonon *et al.* [1996] have demonstrated that long lifetime carriers may easily be discharged by heating the sample. This provides carriers with increasing energy, more importantly increasing lattice vibration resulting in a higher change in momentum energy strong enough to promote other possible indirect transitions.

Gonon *et al.* [1997] and Vaitkus *et al.* [1993] indicated the presence of persistent conductivity in the material after irradiation with UV. The electrons raised in the conduction band were trapped at 1.9eV below the conduction band and the population of free holes left in the valence band will give rise to persistent photoconductivity [Gonon, 1997]. He also showed the presence of acceptor like states at 1.1eV. The I-V characteristic of the intrinsic diamond will have a space charge limited current (SCLC) relationship. A device with a 2μm fingers spacing however, displayed a decay tail of more than 100s clearly demonstrated that it is the nature of the

traps in the material which were excited during the illumination which finally governs the speed of device [Jiang, 1998].

The MSM device demonstrated here offers the advantage of having the depletion region confined below the Schottky contact. With a moderate doping level and a very thin channel, the electric field strength in the depletion region will be extremely high without the need of a large bias voltage. Outside the depletion region the field will be relatively weak. Also note that even for the large electrode spacing used here a bias of only 1.0V is required to operate the device. If a short pulse (to avoid excitation of traps with a long time constant) is incident on these devices, the high field at the depletion region will sweep the carriers to the electrode while those which are in the low field region will recombine. As the sweeping action is fast, a burst of carriers will be detected followed by a rapid decay. The experiment described earlier in this chapter demonstrated the ability of the MSM detector to operate satisfactory in the slow response regime, the next stage is to test these devices for their transient response to very short pulses of varying duration. Compared to some natural diamonds, polycrystalline samples will have a significantly smaller collection distance, which is expressed as the product of mobility, lifetime and electric field [Pan, 1992]. Hence, carriers which were generated farther away from the contacts will recombine faster.

UV Intensity ($\mu W/mm^2$)	Photocurrent (μA)		Responsivity (A/W)		Quantum Efficiency	
	MSM	OPFET	MSM	OPFET	MSM	OPFET
0.30	0.13	2.90	1.41	32.0	7.9	180
0.41	0.20	3.64	1.61	29.8	9.0	168
0.50	0.27	4.35	1.79	28.7	10	162
0.66	0.34	5.07	1.71	25.5	9.6	143
0.82	0.44	5.80	1.77	23.5	9.9	132

Table 1 This table shows the Responsivity and Quantum efficiency of the MSM and OPFET device fabricated illuminated with 220nm wavelength at different intensity. The area of the Al strip is $0.3mm^2$.

Table 1 shows the responsivity and the quantum efficiency of the MSM and OPFET to UV at 220nm. A quantum efficiency greater than unity is recorded for both the MSM device and the OPFET. In order to allow for this comparison the size of the Al gate in the OPFET was similar to the size of a single Al contact in the MSM device. The gain in the MSM device may be caused by carriers trapped in the depletion region. It may also arise because of the photoconductivity mechanism and trapping in the material. This is particularly evident when the photocurrent shows a long decay time. The gain in the OPFET device is much higher compared to the gain on the MSM. This is the primary advantage of using this particular device design. Quantum efficiencies as high as 10^6 have been reported in photoconductive devices [McKeag, 1998]. This very large value derived from the external circuit. Carriers which were trapped in the device allowed further current injection from the external circuit to maintain the space charge neutrality of the device. In addition, McKeag *et al.* [1998] demonstrated that treating the device

in carefully chosen environments could enhance device performance resulting in a faster response. This enhancement might be caused by the passivation of defect states in the material following the treatment. However, in general a device with a higher gain will result in a slower (speed) response and vice versa. The relation between quantum efficiency and speed was roughly displayed here where the OPFET gain (quantum efficiency) is higher but the device displayed a much slower time to switch off (~150s) compared to the faster MSM (80s) but with lower gain. Also note, that the decay measurement in this section was conducted after the material was exposed to UV for a duration of more than 5 minutes. The origin of gain in the OPFET is quite similar to that of the MESFET except that modification to the depletion region was performed by illuminating the gate with UV light instead of applying a negative bias on the gate with respect to the source. E-H pairs generated in the depletion region by UV are swept by the electric field which decreases the size depletion region beneath the gate. This can be explained as the photodiode action. A decrease in the size of the depletion region will allow larger current injection (photocurrent) between the source and drain. This is the amplification or transistor action. In addition, due to the high conductivity in the conductive channel, larger current will be injected between the drain and the source. This explains the origin of the gain in the OPFET. The gain can be increased by reducing the series resistance between the drain and the source (for example decreasing the separation between the drain and the source) for a fixed gate dimension.

Furthermore, if the electrode spacing of the MSM device can be made smaller, for example close to 2 μm, and the dopant concentration reduced to about $10^{15}cm^{-3}$ [Shi, 1992; Figueroa, 1981], the reach through condition could be achieved without a large bias [Sze, 1973]. The reach through condition occurs when the depletion region of the reverse bias contact extends all the way to the forward bias contact. Under this condition the active area for light detection will not be constrained to just the depletion region beneath the metallisation contact.

Section 10.9 Conclusion

The use of the surface conductive layer to detect radiation in the 220nm region has been demonstrated. The detection was based on an active device which is the optically activated field effect transistors (OPFET) and a passive device, the metal-semiconductor-metal (MSM) photodiode. The MSM method of detection relies on using the depletion layer from the metal semiconductor contact to maintain a low dark current. Generation of carriers within or near this region will modify the transport properties within the device. Carriers which are swept by the depletion region will constitute a photocurrent. In the case of the floating gate OPFET, the carriers in the depletion region will modify the width of this region allowing a wider channel for current flow. The quantum efficiency of both devices indicates that the OPFET has significant higher gain than the MSM device. The gain in the MSM device probably arises through carriers which were trapped in long lifetime electronic states causing injection of carriers from the forward bias contact.

The presence of these states were confirmed through the long decay time observed for

both the OPFET and the MSM device. This was also supported by the exponential relation between the responsivity of the device and the radiation wavelength especially in the 300 to 400nm region although a 3 orders of discrimination was achieved between the visible and the UV.

References:-

Bhattacharya, P.'Semiconductor Optoelectronic Devices' (Prentice-Hall, Ebglewood Cliffs, New Jersey, 1994), Chap 9.

Binari, S.C., Marchywka, M., Koolbeck, D.A., Dietrich, H.B. and Moses, D. [1993] Diamond & Relat. Mater., **2**, 1020.

Foulon, F., Bergonzo, P., Jany, C., Gicquel, A. and Pochet, T. [1996] Diamond & Relat. Mater., **5**, 732.

Gammel, J.G. and Ballantyne, J.M. [1978] Tech. Dig. Int. Electron Devices Mett., **24**, 120.

Gluche, P., Aleskov, A., Vescan, A., Ebert, W. and Kohn, E. [1997] IEEE Electron Dev. Lett., **18**, 547.

Gonon, P., Prawer, S., Boiko, Y. and jamieson, D.N. [1996] Appl. Phys. Lett., **68**, 1238.

Gonon, P., Prawer, S., Boiko, Y. and jamieson, D.N. [1997] Diamond & Relat. Mater., **6**, 860.

Hayashi, K., Yamanaka, S., Watanabe, H., Sekiguchi, T., Okushi, H. and Kajimura, K. [1997] J. Appl. Phys., **81**, 744.

Jiang, W., Ahn, J., Xu, F-K., Liaw, C-Y., Chan, Y-C., Zhou, Y. and Lam, Y-L. [1998] Appl. Phys. Lett., **72**, 1131.

Lakshmi, B., Chalapati, K., Srivastava, K., Arora, B.M., Subramaniam, S. and Sharma, D.K. [1990] IEEE Trans. Electron Devices., **37**, 1533.

McKeag, R.D., Chan, S.S.M. and Jackman, R.B. [1995] Appl. Phys. Lett., **67**, 2117.

McKeag, R.D., and Jackman, R.B. [1998] Diamond & Relat. Mater., **7**, 513.

Ng, K.K., 'Complete Guide to Semiconductor Devices' (McGraw Hill, New York, 1995) Chap 5.

Pan, L.S., Kania, D.R., Han, S., Ager III, J.W. Landstrass, M., Landen, O.L. and Pianetta, P. [1992] Science, **255**, 830

Plano, M.A., Zhao, S., Gardinier, C.F., Landstrass, M.I., Karnia. D.R., Kagan, H., Gan, K.K., Kass, R., Pan, L.S., Han, S., Schnetzer, S. and Stone, R. [1994] Appl. Phys. Lett., **62**, 193.

Rogers, D.L., Woodfall, J.M., Pettit, G.D. and McInturff, D. [1988] IEEE Electron Device Lett., **EDL-9**, 515.

Salvatori, S., Vincenzoni, R., Rossi, M.C., Galuzzi, F., Pinazari, F., Cappelli, E. and Ascarelli, P. [1996] Diamond & Relat. Mater., **5**, 775.

Salvatori, S., Pace, E., Rossi, M.C. and Galluzzi, F. [1997] Diamond & Relat. Mater., **6**, 361.

Shi, C-X., Grutzmacher, D., Stollenwerk, M., Wang, Q-K. and Heime, K. [1992] IEEE Trans. Electron Devices, **ED-39**, 1028.

Slayman, C.W. and Figueroa, [1981] IEEE Electron Device Lett., **EDL-2**, 112.

Sugeta, T. and Urisu, [1979] IEEE Trans. Electron. Devices, **ED-26**, 1855

Sugeta, T. and Mizushima, Y. [1980] Jpn. J. Appl. Phys. Part 2, **19**, 27.

Sze, S.M., Coleman, D.J. and Loya, A. [1971] Solid State Electron., **14**, 1209.

Vaitukus, R., Inushima, T. and Yamazaki, S. [1993] Appl. Phys. Lett., **62**, 2384.

Whitfield, M.D., McKeag, R.D. Pang, L.Y.S., Chan, S.S.M. and Jackman, R.B. [1996] Diamond & Relat. Mater., **5**, 829.

Chapter 11

Concluding Remarks

Early predictions that diamond would be a suitable material for high performance and high power devices were not supported by attempts to fabricate diodes and field effect transistors (FET's) on the more commercially accessible material, polycrystalline CVD diamond. Many believe that the poor quality of the material and the difficulty associated with doping have undermined the true potential of diamond. Boron, the only established dopant for PCD displayed a high activation energy of 0.37eV. Hence, at room temperature only a small percentage of the carriers will be activated. The activation energy can be reduced through heavy doping resulting in the formation of an impurity band. This has been demonstrated on smooth (100) single crystal diamond through delta or pulse doping. However, on polycrystalline material with a surface roughness in the microns scale and grain boundaries present, it is very difficult indeed to achieve a doping uniformity over a large area in the nanometer scale. As a result, there are currently no reports of boron doped polycrystalline FETs which display current saturation and pinch off or good performance either at low or high temperature. Electronic devices such as MESFETs have never been successfully developed. Even Schottky diodes with low ideality factor, low leakage currents and high rectification ratios are rarely reported in the literature. Only metal-insulator(oxide)-semiconductor FETs have been attempted where the insulating layer is a necessity in order to prevent the large gate leakage current.

Much research conducted on CVD diamond sensors has been directed towards the development of photoconductive light detectors. This form of detector relies on the intrinsic high resistivity of the material to achieve a low dark current, hence the problem associated with doping is avoided. The specific goal of a visible blind UV detector is only achievable using diamond as other semiconductors will have a visible response. Another important class of devices currently under development are radiation detectors and dosimeters which exploit the

radiation hardness of diamond.

This study describes the introduction and the application of an alternate dopant for PCD. Electrical measurements confirmed the p-type nature of the material with a measured sheet carrier density of $10^{13}cm^{-2}$ and a Hall mobility ranging from 15 to 70 cm^2/Vs on as-grown PCD. This dopant originates from the 'hydrogen terminated' surfaces of diamond film and manifests as shallow acceptor states. Therefore, at room temperature complete impurity ionisation is achieved. Control over the carrier concentration can be achieved through annealing the PCD in air. A significant advantage of using this form of dopant is that the nature of the metallisation contact deposited on this layer depends on the electronegativity of the metal. Au (electronegative value of 2.4) being a more electronegative element displayed near ohmic while compared to Al (electronegative value of 1.5) which displayed a Schottky characteristic. This combination produced Schottky diodes which have an ideality factor close to 1.1, rectification ratios of over 6 orders of magnitude at ±10V and a breakdown over 100V with leakage current in the nA levels throughout. High performance Schottky diodes have been demonstrated at room temperature. Had oxidised surfaces with boron doping been used, similar conduction levels and device performances would not be achievable. In addition, these diodes are capable of operating at 200°C with a rectification ratio of 3 orders of magnitude taken at ±10V.

More advanced switches which exhibit gain, such as the MESFET, have been fabricated. Using Al as the metal gate control and Au as the source and drain contact, both enhancement and depletion mode MESFETs have been demonstrated on PCD. The operational mode of these transistors depends on the thickness of the conductive channel. On the smaller grain material, the depletion mode operation is possible. However, on the larger grain material only the enhancement mode is achievable. In addition, MESFETs displaying a V_{DS} breakdown of more than 100V have been demonstrated. The sheet resistance of the polycrystalline films (10 kΩ/square) on which these MESFETs were fabricated is comparable to homoepitaxial material (7 kΩ/square). Given an improved design, polycrystalline FETs displaying a predicted power handling capability of close to 6kW/mm for the DC characteristic should be achievable. These MESFETs were the first ever to be fabricated and also one of the first transistors which display full pinch off and saturation of drain current on PCD. In terms of DC characteristic there will be no significant advantage of using single crystal diamond if the same device structure can be deposited on PCD with a comparable sheet resistance.

The properties of ohmic contacts played an essential role in determining the electrical characteristic of these devices. The properties of Au contacts were investigated using the circular TLM method. Other metallisation scheme such as Ti/Au and Ti/Al have been explored as well. These metallisation schemes rely on the formation of a conductive carbide interface and offer the advantage of mechanical durability and better adhesion compared to Au contacts. The formation of a reacted interface requires a high temperature anneal. An optimum anneal cycle at 600°C for 20 minutes followed by a hydrogen plasma exposure at 600°C for 5 minutes is necessary to restore the conductivity of the material to its original level. A specific contact resistance ranging from 10^{-1} to $10^{-3}\Omega cm^2$ has been measured. The use of Ti/Au reacted interface is also compatible

with the incorporation of a heavy dose of ion implanted B ($>10^{20}cm^{-3}$) if a lower specific contact resistance is required ($<10^{-5}\Omega cm^2$).

Another attractive application of this surface layer is the detection of radiation which corresponds to the indirect bandgap of diamond. This method relies on using the blocking metal semiconductor contact to maintain a low dark current. Currently only the photoconductive devices are available for this application. The operation of MSM photodiodes and OPFET devices has been demonstrated in this study for the first time and their detection mechanisms have been described. These devices are capable of showing gain with the OPFET displaying higher values. As these devices are fabricated on a doped layer monolithic integration of these detectors with other electronic devices can be made possible.

In the late 1980's, researchers predicted that diamond will have semiconducting properties far superior to existing materials. This results from the combination of extreme physical and electrical properties of diamond. The extreme properties enable applications where devices are exposed to harsh environments and high temperatures to be envisaged. However, the extreme properties also make diamond a material difficult to handle. The mechanical hardness and chemical inertness introduce difficulty in processing stages such as etching. Most of the superior electronic properties of diamond arise through the close packed nature of the diamond lattice which causes difficulty in doping. An impurity dopant which is fully ionised at room temperature with the ability to operate at high temperature has yet to be discovered. If this hurdle can be overcome then diamond electronics will progress rapidly. The doping layer investigated in this study is unusual, ultra thin and stable up to 200°C. More importantly, the performance of the electronic devices on this layer are outstanding even on polycrystalline material. Although the performance of the electronic devices in this study may not be able to surpass the current state-of-the-art Si, SiC or GaN devices, they do significantly advance the field of diamond electronics.

Apart from the dopant problem, the surface roughness of PCD films restricts the fabrication of devices with small dimensions. Improvements in the area of CVD growth to produce films with a smoother surface, higher quality and over a large area are essential. Furthermore, the conductive layer used here is only confined to the surface and disappears above 400°C. The possibility of increasing the depth of this layer is still under investigation. In the next millennium, to compete with existing semiconductors, a breakthrough is needed to overcome the growth, the quality and the dopant problem. Nevertheless, diamond will always find niche applications in specific fields where its extreme properties are the most important factor.

Appendix 1.1: De-grease formulation

Reagents:
(i) 1,1,1-trichloroethane
(ii) acetone
(iii) 2-propanol (IPA)
(iv) de-ionised (DI) water

Procedure:

(i) Place sample in 1,1,1-trichloroethane (55°C) for 3 minutes.
(ii) Transfer sample to acetone at room temperature for 3 minutes
(iii) Transfer sample to 2-propanol at room temperature for 3 minutes
(iv) Transfer sample to DI water at room temperature for 3 minutes
(v) Remove excess of water from sample by blowing with nitrogen

When transferring samples between solvents it is important to prevent the solvent on the sample from drying out as residue which is soluble in the previous solvent may be insoluble in the next.

Appendix 1.2: Acid treatment formulation

Reagents:
(i) concentrated sulphuric acid (H_2SO_4)
(ii) ammonium persulphate ($(NH_4)_2S_2O_8$)
(iii) hydrogen peroxide (H_2O_2)
(iv) ammonium hydroxide (NH_4OH)

Procedure:

(i) Place about 8 teaspoonful of ammonium persulphate in a beaker. Carefully add in about 30ml of concentrated sulphuric acid. This will give the ETCH solution
(ii) Prepare the rinse solution which consists of a 1:1 mix of hydrogen peroxide and ammonium persulphate
(iii) Place the samples in the ETCH solution and heat the ETCH solution gradually to about 200°C. Maintain the temperature at 200°C for 20min. White fumes of SO_3 will be released once temperature exceeds 140°C
(iv) Transfer the sample from the ETCH solution to the rinse solution when the ETCH solution has cooled down to about 50°C.
(v) Heat the rinse solution with the sample to about 50°C for 5 minutes.
(vi) Transfer sample from the rinse solution to DI water
(vii) Remove water from the sample by blowing with nitrogen.

Appendix 2: Experimental setup for Hall measurements

Appendix 2.1: Sample Preparation

Apparatus:

(a) Edwards 306 resistive thermal evaporator
(b) Aluminium foil
(c) As deposited free standing diamond samples
(d) Gold pellets

Preparation of electrical contacts for van der Pauw measurements

(i) Diamond samples for Hall measurements are prepared by breaking the free standing wafer into square tiles approximately 0.5 x 0.5 cm in size.

(ii) The samples together with the Au pellets and Al foil are then degreased according to Appendix 1.

(iii) The samples are secured on a glass slide with a double sided sticky tape.

(iv) The Al foil is cut into long rectangular strips of 0.45 x 3.0 cm and then placed on top of the square tiles as shown in figure A2.1. The Al strips will act as a mask to ensure that metal contacts will only be deposited at the 4 corners of the sample.

(v) Evaporation is performed and the typical thickness of the Au layer required is about 300nm to facilitate bonding.

(vi) After evaporation, the Al strips were removed and the electrical properties of the Au contact is tested to ensure that the current levels were sufficiently high for Hall measurements.

(vii) The samples are bonded to a header as shown in Figure A2.2.

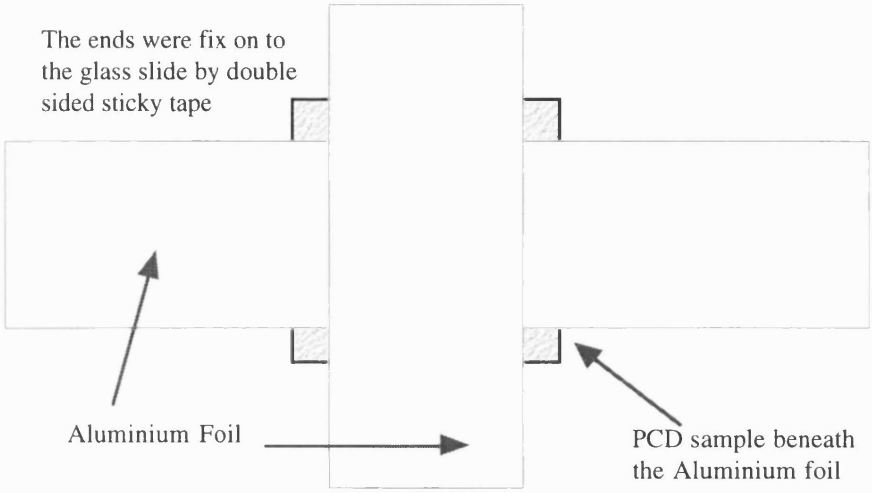

Figure A2.1 The schematic diagram of the diamond tiles masked with aluminium strips

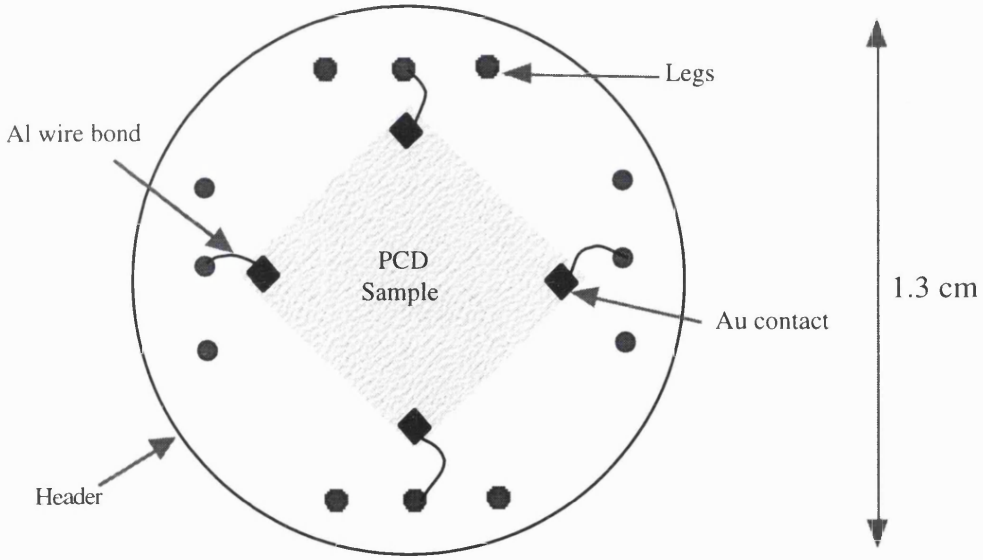

Figure A2.2 The schematic diagram of the samples bonded on to the header.

Appendix 2.2: The Hall measurement

Apparatus :

(a) Constant current source capable of providing 100nA, 1μA, 10μA, 100μA and 1mA.
(b) Electromagnet supplying a magnetic field strength of 0.3T
(c) Keithley multimeter 2000 for voltage measurement
(d) Sample holder as shown in figure A5.3 to position the sample in the magnetic field
(e) Electrical heater.

Measurement Technique

(i) The header with the sample properly bonded is placed on the metal block as shown in figure A5.3. The spring will secure the header into position. The heating element is placed beneath the metal block to vary the temperature of the sample. The surrounding of the metal block is filled with glass wool to provide a more uniform heating.

(ii) The sample holder is positioned between the electromagnet. Changing the power supply to

the heater allows good control over a temperature range of about 200°C with the actual temperature itself being monitored by the thermocouple.

(iii) The 4 wires isolated from each other by ceramic beads will provide the electrical connection to the contacts in the header so that measurement can be made.

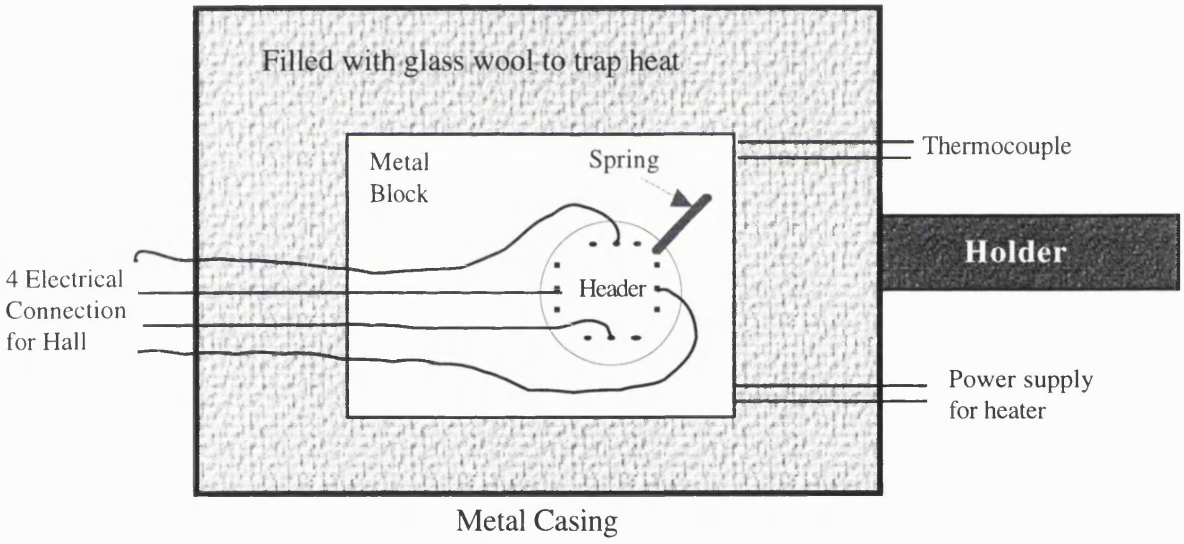

Figure A2.3 The schematic diagram of the sample holder used for the Hall measurement

Appendix 3.1: Photolithography Techniques - Etching

Reagents:

(a) Photoresist AZ 4652
(b) 351 developer
(c) Acetone
(d) Standard Au and Al Etch

Photoresist spinning and developing procedure:

(i) Place the sample on the spinner. Switch on the vacuum to hold the sample so that it will remain on the stage. Set the optimum speed required. Set the first spin setting to about 2000rpm and the second spin setting to about 4500rpm.

(ii) Carefully place a drop of photoresist (AZ 4652) on the sample. Make sure that it is sufficient to cover the entire sample including the 4 corners.

(iii) Use the first spin setting of 2000rpm and spin for approximately 10 seconds. The first spin is for the purpose of planarising the surface roughness.

(iv) Place another drop of photoresist on the 1st layer. Use the 2nd setting of 4500rpm and spin for about 20 seconds. After the second spin, the photoresist will be more uniformly spread out on the sample. The photoresist at the edge will be thicker than the middle of the sample. This is known as the beading effect.

(v) Switch off the vacuum, carefully remove the sample from the spinner and place it on a glass slide. Heat the sample in an oven set to 85°C for 20 minutes.

(vi) A light field mask is used to define the specific pattern on the sample. During UV exposure, set the integrated time on the Karl Suss mask aligner to 700s

(vii) In the developing stage a solution which consists of a 1:3 mix of de-ionised water and 351 developer is prepared. Place the sample in the mixture. Gently swirl the mixture to get a uniform effect for about 60s. Remove excess developer from the sample by cleaning the sample in de-ionised water. Inspect the sample under a microscope.

(viii) Repeat procedure (vii) at 10s developing interval until the desired pattern is successfully defined on the surface. The sample is placed in the etch solution to remove unwanted region. Places which are covered by the photoresist are protected.

(ix) The remaining photoresist on the sample can be removed with acetone.

Appendix 3.2: Photolithography Techniques - Lift off

Photoresist spinning and developing procedure:

(i) Set the spinner to about 5000rpm and place a drop of photoresist on the sample. Spin for about 20s.

(ii) Remove the sample and place it on the glass slide. Bake the sample for about 10 minutes at 85°C. Remove the sample from the oven. Let the sample cool down to room temperature.

(iii) Expose the entire sample to UV without a mask. Set the integrated exposure time to 350s.

(iv) Transfer the exposed sample to the spinner and place another drop of photoresist on the 1st layer. This time set the spin speed to 4500rpm and spin for 20s. Bake the sample in the oven at 85°C for about 15 minutes.

(v) Place the sample in the Karl Suss mask aligner, this time use a dark field mask with the required pattern. Set the integrated exposure time to about 600s.

(vi) Prepare a solution of de-ionised water and 351 developer in a ratio of 3:1. Place the sample in the mixture and swirl gently to get a uniform effect. After about 50s, remove the sample and clean off excess developer by placing the sample in a large beaker of water. Inspect under the microscope.

(vii) Look out for signs of undercutting occurring at the edge of the photoresist. If undercutting did not occur, repeat procedure (vi) with a developing interval of 10s.

(viii) Once the pattern required is properly defined, metal contacts need to be deposited on the sample immediately. Unwanted metal on top of the photoresist can be lifted off by placing sample in acetone.

(ix) Acetone will be able to reach the bottom layer of photoresist beneath the metal contacts easily if the photoresist has an undercut wall structure.

Appendix 4: Computation for the Circular Transmission Line Model using Reeves Method

The actual syntax used in the Matlab is shown below. Text will be included to briefly describe how the formula is used. This section shows determination of $\mathbf{r}_c$

Dimension of UCL Circular Test Structure

```
r0 = 0.01;

r1a = 2.00*r0;
r1  = 4.00*r0;
r2a = 5.63*r0;
r2  = 7.69*r0;

Ar0 = 0.5 : 0.01 : 1.5;

z = 1;
o = 0;

Ar1a = 2.00.*Ar0;
Ar1  = 4.00.*Ar0;
Ar2a = 5.63.*Ar0;
Ar2  = 7.69.*Ar0;
```

r0 is given in the centimeter scale

Formulae for constructing Psi and Delta

```
AAr1 = besseli(z,Ar1) .* besselk(o,Ar1a) + besseli(o,Ar1a) .* besselk(z,Ar1);

AAr2 = besseli(z,Ar2) .* besselk(o,Ar2a) + besseli(o,Ar2a) .* besselk(z,Ar2);

BBr1 = besseli(z,Ar1a) .* besselk(o,Ar1) + besseli(o,Ar1) .* besselk(z,Ar1a);

CCr1 = besseli(z,Ar1) .* besselk(z,Ar1a) - besseli(z,Ar1a) .* besselk(z,Ar1);

CCr2 = besseli(z,Ar2) .* besselk(z,Ar2a) - besseli(z,Ar2a) .* besselk(z,Ar2);

DDr1 = besseli(o,Ar1a) .* besselk(o,Ar1) - besseli(o,Ar1) .* besselk(o,Ar1a);

Er0  = besseli(o,Ar0) ./ besseli(z,Ar0);

K    = AAr1 .* BBr1  ./ CCr1  + DDr1;

Psia = log(r2a ./ r1) .* (Er0 ./ Ar0 + AAr1 ./ (Ar1a .* CCr1) );

Psib = log(r1a ./ r1) .* (BBr1 ./ (Ar1 .* CCr1) + AAr2 ./ (Ar2 .* CCr2) );

Psi  = (Psia - Psib) ./ K;

Delta = 2 .* pi ./ (K .* Ar0 .* Ar0 .* Psi);
```

Formulae for plotting Psi as a function of Ar0 :- Graph Appendix 4.1

```
hold off
semilogy(Ar0,Psi);
hold on
grid
hold on
ylabel('Psi and Delta')
xlabel('Alpha r0');
text(3.8, 10000, 'Psi')
text(4.0,  7.2, 'Delta')
title('Dependence of Psi and Delta on Mike mask')
set(gca, 'ytick', 70  : 4   : 360);
plot(Ar0,Delta);
set(gca, 'xtick', 2.0 :0.04 : 2.82);
```

Formulae for plotting Delta as a function of Ar0 :- Graph Appendix 4.2

```
hold off
grid
semilogy(Ar0,Delta);
hold on
grid
ylabel('Delta')
xlabel( 'Alpha r0')
title('Delta on Mike mask')
set(gca, 'ytick', 3.4 : -0.1 : 2.60);
set(gca, 'xtick', 2.0 : 0.04 : 2.82);
```

Experimental Result is placed here

```
Rin     =  ;
Rout    =  ;
RE      =  ;

Psi     = ( log(r2a/r1) * Rin - log(r1a/r0) * Rout ) / RE
```

From the above Rin = R_{in}
Rout = R_{out}
RE = R_{END2-3}

The value of Ar0 for the Psi calculated above needs to be determined from the Graph in Appendix 4.1

Once Ar0 is known, the Graph in Appendix 4.2 is used to determine the corresponding value for Delta

Once Delta is known, the calculation for specific contact resistance can proceed.

Formula for determining the Specific Contact Resistance

```
Pc   = ( log(r2a/r1) * Rin - log(r1a/ro) * Rout) * r0 * r0 * Delta
```

The value for the rest of the parameters require in the equation above is determined from the calculation given earlier.

Appendix 5: Calculation for the Circular Transmission Line Model using Reeves Method

Solutions from Appendix 4 is placed here

```
Rin   =  ;
Rout  =  ;
RE    =  ;
Ar0   =  ;
Delta =  ;
```

Defining the dimension of UCL c-TLM test Structure

```
z = 1;
o = 0;

r0  = 0.01;
r1a = 2.00*r0;
r1  = 4.00*r0;
r2a = 5.63*r0;
r2  = 7.69*r0;

Ar1a  = 2.00*Ar0;
Ar1   = 4.00*Ar0;
Ar2a  = 5.63*Ar0;
Ar2   = 7.69*Ar0;
```

Formulae for solving the necessary variables required by the next section.

```
AAr1 = besseli(z,Ar1) * besselk(o,Ar1a) + besseli(o,Ar1a) * besselk(z,Ar1);

AAr2 = besseli(z,Ar2) * besselk(o,Ar2a) + besseli(o,Ar2a) * besselk(z,Ar2);

BBr1a = besseli(z,Ar1) * besselk(o,Ar1a) + besseli(o,Ar1a) * besselk(z,Ar1);

CCr1 = besseli(z,Ar1) * besselk(z,Ar1a) - besseli(z,Ar1a) * besselk(z,Ar1);

CCr2 = besseli(z,Ar2) * besselk(z,Ar2a) - besseli(z,Ar2a) * besselk(z,Ar2);

DDr1 = besseli(o,Ar1a) * besselk(o,Ar1) - besseli(o,Ar1) * besselk(o,Ar1a);

Er0  = besseli(o,Ar0) / besseli(z,Ar0);
```

Formulae for sheet resistance below the contact (r_{sk})

```
Pc    = ( log(r2a/r1) * Rin - log(r1a/r0) * Rout) * r0 * r0 * Delta;

Alpha = Ar0 / 0.01;

Rsk = Pc * Alpha*Alpha;
```

Formulae for calculating all the parameters required by the equivalent circuit & r_s

```
Zo   = Rsk / (2*pi*Ar0);
Rc0  = Zo * Er0;

Z1a  = Rsk / (2*pi*Alpha*r1a);
Rc1a = Z1a * BBr1a / CCr1;

RA   = Rin -Rc0 -Rc1a;

Rsh  = RA * 2 * pi / log(r1a/r0);

BBr2a  = besseli(z,Ar2) * besselk(o,Ar2a) + besseli(o,Ar2a) * besselk(z,Ar2);

BBr1 = besseli(z,Ar1a) * besselk(o,Ar1) + besseli(o,Ar1) * besselk(z,Ar1a);

Z1   = Rsk / (2*pi*Alpha*r1);

Z2a  = Rsk / (2*pi*Alpha*r2a);

Rc1  = Z1 * BBr1 / CCr1;

Rc2  = Z2a * BBr2a / CCr2;

RB   = Rout - Rc1 - Rc2;

Rsh2 = RB * 2 * pi / log(r2a/r1);
```

Formulae for calculating the transfer length

```
LT = sqrt(Pc/Rsh);
```

Formulae to calculate the Schotty barrier height

```
k  = 1.38e-23;
T  = 293;
q  = 1.6e-19;
m  = 0.7;
A  = 120*m;

SBH =  ( log (Pc * q * A * T / k)  ) * k * T / q;
```

The value for all of the parameters will be displayed in this section

```
Rsk
Rsh
Rsh2
LT
Pc
Rc0
RA
Rc1a
Rc1
RB
Rc2
SBH
```

Appendix 6: Glossary of Terms

Al	aluminium
Au	gold
B	boron
c-TLM	circular transmission line model
C-V	capacitance-voltage
CVD	chemical vapour deposition
E-H	electron-hole
FET	field effect transistors
UHV	ultra high vacuum
I-V	current -voltage
MESFET	metal semiconductor field effect transistor
MISFET	metal insulator semiconductor field effect transistor
MOSFET	metal oxide semiconductor field effect transistor
MSM	metal semiconductor metal
NEA	negative electron affinity
OPFET	optically activated field effect transistor
PCD	polycrystalline CVD diamond
SBH	Schottky barrier height
SEM	scanning electron microscope
SIMS	secondary ion mass spectroscopy
Ti	titanium
TLM	transfer length method
UPS	ultra-violet photoelectron spectroscopy
UV	ultra-violet

Appendix 7: Related Publications

[1] High carrier mobility in polycrystalline thin film diamond
H.J. Looi, R.B. Jackman and J.S. Foord,
Appl Phys. Lett., **72**, 353, (1998)

[2] Enhancement mode MESFET on thin film diamond
H.J. Looi, L.Y.S. Pang, Y. Wang, M.D. Whitfield, R.B. Jackman,
IEEE Electron Device Lett., **19**, 112, (1998)

[3] High performance MESFET from thin film diamond
H.J.Looi, L.Y.S. Pang, Y. Wang, M.D. Whitfield and R.B. Jackman,
Diamond & Relat. Mater., **7**, 565, (1998)

[4] Thin film diamond field effect transistors for high power applications
H.J. Looi, L.Y.S. Pang and R.B. Jackman,
Mat. Res. Soc. Symp. Proc., vol **483**, 63, (1998)

[5] An insight into the mechanism of surface conductivity in thin film diamond
H.J. Looi, L.Y.S. Pang, A.B. Molloy, F. Jones, J.S. Foord and R.B. Jackman,
Diamond & Relat. Mater., **7**, 550, (1998)

[6] Progress towards high power thin film diamond transistors
H.J. Looi, L.Y.S. Pang, M.D. Whifield, J.S. Foord and R.B. Jackman,
Diamond & Relat. Mater., **8**, 966, (1999)

[7] An optically activated diamond field effect transistor
S.P. Lansley, H.J. Looi, Y. Wang, M.D. Whtfield and R.B. Jackman,
Diamond & Relat. Mater., **8**, 946, (1999)

[8] Optimising electronic and optoelectronic properties of thin film diamond
O. Gaudin, S. Watson, S.P. Lansley, H.J. Looi, M.D. Whitfield and R.B. Jackman,
Diamond & Relat. Mater., **8**, 886, (1999)

[9] The effect of hydrogen on the electronic properties of CVD diamond films
H.J. Looi, M.D. Whitfield, J.S. Foord and R.B. Jackman,
Thin Solid Films, **343-344**, 623, (1999)

[10] A thin film diamond phototransistor
S.P. Lansley, H.J. Looi, Y. Wang, M.D. Whitfield and R.B. Jackman,
Appl. Phys. Lett., **74**, 615, (1999)

[11] Metal-semiconductor-metal photodiodes fabricated from thin film diamond
H.J. Looi, M.D. Whitfield and R.B. Jackman,

Appl. Phys. Lett., **74**, 3332, (1999)

[12] Mechanism of surface conductivity in thin film diamond: Application to high performance devices, H.J. Looi, L.Y.S. Pang, A.B. Molloy, F. Jones, J.S. Foord and R.B. Jackman, Carbon, **37**, 801 (1999)

[13] High performance devices from surface conductivity
R.B. Jackman, H.J.Looi, L.Y.S. Pang, M.D. Whitfield and J.S. Foord.
Carbon, **37**, 817 (1999)

[14] Hydrogen 'doped' thin film diamond field effect transistors for high power applications
H.J. Looi, L.Y.S. Pang, J.S. Foord and R.B. Jackman.
Solid State electronics, **42**, 2215, (1999)

[15] Engineering low resistance contacts on p-type hydrogenated diamond
H.J. Looi, L.Y.S. Pang, M.D. Whitfield, J.S. Foord and R.B. Jackman,
Diamond & Relat. Mater., (submitted Diamond Films 99)

[16] Metal-semiconductor-metal photodiodes on thin film diamond
H.J.Looi, M.D. Whifield and R.B.Jackman, (submitted Diamond Films 99)